

Doctoral thesis

Doctoral theses at NTNU, 2022:53

Atousa Ghanbari Birgani

RKKY interaction and coexistence with magnetism in superconducting systems

NTNU
Norwegian University of Science and Technology
Thesis for the Degree of
Philosophiae Doctor
Faculty of Natural Sciences
Department of Physics



Norwegian University of
Science and Technology

Atousa Ghanbari Birgani

RKKY interaction and coexistence with magnetism in superconducting systems

Thesis for the Degree of Philosophiae Doctor

Trondheim, March 2022

Norwegian University of Science and Technology
Faculty of Natural Sciences
Department of Physics



Norwegian University of
Science and Technology

NTNU

Norwegian University of Science and Technology

Thesis for the Degree of Philosophiae Doctor

Faculty of Natural Sciences

Department of Physics

© Atousa Ghanbari Birgani

ISBN 978-82-326-6602-7 (printed ver.)

ISBN 978-82-326-6330-9 (electronic ver.)

ISSN 1503-8181 (printed ver.)

ISSN 2703-8084 (online ver.)

Doctoral theses at NTNU, 2022:53

Printed by NTNU Grafisk senter

Abstract

Understanding the interplay between superconductivity and magnetism is of crucial importance for e.g. the field of superconducting spintronics. An attractive playground for investigation of this interplay is heterostructures of superconductors and magnetic materials. Much research has been performed on such heterostructures, revealing that interesting features can arise. Such features include Andreev reflections, the proximity effect, as well as the possibility of realizing spin-split superconductors. Through the proximity effect, superconducting pair correlations can leak into neighboring materials. The proximity effect is closely related to the existence of Andreev reflections where an electron approaching a superconductor is reflected as a hole, leading to creation of a Cooper pair in the superconductor. Moreover, a ferromagnet can induce a homogeneous spin-splitting field inside a neighboring thin-film superconductor. In this thesis, we present results from four research papers concerning systems where magnetism and superconductivity interact. We also present the background material which is necessary in order to understand the results of these papers.

The first paper included in this thesis [1] investigates indirect interaction between magnetic materials mediated by a superconductor. The considered system is a superconducting spin-valve consisting of a superconductor sandwiched between two metallic ferromagnets. Whether the magnetization in the two ferromagnets prefer to be aligned or anti-aligned then depends on both the indirect interaction between the ferromagnets mediated by itinerant carriers in the superconductor as well as the influence of the ferromagnets on the superconducting condensation energy. In the second paper [2], a similar system is considered. In this case, a d -wave superconductor mediates the indirect interaction between two metallic ferromagnets located at a diagonal edge of the superconductor. The structure of the superconductor leads to generation of zero-energy bound states at the diagonal edge, which influences the indirect interaction between the ferromagnets.

The third paper included in this thesis [3] studies the RKKY interaction between localized magnetic impurities mediated by the quasiparticles of an isotropic s -wave superconductor which is subjected to a uniform spin-splitting field. In such a spin-split superconductor the quasiparticle excitation energies become spin dependent, which influences the indirect interaction mediated by these quasiparticles. One should in this case make sure that the spin-splitting field is not too strong as this will lead to a tran-

sition from a superconducting to a normal state. The spin-splitting field that a spin-singlet superconductor can coexist with is normally tied to the magnitude of the superconducting gap, meaning that there for a given superconducting gap is a limit on the critical field. This lead us to the topic of the fourth paper [4] included in this thesis. There, we investigate whether it is possible to surpass this limit in a two-band system consisting of one dispersive and one flat energy band.

Preface

This thesis is submitted to the Norwegian University of Science and Technology (NTNU) in Trondheim, Norway as a partial fulfillment of the requirements for the degree of Philosophiae Doctor. The performed work was done under supervision of Professor Jacob Linder and co-supervision of Professor Asle Sudbø from September 2018 until spring 2022. My work has resulted in 4 research articles. The work was funded by The Research Council of Norway through its Centres of Excellence funding scheme Project No. 262633 "QuSpin". Additionally, I have completed 30 ECTS credits of coursework, corresponding workload of one semester.

Atousa Ghanbari Birgani
Trondheim, Norway
March 2022

Acknowledgements

Once, when I was sad about one of my research projects, my friend Mahroo wrote me a poem in Farsi on a sticky note and put it below the screen of my computer. The poem was

تا در هوس لقمه ی نانی نانی
تا در طلب گوهر کانی کانی
هر چیز که در جستن آنی آنی
این نکته ی رمز اگر بدانی دانی

It is from a famous poet named Rumi, which in Iran is better known as Mowlana. In simple words, it says that what you aim for is what you will achieve. I still have the note below my screen, and I got what I aimed for thanks to everyone who was beside me in my journey. I want to use this opportunity to show them my appreciation.

First of all, I want to thank my supervisor professor Jacob Linder who trusted me and gave me the opportunity to do a PhD degree at NTNU. I am grateful for everything he taught me that helped me becoming a better researcher. I will always remember him as an influential person in my life. I also want to thank my co-supervisor professor Asle Sudbø who, among other things, provided valuable insight during the work on my final research project.

I further want to thank my colleagues from the Linder group: Lina, Jabir Ali and Eirik F., as well as the former members Vetle and Morten whom I had many fruitful discussions with as a new PhD student. I must also thank my other colleagues at Quspin, some of which are also my very good friends. I especially want to name Payel, Håvard, Matthias, Håkon, Longfei, Jonas, Marion, Karen-Elisabeth, Alireza and Sol, as well as Even, Akash, Arnau, Fredrik Nicolai, Roberto and Martin who are currently working elsewhere. I have had a lot of fun taking part in different social activities with these people, making my transition to a new country much easier. I have also found very good friends outside of QuSpin. One of them is Azam who was instrumental in getting me through the first part of the pandemic. Thank you for sharing your room with me as our office. I also want to thank my other good friends Maryam, Elina, Hasti, Leila and Lale for all the good times we had together which helped me forget about being so far away from home.

To me, having family close by is very important. One of my greatest fortunes in Norway was to find another family: My partner Eirik, who is also

my colleague and best friend, as well as his parents Roger and Ann-Elise. Their presence, especially during the pandemic, was invaluable.

I also want to send the greatest thanks to my family in Iran, my mom Parvin, my dad Eskandar, and my siblings Datam, Azar, and Atra, who were patient enough to endure not seeing me through out my entire PhD so that I could reach this point. I want to tell them that

پدر و مادر مهربانم از اینکه در تمام این مدت در کنارم بودید سپاس گذارم. با وجود اینکه امکان حضور فیزیکی در کنارم برایتان فراهم نشد هر روز صدا و تصویرتان تسکین دهنده ی بسیاری از مشکلات من بودند. امیدوارم که همیشه شاد و سلامت باشید

Publications

Paper 1:

A. Ghanbari, V. K. Risinggård, and J. Linder,
Self-consistent solution for the magnetic exchange interaction mediated by a superconductor,
Scientific Reports **11**, 5028 (2021) [1].

Paper 2:

A. Ghanbari, E. Erlandsen, and J. Linder,
The effect of midgap states on the magnetic exchange interaction mediated by a d-wave superconductor,
Physical Review B **104**, 054502 (2021) [2].

Paper 3:

A. Ghanbari, and J. Linder,
RKKY interaction in a spin-split superconductor,
Physical Review B **104**, 094527 (2021) [3].

Paper 4:

A. Ghanbari, E. Erlandsen, A. Sudbø, and J. Linder
Going beyond the Chandrasekhar-Clogston limit in a flat-band superconductor,
Preprint: arXiv:2109.13245 (2021) [4].

My contributions to the publications

For Paper 1, I performed the analytical and numerical calculations, and created the figures. The manuscript was written together with Jacob Linder and Vetle K. Risinggård. For Paper 2, I performed the analytical and numerical calculations, and created the figures. The results were interpreted and the manuscript was written in collaboration with Eirik Erlandsen and Jacob Linder. For Paper 3, I performed the analytical and numerical calculations, created the figures, and wrote the manuscript together with Jacob Linder. For Paper 4, I performed the analytical calculations. Together with Eirik Erlandsen, I performed the numerical calculations and created the figures. Further, the manuscript was written together with Eirik Erlandsen and Jacob Linder. In total, Eirik Erlandsen and I contributed equally to this project. For all projects, my coauthors contributed through discussions and feedback throughout the process.

Contents

1	Introduction	1
1.1	Spintronics	1
1.2	Superconductors in spintronics	3
2	The superconducting state	7
2.1	Introduction to superconductivity	7
2.2	Electron-phonon interaction and Coulomb repulsion	8
2.3	Conventional superconductors and BCS theory	10
2.4	BCS Hamiltonian	11
2.5	Mean-field approximation	13
2.6	BCS gap equation	14
2.7	Constant potential	16
2.8	BCS coherence length	18
2.9	Unconventional superconductivity	18
2.10	Extended BCS theory	20
2.11	Pairing amplitudes and mean-field extended Hamiltonian	21
2.12	Unconventional quasiparticles	23
3	Superconductivity and magnetism	27
3.1	Effect of magnetic field on bulk superconductors	27
3.2	Ferromagnetism	29
3.3	Proximity effect	32
3.4	Spin-split superconductor	34
3.5	Chandrasekhar-Clogston limit	35
3.6	Flat-band systems	38
3.7	Going beyond the Chandrasekhar-Clogston limit	39
4	Magnetic impurities and interaction between them	43
4.1	Origin of exchange interaction	43
4.2	Indirect exchange interaction	45
4.3	Ruderman-Kittel-Kasuya-Yosida interaction	47
4.4	RKKY in a spin-split superconductor	50
4.5	Experimental realization	52

5	Bogoliubov-de Gennes method for lattice models	55
5.1	Normal Metal	55
5.2	<i>s</i> -wave pairing	60
5.3	<i>d</i> -wave pairing	63
6	Indirect exchange interaction between ferromagnets	69
6.1	Superconducting spin valve	69
6.2	Andreev reflection and crossed Andreev reflection	71
6.3	Interaction between ferromagnets mediated by an <i>s</i> -wave superconductor	73
6.4	Zero-energy surface bound states	75
6.5	Interaction between ferromagnets mediated by a <i>d</i> -wave superconductor	79
7	Conclusion and outlook	81
A	Evaluation of T_c integral	85
B	Unconventional Cooper pairing	87
C	Free energy of a fermionic system	91
D	Chandrasekhar-Clogston limit	93
E	Schrieffer-Wolff transformation	99
	Bibliography	100
	Papers	110

Introduction

What will you read in this chapter? Starting with a short introduction to spintronics, we move on to a brief summary of the importance of superconductors for spintronics.

1.1 Spintronics

In electronic devices, electrical currents can be used to perform logic operations and store information. Electrical currents consists of moving electrons that carry charge through the system. While flowing, the electrons collide with each other as well as their environment, generating heat. This heat is often lost to the surroundings, representing a loss of useful energy, or it might even require us to spend additional energy to cool down our electrical devices. Finding ways to reduce or reuse this waste heat is therefore an important step towards a more energy efficient future.

While electronics exploit the charge of electrons to represent and transport information, electrons also have other properties. One of these is spin. An alternative to traditional electronics is therefore to attempt to utilize the spin of electrons, rather than the charge. This idea introduced a new field within physics called *spintronics*.

The term spintronics first appeared around the turn of the millennium as the title of a research project concerning magnetic sensors and magnetic random access memories [5, 6]. Spintronics can, however, be traced all the way back to 1936 when, for the itinerant electrons in the metallic ferromagnet Nickel (Ni), Mott introduced different relaxation times for spins parallel and anti-parallel to the magnetization [7], giving rise to spin polarized currents. His model, where the current is treated as carried by two independent spin components, is known in the literature as *the two current conduction model*. This model has been further investigated by e.g. Campbell *et al.* in 1967 [8] and in 1968 by Fert and Campbell [9].

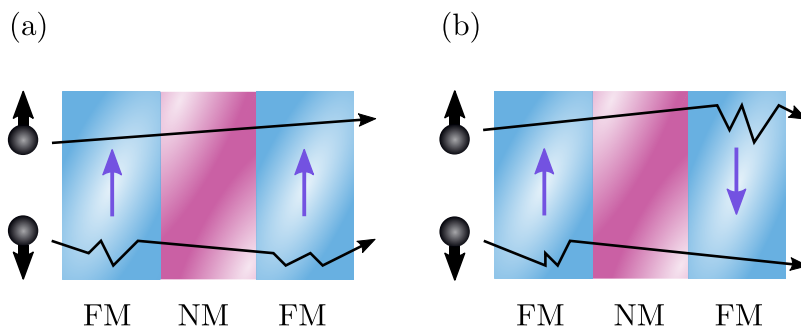


Figure 1.1: Schematic illustration of a GMR structure consisting of a normal metal (NM) layer sandwiched between two ferromagnetic metal (FM) layers. The magnetization of the two ferromagnets are aligned in (a), and anti-aligned in (b).

A breakthrough for spintronics came with the observation of giant magnetoresistance (GMR) in Iron-Chromium (Fe/Cr) superlattices [10] and in trilayers of Iron-Chromium-Iron (Fe/Cr/Fe) [11], introducing the possibility of exploiting the spin properties of electrons in memory devices. This discovery led to Fert and Grünberg being awarded the Nobel Prize in physics in 2007. GMR can be realized in structures where a nonmagnetic metal is sandwiched between two ferromagnetic metals. A current flowing through this system will face different resistance depending on the magnetization alignment of the ferromagnets. If the two ferromagnets have parallel magnetization, the resistance is low. On the other hand, if the magnetization of the ferromagnets are antiparallel, the electrical resistance of the system will be high. A simple picture displaying the motion of electrons in a GMR structure is presented in Fig. 1.1. An electron with spin antiparallel to the magnetization of the ferromagnet it is passing through is here assumed to experience stronger scattering than an electron with spin parallel to the magnetization. Therefore, when the ferromagnets are anti-aligned, as shown in Fig. 1.1 (b), electrons with both spin up and spin down experience strong scattering on their way through the trilayer structure. On the other hand, when the ferromagnets are aligned, as shown in Fig. 1.1 (a), electrons with spin parallel to the magnetization of the ferromagnets experience only weak scattering, leading to a lower electrical resistance. The electrical resistance of the system can, in other words, be magnetically con-

trolled. Soon after the discovery of GMR, magneto-resistive random access memories (MRAMs) based on GMR were developed [12–14].

Later, in 1994, a new layered structure that could give rise to large magnetoresistance (MR) was proposed by Miyazaki and Tezuka [15], as well as Moodera *et al.* [16]. They substituted the central nonmagnetic metal with an insulator. This layered structure, known as a magnetic tunnel junction (MTJ), improved the signal in MRAM at room temperature. It is worth noting that the foundation for these observations was laid already in 1975 by Julliere [17]. He considered a trilayer of Fe/Ge/Co (Ferromagnet-insulator-ferromagnet) at a temperature of 4.2 K. For the first time, he observed that the tunneling conductance in this system depends on the relative orientation of the magnetic moments of the two magnets. The values that he obtained for the relative change of conductance was up to 14%.

Today, spintronics is a broad field with many branches, but with a common objective to pave the way for new spin-based devices. Some crucial factors in realizing such spin-based devices is to be able to generate, transport, and detect spin-currents. Spin currents can be generated in TMR or GMR structures, as well as through the spin Hall effect [18] and the spin Seebeck effect [19]. Detection of spin-currents can similarly be achieved e.g. through inverse spin Hall effect [20]. The spin-currents can for instance be carried by electrons in metallic magnetic materials or by spin-waves (magnons) [21] in magnetic insulators such as yttrium iron garnet (YIG) [22]. The latter alternative opens up the possibility for transferring a spin-current without any movement of electrons, making low energy information transfer possible. Superconductors, as materials with dissipationless currents, also turn out to be good candidates for transport of spin-currents. The subfield of super-spintronics will be further discussed in the next section.

1.2 Superconductors in spintronics

Long before GMR was observed in layered structures, de Gennes proposed in 1966 the idea that superconductivity can be controlled by magnetism [23]. He considered a thin film superconductor, with thickness smaller than the superconducting coherence length, sandwiched between two ferromagnetic insulators (FMI). The temperature was assumed to be well below the critical temperature for the superconducting phase transition. For this system, he showed that the central layer could be either in a superconducting

or normal state depending on the relative angle between the magnetization of the two ferromagnets. For anti-aligned ferromagnets, the induced homogeneous exchange field inside the superconductor vanishes, while for aligned ferromagnets, the induced field is maximized. If this maximal induced exchange field is larger than the critical field of the superconductor, the superconductor transitions to the normal state when the relative angle between the magnetization of the two ferromagnets is made sufficiently small. The system proposed by de Gennes is, in fact, a spintronic storage device based on superconductors, featuring either zero resistance or finite resistance depending on whether the magnetization of the ferromagnets is parallel or antiparallel. In subsequent experiments performed by Deutscher and Meunier [24], and Hauser [25], it was observed that the superconducting transition temperature of a superconductor sandwiched between two ferromagnets was higher when the ferromagnets were anti-aligned than when they were aligned.

Nowadays, the field of superconducting spintronics [26] is attracting much attention due to the possibility of dissipationless transport of spin currents. A central question is then how such superconducting spin currents can be generated. Bergeret *et al.* first predicted leakage of long range spin-triplet Cooper pairs into a ferromagnet with inhomogeneous magnetization in proximity to a spin-singlet superconductor [27]. Ever since then, a lot of studies on generation of spin-polarized supercurrents in different multilayers of superconductors and ferromagnets have been performed. Examples include studies of Josephson junctions (superconductor-ferromagnet-superconductor) [28–30], and superconductor-ferromagnet-ferromagnet structures [31].

Despite of all the progress that has been made within the field of superconducting spintronics there is still much left to explore. In this thesis, we focus on broadening the understanding of the interplay between magnetism and superconductivity. Understanding this interplay is essential for successful integration of superconductivity and spintronics, which relies on both stability of superconductivity in the presence of magnetism as well as taking advantage of the fascinating phenomena that can arise when these two types of order meet. We start with introducing a theoretical description of superconductivity in chapter 2. In chapter 3, we describe the combination of superconductivity and magnetism, either introduced through a superconductor exposed to an external magnetic field, or proximity coupling between superconducting and magnetic materials. This chapter forms the basis for

discussion of paper [4], which is concerned with the critical magnetic field where the system transitions from a superconducting to a normal state. In chapter 4, we introduce the concept of indirect interaction between localized magnetic moments mediated by itinerant electrons. We then turn to how this indirect interaction is influenced by spin-splitting of the electrons mediating the interaction. This leads us to the discussion of paper [3], which is concerned with indirect interaction between magnetic impurities mediated by the quasiparticles in a spin-split superconductor. After having covered indirect interaction between magnetic impurities, we move on to indirect interaction between larger collections of spins such as ferromagnets. Specifically, we are interested in indirect interaction between ferromagnets mediated by different types of superconductors, which is the topic of papers [1] and [2]. To this end, chapter 5 discusses theoretical treatment of superconductors without continuous boundary conditions, while chapter 6 considers systems where superconductors and ferromagnets are coupled together, leading us to the discussion of the two first papers.

The superconducting state

We start with a brief introduction to superconductivity and the origin of the attractive interaction between electrons in conventional superconductors. We then move on to the first microscopic theory explaining superconductivity in conventional superconductors known as BCS theory. Following this, we then transition to unconventional superconductors and the extended BCS theory that can be used to model them.

2.1 Introduction to superconductivity

When cooled down, certain materials enter a phase called superconductivity. This phase is radically different from the normal metal phase that is typically displayed by these systems at higher temperatures. The two main features that distinguish a superconductor from a normal metal are zero electrical resistivity and the Meissner effect. The temperature where these features set in is referred to as the superconducting critical temperature T_c . As a result of their special properties, and especially their ability to conduct electricity without resistive energy loss, superconductors are attractive for a wide range of applications. However, as superconductivity typically arises at low temperatures, the applications of superconductors are constrained to cases where the benefits of the superconducting properties outweigh the cost of cooling down the material [32]. The most popular usage of superconductors is for generation of strong magnetic fields by driving large currents through superconductors without suffering resistive losses. Such superconductor-based electromagnets are used in e.g. MRI [33] (magnetic resonance imaging) and NMR (nuclear magnetic resonance) machines. They are also used in CERN to bend beams of particles [34]. Superconductors are also used in electronics, where the Josephson effect [35] has made superconducting quantum interference devices (SQUIDs) possible, such as SQUIDs

magnetometers [36–38]. Josephson junctions could also be used in transistors [39, 40]. Further technological exploitation of superconductors relies on an improved understanding of their properties and microscopic origin.

In order to categorize different types of superconductors, one can divide them into groups based on their microscopic and macroscopic properties. Superconductors can e.g. be categorized as conventional or unconventional based on the symmetry properties of the superconducting pairing, or as low T_c or high T_c depending on the superconducting critical temperature. We will discuss these classification schemes briefly in the upcoming sections in this chapter. Superconductors are also referred to as type I or type II depending on their response to an external magnetic field. We will get back to this in chapter 3.

2.2 Electron-phonon interaction and Coulomb repulsion

In a crystal, the ions vibrate around their equilibrium positions. The quantized lattice vibrations are referred to as phonons. Electrons living in the system can interact with these phonons. The Fröhlich Hamiltonian describing a system of electrons and phonons that interact with each other using the second quantization notation is

$$H_F = \sum_{\mathbf{k}, \alpha} \varepsilon_{\mathbf{k}} c_{\mathbf{k}, \alpha}^\dagger c_{\mathbf{k}, \alpha} + \sum_{\mathbf{q}} \hbar \omega_{\mathbf{q}} \left(b_{\mathbf{q}}^\dagger b_{\mathbf{q}} + \frac{1}{2} \right) + \sum_{\mathbf{k}, \mathbf{q}} g_{\mathbf{k}, \mathbf{q}} c_{\mathbf{k}+\mathbf{q}, \alpha}^\dagger c_{\mathbf{k}, \alpha} (b_{\mathbf{q}} + b_{-\mathbf{q}}^\dagger). \quad (2.1)$$

The first-term in the above Hamiltonian represents the kinetic energy of the electrons. Here the operator $c_{\mathbf{k}, \alpha}^\dagger$ ($c_{\mathbf{k}, \alpha}$) creates (annihilates) an electron with momentum \mathbf{k} and spin α . The second term represents the phonons, where $b_{\mathbf{q}}^\dagger$ ($b_{\mathbf{q}}$) is a bosonic creation (annihilation) operator. We treat the first two terms as the unperturbed part of the Hamiltonian and the last term as a small perturbation to the system ηH_1 , where η is a smallness parameter. Then, in order to obtain an effective electron-electron interaction, we perform a canonical transformation named the Schrieffer-Wolff transformation, which is discussed in Appendix E. The effective electron-electron interaction mediated by phonons then takes the form

$$H_{\text{eff}} = \sum_{\alpha, \alpha'} \sum_{\mathbf{k}, \mathbf{k}', \mathbf{q}} V_{\text{eff}}(\mathbf{k}, \mathbf{k}', \mathbf{q}) c_{\mathbf{k}+\mathbf{q}, \alpha}^\dagger c_{\mathbf{k}, \alpha} c_{\mathbf{k}'-\mathbf{q}, \alpha'}^\dagger c_{\mathbf{k}', \alpha'}. \quad (2.2)$$

Here, $V_{\text{eff}}(\mathbf{k}, \mathbf{k}', \mathbf{q})$ is an effective potential expressed as

$$V_{\text{eff}} = g_{\mathbf{k}, \mathbf{q}} g_{\mathbf{k}', -\mathbf{q}} \frac{\hbar \omega_{\mathbf{q}}}{(\varepsilon_{\mathbf{k}'} - \varepsilon_{\mathbf{k}'-\mathbf{q}})^2 - (\hbar \omega_{\mathbf{q}})^2}. \quad (2.3)$$

This is an interesting result as it represents that, as a consequence of the interaction between the electrons and phonons, there will be an effective electron-electron interaction which can be attractive. An attractive interaction is, as we will see in the coming sections, what we need in order for electrons to pair up and give rise to superconductivity. The above interaction is attractive when $|\varepsilon_{\mathbf{k}'} - \varepsilon_{\mathbf{k}'-\mathbf{q}}| < \hbar \omega_{\mathbf{q}}$ and vanishes quickly if the difference between the electron energies becomes too large as the electron energy scale typically is much larger than the phonon energy scale. For an electron with momentum \mathbf{k}' situated at the Fermi level, the interaction strength is small unless the outgoing electron with momentum $\mathbf{k}' - \mathbf{q}$ is also close to the Fermi level. The width of the shell around the Fermi level where the interaction is active is typically assumed to be of the order of the maximum energy of the phonon spectrum $\hbar \omega_c$. Within this thin shell, the interaction potential is often taken to be a constant.

Further, the electrons also interact with each other through the repulsive Coulomb interaction. The second-quantised Hamiltonian describing the Coulomb interaction between the electrons is

$$H_C = \sum_{\alpha, \alpha'} \sum_{\mathbf{k}, \mathbf{k}', \mathbf{q}} V_C(\mathbf{q}) c_{\mathbf{k}+\mathbf{q}, \alpha}^\dagger c_{\mathbf{k}', \alpha'}^\dagger c_{\mathbf{k}', \alpha'} c_{\mathbf{k}, \alpha}. \quad (2.4)$$

The above expression describes the scattering processes in which one electron with momentum \mathbf{k} and spin α scatters from another electron with momentum \mathbf{k}' and spin α' . During this scattering a momentum \mathbf{q} is transferred from one electron to the other. Further, $V_C(\mathbf{q}) = 4\pi \frac{e^2}{q^2}$ is the Fourier transform of the normal expression for the Coulomb interaction between two electrons $V_C(\mathbf{r}) = \frac{e^2}{|\mathbf{r}|}$ [41], where e is the electron charge and $|\mathbf{r}|$ is the distance between the two electrons. Taking into account screening of the Coulomb interaction due to the presence of the rest of the electrons in the system,

the renormalized Coulomb interaction takes the form $V_C(\mathbf{q}) = \frac{4\pi e^2}{\mathbf{q}^2 + 4\pi e^2 N(\varepsilon_F)}$ [41], where $N(\varepsilon_F)$ is the density of the states at Fermi-level. Importantly, the screening increases with the density of states at the Fermi level so that the Coulomb interaction typically is significantly weakened in good metals with a large density of states at the Fermi level.

The Coulomb interaction still represents a repulsive interaction between electrons, which is harmful for superconductivity. However, unlike the phonon-mediated electron-electron interaction, the Coulomb interaction is not quickly suppressed when electrons at the Fermi level are scattered away from the Fermi level. In the Green's function formalism, working with frequencies, this would correspond to the phonon-mediated interaction, active only at small frequencies, acting over larger time-scales than the Coulomb interaction. It has then been shown that the effect of Coulomb interaction on superconductivity is further reduced due to the time-scale differences between the interactions [42]. We will return to a simple picture for this effect in one of the coming sections.

2.3 Conventional superconductors and BCS theory

Superconductivity was first discovered in 1911 when H. Kamerlingh Onnes observed that, below a temperature of 4.1 K, the electrical resistivity of Mercury (Hg) vanished. However, it would take 46 years until a microscopic theory of superconductivity was developed. This theory was proposed in an article by J. Bardeen, L. N. Cooper, and J. R. Schrieffer [43]. Their theory, referred to as the BCS theory, was found to be able to explain the superconductivity in most elemental superconductors such as Aluminum (Al), Tin (Sn) and Niobium (Nb). This type of superconductivity is called conventional superconductivity, usually featuring a relatively low transition temperature. Niobium with $T_c \approx 9$ K [44] has one of the highest transition temperatures among conventional superconductors. According to the BCS theory, superconductivity arises from attractive interaction between electrons. Such attractive interaction can, as shown in the previous section, arise from electron-phonon coupling, which is responsible for giving rise to superconductivity in conventional superconductors.

Above the superconducting transition temperature, conventional superconductors are in a metallic state where the electron states below the Fermi level are mostly filled and the states above the Fermi level are mostly unoc-

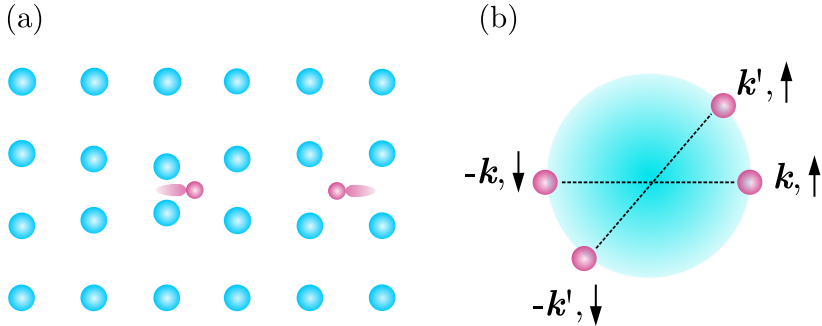


Figure 2.1: (a) An incoming electron polarizes the ionic lattice, leaving behind a larger density of positive charge. Another electron moving in the lattice is attracted to this polarization. (b) Attractive interaction mediated by phonons gives rise to formation of Cooper pairs composed of electrons with opposite spins and momenta.

cupied. BCS theory then states that attractive interaction between electrons leads to electrons close to the Fermi level pairing up into so-called Cooper pairs, named after Leon Cooper, forming a condensate. The Cooper pairs are formed between electrons with opposite spins (\uparrow and \downarrow) and opposite momentum (\mathbf{k} and $-\mathbf{k}$). In the presence of Cooper pairing, the single-particle excitations are combinations of electron and hole excitations and the single-particle excitation spectrum contains a gap around the Fermi level.

2.4 BCS Hamiltonian

We here start out from a real-space Hamiltonian involving attractive on-site interaction between electrons. This Hamiltonian leads us to a momentum space Hamiltonian similar to the one considered in the original formulation of BCS theory. Our real-space Hamiltonian takes the form

$$H = -t \sum_{\langle i,j \rangle, \alpha} c_{i,\alpha}^\dagger c_{j,\alpha} - \sum_{i,\alpha} \mu_i n_{i,\alpha} - \sum_i V_i n_{i,\uparrow} n_{i,\downarrow}. \quad (2.5)$$

Here, $c_{i\alpha}^\dagger$ ($c_{i\alpha}$) creates (annihilates) an electron with spin α at lattice site i . Further μ_i is the chemical potential at lattice site i and $n_{i,\alpha} = c_{i,\alpha}^\dagger c_{i,\alpha}$ is the

number operator. This Hamiltonian represents an intuitive picture describing the mechanism for superconductivity in real-space. A metallic system consists of itinerant electrons that can hop around on a lattice of ions which can vibrate around their equilibrium positions. An incoming electron will, due to its negative charge, pull ions towards itself, as displayed in Fig. 2.1 (a). This leads to a region of increased density of positive charge in the system. This charge polarization remains long after the electron has left due to the ion dynamics being much slower than the electron dynamics. Another electron can then be attracted to this region with increased density of positive charge. As the ions relax slowly back to their equilibrium positions, the two incoming electrons do not have to ever be close to each other, avoiding strong Coulomb interaction. The electrons are therefore able to interact attractively despite the presence of Coulomb interaction, as introduced earlier. The physics contained in this simple picture is in our real-space Hamiltonian captured through an attractive on-site interaction between electrons with strength $V_i > 0$.

Considering continuous boundary conditions, we can do the Fourier transformation $c_{i,\alpha} = \frac{1}{\sqrt{N}} \sum_{\mathbf{k}} e^{-i\mathbf{k}\cdot\mathbf{r}_i} c_{\mathbf{k},\alpha}$. Implementing this into Eq. (2.5) leads to

$$\begin{aligned}
 H = & -\frac{1}{N} \sum_{\substack{\mathbf{k}_1, \mathbf{k}_2 \\ \mathbf{k}_3, \mathbf{k}_4}} V \delta_{\mathbf{k}_1 - \mathbf{k}_2 + \mathbf{k}_3 - \mathbf{k}_4} c_{\mathbf{k}_1, \uparrow}^\dagger c_{\mathbf{k}_2, \uparrow} c_{\mathbf{k}_3, \downarrow}^\dagger c_{\mathbf{k}_4, \downarrow} + \\
 & + \sum_{\mathbf{k}, \alpha} \varepsilon_{\mathbf{k}} c_{\mathbf{k}, \alpha}^\dagger c_{\mathbf{k}, \alpha},
 \end{aligned} \tag{2.6}$$

where we have assumed that the chemical potential and on-site interaction does not vary spatially ($\mu_i = \mu$ and $V_i = V$). The above equation describes a system of electrons that are able to interact through an effective potential. For our simple real-space model, the resulting interaction is constant with respect to momentum. In general, the effective interaction could have a momentum dependence. For generality, we will therefore in the following consider an interaction potential $V_{\mathbf{k}_1, \mathbf{k}_2, \mathbf{k}_3, \mathbf{k}_4}$. For our real-space Hamiltonian, the resulting electron dispersion takes the form $\varepsilon_{\mathbf{k}} = -2t \left(\cos(k_x) + \cos(k_y) \right) - \mu$, in two dimension and considering the lattice constant to be one. The detailed form of this dispersion relation will, however, not matter in the following.

Following the usual BCS approach, we will consider Cooper pairing between electrons with opposite spins and momenta as illustrated in Fig. 2.1

(b). In the above equation, we then restrict the considered scattering processes to those with $\mathbf{k}_1 = -\mathbf{k}_3$. Using fermionic anticommutation relations and renaming the momentum indices, we then obtain the BCS Hamiltonian

$$H_{\text{BCS}} = \sum_{\mathbf{k}, \alpha} \varepsilon_{\mathbf{k}} c_{\mathbf{k}, \alpha}^{\dagger} c_{\mathbf{k}, \alpha} - \frac{1}{N} \sum_{\mathbf{k}, \mathbf{k}'} V_{\mathbf{k}, \mathbf{k}'} c_{\mathbf{k}, \uparrow}^{\dagger} c_{-\mathbf{k}, \downarrow}^{\dagger} c_{-\mathbf{k}', \downarrow} c_{\mathbf{k}', \uparrow}. \quad (2.7)$$

2.5 Mean-field approximation

In order to deal with the Hamiltonian in Eq. (2.7), we will apply a mean-field approximation. If we have an operator A , we can express it as a sum over its expectation value and its deviation from the expectation value. The deviation can then be expressed as $\delta A = A - \langle A \rangle$. Similarly, for an operator B , we have $\delta B = B - \langle B \rangle$. We then write

$$\delta A \delta B = AB - A \langle B \rangle - B \langle A \rangle + \langle A \rangle \langle B \rangle. \quad (2.8)$$

Considering the deviations from the expectation values to be small, we can approximate AB as follows

$$AB \approx A \langle B \rangle + B \langle A \rangle - \langle A \rangle \langle B \rangle. \quad (2.9)$$

Setting $A = c_{\mathbf{k}, \uparrow}^{\dagger} c_{-\mathbf{k}, \downarrow}^{\dagger}$ and $B = c_{-\mathbf{k}', \downarrow} c_{\mathbf{k}', \uparrow}$, the mean-field form of the BCS Hamiltonian becomes

$$\begin{aligned} H_{\text{BCS}}^{\text{MF}} = & -\frac{1}{N} \sum_{\mathbf{k}, \mathbf{k}'} V_{\mathbf{k}, \mathbf{k}'} \left(c_{\mathbf{k}, \uparrow}^{\dagger} c_{-\mathbf{k}, \downarrow}^{\dagger} \langle c_{-\mathbf{k}', \downarrow} c_{\mathbf{k}', \uparrow} \rangle + \langle c_{\mathbf{k}, \uparrow}^{\dagger} c_{-\mathbf{k}, \downarrow}^{\dagger} \rangle c_{-\mathbf{k}', \downarrow} c_{\mathbf{k}', \uparrow} - \right. \\ & \left. \langle c_{\mathbf{k}, \uparrow}^{\dagger} c_{-\mathbf{k}, \downarrow}^{\dagger} \rangle \langle c_{-\mathbf{k}', \downarrow} c_{\mathbf{k}', \uparrow} \rangle \right) + \sum_{\mathbf{k}, \alpha} \varepsilon_{\mathbf{k}} c_{\mathbf{k}, \alpha}^{\dagger} c_{\mathbf{k}, \alpha}. \end{aligned} \quad (2.10)$$

We next define the gap function

$$\Delta_{\mathbf{k}} = \frac{1}{N} \sum_{\mathbf{k}'} V_{\mathbf{k}, \mathbf{k}'} \langle c_{-\mathbf{k}', \downarrow} c_{\mathbf{k}', \uparrow} \rangle, \quad (2.11)$$

so that

$$\Delta_{\mathbf{k}}^* = \frac{1}{N} \sum_{\mathbf{k}'} V_{\mathbf{k},\mathbf{k}'} \langle c_{\mathbf{k},\uparrow}^\dagger c_{-\mathbf{k},\downarrow}^\dagger \rangle. \quad (2.12)$$

The mean field BCS Hamiltonian can then be expressed as

$$H_{\text{BCS}}^{\text{MF}} = \sum_{\mathbf{k},\alpha} \varepsilon_{\mathbf{k}} c_{\mathbf{k},\alpha}^\dagger c_{\mathbf{k},\alpha} - \sum_{\mathbf{k}} \left(\Delta_{\mathbf{k}} c_{\mathbf{k},\uparrow}^\dagger c_{-\mathbf{k},\downarrow}^\dagger + \Delta_{\mathbf{k}}^* c_{-\mathbf{k},\downarrow} c_{\mathbf{k},\uparrow} \right) + H_{\text{BCS}}^0 \quad (2.13)$$

Here, $H_{\text{BCS}}^0 = \frac{1}{N} \sum_{\mathbf{k},\mathbf{k}'} V_{\mathbf{k},\mathbf{k}'} \langle c_{\mathbf{k},\uparrow}^\dagger c_{-\mathbf{k},\downarrow}^\dagger \rangle \langle c_{-\mathbf{k}',\downarrow} c_{\mathbf{k}',\uparrow} \rangle$. In order to diagonalize this Hamiltonian, we use a transformation named the Bogoliubov transformation. Defining new fermionic operators (γ and γ^\dagger) and using the following linear relation between these new operators and the normal creation and annihilation operators (c and c^\dagger)

$$\begin{pmatrix} c_{\mathbf{k},\alpha} \\ c_{-\mathbf{k},-\alpha}^\dagger \end{pmatrix} = \begin{pmatrix} v_{\mathbf{k}} & \alpha \nu_{\mathbf{k}} \\ -\alpha \nu_{\mathbf{k}} & v_{\mathbf{k}} \end{pmatrix} \begin{pmatrix} \gamma_{\mathbf{k},\alpha} \\ \gamma_{-\mathbf{k},-\alpha}^\dagger \end{pmatrix}, \quad (2.14)$$

where

$$v_{\mathbf{k}} = \frac{1}{\sqrt{2}} \sqrt{1 + \frac{\varepsilon_{\mathbf{k}}}{\sqrt{\varepsilon_{\mathbf{k}}^2 + |\Delta_{\mathbf{k}}|^2}}}, \quad \nu_{\mathbf{k}} = \frac{1}{\sqrt{2}} \sqrt{1 - \frac{\varepsilon_{\mathbf{k}}}{\sqrt{\varepsilon_{\mathbf{k}}^2 + |\Delta_{\mathbf{k}}|^2}}}, \quad (2.15)$$

the diagonalized form of the Hamiltonian is

$$H_0 = H_{\text{BCS}}^0 + \sum_{\mathbf{k}} \varepsilon_{\mathbf{k}} - \sum_{\mathbf{k}} E_{\mathbf{k}} + \sum_{\mathbf{k},\alpha} E_{\mathbf{k}} \gamma_{\mathbf{k},\alpha}^\dagger \gamma_{\mathbf{k},\alpha}. \quad (2.16)$$

Here, $E_{\mathbf{k}} = \sqrt{\varepsilon_{\mathbf{k}}^2 + |\Delta_{\mathbf{k}}|^2}$ is the excitation energy of a quasiparticle with momentum \mathbf{k} . The quasiparticle energies $\pm E_{\mathbf{k}}$ are presented in Fig. 2.2 (b) as a function of momentum. This spectrum features a gap around the Fermi level which is referred to as the superconducting gap. This means that there is a minimum energy required in order to create excitations in the system.

2.6 BCS gap equation

The gap around the Fermi level in the band structure is determined by the superconducting gap function defined in Eq. (2.11). We can use the Bogoliubov transformation that we introduced in the previous section to obtain a

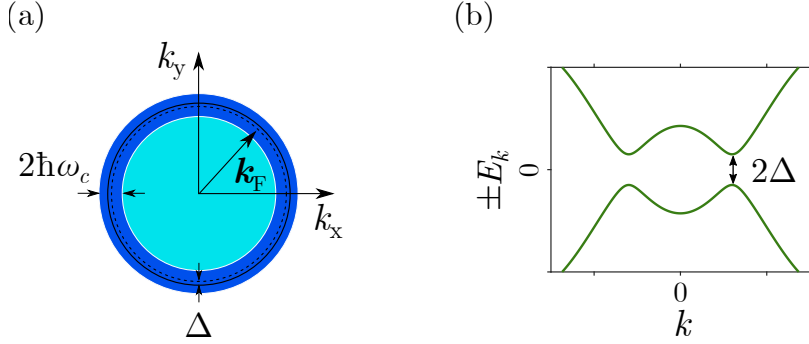


Figure 2.2: (a) Schematic illustration of a circular Fermi-surface with a thin shell of $\hbar\omega_c$ around it where the attractive interaction between electrons is active. The s -wave superconducting gap takes on a constant value within this thin shell, leading to a gap around the Fermi level in the band structure. (b) Quasiparticle spectrum of an s -wave superconductor, displaying the gap in the spectrum. To more clearly display the effect of the gap on the spectrum, the gap has here been taken to be very large.

self-consistent equation for this gap function. Starting from Eq. (2.11) and using the transformation $c_{\mathbf{k},\alpha} = v_{\mathbf{k}}\gamma_{\mathbf{k},\alpha} + \alpha v_{\mathbf{k}}\gamma_{-\mathbf{k},-\alpha}^\dagger$, produces

$$\begin{aligned} \Delta_{\mathbf{k}} &= \frac{1}{N} \sum_{\mathbf{k}'} V_{\mathbf{k},\mathbf{k}'} \langle (v_{-\mathbf{k}'}\gamma_{-\mathbf{k}',\downarrow} - \nu_{-\mathbf{k}'}\gamma_{\mathbf{k}',\uparrow}^\dagger) (v_{\mathbf{k}'}\gamma_{\mathbf{k}',\uparrow} + \nu_{\mathbf{k}'}\gamma_{-\mathbf{k}',\downarrow}^\dagger) \rangle = \\ &= \frac{1}{N} \sum_{\mathbf{k}'} V_{\mathbf{k},\mathbf{k}'} \langle v_{-\mathbf{k}'}\gamma_{-\mathbf{k}',\downarrow} \nu_{\mathbf{k}'}\gamma_{-\mathbf{k}',\downarrow}^\dagger - \langle \nu_{-\mathbf{k}'}\gamma_{\mathbf{k}',\uparrow}^\dagger v_{\mathbf{k}'}\gamma_{\mathbf{k}',\uparrow} \rangle = \\ &= \frac{1}{N} \sum_{\mathbf{k}'} V_{\mathbf{k},\mathbf{k}'} v_{-\mathbf{k}'} \nu_{\mathbf{k}'} (1 - n(E_{-\mathbf{k}',\downarrow})) - \nu_{-\mathbf{k}'} v_{\mathbf{k}'} n(E_{\mathbf{k}',\uparrow}). \end{aligned} \quad (2.17)$$

Here, $n(E_{\mathbf{k}',\alpha}) = \frac{1}{1 + e^{\beta E_{\mathbf{k}',\alpha}}}$ is the Fermi-Dirac distribution function. Using $\tanh(x) = \frac{e^{2x} - 1}{e^{2x} + 1}$, setting $E_{\mathbf{k}',\alpha} = E_{\mathbf{k}'}$, and inserting the expressions for the Bogoliuov transformation coefficients, we obtain for the BCS gap equation

$$\Delta_{\mathbf{k}} = \frac{1}{2N} \sum_{\mathbf{k}'} V_{\mathbf{k},\mathbf{k}'} \frac{\Delta_{\mathbf{k}'}}{\sqrt{\varepsilon_{\mathbf{k}'}^2 + |\Delta_{\mathbf{k}'}|^2}} \tanh\left(\frac{\beta}{2} \sqrt{\varepsilon_{\mathbf{k}'}^2 + |\Delta_{\mathbf{k}'}|^2}\right). \quad (2.18)$$

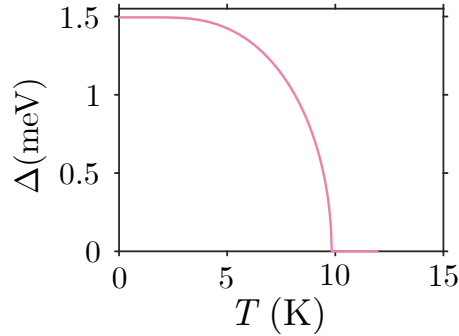


Figure 2.3: Example calculation of superconducting gap as a function of temperature based on Eq. (2.20).

2.7 Constant potential

The next step in the conventional BCS approach to superconductivity is to take the interaction potential to be constant in a thin shell around the Fermi level and zero otherwise

$$V_{\mathbf{k},\mathbf{k}'} = \begin{cases} V > 0, & |\varepsilon_{\mathbf{k}}|, |\varepsilon_{\mathbf{k}'}| \leq \hbar\omega_c, \\ 0, & \text{otherwise.} \end{cases} \quad (2.19)$$

Here, $2\hbar\omega_c$ represents the width of the thin shell around the Fermi-surface, as motivated by the previous discussion of the phonon-mediated interaction potential. If one instead uses the interaction potential arising from our initial real-space Hamiltonian, the difference is that there would no longer be a cutoff on the interaction. This real-space model featuring a constant potential is often used when studying finite systems where the boundaries of the system need to be taken into account, and/or the focus is on the effect of the presence of a superconductor rather than the origin of the superconductivity itself.

Regardless of whether there is a cutoff on the interaction, an interaction potential without any angular dependence on momentum will, based on the gap function definition, give rise to a gap function without angular dependence on momentum, i.e. a gap function with *s*-wave symmetry. For the dependence with respect to radial momentum, we see from Eq. (2.18), keeping the cutoff on the interaction, that the gap function vanishes for momenta \mathbf{k} where $|\varepsilon_{\mathbf{k}}| > \hbar\omega_c$. For momenta \mathbf{k} where $|\varepsilon_{\mathbf{k}}| < \hbar\omega_c$, on the other

hand, the gap function can be taken as a constant Δ , and the gap equation can now be written as

$$1 = \frac{V}{2N} \sum_{\mathbf{k}}^{\left|\varepsilon_{\mathbf{k}}\right| < \hbar\omega_c} \frac{1}{E_{\mathbf{k}}} \tanh\left(\frac{\beta}{2} E_{\mathbf{k}}\right). \quad (2.20)$$

The central quantities involved in this equation are illustrated in Fig. 2.2 (a). The above self-consistent equation can be solved in order to find the superconducting gap as a function of e.g. temperature or interaction strength. An example of the dependence of the gap on the temperature is displayed in Fig. 2.3. What we will focus on, for the time being, is determining the critical temperature, T_c , where the system transitions from a superconducting state to a normal state. At the critical temperature, the gap function vanishes. The critical temperature can therefore be obtained from the gap equation by taking $\Delta = 0$ in the expression for the quasiparticle energies and solving the equation for temperature. Going to the thermodynamic limit, we can write

$$1 = \frac{V}{2N} \int_{-\hbar\omega_c}^{\hbar\omega_c} d\varepsilon \frac{N(\varepsilon)}{|\varepsilon|} \tanh\left(\frac{|\varepsilon|}{2k_B T_c}\right). \quad (2.21)$$

Here, $N(\varepsilon)$ is the density of the states, which we can approximate by the density of states at the Fermi level, N_0 , as the cutoff $\hbar\omega_c$ is assumed to be much smaller than the bandwidth of the system. The density of states is then not expected to vary significantly within the integration region. The gap equation then takes the form

$$1 = \frac{VN_0}{N} \int_0^{\hbar\omega_c} d\varepsilon \frac{1}{\varepsilon} \tanh\left(\frac{\varepsilon}{2k_B T_c}\right). \quad (2.22)$$

Evaluating the integral, as detailed in Appendix A under the assumption that $k_B T_c \ll \hbar\omega_c$, leads to the following expression for the critical temperature

$$k_B T_c = 1.13 \hbar\omega_c e^{-\frac{1}{vN_0/N}}. \quad (2.23)$$

Notably, we see from this equation that the critical temperature increases with the density of states at the Fermi level. This has motivated the study

of superconductivity in systems with flat energy bands, potentially featuring very large density of states at the Fermi level. We will return to the topic of flat-band superconductivity in the next chapter.

2.8 BCS coherence length

An important characteristic length for a superconductor is the superconducting coherence length. Loosely speaking, it represents the average separation of the particles forming a Cooper pair, and it varies for different superconducting materials. Within BCS theory, the coherence length can be expressed on the simple form [45]

$$\xi_{\text{BCS}} = \frac{\hbar v_f}{\pi \Delta(T=0)}. \quad (2.24)$$

Here, \hbar is the reduced Planck constant, and $v_f = \frac{1}{\hbar} \frac{\partial \varepsilon_{\mathbf{k}}}{\partial \mathbf{k}} |_{\mathbf{k}=\mathbf{k}_f}$ is the Fermi velocity. The coherence length is e.g. important for distinguishing between type I and type II superconductors which we will get back to it in next chapter. A list of conventional superconductors and their coherence lengths is presented in Table x.

Table 2.1: Coherence length and T_c in some elemental conventional superconductors. The values are taken from [44, 46–49]

	Al	Cd	Nb	Sn	Pb
ξ_{BCS} (nm)	1600	760	38	230	83
T_c (K)	1.2	0.52	9.2	3.72	7.19

2.9 Unconventional superconductivity

So far, we have considered isotropic s -wave superconductors arising from phonon-mediated electron-electron interactions. In 1972, superfluidity was observed in liquid He^3 [50]. An interesting aspect of this new discovery was that the pairing in He^3 does not have isotropic s -wave symmetry. This

opened up possibilities for new types of superconductors with different pairing symmetries and/or different pairing mechanisms, broadly referred to as unconventional superconductors.

Superconductors within this class have a broad range of critical temperatures. The early unconventional superconductors were heavy fermion superconductors. The first one that was discovered was CeCu_2Si_2 , which has a critical temperature of $T_c = 0.5$ K [51]. Other heavy fermion superconductors with slightly higher critical temperatures include UNi_2Al_3 , UPd_2Al_3 , and CeCoIn_5 with critical temperatures $T_c = 1$ K [52], $T_c = 2$ K [53], and $T_c = 2.3$ K [54], respectively. Organic materials, such as $(\text{TMTSF})_2\text{PF}_6$ [55], can also host unconventional superconductivity at relatively low temperatures.

The discovery of superconductivity in Lanthanum-barium-copper-oxide (LaBaCuO_4) was a breakthrough in high- T_c superconductivity. The critical temperature was observed to be $T_c \approx 30$ K [56], which was the highest so far. Ever since then, cuprate-based superconductors have been of high interest. A famous example is Yttrium-barium-copper-oxide (YBCO) with $T_c \approx 90$ K [57], while the current record for highest critical temperature at atmospheric pressure is held by mercury barium calcium copper oxide ($\text{HgBa}_2\text{Ca}_2\text{Cu}_3\text{O}_x$) with a critical temperature slightly below 140 K [58]. In more recent years, high critical temperatures up to around 100 K have been observed in Iron-based superconductors [59].

Unconventional superconductors feature a wide variety of, often strongly debated, pairing symmetries. Many studies support that cuprate based superconductors feature d -wave pairing [60], while e.g. iron-based superconductors seem to have some kind of extended s -wave pairing symmetry [61, 62]. It was long thought that Sr_2RuO_4 features p -wave pairing [63], while recent studies indicate that this might not be the case [64, 65].

Within the BCS framework, the pairing symmetries of the order parameter are dictated by the symmetry properties of the interaction potential. Unconventional superconductivity can then be introduced by an interaction potential with suitable properties. An interaction potential that changes sign when $\mathbf{k} \rightarrow -\mathbf{k}$ can e.g. give rise to p -wave pairing. Although it is possible to describe unconventional superconductivity within a generalized BCS formalism, unconventional superconductors can often not be well described using this framework. Understanding the superconductivity in the cuprates has e.g. proved to be a difficult challenge. Many different pairing mechanisms have been proposed, including attractive interactions mediated by

spin-fluctuations. Understanding the superconductivity in unconventional superconductors is often difficult because the systems can be complicated and hard to describe also above the critical temperature. Nevertheless, we introduce the generalized BCS formalism, able to describe unconventional superconductivity, in the next section.

2.10 Extended BCS theory

In order to showcase how the BCS theory can be generalized to describe unconventional superconductors, we will start out from a real-space model that can give rise to unconventional superconductivity. This tight-binding Hamiltonian is used in the second paper [2] included in this thesis and introduces attractive interaction between electrons on nearest-neighbor lattice sites. The Hamiltonian, referred to as an extended BCS Hamiltonian, takes the form

$$H_{\text{EBCS}} = - \sum_{\langle i,j \rangle, \alpha} t_{ij} c_{i,\alpha}^\dagger c_{j,\alpha} - \sum_{i,\alpha} \mu_i n_{i,\alpha} - \frac{1}{2} \sum_{\langle ij \rangle, \alpha, \alpha'} V_{ij}^{\alpha, \alpha'} n_{i,\alpha} n_{j,\alpha'}. \quad (2.25)$$

The first and second terms in the above Hamiltonian are the hopping and chemical potential terms, respectively. The final term represents the attractive interaction between electrons on neighboring lattice sites with both equal and opposite spins. The microscopic origin of such nearest neighbour attractive interactions could e.g. be long-range electron-phonon interactions [66]. This term can give rise to both spin-singlet and spin-triplet pairing symmetries, including anisotropic *s*-wave, *d*-wave and *p*-wave pairing. Depending on the value of chemical potential [67], as well as the strength of the attractive interaction, one pairing symmetry will dominate over the others.

In the following, we consider a thin-film system with periodic boundary conditions in both in-plane directions. Implementing the Fourier transformation $c_{i\alpha} = \frac{1}{\sqrt{N}} \sum_{\mathbf{k}} e^{-i\mathbf{k}\cdot\mathbf{r}_i} c_{\mathbf{k},\alpha}$, the *k*-space form of the extended BCS Hamiltonian is

$$H_{\text{EBCS}} = - \frac{1}{2N} \sum_{\alpha \neq \alpha'} \sum_{\mathbf{k}_1, \mathbf{k}_2} V^{\alpha, \alpha'} \left(e^{i\mathbf{k}_3 \cdot \hat{x}} e^{-i\mathbf{k}_4 \cdot \hat{x}} + e^{-i\mathbf{k}_3 \cdot \hat{x}} e^{i\mathbf{k}_4 \cdot \hat{x}} + e^{i\mathbf{k}_3 \cdot \hat{y}} e^{-i\mathbf{k}_4 \cdot \hat{y}} + e^{-i\mathbf{k}_3 \cdot \hat{y}} e^{i\mathbf{k}_4 \cdot \hat{y}} \right) \delta_{\mathbf{k}_1 - \mathbf{k}_2 + \mathbf{k}_3 - \mathbf{k}_4} c_{\mathbf{k}_1, \alpha}^\dagger c_{\mathbf{k}_2, \alpha} c_{\mathbf{k}_3, \alpha'}^\dagger c_{\mathbf{k}_4, \alpha'} + \sum_{\mathbf{k}, \alpha} \varepsilon_{\mathbf{k}} c_{\mathbf{k}, \alpha}^\dagger c_{\mathbf{k}, \alpha}, \quad (2.26)$$

where we have assumed that the interaction potential is spatially uniform ($V_{ij}^{\alpha\alpha'} = V^{\alpha\alpha'}$ for nearest neighbors). Focusing on scattering processes that can give rise to pairing between electrons with opposite momenta, we further write

$$H_{\text{EBCS}} = -\frac{1}{2N} \sum_{\substack{\mathbf{k}, \mathbf{k}' \\ \alpha, \alpha'}} V^{\alpha, \alpha'} \left(e^{-i\mathbf{k}\cdot\hat{x}} e^{i\mathbf{k}'\cdot\hat{x}} + e^{i\mathbf{k}\cdot\hat{x}} e^{-i\mathbf{k}'\cdot\hat{x}} + e^{-i\mathbf{k}\cdot\hat{y}} e^{i\mathbf{k}'\cdot\hat{y}} + e^{i\mathbf{k}\cdot\hat{y}} e^{-i\mathbf{k}'\cdot\hat{y}} \right) \times \\ c_{\mathbf{k}, \alpha}^\dagger c_{-\mathbf{k}, \alpha'}^\dagger c_{-\mathbf{k}', \alpha'} c_{\mathbf{k}', \alpha} + \sum_{\mathbf{k}, \alpha} \varepsilon_{\mathbf{k}} c_{\mathbf{k}, \alpha}^\dagger c_{\mathbf{k}, \alpha}. \quad (2.27)$$

2.11 Pairing amplitudes and mean-field extended Hamiltonian

Similar to the treatment of the normal BCS Hamiltonian, we introduce a mean-field approximation

$$H_{\text{EBCS}}^{\text{MF}} = -\frac{1}{2N} \sum_{\substack{\mathbf{k}, \mathbf{k}' \\ \alpha, \alpha'}} V^{\alpha, \alpha'} \left(e^{-i\mathbf{k}\cdot\hat{x}} e^{i\mathbf{k}'\cdot\hat{x}} + e^{i\mathbf{k}\cdot\hat{x}} e^{-i\mathbf{k}'\cdot\hat{x}} + e^{-i\mathbf{k}\cdot\hat{y}} e^{i\mathbf{k}'\cdot\hat{y}} + e^{i\mathbf{k}\cdot\hat{y}} e^{-i\mathbf{k}'\cdot\hat{y}} \right) \times \\ \left(\langle c_{\mathbf{k}, \alpha}^\dagger c_{-\mathbf{k}, \alpha'}^\dagger \rangle c_{-\mathbf{k}', \alpha'} c_{\mathbf{k}', \alpha} + c_{\mathbf{k}, \alpha}^\dagger c_{-\mathbf{k}, \alpha'}^\dagger \langle c_{-\mathbf{k}', \alpha'} c_{\mathbf{k}', \alpha} \rangle - \langle c_{\mathbf{k}, \alpha}^\dagger c_{-\mathbf{k}, \alpha'}^\dagger \rangle \times \right. \\ \left. \langle c_{-\mathbf{k}', \alpha'} c_{\mathbf{k}', \alpha} \rangle \right) + \sum_{\mathbf{k}, \alpha} \varepsilon_{\mathbf{k}} c_{\mathbf{k}, \alpha}^\dagger c_{\mathbf{k}, \alpha}. \quad (2.28)$$

We then define the pairing amplitudes

$$F_{\alpha, \alpha'}^{x\pm}(\mathbf{k}) = -\frac{1}{N} \sum_{\mathbf{k}'} e^{\mp i\mathbf{k}'\cdot\hat{x}} \langle c_{-\mathbf{k}', \alpha'} c_{\mathbf{k}', \alpha} \rangle, \\ F_{\alpha, \alpha'}^{y\pm}(\mathbf{k}) = -\frac{1}{N} \sum_{\mathbf{k}'} e^{\mp i\mathbf{k}'\cdot\hat{y}} \langle c_{-\mathbf{k}', \alpha'} c_{\mathbf{k}', \alpha} \rangle, \quad (2.29)$$

together with

$$A_{\alpha,\alpha'}(\mathbf{k}) = V^{\alpha,\alpha'} \left(e^{i\mathbf{k}\cdot\hat{x}} F_{\alpha,\alpha'}^{x+}(\mathbf{k}) + e^{-i\mathbf{k}\cdot\hat{x}} F_{\alpha,\alpha'}^{x-}(\mathbf{k}) \right. \\ \left. + e^{i\mathbf{k}\cdot\hat{y}} F_{\alpha,\alpha'}^{y+}(\mathbf{k}) + F_{\alpha,\alpha'}^{y-}(\mathbf{k}) e^{-i\mathbf{k}\cdot\hat{y}} \right), \quad (2.30)$$

the mean-field Hamiltonian then takes the form

$$H_{\text{EBCS}}^{\text{MF}} = \frac{1}{2} \sum_{\mathbf{k},\alpha,\alpha'} \left(A_{\alpha,\alpha'}^*(\mathbf{k}) c_{-\mathbf{k},\alpha'} c_{\mathbf{k},\alpha} + A_{\alpha,\alpha'}(\mathbf{k}) c_{\mathbf{k},\alpha}^\dagger c_{-\mathbf{k},\alpha'}^\dagger \right) + \\ \sum_{\mathbf{k},\alpha} \varepsilon_{\mathbf{k}} c_{\mathbf{k},\alpha}^\dagger c_{\mathbf{k},\alpha} + H_{\text{EBCS}}^0, \quad (2.31)$$

where,

$$H_{\text{EBCS}}^0 = \frac{1}{N} \sum_{\substack{\mathbf{k},\mathbf{k}' \\ \alpha,\alpha'}} V^{\alpha,\alpha'} \left(e^{-i\mathbf{k}\cdot\hat{x}} e^{i\mathbf{k}'\cdot\hat{x}} + e^{i\mathbf{k}\cdot\hat{x}} e^{-i\mathbf{k}'\cdot\hat{x}} + e^{-i\mathbf{k}\cdot\hat{y}} e^{i\mathbf{k}'\cdot\hat{y}} + e^{i\mathbf{k}\cdot\hat{y}} e^{-i\mathbf{k}'\cdot\hat{y}} \right) \times \\ \langle c_{\mathbf{k},\alpha}^\dagger c_{-\mathbf{k},\alpha'}^\dagger \rangle \langle c_{-\mathbf{k}',\alpha'} c_{\mathbf{k}',\alpha} \rangle. \quad (2.32)$$

The definitions are here chosen to match the definitions of the second paper [2] included in this thesis. The spin dependent interaction strength as well as the momentum dependent exponential functions could be combined to a spin and momentum dependent interaction potential

$$V_{\mathbf{k},\mathbf{k}'}^{\alpha,\alpha'} = V^{\alpha,\alpha'} \left(e^{-i\mathbf{k}\cdot\hat{x}} e^{i\mathbf{k}'\cdot\hat{x}} + e^{i\mathbf{k}\cdot\hat{x}} e^{-i\mathbf{k}'\cdot\hat{x}} + e^{-i\mathbf{k}\cdot\hat{y}} e^{i\mathbf{k}'\cdot\hat{y}} + e^{i\mathbf{k}\cdot\hat{y}} e^{-i\mathbf{k}'\cdot\hat{y}} \right), \quad (2.33)$$

producing

$$A_{\alpha,\alpha'}(\mathbf{k}) = -\frac{1}{N} \sum_{\mathbf{k}'} V_{\mathbf{k},\mathbf{k}'}^{\alpha,\alpha'} \langle c_{-\mathbf{k}',\alpha'} c_{\mathbf{k}',\alpha} \rangle. \quad (2.34)$$

In general, varying the starting model, this interaction potential could have an arbitrary spin and momentum dependence, giving rise to pairing amplitudes $A_{\alpha,\alpha'}(\mathbf{k})$ with different spin and momentum symmetries. Writing out the pairing amplitudes $A_{\alpha,\alpha'}(\mathbf{k})$ as a momentum dependent matrix, we obtain

$$A(\mathbf{k}) = \begin{pmatrix} A_{\uparrow,\uparrow}(\mathbf{k}) & A_{\uparrow,\downarrow}(\mathbf{k}) \\ A_{\downarrow,\uparrow}(\mathbf{k}) & A_{\downarrow,\downarrow}(\mathbf{k}) \end{pmatrix}. \quad (2.35)$$

From fermionic anticommutation relations, it follows that the spin and momentum dependent interaction potential $V_{\mathbf{k}\mathbf{k}'}^{\alpha\alpha'}$ needs to be even under the combined operation of inversion of momentum and exchange of spin ($V_{\mathbf{k},\mathbf{k}'}^{\alpha,\alpha'} = V_{-\mathbf{k},-\mathbf{k}'}^{\alpha',\alpha}$). From their definitions, the pairing amplitudes $A_{\alpha,\alpha'}(\mathbf{k})$ then become odd under the combined operation of inversion of momentum and exchange of spin, representing that they are odd with respect to exchange of the fermionic particles that go into the Cooper pairs. We can write this compactly as $A(\mathbf{k}) = -A(-\mathbf{k})^T$, where T is the matrix transpose, or write out explicitly

$$\begin{cases} A_{\alpha,\alpha'}(\mathbf{k}) = -A_{\alpha',\alpha}(-\mathbf{k}) = A_{\alpha,\alpha'}(-\mathbf{k}) = -A_{\alpha',\alpha}(\mathbf{k}), & \text{EP} \rightarrow \text{spin-singlet}, \\ A_{\alpha,\alpha'}(\mathbf{k}) = -A_{\alpha',\alpha}(-\mathbf{k}) = -A_{\alpha,\alpha'}(-\mathbf{k}) = A_{\alpha',\alpha}(\mathbf{k}), & \text{OP} \rightarrow \text{spin-triplet}, \end{cases} \quad (2.36)$$

Here, EP stands for *even under parity*, and OP stands for *odd under parity*. It is common to rewrite $A(\mathbf{k})$ by means of a three dimensional vector $\mathbf{d}(\mathbf{k})$ [68] and a scalar $\Delta_0(\mathbf{k})$. Then,

$$A(\mathbf{k}) = \begin{pmatrix} -d_x(\mathbf{k}) + id_y(\mathbf{k}) & d_z(\mathbf{k}) + \Delta_0(\mathbf{k}) \\ d_z(\mathbf{k}) - \Delta_0(\mathbf{k}) & d_x(\mathbf{k}) + id_y(\mathbf{k}) \end{pmatrix}, \quad (2.37)$$

where

$$\begin{cases} d_x(\mathbf{k}) = \frac{1}{2}(-A_{\uparrow,\uparrow}(\mathbf{k}) + A_{\downarrow,\downarrow}(\mathbf{k})), \\ d_y(\mathbf{k}) = \frac{1}{2i}(A_{\uparrow,\uparrow}(\mathbf{k}) + A_{\downarrow,\downarrow}(\mathbf{k})), \\ d_z(\mathbf{k}) = A_{\uparrow,\downarrow}(\mathbf{k}) - \Delta_0(\mathbf{k}). \end{cases} \quad (2.38)$$

The Cooper pairs which are described by the vector $\mathbf{d}(\mathbf{k})$ form a spin-triplet state, while $\Delta_0(\mathbf{k})$ is the pairing amplitude for spin-singlet Cooper pairs.

2.12 Unconventional quasiparticles

Starting from Eq. (2.31) and defining $H_{\text{eff}} = H_{\text{EBCS}}^{\text{MF}} - H_{\text{EBCS}}^0$, we can write

$$H_{\text{eff}} = \frac{1}{2} \sum_{\mathbf{k}} \Psi_{\mathbf{k}}^{\dagger} \begin{pmatrix} \varepsilon_{\mathbf{k}} \sigma_0 & A(\mathbf{k}) \\ A^{\dagger}(\mathbf{k}) & -\varepsilon_{\mathbf{k}} \sigma_0 \end{pmatrix} \Psi_{\mathbf{k}} + \sum_{\mathbf{k}} \varepsilon_{\mathbf{k}}, \quad (2.39)$$

where, $\sigma_0 = \begin{pmatrix} 1 & 0 \\ 0 & 1 \end{pmatrix}$, and $\Psi_{\mathbf{k}}^{\dagger} = (c_{\mathbf{k},\uparrow}^{\dagger} \quad c_{\mathbf{k},\downarrow}^{\dagger} \quad c_{-\mathbf{k},\uparrow} \quad c_{-\mathbf{k},\downarrow})$. The eigenvalues of the above 4×4 matrix are the quasiparticle energies. In order to calculate them, we limit ourselves to the case of so-called unitary pairing with $A(\mathbf{k})A(\mathbf{k})^{\dagger} = |A_{\mathbf{k}}|^2 \sigma_0$, where $|A_{\mathbf{k}}|^2 = |\Delta_0(\mathbf{k})|^2$ or $A_{\mathbf{k}} = |\mathbf{d}(\mathbf{k})|^2$. Then, the eigenvalues of the above matrix become $E_{\mathbf{k}}^{\pm} = \pm \sqrt{\varepsilon_{\mathbf{k}}^2 + |A_{\mathbf{k}}|^2}$. Further, the Bogoliubov transformation used to diagonalize this matrix is of the form

$$\Psi_{\mathbf{k}} = \begin{pmatrix} \hat{v}_{\mathbf{k}} & \hat{v}_{\mathbf{k}} \\ -\hat{u}_{\mathbf{k}}^{\dagger} & \hat{u}_{\mathbf{k}} \end{pmatrix} \Phi_{\mathbf{k}}, \quad (2.40)$$

where, $\Phi_{\mathbf{k}}^{\dagger} = (\gamma_{\mathbf{k},\uparrow}^{\dagger} \quad \gamma_{\mathbf{k},\downarrow}^{\dagger} \quad \gamma_{-\mathbf{k},\uparrow} \quad \gamma_{-\mathbf{k},\downarrow})$ is a vector of quasiparticle operators. The Bogoliubov transformation matrices are

$$\hat{u}_{\mathbf{k}} = \frac{E_{\mathbf{k}} + \varepsilon_{\mathbf{k}}}{\sqrt{(E_{\mathbf{k}} + \varepsilon_{\mathbf{k}})^2 + |A_{\mathbf{k}}|^2}} \sigma_0, \quad \hat{v}_{\mathbf{k}} = \frac{-1}{\sqrt{(E_{\mathbf{k}} + \varepsilon_{\mathbf{k}})^2 + |A_{\mathbf{k}}|^2}} A(\mathbf{k}), \quad (2.41)$$

where $E_{\mathbf{k}} = |E_{\mathbf{k}}^{\pm}|$. Finally, the diagonalized form of the full Hamiltonian is

$$H_{\text{EBCS}}^{\text{MF}} = \frac{1}{2} \sum_{\mathbf{k}} \Phi_{\mathbf{k}}^{\dagger} E \Phi_{\mathbf{k}} + H_{\text{EBCS}}^0 + \sum_{\mathbf{k}} \varepsilon_{\mathbf{k}}, \quad (2.42)$$

where E is the quasiparticle energies matrix of the form

$$E = \begin{bmatrix} E_{\mathbf{k}} & 0 & 0 & 0 \\ 0 & E_{\mathbf{k}} & 0 & 0 \\ 0 & 0 & -E_{\mathbf{k}} & 0 \\ 0 & 0 & 0 & -E_{\mathbf{k}} \end{bmatrix}. \quad (2.43)$$

A detailed derivation of the eigenvalues and the Bogoliubov transformation can be found in Appendix B. Later in chapter 5, will return to obtaining eigenvalues and transformation matrices from a more numerical point of view.

Superconductivity and magnetism

Superconductivity and magnetism are two phenomena that typically do not go well together. Superconductors tend to expel applied magnetic fields and any magnetic field that makes it way into a superconductor tends to tear Cooper pairs apart. In this chapter, we will first discuss the effect of an external magnetic field on a bulk superconductor and then briefly introduce proximity effects in superconducting heterostructures. We then proceed to discussing the Chandrasekhar-Clogston limit, which normally limits the spin-splitting field a spin-singlet superconductor can coexist with. Finally, we propose a mechanism for surpassing the Chandrasekhar-Clogston limit in multi-band systems.

3.1 Effect of magnetic field on bulk superconductors

When applying an external magnetic field to a superconductor, interesting phenomena can take place. Twenty-two years after the zero resistance property of superconductors was discovered, Meissner and Ochsenfeld observed that a material cooled down below its superconducting critical temperature in the presence of an applied magnetic field expels the magnetic flux at the superconducting transition point [69]. This effect, called the Meissner effect, causes the magnetic field inside a superconductor to vanish, as illustrated in Fig. 3.1 (b). The screening of the magnetic field is caused by formation of supercurrents in the superconductor, setting up an opposing magnetic field ($\mathbf{B} = 0$). Increasing the magnetic field, it eventually becomes more energetically favorable to break the superconductivity and let magnetic flux penetrate the material. This represents a phase transition from a superconducting state to a normal state. A direct phase transition from a

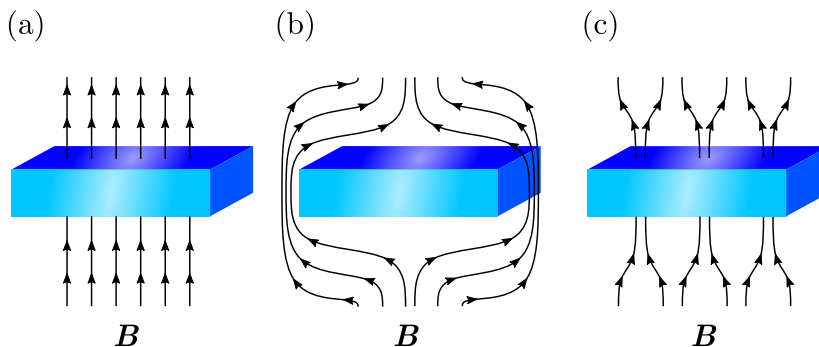


Figure 3.1: A superconductor in an external magnetic field. (a) When the system is in its normal state, magnetic flux penetrates the system. (b) In the superconducting state, the magnetic field is normally screened so that no magnetic flux penetrates the system. (c) In a type II superconductor, there exists an intermediate superconducting phase where magnetic flux is able to penetrate the system at specific points.

superconducting state without magnetic flux penetration to a normal state categorizes type I superconductors. Most of the elemental superconductors such as aluminium (Al), mercury (Hg), lead (Pb), and zinc (Zn) are type I superconductors. Type II superconductors such as niobium (Nb), vanadium (V) and Yttrium-Barium-Copper-Oxide (YBCO), are superconductors featuring an additional intermediate superconducting phase between two critical magnetic fields H_{c1} and H_{c2} . In this intermediate phase, the system features vortices, i.e. non-superconducting regions surrounded by circulating supercurrents, where magnetic flux penetrates the system. This phase, illustrated in Fig. 3.1 (c), is referred to as the vortex phase, while the phase below H_{c1} is referred to as the Meissner phase. Evidence of the presence of a vortex phase was observed in early experiments on niobium (Nb) [70] and vanadium (V) [71]. This phase was described by Abrikosov as a formation of a lattice of vortices [72], which was directly observed through electron microscopy performed on lead and indium alloys in 1967 [73].

Although there is typically no magnetic flux penetrating the bulk of a superconductor in the Meissner phase, magnetic fields are still able to penetrate some finite length into such a superconductor. The characteristic decay length for this penetration is referred to as the *penetration depth* λ_m . In the case of type II superconductors, the penetration depth is equal to the Lon-

don penetration depth (λ_L), arising from the London equation [74]. Type II superconductors are therefore sometimes referred to as London superconductors. In this type of superconductors, the London penetration depth is typically much larger than the coherence length (ξ_{BCS}). Type I superconductors, also called Pippard superconductors [75], typically have coherence lengths that are much larger than their London penetration depths, in which case the London equation no longer holds [76]. In this type of superconductors, the penetration depth is larger than the London penetration depth, and it can be expressed as $\lambda_m \sim (\lambda_L^2 \xi_{\text{BCS}})^{1/3}$ [76]. For both type I and type II superconductors, the strength of the magnetic field decays approximately exponentially with the penetration z as $B(z) = B(0)e^{-z/\lambda_m}$ [76].

Although, magnetic fields are normally screened in bulk superconductors, it is under certain conditions possible to combine magnetism and superconductivity. While an inhomogeneous magnetization can e.g. be induced in somewhat thick superconductors through proximity to ferromagnets, homogeneous spin-splitting of the single-particle states can be achieved in thin-film superconductors through either proximity to a ferromagnet or the application of a magnetic field. In the following, we will focus on these types of systems, where the interplay between superconductivity and magnetism can be studied.

3.2 Ferromagnetism

Magnetic materials are often divided into groups such as paramagnets, diamagnets, and ferromagnets. In paramagnets, magnetic moments in the material align themselves with an external field. In diamagnets, the dominant effect in the presence of a magnetic field is instead induced orbital motion of charged particles, setting up an opposing magnetic field. Ferromagnets are materials with magnetic moments that can align themselves, giving rise to magnetism, even at zero applied magnetic field. This takes place below a critical temperature T_C , referred to as the Curie temperature. Above this temperature, the system is usually in a paramagnetic state. In the presence of an applied field, ferromagnets exhibit hysteresis, meaning that the state of the system depends on the history of the system. At a large applied magnetic field, the magnetization of the system takes on its saturation value $M_S(T)$. Lowering the magnetic field to zero, the magnetization decreases, but it does not vanish. When applying a negative magnetic field, the magnetization eventually vanishes, changes sign and saturates at $-M_S(T)$. Then,

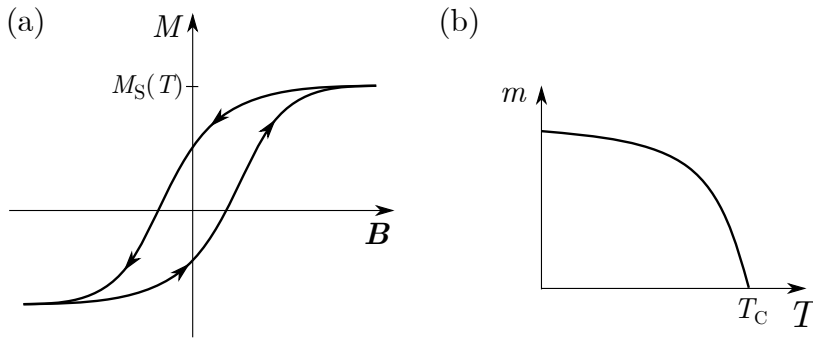


Figure 3.2: Schematic illustrations of (a) hysteresis loop of a ferromagnet, (b) the dependence of the magnetization of a domain with respect to temperature.

when performing the whole procedure in the opposite direction, the magnetization once again ends up at its positive saturation value. However, along the way, the magnetization now traces out a different path than what it did on the way from $M_S(T)$ to $-M_S(T)$, giving rise to the loop displayed in Fig. 3.2 (a).

Both the hysteresis loop and the Curie temperature can be understood from the assumptions of Weiss [77]. These assumptions include: the formation of domains, and the presence of molecular or background fields giving rise to magnetization of the domains. Each domain was taken to be magnetized up to a value $m(T)$, with varying direction of the magnetization from one domain to another. The total magnetization is then the sum of the magnetization of all these domains, which can be zero if the domains are randomly oriented. If one applies an external magnetic field to the system, the domains will start aligning themselves with the field until the system reaches its saturation magnetization $M_S(T)$ when all the domains are aligned. When lowering the magnetic field to zero, the domains tend to stay aligned, giving rise to the hysteresis effect. Moreover, in order to ensure magnetic ordering within a domain, the background field needs to defeat the effect of temperature, which acts to destroy the ordering. The magnetization of a domain therefore decreases with temperature until it vanishes at some critical temperature, as displayed in Fig. 3.2 (b).

Ferromagnetic materials can be insulators, featuring localized magnetic moments, or metals where the electrons can move, more or less freely, around

in the system. For the case of localized magnetic moments, giving rise to a ferromagnetic state, Heisenberg introduced, in 1928, a model that could explain the origin of the Weiss background field [78]. He related the origin of the background field to exchange interaction between the magnetic moments. In the next chapter we will get back to this exchange interaction between the magnetic moments. For now, we just present the Heisenberg model

$$H_{\text{eff}} = - \sum_{i \neq j} J_{ij} \mathbf{S}_i \cdot \mathbf{S}_j, \quad (3.1)$$

where \mathbf{S}_i is a localized magnetic moment at lattice point i which interacts with another localized magnetic moment at lattice point j in the system. Further, J_{ij} is the exchange integral, and $J_{ij} = J_{ji}$ so that we can limit the summation

$$H_{\text{eff}} = - 2 \sum_{i < j} J_{ij} \mathbf{S}_i \cdot \mathbf{S}_j. \quad (3.2)$$

As mentioned above, the physical origin of J_{ij} will be discussed in next chapter. For $J_{ij} > 0$, the Heisenberg model describes ferromagnetism. The localized spins then prefer to align themselves with their neighbors. The Heisenberg model is, however, able to also describe different magnetic states. If one e.g. takes $J_{ij} < 0$, neighboring spins, which typically interact the strongest, will prefer to anti-align, potentially giving rise to antiferromagnetism. Focusing on ferromagnetism, we perform a mean-field treatment of the Heisenberg Hamiltonian, producing

$$H_{\text{eff}}^{\text{MF}} = - 2 \sum_{i < j} J_{ij} (\langle \mathbf{S}_i \rangle \cdot \mathbf{S}_j + \langle \mathbf{S}_j \rangle \cdot \mathbf{S}_i - \langle \mathbf{S}_i \rangle \cdot \langle \mathbf{S}_j \rangle), \quad (3.3)$$

describing individual localized spins interacting with a background field set up by the localized spins themselves. This background field is similar to the background field assumed by Weiss, giving rise to magnetization within a domain.

In metallic ferromagnets, such as Iron (Fe) and Cobalt (Co), the magnetization can originate with the itinerant electrons through e.g. the Stoner mechanism. An effective model for metallic ferromagnetism can, however, be achieved through a Heisenberg Hamiltonian involving exchange interaction between electron spins, similar to the insulating case. Once again,

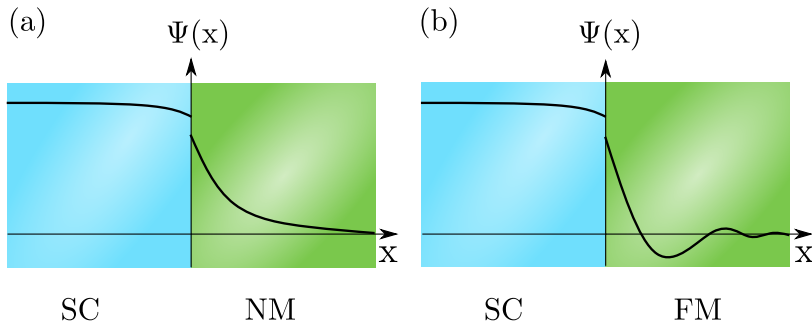


Figure 3.3: Superconductor located next to (a) normal metal and (b) ferromagnet, the solid line in both figures represent the spatial dependence of the superconducting pair correlations.

performing a mean-field treatment then leads to itinerant electrons interacting with a background field

$$H_{\text{eff}}^{\text{MF}} = \sum_{i\alpha\beta} (\mathbf{h}_i \cdot \boldsymbol{\sigma})_{\alpha\beta} c_{i\alpha}^\dagger c_{i\beta}, \quad (3.4)$$

giving rise to a magnetization in the system. The background field h is here proportional to the magnetization of the electrons. The strength of the background field can be taken as an input parameter to the theory or be determined self-consistently.

3.3 Proximity effect

In the previous chapter, we discussed the interesting properties of superconducting materials. In this chapter, we touch on the physics arising when another material is brought into contact with a superconductor, allowing the two materials to affect each other. A simple example of such a hybrid structure is a superconductor-normal metal (SC/N) bilayer. In such a system, some superconducting pair correlations will leak into the normal metal. This is often referred to as the *proximity effect*. As the normal metal does not support superconducting pair correlations, the amplitude of the correlations leaking into the normal metal decays with the distance from the interface, as displayed in Fig. 3.3 (a). In case of a clean normal metal, the decay length of the pair correlations is $\xi_T \sim v_F/T$ [79], where v_F is the

Fermi-velocity and T is temperature. As a result of the leaking across the interface, the superconducting gap and T_c on the superconductor side are reduced close to the interface. This is called the *inverse proximity effect*.

In a superconductor-ferromagnet (SC/FM) bilayer, the amplitude of the pair correlations leaking into the ferromagnet is damped, as was the case for the normal metal. However, there is also an additional oscillatory behavior, as displayed in Fig. 3.3 (b). A simple intuitive picture explaining the origin of these oscillations is provided by Demler *et al.* [80]. Consider an s -wave superconductor in proximity with a metallic ferromagnet. The electrons forming a Cooper pair have opposite spins, making the singlet state $\langle \uparrow\downarrow - \downarrow\uparrow \rangle$. We consider a Cooper pair where the spin up electron has momentum \mathbf{k} and the spin down electron has momentum $-\mathbf{k}$. When entering the ferromagnet, we assume that the energies of the electrons are conserved while the momenta normal to the interface are not. Due to the magnetization of the ferromagnet, the potential energy of the spin up electron is lowered by h , while the potential energy of the spin down electron is increased by h . In order to conserve its energy, the momentum of the spin up electron is shifted $\mathbf{k} \rightarrow \mathbf{k} + \mathbf{q}$, leading to an increased kinetic energy. Similarly, the spin down electron has its momentum shifted $-\mathbf{k} + \mathbf{q}$, lowering its kinetic energy. Inside the ferromagnet, we then have a pair correlation with center of mass momentum $2\mathbf{q} \sim 2h/v_F$. If we exchange the spins of the electrons, we instead end up with correlations with center of mass momentum $2\mathbf{q} \sim -2h/v_F$. Finite-momentum pairing is well known to give rise to spatial modulation of the amplitude of the pairing correlations [81, 82], which gives rise to the oscillations in Fig. 3.3 (b). In order to see how finite momentum Cooper pairing gives rise to spatial modulation of the pair correlations, we consider

$$\langle c_{i,\uparrow} c_{i,\downarrow} \rangle = \frac{1}{N} \int d\mathbf{k}' d\mathbf{k}'' \langle c_{\mathbf{k}',\uparrow} c_{\mathbf{k}'',\downarrow} \rangle e^{i\mathbf{k}' \cdot \mathbf{r}_i} e^{i\mathbf{k}'' \cdot \mathbf{r}_i}. \quad (3.5)$$

Normally, $\langle c_{\mathbf{k}',\uparrow} c_{\mathbf{k}'',\downarrow} \rangle = \delta_{\mathbf{k}',-\mathbf{k}''} \langle c_{\mathbf{k}',\uparrow} c_{\mathbf{k}'',\downarrow} \rangle$, leading to a cancellation of the spatial dependence on the right-hand-side of the equation. In order to consider finite-momentum pairing, we instead take $\langle c_{\mathbf{k}',\uparrow} c_{\mathbf{k}'',\downarrow} \rangle = \langle c_{\mathbf{k}+\mathbf{p},\uparrow} c_{-\mathbf{k}+\mathbf{p},\downarrow} \rangle$, where we e.g. consider pairing correlations for specific momenta $\mathbf{p} = \pm\mathbf{q}$, leading to $\delta_{\mathbf{p},\pm\mathbf{q}} \langle c_{\mathbf{k}+\mathbf{p},\uparrow} c_{-\mathbf{k}+\mathbf{p},\downarrow} \rangle$. We then obtain

$$\begin{aligned}
\langle c_{i,\uparrow} c_{i,\downarrow} \rangle &= \frac{1}{N} \int d\mathbf{k} d\mathbf{p} \delta_{\mathbf{p},\pm\mathbf{q}} \langle c_{\mathbf{k}+\mathbf{p},\uparrow} c_{-\mathbf{k}+\mathbf{p},\downarrow} \rangle e^{i(\mathbf{k}+\mathbf{p})\cdot\mathbf{r}_i} e^{i(-\mathbf{k}+\mathbf{p})\cdot\mathbf{r}_i} \\
&= \frac{1}{N} \int d\mathbf{k} \left(\langle c_{\mathbf{k}+\mathbf{q},\uparrow} c_{-\mathbf{k}+\mathbf{q},\downarrow} \rangle e^{i(\mathbf{k}+\mathbf{q})\cdot\mathbf{r}_i} e^{i(-\mathbf{k}+\mathbf{q})\cdot\mathbf{r}_i} \right. \\
&\quad \left. \langle c_{\mathbf{k}-\mathbf{q},\uparrow} c_{-\mathbf{k}-\mathbf{q},\downarrow} \rangle e^{i(\mathbf{k}-\mathbf{q})\cdot\mathbf{r}_i} e^{i(-\mathbf{k}-\mathbf{q})\cdot\mathbf{r}_i} \right). \tag{3.6}
\end{aligned}$$

Assuming e.g. that $\langle c_{\mathbf{k}+\mathbf{q},\uparrow} c_{-\mathbf{k}+\mathbf{q},\downarrow} \rangle = \langle c_{\mathbf{k}-\mathbf{q},\uparrow} c_{-\mathbf{k}-\mathbf{q},\downarrow} \rangle$, we then obtain

$$\langle c_{i,\uparrow} c_{i,\downarrow} \rangle = \frac{2 \cos(2\mathbf{q} \cdot \mathbf{r}_i)}{N} \int d\mathbf{k} \langle c_{\mathbf{k}+\mathbf{q},\uparrow} c_{-\mathbf{k}+\mathbf{q},\downarrow} \rangle. \tag{3.7}$$

We then see that the pair correlations have a periodic spatial dependence determined by the center of mass momentum $2\mathbf{q}$.

3.4 Spin-split superconductor

It is in thin-film superconductors possible to induce a uniform spin-splitting of the single-particle states. Such superconductors are referred to as spin-split superconductors. Further, the spin-splitting can be induced through proximity to a ferromagnet, as a result of the exchange interaction between the spins of the quasiparticles and the spins in the ferromagnet [83], which can give rise to a homogeneous spin-splitting for superconducting thin-films with thickness smaller than the superconducting coherence length. The spin-splitting field induced by coupling to a ferromagnetic insulator can then be expressed as $h \approx J m \frac{a}{d_S}$ [23]. Here J is the strength of the coupling between itinerant electrons in the superconductor and magnetic moments in the ferromagnet, d_S is the thickness of the superconducting thin-film, a is the lattice constant inside the superconductor, and $m = \langle S_i \rangle$ is the magnetization of the lattice site spins in the ferromagnet. A potential benefit of using a ferromagnetic insulator rather than a metallic one is that in the latter case Cooper pairs will not be able to leak into the ferromagnet, avoiding the associated modification of the superconducting gap close to the interface. Similarly, the induced spin-splitting can also be introduced through an external magnetic field.

Normally, an external magnetic field (or a stray field arising from a neighboring ferromagnet) would give rise to orbital motion in the superconductor, attempting to screen the magnetic field. Although the screening

will be weak when the superconductor is much thinner than the penetration depth, such orbital effects can still cause superconductivity to break down if the field becomes too large. However, if the field is directed in-plane, it will typically not be able to induce orbital motion [83]. The only effect on the superconductor is then the induced spin-splitting, which also becomes the factor that determines the critical magnetic field the superconductor can coexist with. Starting from our description of a spin-singlet superconductor from chapter 2, taking into account the effect of spin-splitting, we then obtain the Hamiltonian

$$H_0 = \frac{1}{2} \sum_{\mathbf{k}, \alpha} \begin{pmatrix} c_{\mathbf{k}, \alpha}^\dagger & c_{-\mathbf{k}, -\alpha} \end{pmatrix} \begin{pmatrix} \varepsilon_{\mathbf{k}} - \alpha h & -\alpha \Delta \\ -\alpha \Delta & -\varepsilon_{\mathbf{k}} - \alpha h \end{pmatrix} \begin{pmatrix} c_{\mathbf{k}, \alpha} \\ c_{-\mathbf{k}, -\alpha}^\dagger \end{pmatrix} - \frac{|\Delta|^2}{V} + \sum_{\mathbf{k}} \varepsilon_{\mathbf{k}}. \quad (3.8)$$

where h is the induced homogeneous spin-splitting field inside the superconductor. Performing the usual Bogoliubov transformation Eq. 2.14, the diagonalized form of the Hamiltonian is

$$H_0 = -\frac{|\Delta|^2}{V} + \sum_{\mathbf{k}} \varepsilon_{\mathbf{k}} - \sum_{\mathbf{k}} E_{\mathbf{k}} + \sum_{\mathbf{k}, \alpha} E_{\mathbf{k}, \alpha} \gamma_{\mathbf{k}, \alpha}^\dagger \gamma_{\mathbf{k}, \alpha}. \quad (3.9)$$

The quasiparticle energies are now $E_{\mathbf{k}, \alpha} = E_{\mathbf{k}} - \alpha h$ with $E_{\mathbf{k}} = \sqrt{\varepsilon_{\mathbf{k}}^2 + \Delta^2}$, showing a spin-splitting of the quasiparticle states. This splitting leads to a modification of the self-consistent equation for the superconducting gap

$$1 = -\frac{V}{2} \sum_{\mathbf{k}} \frac{1}{2} \frac{1}{\sqrt{\varepsilon_{\mathbf{k}}^2 + \Delta^2}} \left[\tanh\left(\frac{\beta}{2} (\sqrt{\varepsilon_{\mathbf{k}}^2 + \Delta^2} - h)\right) + \tanh\left(\frac{\beta}{2} (\sqrt{\varepsilon_{\mathbf{k}}^2 + \Delta^2} + h)\right) \right]. \quad (3.10)$$

3.5 Chandrasekhar-Clogston limit

As we introduced in the previous section, in the absence of orbital effects, spin-splitting effects determine the critical magnetic field that a superconductor can coexist with. For a spin-singlet superconductor, in the absence of spin-orbit coupling and spin-flip scattering [83], the critical magnetic field

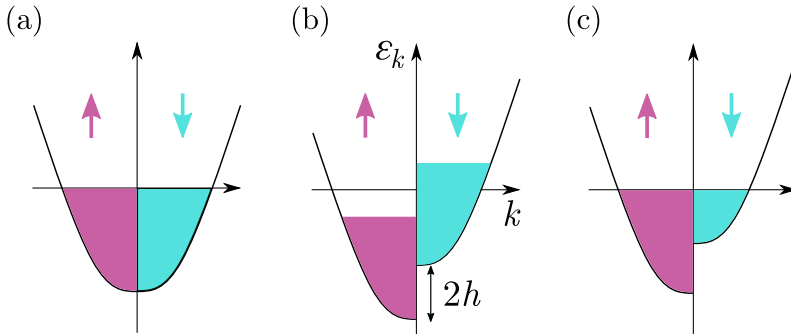


Figure 3.4: Single-band model for a normal metal (a) in the absence of spin-splitting, and (b) immediately after a spin-splitting field h is applied to the system. The spin degeneracy of the bands is then broken. (c) Spin down electrons are then converted into spin up electrons via relaxation mechanisms, spin-polarizing the system and lowering the energy.

is given by the so-called Chandrasekhar-Clogston limit [84, 85]. This limit is derived by considering how the free energy (which, at zero temperature, is simply the energy of the system) of the normal and superconducting state varies with a spin-splitting field. A detailed derivation can be found in Appendix D.

We begin by considering how the free energy of the normal state is affected by a spin-splitting field. Starting from the free energy of the superconducting state and setting $\Delta = 0$, the free energy of the normal state can be expressed as

$$F^N = \sum_{\mathbf{k}} (\varepsilon_{\mathbf{k}} - |\varepsilon_{\mathbf{k}}|) - \frac{1}{\beta} \sum_{\mathbf{k}, \alpha} \ln(1 + e^{-\beta(|\varepsilon_{\mathbf{k}}| - \alpha h)}). \quad (3.11)$$

In the absence of a spin-splitting field, the two spin-bands are degenerate, as illustrated in Fig. 3.4 (a). In the presence of a spin-splitting field, the states in the spin up band are e.g. shifted down in energy, while the states in the spin down band are shifted up. As displayed in Fig. 3.4 (b), this leads to some occupied states being shifted above the Fermi level, while some unoccupied states are shifted below the Fermi level. Redistributing themselves, spin down electrons are then flipped into spin up electrons in order to fill the states below the Fermi level. The system then becomes

spin-polarized and lowers its energy, which can be seen from Fig. 3.4 (c). The magnitude of the change in free energy at zero temperature is then, as detailed in Appendix D,

$$F^N(h=0) - F^N(h \neq 0) = N_0 h^2. \quad (3.12)$$

Reinstating $\Delta \neq 0$, the free energy of the superconducting state is

$$F^S = N \frac{\Delta^2}{V} + \sum_{\mathbf{k}} (\varepsilon_{\mathbf{k}} - E_{\mathbf{k}}) - \frac{1}{\beta} \sum_{\mathbf{k}, \alpha} \ln(1 + e^{-\beta E_{\mathbf{k}, \alpha}}). \quad (3.13)$$

At zero temperature, this expression is not affected by a spin-splitting field smaller than the superconducting gap. No states are shifted above the Fermi level and the energy gain of the occupied spin up states is therefore compensated by the increased cost of the occupied spin down states.

At zero field, still working at zero temperature, the free energy of the superconducting state is lower than the free energy of the normal state by an amount referred to as the condensation energy $F^N(h=0) - F^S(h=0) = N_0 \Delta_0^2/2$, as outlined in the Appendix D. Here, Δ_0 is the superconducting gap at zero field and temperature. As the normal state free energy is lowered in the presence of a spin-splitting field, the system will eventually transition to the normal state when the spin-splitting field is increased. At the transition point, the free energy of the normal state is equal to the free energy of the superconducting state, $F^N(h \neq 0) = F^S(h \neq 0)$. As the free energy of the superconducting state typically is not affected by the spin-splitting field, we can instead write $F^N(h \neq 0) = F^S(h=0)$. Subtracting the zero field free energy of the normal state on both sides of the equation, we then obtain

$$F^N(h=0) - F^N(h \neq 0) = F^N(h=0) - F^S(h=0). \quad (3.14)$$

This means that when the transition to normal state happens, the paramagnetic energy gain in the normal state is equal to the superconducting condensation energy, i.e. when

$$N_0 h_c^2 = N_0 \frac{\Delta_0^2}{2}. \quad (3.15)$$

We then directly obtain the Chandrasekhar-Clogston limit, restricting the spin-splitting field that the superconductor can coexist with

$$h_c = \frac{\Delta_0}{\sqrt{2}}. \quad (3.16)$$

In the above calculation, we see that the density of states at the Fermi level enters on both sides of the final equation. In fermionic systems, especially at low temperatures, it is indeed the case that much of the physics is dominated by the particles that are close to the Fermi level and that the density of states often varies little in the relevant region. There do, however, exist systems featuring significant variations in the density of states around the Fermi level. For such systems, the above derivation of the critical spin-splitting field does not apply. One could therefore wonder if it is then possible to go beyond the Chandrasekhar-Clogston limit. An example of systems that could feature rapid variations in the electronic density of states around the Fermi level is multi-band systems containing so-called flat-bands, i.e. energy bands with little or no dispersion. In the following, we give a brief introduction to such flat-band systems, as well as the topic of flat-band superconductivity, before we discuss whether it could be possible to go beyond the Chandrasekhar-Clogston limit in flat-band superconductors.

3.6 Flat-band systems

As explained above, flat-band systems are systems containing one or more energy bands with little or no dispersion, meaning that these energy spectra have little or no dependence on momentum. Theoretical studies of flat-band systems goes back to the 1980s. Sutherland, in 1986, presented a model featuring localized states with zero-energy [86]. The system he considered was a bipartite lattice, consisting of two sublattices, known as the Dice lattice. Later, in 1989, Lieb was investigating the magnetic ground state of the Hubbard model for both attractive and repulsive interaction. For certain bipartite lattices hosting flat-bands, now known as Lieb lattices, he found that the repulsive Hubbard model could give rise to a net magnetization at half-filling [87]. Since then, flat-band ferromagnetism in multi-band systems has been further investigated [88–91]. Lately, the possibility of instead realizing superconductivity in such multi-band systems featuring flat-bands has attracted much attention.

As mentioned earlier, increasing the density of states at the Fermi level can be a way to enhance the critical temperature of a superconductor, making flat-band systems interesting from the perspective of superconductivity. Theoretical studies have found that the dependence of the critical temperature on the interaction strength in such systems can be linear [92, 93], rather than the typical exponential behavior resulting from normal BCS theory. A breakthrough for flat-band superconductivity came with the discovery of superconductivity in twisted bilayer graphene. Twisted bilayer graphene consists of two graphene layers which are grown on top of each other with a relative twist angle. For certain twist angles, referred to as magic angles, the band structure of the system features flat-bands giving rise to a strongly peaked density of states [94]. In this material, at certain doping levels, it was discovered that superconductivity can be realized up to a temperature of $T_c = 1.7\text{ K}$ [95]. Although the critical temperature is not that impressive, the discovery has received much attention due to the combination of the strongly correlated nature and tunability of the system. Due to these properties, twisted bilayer graphene, as well as similar systems, might e.g. be able to shed some light on the physics of high- T_c superconductors.

3.7 Going beyond the Chandrasekhar-Clogston limit

Motivated by the above discussion of the Chandrasekhar-Clogston limit and systems with rapidly varying density of states around the Fermi level, we consider a simple model for such a system. Our model contains a dispersive band crossing the Fermi level and a flat-band that is located μ_0 below the Fermi level. The superconductivity in this system is assumed to originate from an attractive interaction on the form $c_{i,\mathbf{k},\uparrow}^\dagger c_{i,-\mathbf{k},\downarrow}^\dagger c_{j,-\mathbf{k}',\downarrow} c_{j,\mathbf{k}',\uparrow}$, where i and j are band-indices, allowing for intraband and interband scattering [92, 96]. We assume that the interaction is active in a thin shell $2\hbar\omega_c$ around the Fermi level. Therefore, in order for the flat band to contribute to the pairing we need $\mu_0 < \hbar\omega_c$.

Performing the usual mean-field approach leads to two coupled gap equations

$$\Delta_i(\mathbf{k}) = \frac{1}{N} \sum_{j,\mathbf{k}'} V_{ij}(\mathbf{k}, \mathbf{k}') \frac{\Delta_j(\mathbf{k}')}{2E_{j,\mathbf{k}'}} \times \frac{1}{2} \left[\tanh\left(\frac{\beta}{2} E_{j,\mathbf{k}',\uparrow}\right) + \tanh\left(\frac{\beta}{2} E_{j,\mathbf{k}',\downarrow}\right) \right], \quad (3.17)$$

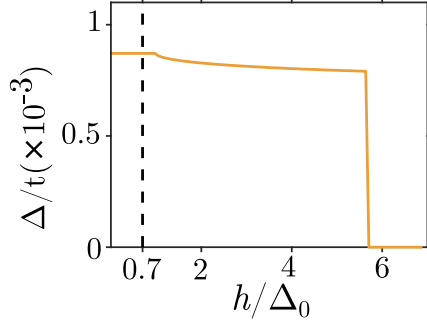


Figure 3.5: Example of superconducting gap as a function of spin-splitting field for our model system featuring both a dispersive and a flat band. It has been checked that the superconducting state minimizes the free energy for $\Delta \neq 0$.

for the order parameters associated with the two bands. Here $E_{i,\mathbf{k},\alpha} = E_{i,\mathbf{k}'} - \alpha h$ is the quasiparticle energy for band i in the presence of a spin-splitting field h . For simplicity, we here consider the interaction strength to be independent of the band-indices. The more general case is discussed in paper [4] contained in this thesis. The gaps associated with the two bands then become equal such that we are left with a single self-consistent equation for the gap $\Delta = \Delta_1 = \Delta_2$,

$$\Delta = \frac{1}{N} \sum_{j,\mathbf{k}'}^{|\varepsilon_{j,\mathbf{k}'}| \leq \hbar\omega_c} V \frac{\Delta}{2E_{j,\mathbf{k}'}} \times \frac{1}{2} \left[\tanh\left(\frac{\beta}{2} E_{j,\mathbf{k}',\uparrow}\right) + \tanh\left(\frac{\beta}{2} E_{j,\mathbf{k}',\downarrow}\right) \right], \quad (3.18)$$

where we have assumed that the interaction strength is constant within the thin shell around the Fermi level.

As we are dealing with a spin-split superconductor, it is not enough to find a nontrivial solution to the gap equation in order to conclude that the system is in a superconducting state. We also have to check that the superconducting state has lowered free energy than the normal state. The free energy is expressed as

$$F = \frac{1}{4} \sum_{i,\mathbf{k},\alpha} \frac{\Delta_i^2(\mathbf{k})}{E_{i,\mathbf{k}}} \tanh\left(\frac{\beta}{2} E_{i,\mathbf{k},\alpha}\right) + \sum_{i,\mathbf{k}} (\varepsilon_{i,\mathbf{k}} - E_{i,\mathbf{k}}) - \frac{1}{\beta} \sum_{i,\mathbf{k},\alpha} \ln(1 + e^{-\beta E_{i,\mathbf{k},\alpha}}). \quad (3.19)$$

Solving the gap equation and setting the gap to the value that minimizes the free energy, we obtain the curve in Fig. 3.5 for a given set of parameters. This figure shows that superconductivity in this case can coexist with a spin-splitting field considerably larger than the critical field arising from the Chandrasekhar-Clogston limit $h_c/\Delta_0 \approx 0.7$. This result can be understood from the above equations. From Eq. (3.18), we see that when $h < \Delta$ and the temperature is zero, the contributions from both the dispersive band and the flat-band are unaffected by the spin-splitting field as still $\tanh\left(\frac{\beta}{2}E_{j,\mathbf{k}',\alpha}\right) \rightarrow 1$. However, as soon as $h > \Delta$, some contributions from the dispersive band are lost as the two tanh terms cancel each other. The first contributions that are lost are the most important contributions where $\varepsilon_{\mathbf{k}} \rightarrow 0$, allowing the spin-splitting field to change the sign of the spin-up quasiparticle energy. This effect causes the decrease in the gap with respect to spin-splitting field which is observed in Fig. 3.4 when the strength of the spin-splitting field surpasses Δ_0 . On the other hand, the contributions from the flat-band are robust towards spin-splitting fields smaller than μ_0 . The flat-band can then guarantee a nontrivial solution to the gap equation for $h < \mu_0$, as long as V is sufficiently large. For $\mu_0 > \Delta_0$, solutions to the gap equation can then be obtained for $h > \Delta_0$.

As mentioned above, it is not sufficient to have a nontrivial solution to the gap equation, the superconducting state must also minimize the free energy. Inspecting the free energy in Eq. (3.19), the term $\varepsilon_{i,\mathbf{k}}$ is the same for the superconducting and normal state. The combination of the first term and the term $-E_{i,\mathbf{k}}$ decreases with increasing magnitude of the superconducting gap, giving rise to the condensation energy which favors the superconducting state at zero field. Importantly, the flat-band contributes significantly to the condensation energy due to its large density of states close to the Fermi level. Inspecting the free energy in Eq. (3.19), the term $\varepsilon_{i,\mathbf{k}}$ is the same for the superconducting and normal state. The combination of the first term and the term $-E_{i,\mathbf{k}}$ decreases with increasing magnitude of the superconducting gap, giving rise to the condensation energy which favors the superconducting state at zero field. Importantly, the flat-band contributes significantly to the condensation energy due to its large density of states close to the Fermi level. In the presence of a spin-splitting field, the quasiparticle energies in the last logarithmic term can, for the normal state, turn negative, lowering the free energy of the normal state. This does, however, only apply to the quasiparticle energies associated with the dispersive band as long as $h < \mu_0$. For $h < \mu_0$, the presence of the flat-band there-

fore only increases the condensation energy without affecting how much the normal state lowers its free energy. Superconductivity can therefore survive beyond the Chandrasekhar-Clogston limit.

Above, we have introduced a general mechanism for how spin-singlet superconductivity can survive beyond the Chandrasekhar-Clogston limit. Future studies should attempt to identify real systems where this mechanism can be realized by performing more detailed calculations. Possible candidates for real systems are twisted multi-layered materials or artificial electronic lattice systems realizing some specific lattice model giving rise to a suitable band structure.

Magnetic impurities and interaction between them

Two spins located close to each other can constitute an interacting spin system. Even if the direct interaction between the two spins is negligible, the spins can interact indirectly if they are part of a bigger system that can mediate interaction between them. In this chapter, we discuss different types of interactions between localized spins, ending with a discussion of RKKY interaction mediated by itinerant particles. We then consider the RKKY interaction between localized spins in a spin-split superconductor and introduce a potential experimental method for measurement of RKKY interaction in such a system.

4.1 Origin of exchange interaction

In the previous chapter, we explained that ferromagnetism can originate with the exchange interaction between localized or itinerant spins. In this section, we will further discuss the origin of exchange interaction between localized spins.

The Hamiltonian we introduced in Eq. (3.1) as the effective Heisenberg Hamiltonian is actually the generalized form of the first two-spin Hamiltonian that Heisenberg presented for the hydrogen molecule, H_2 , in 1928 [78]. We consider the two electrons in the Hydrogen molecule to be identical particles, having \mathbf{r}_1 and \mathbf{r}_2 as their spatial coordinates. They further have spins $s_1 = \frac{1}{2}$ and $s_2 = \frac{1}{2}$. The total wave function of this fermionic two-spin system should be antisymmetric under exchange of the two particles. This wave function consists of a spatial part and a spin part. If the electron spins form a spin-singlet state with $s = 0$, which is odd under exchange of the particles, the spatial part should be symmetric. On the other hand, if the spins are in the spin-triplet state with total spin $s = 1$, the spatial part

needs to be antisymmetric. We therefore express the wave function for the singlet and triplet state as

$$\Psi_S = \frac{|\uparrow\downarrow\rangle - |\downarrow\uparrow\rangle}{\sqrt{2}} \times \frac{\phi_1(\mathbf{r}_1)\phi_2(\mathbf{r}_2) + \phi_1(\mathbf{r}_2)\phi_2(\mathbf{r}_1)}{\sqrt{2}}, \quad (4.1)$$

and

$$\Psi_T = \chi_T \times \frac{\phi_1(\mathbf{r}_1)\phi_2(\mathbf{r}_2) - \phi_1(\mathbf{r}_2)\phi_2(\mathbf{r}_1)}{\sqrt{2}}, \quad (4.2)$$

where

$$\chi_T = \begin{cases} |\uparrow\uparrow\rangle, \\ \frac{|\uparrow\downarrow\rangle + |\downarrow\uparrow\rangle}{\sqrt{2}}, \\ |\downarrow\downarrow\rangle. \end{cases} \quad (4.3)$$

We further express the energy of the singlet state as

$$E_S = \int d\mathbf{r}_1 d\mathbf{r}_2 \Psi_S^* H_{12} \Psi_S, \quad (4.4)$$

where H_{12} is the Hamiltonian of the two-electron system, including e.g. Coulomb repulsion. This Hamiltonian is assumed to not depend explicitly on the spins of the electrons. Due to the requirement that the wave function needs to be antisymmetric under exchange of particles, we will however see that the energy of the system still ends up depending on the spin-state. Further, the energy of the triplet state is

$$E_T = \int d\mathbf{r}_1 d\mathbf{r}_2 \Psi_T^* H_{12} \Psi_T. \quad (4.5)$$

As the Hamiltonian does not care about the spin-state of the system, the difference between the energies of the singlet and triplet states only depends on the spatial part of the wave function. Using that the Hamiltonian is Hermitian, $H_{12}^\dagger = H_{12}$, the energy difference is obtained from

$$E_S - E_T = 2 \int d\mathbf{r}_1 d\mathbf{r}_2 \phi_1(\mathbf{r}_1)^* \phi_2(\mathbf{r}_2)^* H_{12} \phi_1(\mathbf{r}_2) \phi_2(\mathbf{r}_1). \quad (4.6)$$

We can then use this expression to obtain an effective Hamiltonian expressing the energy of the system in terms of the product of the two spin operators $\mathbf{s}_1 \cdot \mathbf{s}_2$. To do this, we use that $\mathbf{s}_{\text{tot}} = \mathbf{s}_1 + \mathbf{s}_2$, leading to

$$(\mathbf{s}_{\text{tot}})^2 = (\mathbf{s}_1)^2 + (\mathbf{s}_2)^2 + 2\mathbf{s}_1 \cdot \mathbf{s}_2. \quad (4.7)$$

The eigenvalue of \mathbf{s}_{tot} is $s(s+1)$, which is 0 for the spin-singlet state and 2 for spin-triplet state. Further, the eigenvalue of $(\mathbf{s}_i)^2$ is $s_i(s_i+1) = \frac{3}{4}$ for the case of spin- $\frac{1}{2}$. We then obtain that $\mathbf{s}_1 \cdot \mathbf{s}_2 = -\frac{3}{4}$ for the spin-singlet case, and that $\mathbf{s}_1 \cdot \mathbf{s}_2 = \frac{1}{4}$ for the spin-triplet case. We can then introduce an effective Hamiltonian

$$H_{\text{eff}} = \frac{1}{4}(E_S + E_T) - (E_S - E_T)\mathbf{s}_1 \cdot \mathbf{s}_2, \quad (4.8)$$

expressing the energy of the system in the spin-singlet and spin-triplet case. From above, we already have the expression for $E_S - E_T$, while the first term is just a constant term. The exchange integral that we discussed in the previous chapter can then be obtained from

$$J_{12} = \frac{E_S - E_T}{2} = \int d\mathbf{r}_1 d\mathbf{r}_2 \phi_1(\mathbf{r}_1)^* \phi_2(\mathbf{r}_2)^* H_{12} \phi_1(\mathbf{r}_2) \phi_2(\mathbf{r}_1). \quad (4.9)$$

4.2 Indirect exchange interaction

What we have have discussed above for a hydrogen molecule is a direct exchange interaction between the spins of the two electrons associated with the two hydrogen atoms in the hydrogen molecule. In general, exchange interaction can also take place between two spins via a third component which mediates the interaction between them. This type of exchange interaction is called an indirect exchange interaction. Three types of indirect exchange interaction are superexchange, double exchange, and RKKY exchange interaction.

If the interaction between two magnetic ions is mediated by an intermediate non-magnetic ion, the interaction is referred to as a superexchange interaction. A famous example of a material featuring this type of interaction is Manganese oxide (MnO) which is a magnetic insulator. Existence of superexchange interaction in MnO crystals was first proposed by Kramer

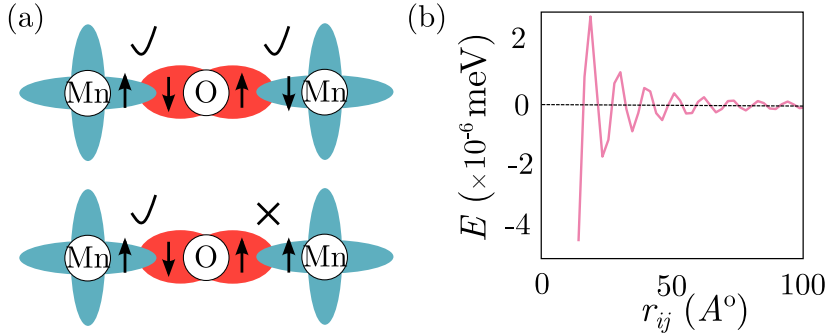


Figure 4.1: (a) An O^{2-} ion sandwiched between two Mn^{2+} ions. Two $2p$ -orbital electrons associated with the O^{2-} ion that can potentially hop to the neighboring Mn^{2+} ions are displayed. In order for such hopping processes to be possible, there needs to be suitable unoccupied $3d$ -orbital states associated with the Mn^{2+} ions. For the configuration in the upper half of the figure, hopping is possible in both directions, while for the configuration in the lower half, hopping is only possible in one direction. (b) The RKKY energy coefficient $E = J(r_{ij})$ of Eq. (4.13), expressing the interaction between two localized magnetic impurities mediated by the itinerant electrons of a normal metal, as a function of the distance between the impurity spins. The results are presented for some set of parameters used in the third paper included in this thesis [3].

in 1934 [97], and later expanded on in 1950 by Anderson [98]. In MnO , the magnetic ions are Mn^{2+} and the non-magnetic ions are O^{2-} . An interaction takes place between the spins associated with the $3d$ -orbital of Mn^{2+} and the spin associated with the $2p$ -orbital of O^{2-} . Here, four electrons take part in the interaction, two from O^{2-} and one from each Mn^{2+} ion. Depending on the filling of the orbitals, as well as spatial location of the Mn^{2+} ions, the interaction between the spins associated with the two Mn^{2+} ions can prefer alignment or anti-alignment of the spins.

We can e.g. consider two Mn^{2+} ions located on opposite sides of a O^{2-} ion (forming a 180° angle). The system can lower its kinetic energy by allowing the $2p$ electrons of the O^{2-} ion to hop to the neighboring Mn^{2+} ions. However, for this to be possible, the $3d$ -orbital electrons of the magnetic ions need to be in a suitable configuration. For hopping to our two considered Mn^{2+} ions, there will be two relevant $2p$ electrons with opposite spins.

If there then e.g. are $3d$ electrons with parallel spins on the two sides of the O^{2-} ion, only one of the $2p$ electrons will be able to hop over to the neighboring ions due to the Pauli principle. An anti-alignment of the two $3d$ electrons will therefore be favored. This is illustrated in Fig. 4.1 (a). One can similarly also discuss interaction between two Mn^{2+} ions that form a 90° angle with the neighboring O^{2-} ion, rather than a 180° angle, as well as different filling of the $3d$ -orbitals. The overall conclusion is then that this type of superexchange interaction gives rise to antiferromagnetism in MnO .

During the above process no charge transfer happens as the Mn^{2+} ions all have the same number of electrons. The double exchange interaction is another type of indirect exchange interaction which can take place when the two magnetic ions that interact with each other via a non-magnetic ion do not have the same number of electrons. A transfer of charge can then take place. This type of interaction was first proposed by Zener in 1951 [99]. A famous example is $La_{1-x}Sr_xMnO_3$, which is a metallic ferromagnet. One electron from a Mn^{3+} ion can in this case hop to a Mn^{4+} ion via a O^{2-} ion if the spins of the two Mn atoms are aligned.

Indirect exchange interaction can also be mediated by conduction electrons, referred to as RKKY interaction. Below we discuss RKKY interaction in more detail as it is the subject of the third paper [3] included in this thesis.

4.3 Ruderman–Kittel–Kasuya–Yosida interaction

In 1954, Ruderman and Kittel calculated the indirect interaction between local magnetic moments, originating with nuclei in a metal mediated by itinerant electrons [100]. Later, in 1956, Kasuya performed a similar study for indirect interaction between inner shell electrons [101] which have a weak direct interaction as they are strongly localized, leading to a small overlap of their wavefunctions. In 1957, Yoshida investigated the same effect as Kasuya in $CuMn$ alloys [102]. All these studies found that two localized magnetic moments in a metal can interact with each other indirectly via spin polarizing the conduction electrons around themselves. This indirect exchange interaction is known as the RKKY interaction in honor of these four researchers. The famous characteristic of this interaction is that it, in a normal metal, exhibits a damped oscillatory behaviour as a function of the distance between the localized magnetic moments. The oscillations are caused by interference effects possible due to the dual particle-wave nature of electrons. Itinerant electrons approaching a localized magnetic

moment can scatter from it. The wave functions of the scattered electrons then interfere with each other either constructively or destructively, creating regions in the space that have higher density of spin up electrons than spin down electrons, as well as regions with higher density of spin down. This gives rise to an oscillatory pattern of electron spin density which leads to a spatial variation in the preferred direction of a second, nearby, localized spin. The resulting, spatially dependent, interaction between the localized spins is what we refer to as the RKKY interaction.

We proceed by showing how the interaction between local magnetic moments in a metal can be calculated through the Schrieffer-Wolff transformation, presented in Appendix E. A normal metal with localized magnetic moments interacting with the conduction electrons can be described through a Hamiltonian

$$H = -t \sum_{\langle i,j \rangle, \alpha} c_{i,\alpha}^\dagger c_{j,\alpha} - \mu \sum_{i,\alpha} c_{i,\alpha}^\dagger c_{i,\alpha} + J \sum_i \mathbf{S}_i \cdot \mathbf{s}_i. \quad (4.10)$$

The final term is here treated as a perturbation to a system of non-interacting electrons and lattice site spins. The lattice site spins are treated as classical spins, and their coupling strength J to the conduction electrons spins $\mathbf{s}_i = \sum_{\alpha\beta} c_{i,\alpha}^\dagger \boldsymbol{\sigma}_{\alpha,\beta} c_{i,\beta}$ is assumed to not be too strong. Performing the Fourier transformation $c_{i,\alpha} = \frac{1}{\sqrt{N}} \sum_{\mathbf{k}} e^{-i\mathbf{k}\cdot\mathbf{r}_j} c_{\mathbf{k},\alpha}$, the Hamiltonian takes the form

$$H = \sum_{\mathbf{k},\alpha} \varepsilon_{\mathbf{k}} c_{\mathbf{k},\alpha}^\dagger c_{\mathbf{k},\alpha} + \frac{J}{N} \sum_i \mathbf{S}_i \cdot \sum_{\substack{\mathbf{k},\mathbf{k}' \\ \alpha,\alpha'}} \left[\sigma_{\alpha\beta} e^{i(\mathbf{k}-\mathbf{k}')\cdot\mathbf{r}_j} c_{\mathbf{k},\alpha}^\dagger c_{\mathbf{k}',\beta} \right]. \quad (4.11)$$

We then consider the following Ansatz in the Schrieffer-Wolff transformation

$$S = \sum_{\substack{\mathbf{k},\mathbf{k}' \\ \alpha,\alpha'}} A_{\mathbf{k},\mathbf{k}'} c_{\mathbf{k},\alpha}^\dagger c_{\mathbf{k}',\alpha}. \quad (4.12)$$

Following the steps in Appendix E, we end up with an effective Hamiltonian representing the indirect interaction between localized spins. Further calculating the expectation value of this effective Hamiltonian, we obtain the RKKY energy

$$E_{\text{RKKY}} = \sum_{i,j} J(\mathbf{r}_{ij}) (\mathbf{S}_i \cdot \mathbf{S}_j), \quad (4.13)$$

where

$$J(\mathbf{r}_{ij}) = -\left(\frac{J}{N}\right)^2 \sum_{\mathbf{k}, \mathbf{k}'} \frac{e^{i(\mathbf{k}-\mathbf{k}') \cdot (\mathbf{r}_i - \mathbf{r}_j)}}{\varepsilon_{\mathbf{k}} - \varepsilon_{\mathbf{k}'}} \left(n(\varepsilon_{\mathbf{k}}) - n(\varepsilon_{\mathbf{k}'}) \right). \quad (4.14)$$

Here, $\mathbf{r}_{ij} = \mathbf{r}_i - \mathbf{r}_j$ is the distance between the two localized spins. The electron energies are even under $\mathbf{k} \rightarrow -\mathbf{k}$, making the Fermi-Dirac distribution function $n(\varepsilon_{\mathbf{k}})$ also even under inversion of momentum. Therefore, only the part of the exponential function which is even under $\mathbf{k} \rightarrow -\mathbf{k}$ and $\mathbf{k}' \rightarrow -\mathbf{k}'$ will survive in the summation. This gives rise to an oscillatory factor $\cos((\mathbf{k} - \mathbf{k}') \cdot (\mathbf{r}_i - \mathbf{r}_j))$. For large r_{ij} , this factor oscillates rapidly when the momenta are summed over, leading to the contributions to the sums cancelling out and the result becoming small. Whether the result ends up as positive or negative depends on the specific value of r_{ij} . The overall behavior of the RKKY interaction is therefore that it exhibits damped oscillations as a function of increasing distance between the localized spins as displayed in Fig 4.1 (b).

4.3.1 Collinear and non-collinear RKKY interaction

What we calculated above represents a collinear symmetric type of RKKY interaction known as Heisenberg-like RKKY interaction. Such an interaction prefers alignment or anti-alignment of the interacting spins, without any preference for alignment or anti-alignment along any specific direction. This type of interaction is usually present in systems with spin-degeneracy, where we e.g. can mention graphene [103, 104], topological insulators [105] and superconducting materials [106–109].

In a spin-polarized system, i.e. a system without spin-degeneracy, the RKKY interaction is no longer collinear symmetric, but rather what is referred to as collinear nonsymmetric. In addition to a Heisenberg term, the RKKY interaction then features an Ising term. The Ising term represents that a specific direction in spin-space is special, meaning that the interaction is no longer isotropic in spin-space. Examples of such system which have been studied in the literature is a one-dimensional spin-polarized electron gas [110] or spin-polarized graphene [111].

In systems with spin-orbit interactions, however, the RKKY interaction can become more complicated and exhibit non-collinear features [112, 113]. In this case, the RKKY interaction between localized spins has been shown

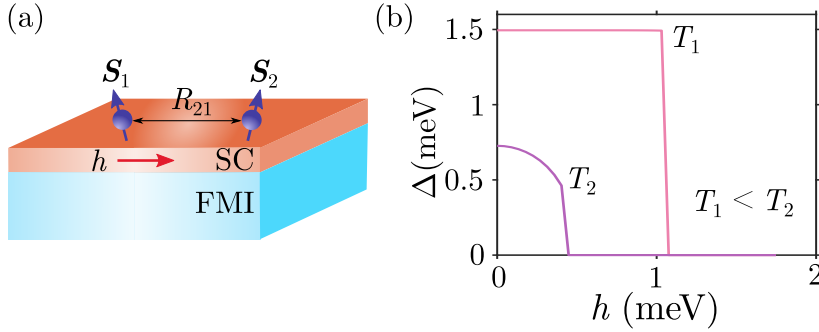


Figure 4.2: (a) A thin film superconductor is located on top of a ferromagnetic insulator (FMI). The FMI induces a homogeneous exchange field (h) inside the superconductor. Two impurity spins S_1 and S_2 in the superconductor are separated by a distance R_{21} . (b) The superconducting gap for an s -wave spin-split superconductor as a function of the spin-splitting field for two different values of the temperature.

to include Dzyaloshinskii-Moriya interaction[114, 115], which favours twisting of the localized spins away from a collinear orientation.

All in all, RKKY interaction between two localized spins, S_1 and S_2 , can typically be summarized as $\alpha_H \mathbf{S}_1 \cdot \mathbf{S}_2 + \alpha_I (S_1^i S_2^i) + \alpha_D \cdot \mathbf{S}_1 \times \mathbf{S}_2$. Where the first term is a Heisenberg term, the second one is an Ising term and the last one represents a Dzyaloshinskii-Moriya type interaction. In the following section, we will investigate the RKKY interaction between magnetic impurities in a spin-split superconductor. The relevant types of RKKY interaction will then be the Heisenberg and Ising types.

4.4 RKKY in a spin-split superconductor

In the previous chapter, we discussed how one can induce a homogeneous spin-splitting field inside a superconductor. The aim of this section is to discuss the RKKY interaction between impurity spins mediated by the quasiparticles of an s -wave spin-split superconductor, considered in paper [3]. One possible experimental realization of such a system is illustrated in Fig. 4.2 (a), where a superconductor is located on top of a ferromagnetic insulator (FMI). The tight-binding Hamiltonian describing our system consists of two terms: a non-perturbative term, and a perturbative term. The

non-perturbative part is simply the mean-field Hamiltonian in Eq. (3.8) describing a spin-split superconductor. Rather than going to the thermodynamic limit, we here consider a finite system with continuous boundary conditions in-plane. The interaction potential is taken to be constant, without any momentum-space structure, arising from a constant attractive on-site interaction. Fig. 4.2 (b) shows the solution to the gap equation that minimizes the free energy for different spin-splitting fields, as well as the temperature dependence of the curves. At low temperatures, the gap equation is barely affected by the spin-splitting field. The gap is then almost constant until the spin-splitting field approaches the Chandrasekhar-Clogston limit. At higher temperatures, closer to the critical temperature, the spin-splitting field is able to affect the gap equation, leading to a gap that more gradually decreases until it vanishes at some field value smaller than the Chandrasekhar-Clogston limit.

The perturbative part of the Hamiltonian includes the interaction between localized impurity spins, \mathbf{S}_i and the itinerant electrons inside the superconductor with spin $\mathbf{s}_i = \sum_{\alpha\beta} c_{i\alpha} \boldsymbol{\sigma}_{\alpha\beta} c_{i\beta}$ where $\boldsymbol{\sigma}$ is the Pauli matrix. The localized impurity spins are treated as classical spins. The perturbative term in the Hamiltonian takes the form

$$\Delta H = J \sum_{i=1}^2 \mathbf{S}_i \cdot \mathbf{s}_i, \quad (4.15)$$

where J is the strength of the interaction between a localized impurity spin and an itinerant electron at site i . In order to calculate the indirect interaction between one impurity spin and the other impurity spin, we perform a Schrieffer-Wolff transformation, as detailed in Appendix E. After performing this transformation, we are left with an effective interaction between impurity spins mediated by the quasiparticles in the superconductor. When the quasiparticles are affected by a spin-splitting field, this effective interaction is not isotropic in spin-space. The effective interaction has one term for the interaction between the component of the spins in the direction of the spin-splitting field, which we refer to as an Ising term with RKKY energy E_I determining whether the RKKY interaction prefers this component of the spins to be aligned or anti-aligned. The effective interaction also has a term for the plane perpendicular to the direction of the spin-splitting field, which we refer to as a Heisenberg term with RKKY energy E_H . The total RKKY energy, representing the interaction between two impurity spins, then takes the form

$$E_{\text{RKKY}} = E_0 + 2E_H(R_{21})(S_1^x S_2^x + S_1^y S_2^y) + 2E_I(R_{21})(S_1^z S_2^z). \quad (4.16)$$

Here, E_0 is a term which does not depend on the relative orientation of the two impurity spins. It contains e.g. $\sum_{\mathbf{k},\alpha} E_{\mathbf{k},\alpha} n(E_{\mathbf{k},\alpha})$, where $E_{\mathbf{k},\alpha}$ is the excitation energy of a quasiparticle affected by the spin-splitting field and $n(E_{\mathbf{k},\alpha})$ is the Fermi-Dirac distribution function. More importantly, E_0 also includes anisotropy terms of the form $E_I[(S_1^z)^2 + (S_2^z)^2]$ and $E_H[(S_1^x)^2 + (S_2^x)^2 + (S_1^y)^2 + (S_2^y)^2]$, which can influence the preferred direction of the impurity spins. Moreover, in our Schrieffer-Wolff transformation, we ignored another term which can also influence the preferred direction of the impurity spins. This term is a first-order term on the form $\langle \Delta H \rangle = \sum_i \langle \mathbf{S}_i \rangle \cdot \langle \mathbf{s}_i \rangle$ leading to a coupling between the impurity spins and the spin-splitting field. This coupling can be quite strong, dictating the preferred direction of the impurity spins. However, despite the fact that the RKKY interaction might not be the dominant effect, it will still be present in these types of systems and should therefore be understood. Measuring the RKKY interaction in such systems could also still be possible, as introduced in the next section.

4.5 Experimental realization

We here introduce a potential method that could be used in order to measure RKKY interaction between two impurity spins in a spin-polarized system. We consider the system presented in Fig. 4.2 (a), where a thin film superconductor is placed on top a ferromagnetic insulator. The ferromagnet will induce an exchange field h inside the superconductor. We consider two impurity spins (\mathbf{S}_1 and \mathbf{S}_2) in the superconductor. As discussed above, the presence of the uniform exchange field is likely to dictate the direction of the impurity spins, leading to an aligned configuration. In this case, the directionally dependent energy of the impurity spin subsystem will be the sum of the coupling between the two individual impurity spins and the background field, as well as the RKKY interaction between the two impurity spins. This energy can, assuming that the impurity spins are aligned due to the background field, be expressed as

$$E_1 = -\zeta S_1 h - \zeta S_2 h + E_{\text{RKKY}}. \quad (4.17)$$

Here, the RKKY term is then of the form $E_{\text{RKKY}} = J(R_{21})$, where R_{21} is the distance between the two impurity spins, and the spins are normalized to 1. With spins aligned with the background field we further have $J(R_{21}) = 2E_I(R_{21})$. Moreover, ζ is some constant determining the strength of the interaction between the impurities and h . Using e.g. spin-polarized scanning tunneling microscopy (STM), as discussed in [116, 117], we flip one of the spins (e.g. S_2). The impurity spin energy then becomes

$$E_2 = -\zeta S_1 h + \zeta S_2 h - J(R_{21}). \quad (4.18)$$

The first term is the same as in E_1 , but the second and third term have changed sign as the two impurity spins are now anti-aligned. The energy cost to flip S_2 , which can be related to the current that is applied through the STM-tip to provide the spin-transfer torque, is the energy difference between E_1 and E_2 . We then have that

$$E_{\text{flip}} = E_2 - E_1 = 2\zeta S_2 h - 2J(R_{21}). \quad (4.19)$$

In order to determine the RKKY interaction $J(R_{21})$, we consider an additional measurement where the impurity spins are far away from each other so that the RKKY interaction can be neglected. The spin-flip energy is in this case named E'_{flip} which is simply equal to $2\zeta S_2 h$. The strength of the RKKY interaction at a specific separation distance R_{21} can then be calculated from

$$J(R_{21}) = \frac{E'_{\text{flip}} - E_{\text{flip}}}{2}. \quad (4.20)$$

Repeating this process for different separation distances leads to knowledge of the distance dependence of the RKKY interaction.

The above outlined method should be viewed as a proof of principle, showing that it could be possible to extract information about the RKKY interaction in experiments despite the fact that the RKKY interaction is masked by interaction between the impurity spins and the background field.

Bogoliubov-de Gennes method for lattice models

The purpose of this chapter is to go through the method which has been used in the first two papers. First, the Bogoliubov-de Gennes (BdG) equations for a normal metal on a square lattice will be derived, treating the problem in real-space. We then generalize this derivation to the case of an s -wave superconductor as well as a d -wave superconductor. We end the chapter by going to momentum space and mapping out the phase diagram of the model used to describe d -wave pairing.

5.1 Normal Metal

5.1.1 Hamiltonian

We first consider a Hamiltonian describing a normal metal on a square lattice

$$H = - \sum_{\langle ij \rangle, \alpha} t_{ij} c_{i, \alpha}^\dagger c_{j, \alpha} - \sum_{i, \alpha} \mu_i c_{i, \alpha}^\dagger c_{i, \alpha}. \quad (5.1)$$

This simple Hamiltonian includes no interaction between electrons, and it can therefore be numerically diagonalized without any further treatment. We will, however, take some extra steps in the treatment of this simple Hamiltonian in order to establish a method that can also be applied in more complicated cases such as for s -wave and d -wave superconductors. We begin by introducing a basis $B_i^\dagger = (c_{i, \uparrow}^\dagger \ c_{i, \downarrow}^\dagger \ c_{i, \uparrow} \ c_{i, \downarrow})$ where $i = (i_x, i_y)$ in the xy plane of an assumed two-dimensional structure. This basis is chosen with future application to superconductivity in mind. Using this basis the Hamiltonian is rewritten as $H = H_0 + \frac{1}{2} \sum_{i, j} B_i^\dagger h_{i, j} B_j = H_0 + \frac{1}{2} W^\dagger S W$. Here,

W is a $4N$ -dimensional vector of electron operators, where $N = N_x N_y$ is the number of lattice sites in the system. Further, S is a $4N \times 4N$ -dimensional matrix which should be diagonalized. The vector W is expressed as

$$W^\dagger = \left(D_1^\dagger \cdots D_{i_y}^\dagger \cdots D_{N_y}^\dagger \right), \quad (5.2)$$

where

$$D_{i_y}^\dagger = \left(B_{1,i_y}^\dagger \cdots B_{i_x,i_y}^\dagger \cdots B_{N_x,i_y}^\dagger \right), \quad (5.3)$$

and $B_{i_x,i_y} = B_i$. Further, the matrix S is expressed as

$$S = \begin{pmatrix} S_{1,1} & \cdots & S_{1,N_y} \\ \vdots & \ddots & \vdots \\ S_{N_y,1} & \cdots & S_{N_y,N_y} \end{pmatrix}, \quad (5.4)$$

where

$$S_{i_y,j_y} = \begin{pmatrix} h_{(1,i_y),(1,j_y)} & \cdots & h_{(1,i_y),(N_x,j_y)} \\ \vdots & \ddots & \vdots \\ h_{(N_x,i_y),(1,j_y)} & \cdots & h_{(N_x,i_y),(N_x,j_y)} \end{pmatrix}. \quad (5.5)$$

Here, $h_{(i_x,i_y),(j_x,j_y)} = h_{i,j}$, which has the form

$$h_{i,j} = \begin{pmatrix} a_{i,j} & 0 & 0 & 0 \\ 0 & a_{i,j} & 0 & 0 \\ 0 & 0 & -a_{i,j} & 0 \\ 0 & 0 & 0 & -a_{i,j} \end{pmatrix}, \quad (5.6)$$

with $a_{i,j} = -\mu\delta_{i,j} - t(\delta_{i,j+1} + \delta_{i,j-1})$.

5.1.2 BdG equations

In order to diagonalize the matrix S , we introduce a unitary matrix P such that $S_d = PSP^\dagger$ becomes a diagonal matrix. Then, $H = H_0 + \frac{1}{2}W^\dagger P^\dagger PSP^\dagger \times PW = H_0 + \frac{1}{2}\tilde{W}^\dagger S_d \tilde{W}$, where S_d now contains the eigenvalues of S , i.e. the quasiparticle energies E_m with $m \in [1, 4N_x N_y]$. Further, the vector \tilde{W} is a vector which contains the quasiparticle creation and annihilation operators (γ and γ^\dagger), which are linear combinations of the original electron operators. We write out S_d and \tilde{W}^\dagger as

$$S_d = \begin{pmatrix} E_1 & \dots & 0 \\ \vdots & \ddots & \vdots \\ 0 & \dots & E_{4N_x N_y} \end{pmatrix}, \quad (5.7)$$

and

$$\tilde{W}^\dagger = \left(\gamma_1^\dagger \quad \gamma_2^\dagger \quad \gamma_3^\dagger \quad \dots \quad \gamma_{4N_x N_y}^\dagger \right). \quad (5.8)$$

In order to determine the unitary matrix P , we need the eigenstates of S which we express as

$$\Phi_m^\dagger = \left(\phi_{1,m}^\dagger \quad \dots \quad \phi_{i_y,m}^\dagger \quad \dots \quad \phi_{N_y,m}^\dagger \right), \quad (5.9)$$

where

$$\phi_{i_y,m}^\dagger = \left(\varphi_{(1,i_y),m}^\dagger \quad \dots \quad \varphi_{(i_x,i_y),m}^\dagger \quad \dots \quad \varphi_{(N_x,i_y),m}^\dagger \right), \quad (5.10)$$

and with $\varphi_{(i_x,i_y),m} = \varphi_{i,m}$, where

$$\varphi_{i,m}^\dagger = \left(v_{i,m}^* \quad \nu_{i,m}^* \quad \omega_{i,m}^* \quad \chi_{i,m}^* \right). \quad (5.11)$$

These eigenstates, together with their corresponding eigenvalues, can be obtained by numerically diagonalizing the matrix S . Then, for the matrix P , represents the transformation from normal creation and annihilation operators ($c_{i\alpha}$ and $c_{i\alpha}^\dagger$) into quasiparticle operators ($\gamma_{m\alpha}$ and $\gamma_{m\alpha}^\dagger$), we can write

$$P^\dagger = \left(\Phi_1 \quad \Phi_2 \quad \dots \quad \Phi_{4N_x N_y} \right). \quad (5.12)$$

Using that $P^\dagger \tilde{W} = W$, we further have that

$$\begin{pmatrix} \phi_{1,1} & \dots & \phi_{1,m} & \dots & \phi_{1,4N_x N_y} \\ \vdots & \ddots & \vdots & \ddots & \vdots \\ \phi_{i_y,1} & \dots & \phi_{i_y,m} & \dots & \phi_{i_y,4N_x N_y} \\ \vdots & \ddots & \vdots & \ddots & \vdots \\ \phi_{N_y,1} & \dots & \phi_{N_y,m} & \dots & \phi_{N_y,4N_x N_y} \end{pmatrix} \tilde{W} = \begin{pmatrix} D_1 \\ \vdots \\ D_{i_y} \\ \vdots \\ D_{N_y} \end{pmatrix}. \quad (5.13)$$

From this equation, the original creation and annihilation operators can be written in terms of quasiparticle operators as

$$\begin{aligned}
c_{i\uparrow} &= \sum_{m=1}^{4N_x N_y} v_{i,m} \gamma_m, & c_{i\downarrow} &= \sum_{m=1}^{4N_x N_y} \nu_{i,m} \gamma_m, \\
c_{i\uparrow}^\dagger &= \sum_{m=1}^{4N_x N_y} \omega_{i,m} \gamma_m, & c_{i\downarrow}^\dagger &= \sum_{m=1}^{4N_x N_y} \chi_{i,m} \gamma_m.
\end{aligned} \tag{5.14}$$

By means of $\tilde{W} = PW$, the reverse relation between the c (c^\dagger) operators and γ (γ^\dagger) is

$$\gamma_m = \sum_i v_{i,m}^* c_{i,\uparrow} + \nu_{i,m}^* c_{i,\downarrow} + \omega_{i,m}^* c_{i,\uparrow}^\dagger + \chi_{i,m}^* c_{i,\downarrow}^\dagger. \tag{5.15}$$

In the above equations for the quasiparticle operators, only half of the operators are independent as the system only contains $2N_x N_y$ independent single particle states. The other half of the operators can be related to the first half, meaning that some of the coefficients $v_{i,m}^*$ with $\omega_{i,m}^*$, and $\nu_{i,m}^*$ with $\chi_{i,m}^*$ are related to each other. To show this, we consider the eigenvalue problem associated with S , giving rise to an equation for the i th row

$$\sum_j \begin{pmatrix} a_{i,j} & 0 & 0 & 0 \\ 0 & a_{i,j} & 0 & 0 \\ 0 & 0 & -a_{i,j} & 0 \\ 0 & 0 & 0 & -a_{i,j} \end{pmatrix} \begin{pmatrix} v_{j,m} \\ \nu_{j,m} \\ \omega_{j,m} \\ \chi_{j,m} \end{pmatrix} = E_m \begin{pmatrix} v_{i,m} \\ \nu_{i,m} \\ \omega_{i,m} \\ \chi_{i,m} \end{pmatrix}. \tag{5.16}$$

We start from

$$\sum_j \begin{pmatrix} a_{i,j} v_{j,m} \\ a_{i,j} \nu_{j,m} \\ -a_{i,j} \omega_{j,m} \\ -a_{i,j} \chi_{j,m} \end{pmatrix} = \begin{pmatrix} E_m v_{i,m} \\ E_m \nu_{i,m} \\ E_m \omega_{i,m} \\ E_m \chi_{i,m} \end{pmatrix}, \tag{5.17}$$

multiply each row with -1 , and then take the complex conjugate. Next, we swap the first row with the third row and the second row with the fourth row. We then obtain a new equation

$$\sum_j \begin{pmatrix} a_{i,j} & 0 & 0 & 0 \\ 0 & a_{i,j} & 0 & 0 \\ 0 & 0 & -a_{i,j} & 0 \\ 0 & 0 & 0 & -a_{i,j} \end{pmatrix} \begin{pmatrix} \omega_{j,m}^* \\ \chi_{j,m}^* \\ v_{j,m}^* \\ \nu_{j,m}^* \end{pmatrix} = -E_m \begin{pmatrix} \omega_{i,m}^* \\ \chi_{i,m}^* \\ v_{i,m}^* \\ \nu_{i,m}^* \end{pmatrix}. \tag{5.18}$$

This equation implies the existence of an eigenvector with elements related to the elements of our original eigenvector and opposite eigenvalue. We can then e.g. write

$$\begin{pmatrix} v_{1,m+2} \\ \nu_{1,m+2} \\ \omega_{1,m+2} \\ \chi_{1,m+2} \\ \vdots \\ v_{N_x N_y, m+2} \\ \nu_{N_x N_y, m+2} \\ \omega_{N_x N_y, m+2} \\ \chi_{N_x N_y, m+2} \end{pmatrix} = \begin{pmatrix} \omega_{1,m}^* \\ \chi_{1,m}^* \\ v_{1,m}^* \\ \nu_{1,m}^* \\ \vdots \\ \omega_{N_x N_y, m}^* \\ \chi_{N_x N_y, m}^* \\ v_{N_x N_y, m}^* \\ \nu_{N_x N_y, m}^* \end{pmatrix}, \quad (5.19)$$

where the eigenvalue associated with this eigenvector is $E_{m+2} = -E_m$. Using the above relationship between the elements of the eigenvectors, we can then show directly that $\gamma_{m+2} = (\gamma_m)^\dagger$. We then obtain the final expressions for the original electron operators in terms of the quasiparticle operators

$$\begin{aligned} c_{i\uparrow} &= \sum_{m=1}^{2N_x N_y} \left(v_{i,m} \gamma_m + \omega_{i,m}^* \gamma_m^\dagger \right), \\ c_{i\downarrow} &= \sum_{m=1}^{2N_x N_y} \left(\nu_{i,m} \gamma_m + \chi_{i,m}^* \gamma_m^\dagger \right), \\ c_{i\uparrow}^\dagger &= \sum_{m=1}^{2N_x N_y} \left(\omega_{i,m} \gamma_m + v_{i,m}^* \gamma_m^\dagger \right), \\ c_{i\downarrow}^\dagger &= \sum_{m=1}^{2N_x N_y} \left(\chi_{i,m} \gamma_m + \nu_{i,m}^* \gamma_m^\dagger \right). \end{aligned} \quad (5.20)$$

5.1.3 Diagonalized Hamiltonian

The diagonalized form of the Hamiltonian can now, using Eqs. (5.7) and (5.8), be written out as

$$H = H_0 + \frac{1}{2} \sum_m \left[E_m \gamma_m^\dagger \gamma_m + E_{m+2} \gamma_{m+2}^\dagger \gamma_{m+2} \right]. \quad (5.21)$$

In the previous section, we concluded that $E_{m+2} = -E_m$ and $\gamma_{m+2} = (\gamma_m)^\dagger$. Inserting these relations in the above equation, and using the fermionic anti-commutation relations, provides us with the final diagonalized form of the Hamiltonian

$$H = H_0 - \frac{1}{2} \sum_{m=1}^{2N_x N_y} E_m + \sum_{m=1}^{2N_x N_y} E_m \gamma_m^\dagger \gamma_m. \quad (5.22)$$

From this Hamiltonian, we then see that the expression for the expectation value of the number operators for the quasiparticles will be $\langle \gamma_m^\dagger \gamma_m \rangle = n(E_m)$, where $n(E_m)$ is the Fermi-Dirac distribution function. Moreover, the free energy of the system, using the expression for the free energy derived in Appendix C, is

$$F = H_0 - \frac{1}{2} \sum_{m=1}^{2N_x N_y} E_m - \frac{1}{\beta} \sum_{m=1}^{2N_x N_y} \ln(1 + e^{-\beta E_m}). \quad (5.23)$$

5.2 *s*-wave pairing

5.2.1 Hamiltonian

As explained previously, the tight-binding Hamiltonian in Eq. (2.5), featuring an attractive on-site interaction, can give rise to isotropic *s*-wave pairing. Applying mean-field theory together with the real-space definition of the superconducting gap $\Delta_i = -V_i \langle c_{i\downarrow} c_{i\uparrow} \rangle$, $h_{i,j}$ takes the following form

$$h_{i,j} = \begin{pmatrix} a_{i,j} & 0 & 0 & d_{i,j} \\ 0 & a_{i,j} & -d_{i,j} & 0 \\ 0 & -d_{i,j}^* & -a_{i,j} & 0 \\ d_{i,j}^* & 0 & 0 & -a_{i,j} \end{pmatrix}. \quad (5.24)$$

We have here defined $d_{i,j} = \Delta_i \delta_{i,j}$, and the definition of $a_{i,j}$ is as in the normal metal case. Following the outlined method, we start by investigating the i th row of eigenvalue equation for the m th eigenvector of S

$$\sum_j \begin{pmatrix} a_{i,j} & 0 & 0 & d_{i,j} \\ 0 & a_{i,j} & -d_{i,j} & 0 \\ 0 & -d_{i,j}^* & -a_{i,j} & 0 \\ d_{i,j}^* & 0 & 0 & -a_{i,j} \end{pmatrix} \begin{pmatrix} v_{j,m} \\ \nu_{j,m} \\ \omega_{j,m} \\ \chi_{j,m} \end{pmatrix} = E_m \begin{pmatrix} v_{i,m} \\ \nu_{i,m} \\ \omega_{i,m} \\ \chi_{i,m} \end{pmatrix}. \quad (5.25)$$

As before, this expression can be rewritten in order to obtain an equation for an eigenvector with a corresponding eigenvalue which has the opposite sign of the original eigenvalue

$$\sum_j \begin{pmatrix} a_{i,j} & 0 & 0 & d_{i,j} \\ 0 & a_{i,j} & -d_{i,j} & 0 \\ 0 & -d_{i,j}^* & -a_{i,j} & 0 \\ d_{i,j}^* & 0 & 0 & -a_{i,j} \end{pmatrix} \begin{pmatrix} \omega_{j,m}^* \\ \chi_{j,m}^* \\ \nu_{j,m}^* \\ \nu_{j,m}^* \end{pmatrix} = -E_m \begin{pmatrix} \omega_{i,m}^* \\ \chi_{i,m}^* \\ \nu_{i,m}^* \\ \nu_{i,m}^* \end{pmatrix}. \quad (5.26)$$

A relationship can therefore be established between the elements of the m th and $(m+2)$ th eigenvectors. A similar relationship can also be obtained for the elements of the $(m+1)$ th and $(m+3)$ th eigenvectors. As before, with help of these relations, we can express the original electron operators in terms of the new quasiparticle operators, obtaining the expressions in Eq. (5.20). Similarly, the diagonalized Hamiltonian and free energy takes the same form as in Eqs. (5.22) and (5.23). The difference is that, since the matrix $h_{i,j}$ is now modified, the eigenvector elements and eigenvalues will be different from the normal metal case. We now also need to self-consistently determine the superconducting gap. Starting out from the definition of the gap, we then use the expressions for the original electron operators in terms of the new quasiparticle operators to obtain

$$\Delta_i = -V_i \sum_{m=1}^{2N_x N_y} \left[\nu_{i,m} \omega_{i,m}^* + (\chi_{i,m}^* \nu_{i,m} - \nu_{i,m} \omega_{i,m}^*) n(E_m) \right]. \quad (5.27)$$

5.2.2 Magnetization and local density of states

An important quantity in the two first papers [1, 2] included in this thesis is the local magnetization $\mathbf{M}_i = \langle \mathbf{S}_i \rangle$. Here $\mathbf{S}_i = \sum_{\alpha\beta} c_{i\alpha}^\dagger \boldsymbol{\sigma}_{\alpha\beta} c_{i\beta}$. Using the BdG equations in Eq. (5.20), we obtain for the different directions in spin-space

$$M_i^x = \langle S_i^x \rangle = \langle c_{i\uparrow}^\dagger c_{i\downarrow} + c_{i\downarrow}^\dagger c_{i\uparrow} \rangle = \sum_m \left[\chi_{i,m} \omega_{i,m}^* + \omega_{i,m} \chi_{i,m}^* + (\nu_{i,m}^* \nu_{i,m} - \omega_{i,m} \chi_{i,m}^* - \chi_{i,m} \omega_{i,m}^* + \nu_{i,m} \nu_{i,m}^*) n(E_m) \right], \quad (5.28)$$

$$M_i^y = \langle S_i^y \rangle = \langle -i c_{i\uparrow}^\dagger c_{i\downarrow} + i c_{i\downarrow}^\dagger c_{i\uparrow} \rangle = i \sum_m \left[\chi_{i,m} \omega_{i,m}^* - \omega_{i,m} \chi_{i,m}^* + (\omega_{i,m} \chi_{i,m}^* - v_{i,m}^* \nu_{i,m} - \chi_{i,m} \omega_{i,m}^* + v_{i,m} \nu_{i,m}^*) n(E_m) \right], \quad (5.29)$$

$$M_i^z = \langle S_i^z \rangle = \langle c_{i\uparrow}^\dagger c_{i\uparrow} - c_{i\downarrow}^\dagger c_{i\downarrow} \rangle = \sum_m \left[|\omega_{i,m}|^2 - |\chi_{i,m}|^2 + (|v_{i,m}|^2 - |\nu_{i,m}|^2 - |\omega_{i,m}|^2 + |\chi_{i,m}|^2) n(E_m) \right]. \quad (5.30)$$

Another important quantity is the local density of states (LDOS), which represents the density of states associated with a specific lattice site. In order to derive this quantity, we start with the expression for the charge at a given lattice site

$$\rho_i = \sum_\alpha \langle c_{i,\alpha}^\dagger c_{i,\alpha} \rangle = \sum_m \left[(|\omega_{i,m}|^2 + |\chi_{i,m}|^2) (1 - n(E_m)) + (|v_{i,m}|^2 + |\nu_{i,m}|^2) n(E_m) \right]. \quad (5.31)$$

The charge density at a lattice site can be expressed as the local density of states, $D_i(E)$, multiplied by the probability that a state with energy E is occupied, integrated over all energies. In equation form, we write this as $\rho_i = \int_{-\infty}^{+\infty} D_i(E) n(E) dE$. When working at low temperatures, which is often necessary when considering superconductivity, the Fermi-Dirac distribution can be approximated by a step function. Then, $\rho_i = \int_{-\infty}^0 D_i(E) dE$, and the charge density in Eq. (5.31) can be written as

$$\begin{aligned} & \sum_m \left[(|\omega_{i,m}|^2 + |\chi_{i,m}|^2) \Theta(E_m) + (|v_{i,m}|^2 + |\nu_{i,m}|^2) \Theta(-E_m) \right] \\ &= \int_{-\infty}^0 N_i(E) dE, \end{aligned} \quad (5.32)$$

where $\Theta(E_m)$ is the Heaviside step function. We can then obtain an expression for the local density of states

$$D_i(E) = \sum_m \left[(|\omega_{i,m}|^2 + |\chi_{i,m}|^2) \delta(E + E_m) + (|\nu_{i,m}|^2 + |\nu_{i,m}|^2) \delta(E - E_m) \right]. \quad (5.33)$$

5.3 *d*-wave pairing

5.3.1 Hamiltonian

In order to describe *d*-wave superconductivity, we start from the tight-binding Hamiltonian in Eq. (2.25). We limit ourselves to nearest-neighbor interaction between electrons with opposite spins and work with a thin-film system. The possibility of interaction between electrons with spins pointing in the same direction can give rise to polarized spin-triplet, which we will not consider in the following. Using the fermionic anticommutation relations, we can rewrite the Hamiltonian on the form

$$H_{\text{EBCS}} = - \sum_{\langle i,j \rangle, \alpha} t_{ij} c_{i,\alpha}^\dagger c_{j,\alpha} - \sum_{i,\alpha} \mu_i n_{i,\alpha} - 2V \sum_{\langle ij \rangle} n_{i,\uparrow} n_{j,\downarrow}, \quad (5.34)$$

where $V = V_{ij}^{\alpha,\alpha'}/2$. After doing the usual mean-field approximation, we obtain for $h_{i,j}$

$$h_{i,j} = \begin{pmatrix} a_{i,j} & 0 & 0 & -n_{i,j} \\ 0 & a_{i,j} & m_{i,j} & 0 \\ 0 & n_{i,j}^* & -a_{i,j} & 0 \\ -m_{i,j}^* & 0 & 0 & -a_{i,j} \end{pmatrix}, \quad (5.35)$$

where

$$\begin{aligned} a_{i,j} &= -\mu \delta_{ij} - t(\delta_{i,j+1} + \delta_{i,j-1}), \\ n_{i,j} &= 2V F_{i,j}(\delta_{ij+1} + \delta_{ij-1}), \\ m_{i,j} &= 2V F_{j,i}(\delta_{ij+1} + \delta_{ij-1}). \end{aligned} \quad (5.36)$$

The pairing amplitudes are now defined as

$$F_{i,j} = F_{i,j}^{\uparrow\downarrow} = \langle c_{i\uparrow} c_{j\downarrow} \rangle. \quad (5.37)$$

Following the method outlined above, and using the BdG transformation Eq. (5.20), we need to evaluate eight pairing amplitudes relating to different directions in the plane of the thin-film. They are

$$\begin{aligned}
F_i^{x\pm} &= \sum_{m=1}^{2N_x N_y} \left[(\omega_{i,m}^* \nu_{i\pm\hat{x},m} - v_{i,m} \chi_{i\pm\hat{x},m}^*) n(E_m) + v_{i,m} \chi_{i\pm\hat{x},m}^* \right], \\
F_i^{\pm x} &= \sum_{m=1}^{2N_x N_y} \left[(\omega_{i\pm\hat{x},m}^* \nu_{i,m} - v_{i\pm\hat{x},m} \chi_{i,m}^*) n(E_m) + v_{i\pm\hat{x},m} \chi_{i,m}^* \right], \\
F_i^{y\pm} &= \sum_{m=1}^{2N_x N_y} \left[(\omega_{i,m}^* \nu_{i\pm\hat{y},m} - v_{i,m} \chi_{i\pm\hat{y},m}^*) n(E_m) + v_{i,m} \chi_{i\pm\hat{y},m}^* \right], \\
F_i^{\pm y} &= \sum_{m=1}^{2N_x N_y} \left[(\omega_{i\pm\hat{y},m}^* \nu_{i,m} - v_{i\pm\hat{y},m} \chi_{i,m}^*) n(E_m) + v_{i\pm\hat{y},m} \chi_{i,m}^* \right],
\end{aligned} \tag{5.38}$$

where we have used the notation $F_{i+\hat{x},i} \equiv F_i^{+\hat{x}}$ and similarly $F_{i,i+\hat{x}} \equiv F_i^{\hat{x}+}$. As before, we diagonalize the system numerically to obtain the eigenenergies E_m as well as the BdG transformation coefficients $v_{i,m}$, $\nu_{i,m}$, $\omega_{i,m}$ and $\chi_{i,m}$. Further, we calculate the pairing amplitudes self-consistently. This is done by starting from some set of initial values for the pairing amplitudes, diagonalizing the system, calculating the pairing amplitudes in Eq. (5.38), and diagonalizing the system with updated values for the pairing amplitudes. This procedure is repeated until convergence is achieved. The relevant BdG transformation coefficients and eigenenergies that give rise to the converged values for the pairing amplitudes are then used to obtain the free energy, LDOS, and magnetization if necessary.

5.3.2 Phase diagram

The above discussed model for a d -wave superconductor is used in the second paper [2] contained in this thesis. In order to make sure that the parameters are chosen so that the considered model actually features d -wave superconductivity, we in this section consider a system with continuous boundary conditions and map out the phase diagram of the model. We start out from Eq. (2.31) where now, again, restrict ourselves to interaction between

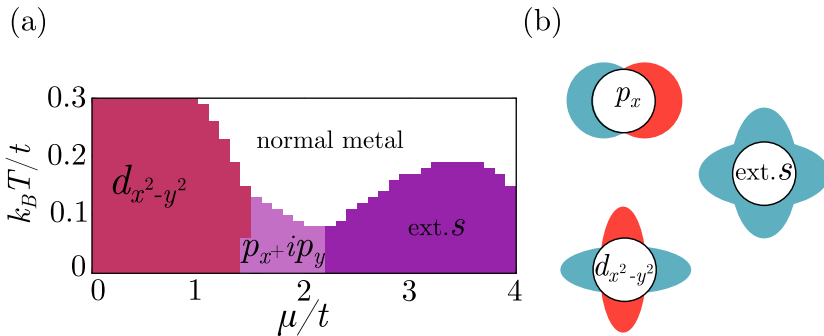


Figure 5.1: (a) Phase diagram for the model introduced in this chapter for nearest-neighbour attractive interaction between opposite spins. (b) Superconducting gap pairing symmetries appearing in the phase diagram, which, starting from the top, represent p_x -wave, extended s -wave, and $d_{x^2-y^2}$ -wave symmetries. Red color and blue colors are used to show a sign change of the superconducting gap as we move around the Fermi surface.

electrons with opposite spins, setting $V = V_{ij}^{\alpha,\alpha'}/2$ in this case. Using the fermionic anticommutation relations together with $A_{\alpha,\alpha'}(\mathbf{k}) = -A_{\alpha',\alpha}(-\mathbf{k})$, we can write Eq. (2.31) as

$$H_{\text{EBCS}}^{\text{MF}} = \sum_{\mathbf{k}} \left(A_{\uparrow,\downarrow}^*(\mathbf{k}) c_{-\mathbf{k},\downarrow} c_{\mathbf{k},\uparrow} + A_{\uparrow,\downarrow}(\mathbf{k}) c_{\mathbf{k},\uparrow}^\dagger c_{-\mathbf{k},\downarrow}^\dagger \right) + \sum_{\mathbf{k},\alpha} \varepsilon_{\mathbf{k}} c_{\mathbf{k},\alpha}^\dagger c_{\mathbf{k},\alpha} + H_{\text{EBCS}}^0, \quad (5.39)$$

Taking advantage of the framework developed in this chapter, we proceed to diagonalize this mean-field extended BCS Hamiltonian numerically. Using Eq. (2.39), the matrix that should be diagonalized can be expressed as

$$H_{\mathbf{k}} = \begin{pmatrix} \varepsilon_{\mathbf{k}} & 0 & 0 & -A_{\uparrow,\downarrow}(\mathbf{k}) \\ 0 & \varepsilon_{\mathbf{k}} & A_{\uparrow,\downarrow}(\mathbf{k}) & 0 \\ 0 & A_{\uparrow,\downarrow}^*(\mathbf{k}) & -\varepsilon_{\mathbf{k}} & 0 \\ -A_{\uparrow,\downarrow}^*(\mathbf{k}) & 0 & 0 & -\varepsilon_{\mathbf{k}} \end{pmatrix}. \quad (5.40)$$

Diagonalization of this matrix gives rise to the eigenvalues $E_{m,\mathbf{k}}$ and eigenvectors $\varphi_{\mathbf{k},m}^\dagger = (\nu_{\mathbf{k},m}^* \ \nu_{\mathbf{k},m}^* \ \omega_{\mathbf{k},m}^* \ \chi_{\mathbf{k},m}^*)$, where we again have that half of the eigenvectors can be expressed in terms of the elements of the other half. We can then consider different sets of initial values for the pairing amplitudes that go into

$$A(\mathbf{k}) = 2V \left(e^{i\mathbf{k}\cdot\hat{x}} F_{\uparrow,\downarrow}^{x+}(\mathbf{k}) + e^{-i\mathbf{k}\cdot\hat{x}} F_{\uparrow,\downarrow}^{x-}(\mathbf{k}) + e^{i\mathbf{k}\cdot\hat{y}} F_{\uparrow,\downarrow}^{y+}(\mathbf{k}) + F_{\uparrow,\downarrow}^{y-}(\mathbf{k}) e^{-i\mathbf{k}\cdot\hat{y}} \right), \quad (5.41)$$

in order to make different pairing symmetries, such as the ones displayed in Fig. 5.1 (b),

$$\begin{aligned} \Delta_d &= (V/4)(F_{\uparrow,\downarrow}^{\hat{x}+} + F_{\uparrow,\downarrow}^{\hat{x}-} - F_{\uparrow,\downarrow}^{\hat{y}+} - F_{\uparrow,\downarrow}^{\hat{y}-}), \\ \Delta_s &= (V/4)(F_{\uparrow,\downarrow}^{\hat{x}+} + F_{\uparrow,\downarrow}^{\hat{x}-} + F_{\uparrow,\downarrow}^{\hat{y}+} + F_{\uparrow,\downarrow}^{\hat{y}-}), \\ \Delta_{p_x} &= (V/2)(F_{\uparrow,\downarrow}^{\hat{x}+} - F_{\uparrow,\downarrow}^{\hat{x}-}), \\ \Delta_{p_y} &= (V/2)(F_{\uparrow,\downarrow}^{\hat{y}+} - F_{\uparrow,\downarrow}^{\hat{y}-}). \end{aligned} \quad (5.42)$$

For a given set of initial values, we iteratively diagonalize the system and calculate new values for the pairing amplitudes using the self-consistent expressions

$$F_{\uparrow,\downarrow}^{x\pm(y\pm)} = -\frac{1}{N} \sum_{\mathbf{k},m} \left[e^{\mp i\mathbf{k}\cdot\hat{x}(\hat{y})} \nu_{\mathbf{k},m} \chi_{\mathbf{k},m}^* (1 - n(E_{\mathbf{k},m})) + e^{\pm i\mathbf{k}\cdot\hat{x}(\hat{y})} \omega_{\mathbf{k},m}^* \nu_{\mathbf{k},m} n(E_{\mathbf{k},m}) \right], \quad (5.43)$$

until convergence is reached. For each set of initial values we reach convergence and evaluate the free energy of the system

$$F = H_0 - \frac{1}{2} \sum_{\mathbf{k},m} E_{\mathbf{k},m} - \frac{1}{\beta} \sum_{\mathbf{k},m} \ln(1 + e^{-\beta E_{\mathbf{k},m}}). \quad (5.44)$$

The ground state of the system for a set of parameters can then be established. Repeating this procedure for different values of the temperature and the chemical potential, the phase diagram in Fig. 5.1 (a) is obtained.

Indirect exchange interaction between ferromagnets

Previously, we discussed indirect exchange interaction between impurity spins mediated by the quasiparticles of a spin-split s -wave superconductor. In this chapter, we investigate the interaction between groups of spin, such as ferromagnets. We first consider the interaction between two metallic ferromagnets connected by an s -wave superconductor. Next, we explore the effect of the existence of zero-energy states, as in a d -wave superconductor with a diagonal edge, on the indirect interaction between two metallic ferromagnets.

6.1 Superconducting spin valve

Historically, the word *spin-valve effect* was first used in a work by Dieny *et al.* [118]. They considered two uncoupled metallic ferromagnets, e.g. Ni, separated by a nonmagnetic metal, such as Cu or Ag. One of the ferromagnets was coupled to an uncompensated antiferromagnet, i.e. an antiferromagnet where only one spin sublattice is exposed at the surface [119, 120]. As a result of the exchange bias effect [121, 122], the magnetization of this ferromagnet was then pinned, making it difficult to change the magnetization through an external magnetic field. In contrast to this *fixed* ferromagnet, the magnetization of the second *free* ferromagnet could easily be altered through an external field. In their study, they observed large magnetoresistive effects in this free-fixed layered structure which they named a spin-valve.

We mentioned in the introduction chapter that de Gennes was the first to introduce a structure consisting of two ferromagnetic insulators sandwiching a superconductor. Such structures are usually referred to as superconducting spin-valves and can consist of both metallic and insulating ferromagnets sandwiching a superconductor. As a result of presence of a

superconductor, these structures feature different physics than the normal spin-valve structure. One feature, which we have mentioned earlier, is that $T_c^{\text{AP}} > T_c^{\text{P}}$ for a superconductor sandwiched between two ferromagnetic insulators, FMI/SC/FMI. Considering the thickness of the ferromagnetic layers to be large enough, one can easily ignore the effect of the superconductor on the ferromagnets. However, considering the effect that the superconductor can have on the ferromagnets can also be of interest. Therefore, Zhu *et al.* considered a superconducting spin-valve of GdN/Nb/GdN, i.e. of the type FMI/SC/FMI [123], where the GdN layers that they used were thin enough so that the effect of the superconductor was no longer negligible. They were then able to probe the superconducting exchange coupling between the ferromagnets, leading to an antiferromagnetic alignment of the ferromagnets. This result was interpreted as arising from the superconducting condensation energy being maximized for the antiparallel configuration.

As the ferromagnets in these works are insulators, the proximity effect is not of importance. The proximity effect can, however, become important in superconducting spin-valve structures including metallic ferromagnets. One of the early theoretical works on superconducting spin-valves involving metallic ferromagnets was performed in 1999 by Tagirov [124], based on the structure proposed by Diény. These calculations showed that in a spin-valve structure with free-fixed metallic ferromagnets, the superconducting transition temperature is larger for anti-parallel alignment than parallel alignment of the ferromagnets. Further, they showed that this device can be used as a switch where the superconducting current can be turned on and off by means of rotating the magnetization of the free ferromagnet. At around the same time, Buzdin obtained similar results for a similar FM/SC/FM structure, finding that the parallel magnet configuration most efficiently breaks Cooper pairs, which can be used to switch off superconductivity [125].

These two latter works were done in diffusive limit. Many studies have also focused on dirty superconductors and/or ferromagnets, as well as different combinations of ferromagnets with varying properties. Later in this chapter, we will investigate the exchange interaction between two metallic ferromagnets in a superconducting spin valve. Importantly, the superconducting gap equation is being solved self-consistently, allowing us to consider both the effect of the superconducting gap on the interaction between the ferromagnets, as well as the effect of the ferromagnets on the superconducting gap. In our case, instead of determining the superconducting transition temperature for parallel and anti-parallel magnet configurations, we deter-

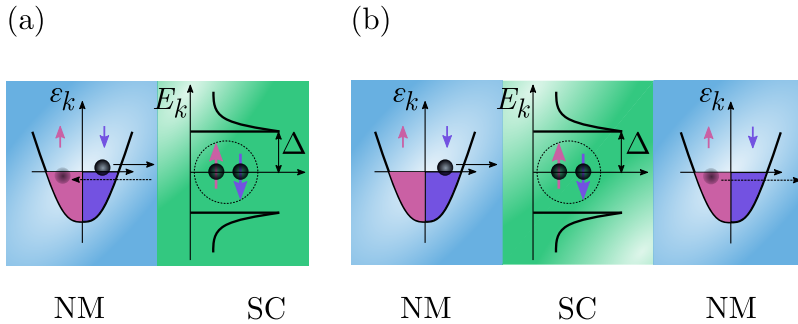


Figure 6.1: (a) Andreev reflection: An electron from the spin-down band inside the normal metal with an energy inside a superconducting gap hits the interface. It will pair up with an electron from the spin-up band and leave behind a hole in the normal metal. These two electrons enter the superconductor and generate a Cooper pair inside of it. (b) Crossed Andreev reflection: An electron from the spin-down band of the left electrode, with energy inside the superconducting gap, pairs up with an electron from the opposite spin band of the right electrode and form a Cooper pair inside the superconductor.

mine the ground state of the system by calculating the free energy difference between these two configurations.

6.2 Andreev reflection and crossed Andreev reflection

As we mentioned in the previous chapters, interesting physics can arise at the interface between a superconductor and another material. The phenomena we will discuss in this section takes place when a normal conductor like a metal or a metallic ferromagnet is brought into contact with a superconductor. An electron approaching the interface from the metallic side can then experience two different types of reflections. One type is normal specular reflection, while the other is Andreev reflection (AR) [126, 127]. During specular reflection, an electron that hits the interface is simply reflected back as an electron. The total number of charge being transferred to the other side of the interface is zero in this type of reflection, and there is

clearly no requirement on the other side of the interface being a superconductor. Andreev reflection, on the other hand, does require the material on the other side to be a superconductor and leads to transfer of a total charge of $-2e$. In this case, an incoming electron hits the interface and is reflected back as a hole representing the absence of a particle with spin opposite to the incoming electron. In this process, a Cooper pair is generated inside the superconductor, as illustrated in Fig. 6.1 (a).

In order to better understand the origin of Andreev reflections, we first consider an electron with the energy larger than the superconducting energy gap ($\varepsilon_{\mathbf{k}} > \Delta$) propagating towards the interface from the metallic side. Such an electron can be normally transmitted into the superconductor as an electron-like quasiparticle. However, if the energy of the incoming electron is smaller than the superconducting gap ($\varepsilon_{\mathbf{k}} < \Delta$), there are no available states inside the gap that the electron can fill on the superconducting side of the interface. Instead, this electron needs to pair up with another electron with opposite spin and momentum to form a Cooper pair. This additional electron is taken from the metallic side of the interface, leaving behind a hole. In other words, the incoming electron is reflected as a hole. The inverse processes involves a hole, approaching the interface from the metallic side, being reflected as an electron. During this scattering process, a Cooper pair inside the superconductor is destroyed. Both normal and inverse Andreev reflection contribute to the proximity effect as both processes introduce correlations between electrons and holes.

Andreev reflection is a local phenomenon in the sense that both particles that contribute to the generation of an additional Cooper pair inside the superconductor come from one metallic contact. On the other hand, Crossed Andreev reflection (CAR) is a non-local phenomenon where the particles that generate the Cooper pair originate with two different metallic contacts. In CAR, the hole is reflected back inside the second metallic contact, as displayed in Fig. 6.1 (b). The existence of crossed Andreev reflection was first theoretically predicted [128, 129], and later observed in layered structures of superconductors and ferromagnetic [130] or normal metals [131].

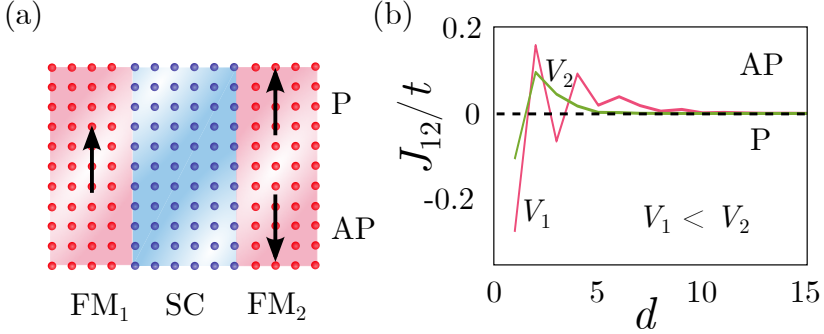


Figure 6.2: (a) An s -wave superconductor is sandwiched between two metallic ferromagnets which are assumed to have either parallel or anti-parallel magnetization. The configuration where the two ferromagnets have parallel magnetization is denoted by P, while the anti-parallel configuration is denoted by AP. (b) The indirect interaction between the two ferromagnets, as a function of the (horizontal) length of the superconductor, is displayed for different strengths of the attractive interaction ($V > 0$) inside the superconductor.

6.3 Interaction between ferromagnets mediated by an s -wave superconductor

The system we consider in this section is a superconducting spin-valve where a conventional s -wave superconductor is sandwiched between two metallic ferromagnets. This structure is illustrated in Fig. 6.2 (a). The s -wave superconductor will be described using the Hamiltonian in Eq. (2.5). The metallic ferromagnets are described through itinerant electrons coupling to a background field as introduced in Eq. (3.4). The aim is to investigate how the two ferromagnets interact with each other via this superconductor. The magnetic ground state of the system is determined from the dependence of the free energy of the system on the relative orientation of the magnetization in the two ferromagnets. To this end, we define

$$J_{12} = F^{\uparrow\uparrow} - F^{\uparrow\downarrow}, \quad (6.1)$$

where $F^{\uparrow\uparrow}$ is the free energy of the system when the magnetization in the two ferromagnets is parallel, and $F^{\uparrow\downarrow}$ is the free energy for the case of anti-

parallel ferromagnets. The sign of J_{12} then expresses whether the free energy is minimized by the parallel or anti-parallel configuration. The reason why we only consider the magnetization of the two ferromagnets to be either aligned or anti-aligned is that we are considering a spin-rotationally invariant superconductor without any spin-orbit coupling or spin-splitting. The system is then expected to either prefer a parallel or anti-parallel magnet configuration.

The distance between the ferromagnets can be varied by changing the length of the superconductor in the horizontal direction, denoted by d . The free energy difference, as a function of d , is plotted in Fig. 6.2 (b) for two different values of the strength of the attractive interaction in the superconductor, V_1 and V_2 . From Fig. 6.2 (b), two types of behaviour can be observed. For the weaker interaction potential V_1 , J_{12} displays damped oscillations with a preference for the AP orientation ($J_{12} > 0$) for larger d . This behaviour can be viewed as competition between two types of behaviour: oscillations, as well as damping with preference for anti-alignment. For the stronger interaction potential V_2 , the oscillations of J_{12} are dominated by damping with preference for anti-alignment.

The above discussed behaviour arises from competing effects. One is the normal RKKY oscillations, arising from indirect interaction mediated by itinerant particles. Another effect is that the superconducting gap pushes the quasiparticle states away from the Fermi level, limiting the normal RKKY interaction. With these two effects in mind, we can explain the above presented oscillatory and damping behaviour. For the case of weaker interaction V_1 , there are normal RKKY oscillations at small d . Then, as d increases, the superconductor becomes larger, leading to a larger gap. The RKKY interaction is then quickly weakened, giving rise to a behaviour dominated by damping rather than oscillations. Moreover, for a stronger attractive interaction V_2 , the superconducting gap is sufficiently large for the damping behaviour to dominate even for small d .

The remaining feature of the J_{12} curves that is left to explain is then the preference for an anti-parallel configuration in the damped regime. Seeking to understand the sign of J_{12} in this region, we checked the superconducting gap for both the P and AP configuration, surprisingly finding that $\Delta_P > \Delta_{AP}$. This was unexpected as the induced magnetization inside the superconductor is larger for the P configuration. One would therefore expect pair-breaking to give rise to $\Delta_P < \Delta_{AP}$. However, there are in general three different pair-breaking mechanisms in this type of superconducting

spin valves: induced magnetization, inverse Andreev reflection, and inverse crossed Andreev reflection. For sufficiently large background field h in the ferromagnets, there are few states close to the Fermi level in the spin minority bands of the ferromagnets, making pair breaking from inverse AR less important regardless of the relative orientation of the two ferromagnets. Pair breaking from inverse CAR also becomes a weak effect in the P configuration, but not in the AP configuration where there are still available states close to the Fermi level associated with opposite spin directions. Based on our results in the discussed region, it then appears that the pair breaking is dominated by inverse CAR, which then leads to the somewhat surprising result that the superconducting gap is larger for the parallel configuration. As $\Delta_P > \Delta_{AP}$, the condensation energy should be expected to be larger for the P configuration, which one could imagine would lead to a preference for the P configuration. This is, however, not the full story as the ground state of the system is affected by both the condensation energy and the RKKY interaction mediated by itinerant quasiparticles, which is more efficiently suppressed for a larger gap. As there are more available quasiparticles around the Fermi level in the AP configuration, featuring a smaller superconducting gap, this configuration actually ends up minimizing the free energy.

6.4 Zero-energy surface bound states

After the discovery of cuprate based superconductors in 1986 [56], the pairing symmetry in these superconductors has been much discussed. As we mentioned in the first chapter, these superconductors are high- T_c unconventional superconductors that were early proposed to have a pairing symmetry different from the normal s -wave pairing symmetry found in conventional superconductors. One proposed candidate was d -wave pairing which differs from isotropic and anisotropic s -wave pairing by changing sign when moving around the Fermi-surface. Many of the performed experiments were, however, not able to probe the sign changes of the gap, meaning that d -wave pairing could not be distinguished from anisotropic s -wave pairing. A possible solution to this problem was proposed by Hu in 1994 [132]. Hu's proposal was motivated by the possibility of existence of zero-energy bound states (ZES) at the surface of superconductors with d -wave pairing symmetry.

Consider a d -wave superconductor with pairing symmetry $d_{x^2-y^2}$. In

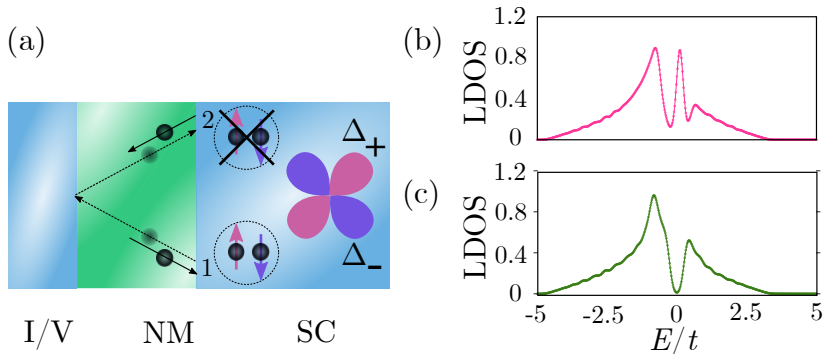


Figure 6.3: (a) A schematic illustration of scattering processes leading to generation of midgap states in a heterostructure consisting of a normal metal layer located between a d_{xy} superconductor, and an insulating layer/vacuum. An electron inside the normal metal performs subsequent Andreev reflections and specular reflections at the two interfaces, leading to a confined electron-hole state. As the incoming quasiparticle in two subsequent Andreev reflections face different signs of the superconducting gap, Δ_+ and Δ_- , the resulting bound states have zero energy relative to the Fermi level. In (b) and (c), we present the local density of states on a diagonal edge of a d -wave and an s -wave superconductor, respectively. For the d -wave superconductor, a peak close to zero energy can be observed.

a rotated coordinate system aligned with a diagonal $\{110\}$ edge of such a superconductor, the order parameter will instead have a d_{xy} symmetry. In order to discuss the presence of zero-energy bound states at such an edge we simply consider a superconductor with d_{xy} symmetry. The specific setup we will investigate is displayed in Fig. 6.3(a), consisting of a normal metal layer sandwiched between a d_{xy} superconductor and an insulating material/vacuum. The same arguments as presented for this system setup can be extended to the case without the normal metal layer by considering that there will be some region close to the interface where the superconducting order parameter decays from its bulk value, which can play the role of the normal metal layer present in our setup.

We then consider an electron, with energy within the superconducting gap, approaching the interface between the normal metal layer and the superconductor from the normal metal side. This electron will be Andreev reflected as a hole, leading to the generation of a Cooper pair inside the

superconductor. This hole will propagate to the other side of the normal metal layer, collide with the vacuum interface, and be specularly reflected back. Further, returning to the superconductor interface, the hole will experience inverse Andreev reflection and be reflected back as an electron. This repeated process, illustrated in Fig 6.3 (a), leads to an electron-hole bound state which is confined to the normal metal layer. In order to better understand these bound states, we need to go into a bit more details.

The above picture represents a closed quasiparticle trajectory where the phase picked up along the way consists of two important parts. The first part is due to the Andreev reflection which gives rise to a phase θ_A . The second part is the phase picked up by the quasiparticle when propagating inside the normal metal, θ_P . During the Andreev reflection where an electron (hole) is reflected back as a hole (electron), a phase shift of $-\arccos(E/|\Delta|) \mp \phi$ takes place [133], where E is the electron energy relative to Fermi-level and ϕ is the phase of the superconducting order parameter. The minus (plus) sign applies for an electron (hole) hitting the interface and being reflected back as a hole (electron). Therefore, the first Andreev reflection introduces a phase shift $-\arccos(E/|\Delta_1|) - \phi_1$, while the second Andreev reflection introduces a phase shift $-\arccos(E/|\Delta_2|) + \phi_2$. This leads to

$$\theta_A = - \left(\arccos(E/|\Delta_1|) + \arccos(E/|\Delta_2|) \right) + \left(\phi_2 - \phi_1 \right). \quad (6.2)$$

On the other hand

$$\theta_P = \frac{2l}{\cos(\theta)} (|k_e| - |k_h|), \quad (6.3)$$

where l is the length of the normal metal layer, and θ is the angle between the trajectory of the incident electron and the interface normal. The electron and hole momenta are given by $k_{e,h} = (2m(E_F \pm E))^{1/2}$. The Bohr-Sommerfeld quantization condition requires the phase obtained during this closed trajectory to sum up to $\theta_A + \theta_P = 2\pi n$, where n is an integer. For completeness, we here discuss the resulting bound states for three different choices of the superconductor.

- Isotropic s -wave: For this type of superconductor $|\Delta_1| = |\Delta_2|$ and $\phi_1 = \phi_2$, therefore $-2\arccos(E/|\Delta_1|) + \theta_P = 2\pi n$. For $n = 0$, this equation leads to $E = |\Delta_1| \cos(\theta_P/2)$. This expression shows that bound

states with nonzero energy are possible even for an isotropic s -wave superconductor. In fact, the idea of existence of quasiparticle surface bound states inside a normal metal layer sandwiched between an s -wave superconductor and an insulator was introduced by de Gennes and Saint-James as early as in 1963 [134].

- **Anisotropic s -wave:** In an anisotropic s -wave superconductor, as we mentioned in the previous chapters, the magnitude of the gap is not the same as we move around the Fermi-surface but the sign of it remains unchanged. As a result of this character, we will typically have $|\Delta_1| \neq |\Delta_2|$ and $\phi_1 = \phi_2$. Therefore, we instead end up with the expression $\arccos(E/|\Delta_1|) + \arccos(E/|\Delta_2|) = \theta_P$, when $n = 0$, simply expressing that the bound state energies are altered by the anisotropy of the order parameter.
- **d -wave:** Finally, we consider the case of a d_{xy} superconductor, as displayed in Fig. 6.3 (a). For the two Andreev reflections the gap then has opposite sign but the same value, $\phi_1 = \pi$, $\phi_2 = 0$, and $|\Delta_1| = |\Delta_2|$. The energy of the bound states can then be obtained from $-2\arccos(E/|\Delta_1|) - \pi + \theta_P = 2\pi n$. If we set $E = 0$ in this equation, then $-2\arccos(0) - \pi + \theta_P(0) = 2\pi n$. This leads to $-2(\pi/2) - \pi + 0 = 2\pi n$ which shows that $n = -1$ allows for the presence of zero-energy bound states.

Existence of such bound states with zero energy at the surface of a d -wave superconductor was also pointed out by Tanaka *et al.* [135], Matsumoto and Shiba [136], and Barash *et al.* [137]. These zero-energy surface states are the origin of the observation of zero bias conductance peaks for tunnel junctions of $\text{YBa}_2\text{Cu}_3\text{O}_7$ by Greek *et al.*, in 1988 [138], and later by other groups such as [139, 140].

In order to investigate the existence of zero-energy surface bound states at the surface of a d -wave superconductor, we consider a two dimensional square lattice structure with one diagonal edge similar to Fig. 6.4 (a), apart from the absence of the ferromagnetic contacts. Using Eq. (5.33), we calculate the local density of states for one lattice point at the diagonal edge. We consider two cases. First a d -wave superconductor described by Eq. (5.34), leading to the LDOS plot in Fig. (6.3) (b) showing a zero-energy peak. We also consider an s -wave superconductor, leading to an LDOS plot that does not feature a zero-energy peak, as displayed in Fig. 6.3 (c).

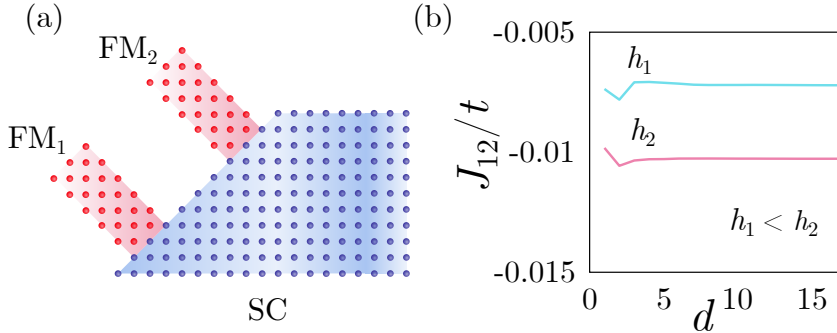


Figure 6.4: (a) Two metallic ferromagnets are located on the diagonal edge of a d -wave superconductor. (b) The indirect interaction between the two ferromagnets, as a function of their separation distance, for two different values of the background field h inside the ferromagnets.

6.5 Interaction between ferromagnets mediated by a d -wave superconductor

Earlier in this chapter, we investigated the indirect exchange interaction between two metallic ferromagnets mediated by an s -wave superconductor. We found that the RKKY oscillations in this case could be dominated by a damping behaviour arising from the superconducting gap pushing quasi-particle states away from the Fermi-level. One could then wonder how this picture changes if one introduces available states inside the gapped region of the excitation spectrum of the superconductor. Motivated by this, we discussed, in the previous section, the existence of localized zero-energy surface states, referred to as midgap states. We concluded that such midgap states can be realized for d -wave superconductors with a diagonal edge in contact with e.g. vacuum.

In order to investigate how such midgap states affect the indirect interaction between ferromagnets, we therefore consider a thin-film d -wave superconductor with one diagonal edge in contact with vacuum and locate two metallic ferromagnets on the diagonal edge Fig. 6.4 (a). The Hamiltonian used to describe the d -wave superconductor is presented in Eq. (5.34), and suitable chemical potential can be determined from the phase plot in Fig. 5.1 (a). The magnetization inside the ferromagnets is introduced through a background field, as in Eq. (3.4). The indirect interaction between the fer-

romagnets is expressed, as earlier in this chapter, through J_{12} , which is the free energy difference between the aligned and anti-aligned magnetization configurations. Results for this indirect interaction is presented in Fig. 6.4 (b). Opposite of the indirect interaction between the ferromagnets in our earlier considered spin-valve structure, the indirect exchange interaction now prefers alignment of the two ferromagnets leading to $J_{12} < 0$. Further, J_{12} now varies very little with the distance between the two ferromagnets. Further, varying the strength of the background field inside the ferromagnets, h , we find that the behaviour is similar, but that the magnitude of J_{12} increases with increasing h .

This result is somewhat surprising as one might expect that the parallel configuration of magnets will more efficiently induce a spin-splitting in the superconductor, leading to a reduced superconducting gap and a lower condensation energy. However, the superconducting gap at the diagonal edge is, even in the absence of the ferromagnets, suppressed due to the presence of the midgap states. The effect of the ferromagnets is then mainly to spin-split midgap states associated with opposite spin directions. This shifts the midgap states away from their resonance energy $E = 0$, leading to a suppression of the midgap states and a recovery of the superconducting gap at the edge. As, the parallel magnet configuration suppresses the midgap states most efficiently, this configuration features a larger superconducting gap along the edge and therefore also a larger condensation energy.

The induced spin-splitting can be easily observed as the midgap states represents many states located around zero energy. A spin-splitting then leads to the formation of a giant magnetic moment due to the large density of states at zero energy [132, 141, 142]. For the case of aligned magnets, this magnetization is uniform along the edge, while for the case of anti-aligned magnets, the magnetization has to change sign along the way. The latter case leads to a transition region with small magnetization, corresponding to weak spin-splitting and weak suppression of the midgap states. This transition region, not present for the aligned magnet configuration, makes the condensation energy larger for the aligned configuration.

Conclusion and outlook

In this thesis, we have presented concepts needed to understand the results in the four included research papers. We have also introduced the main findings of these papers.

We started with a brief introduction to the historical background and current state of the field of spintronics, as well as its subfield superconducting spintronics. We then moved on to describing the superconducting state as well as how it can arise from attractive electron-electron interaction mediated by phonons, as explained by the BCS theory. The extended BCS theory, suitable for describing unconventional superconductivity, was also covered.

We then proceeded to consider the effect of magnetism on superconductivity, either introduced through an external magnetic field or proximity to a magnetic material. This led us to a discussion of the Chandrasekhar-Clogston limit, which normally restricts the spin-splitting field that a spin-singlet superconductor can coexist with. With this background, we turned to paper [4], which considers the critical spin-splitting field of a superconductor with a dispersive band crossing the Fermi level, and an additional flat-band located close to the Fermi level. We explained why such a system might feature superconductivity for spin-splitting fields larger than those permitted by the Chandrasekhar-Clogston limit.

In the next chapter, we shifted the focus to the interaction between magnetic impurities and especially the indirect interaction between them mediated by itinerant particles, known as RKKY interaction. This led us to a discussion of paper [3], which investigates the indirect interaction between magnetic impurities mediated by the quasiparticles in a spin-split superconductor. The indirect interaction was in this case found to not be homogeneous in spin space, but rather consist of two terms referred to as Heisenberg and Ising terms. The Heisenberg term represents the interaction strength for the components of the impurity spins in the plane perpendicular to the magnetic field, while the Ising term describes the interaction

strength for the component of the spins along the axis of the field. As impurity spins in a magnetic environment will have a tendency of aligning with the local magnetization, masking the effect of the RKKY interaction, we further presented a proposal for how the RKKY interaction could be extracted in experiments.

We then introduced the Bogoliubov-de Gennes method for different lattice models, laying the foundation for a discussion of papers [1] and [2], which consider indirect interaction between ferromagnets connected by superconductors.

Before the discussion of these articles, we, however, had to touch on the physics taking place at interfaces between superconductors and non-superconducting materials. We here introduced the concept of Andreev reflections as well as the possibility of zero-energy surface states at specific edges of d -wave superconductors. With this we turned to paper [1], where the indirect interaction between two ferromagnets mediated by an s -wave superconductor is investigated in a spin-valve structure, and contrasted with the case where the superconductor is substituted with a normal metal. Importantly, rather than just investigating how the presence of the superconductor influences the ferromagnets, this study also captures the effect of the presence of the ferromagnets on the superconductor, which again influences the indirect interaction. The indirect interaction was in this article found to show a different behavior depending on whether the interaction was mediated by a normal metal or a superconductor. In the former case, normal RKKY oscillations were obtained, while in the latter case the interaction was found to be more quickly suppressed with increasing length of the central layer of the superconducting spin-valve and to prefer anti-alignment of the magnets when the superconducting gap was sufficiently large.

Finally, we moved to a discussion of paper [2], where the indirect interaction between two magnetic contacts is mediated by a d -wave superconductor. When attached to a diagonal edge of the superconductor, featuring zero-energy bound states, the indirect interaction was found to show a completely different behaviour than the indirect interaction investigated in paper [1]. The indirect interaction was in this case found to vary little with distance and favour alignment of the ferromagnets due to the presence of the midgap states.

Something all the papers included in this thesis have in common is that they are focused on general model systems rather than being oriented towards specific material choices. It would therefore be of interest to con-

nect these studies closer to experiments. A good example is paper [4], which introduces a general mechanism for how superconductivity in multi-band systems containing flat-bands can survive beyond the Chandrasekhar-Clogston limit. A natural next step would be to consider more realistic models in order to learn more about in which realistic systems the outlined mechanism can be realized. One particular system that comes to mind is magic-angle twisted trilayer graphene, featuring closely located dispersive and flat-bands [143], where violation of the Chandrasekhar-Clogston limit has been observed in experiments [144]. This violation has so far been attributed to spin-triplet pairing [144, 145]. As spin-split superconductors have been found to feature large thermoelectric effects [146], it could also be of interest to investigate thermoelectric effects in spin-split flat-band superconductors in general.

It could also be possible to consider indirect interaction mediated by an intrinsic spin-triplet superconductor, or a spin-singlet superconductor with proximity-induced triplet correlations. Going in a slightly different direction, one could also imagine substituting the superconductor with e.g. an antiferromagnetic insulator in order to consider indirect interaction mediated by magnons.

Evaluation of T_c integral

Here, we want to evaluate the integral in Eq. (2.22).

$$1 = \frac{VN_0}{N} \int_0^{\hbar\omega_c} d\varepsilon \frac{1}{\varepsilon} \tanh\left(\frac{\varepsilon}{2k_B T_c}\right). \quad (\text{A.1})$$

Using the change of variable $x = \frac{\varepsilon}{2k_B T_c}$, we obtain

$$1 = \frac{VN_0}{N} \int_0^{\frac{\hbar\omega_c}{2k_B T_c}} dx \frac{1}{x} \tanh(x). \quad (\text{A.2})$$

Further, doing integration by parts

$$1 = \frac{VN_0}{N} \left[\ln\left(\frac{\hbar\omega_c}{2k_B T_c}\right) \tanh\left(\frac{\hbar\omega_c}{2k_B T_c}\right) - \int_0^{\frac{\hbar\omega_c}{2k_B T_c}} dx \frac{\ln(x)}{\cosh^2(x)} \right]. \quad (\text{A.3})$$

In order to evaluate $\tanh\left(\frac{\hbar\omega_c}{2k_B T_c}\right)$ in the first term, we make the assumption $2k_B T_c \ll \hbar\omega_c$, which we will see holds as long as we are in the weak-coupling regime. The upper limit on the integral in the second term can then be taken to infinity as the integral converges quickly for $x \gg 1$. We then obtain

$$\begin{aligned} 1 &= \frac{VN_0}{N} \left[\ln\left(\frac{\hbar\omega_c}{2k_B T_c}\right) - \int_0^\infty dx \frac{\ln(x)}{\cosh^2(x)} \right] \\ &= \frac{VN_0}{N} \left[\ln\left(\frac{\hbar\omega_c}{2k_B T_c}\right) + I \right], \end{aligned} \quad (\text{A.4})$$

where $I \approx 0.81878$, and further

$$\left(\frac{N}{VN_0} - I\right) = \ln\left(\frac{\hbar\omega_c}{2k_B T_c}\right). \quad (\text{A.5})$$

Solving for the critical temperature, we then obtain

$$k_B T_c = 1.13 \hbar\omega_c e^{-\frac{N}{VN_0}}. \quad (\text{A.6})$$

For $\lambda = VN_0/N \ll 1$ (weak-coupling), we then see that the assumption $2k_B T_c \ll \hbar\omega_c$ holds.

Unconventional Cooper pairing

B.1 Unconventional Quasiparticle energies

In this Appendix, we are aiming to determine the unconventional quasiparticle energies that we have introduced in chapter 2. We then need to calculate the eigenenergies of the 4×4 matrix in Eq. (2.39). To this end, we consider the following determinant

$$\begin{vmatrix} (\varepsilon_{\mathbf{k}} - E)\sigma_0 & A(\mathbf{k}) \\ A^\dagger(\mathbf{k}) & -(\varepsilon_{\mathbf{k}} + E)\sigma_0 \end{vmatrix} = 0. \quad (\text{B.1})$$

If A, B, C and D are square matrices of the same size and $CD = DC$, meaning that C and D commute, then $\det \begin{pmatrix} A & B \\ C & D \end{pmatrix} = \det(AD - BC)$. Therefore, our determinant can be expressed as

$$\det\left(-(\varepsilon_{\mathbf{k}}^2 - E^2)\sigma_0 - A(\mathbf{k})A(\mathbf{k})^\dagger\right) = 0. \quad (\text{B.2})$$

This expression can, in general, be complicated, but if we consider $A(\mathbf{k})A^\dagger(\mathbf{k}) = |A_{\mathbf{k}}|^2\sigma_0$, then

$$\begin{vmatrix} -(\varepsilon_{\mathbf{k}}^2 - E^2)\sigma_0 - |A_{\mathbf{k}}|^2\sigma_0 & 0 \\ 0 & -(\varepsilon_{\mathbf{k}}^2 - E^2)\sigma_0 - |A_{\mathbf{k}}|^2\sigma_0 \end{vmatrix} = 0, \quad (\text{B.3})$$

which leads to

$$E = \pm \sqrt{\varepsilon_{\mathbf{k}}^2 + |A_{\mathbf{k}}|^2}. \quad (\text{B.4})$$

B.2 Bogoliubov transformation

In order to diagonalize the 4×4 matrix in Eq. (2.39), we consider $\begin{pmatrix} \hat{a} \\ \hat{b} \end{pmatrix}$ as an eigenvector of the 4×4 matrix with the eigenenergy $E_{\mathbf{k}} = \sqrt{\varepsilon_{\mathbf{k}}^2 + |A_{\mathbf{k}}|^2}$. The eigenvalue problem can then be expressed as

$$\begin{pmatrix} \varepsilon_{\mathbf{k}}\sigma_0 & A(\mathbf{k}) \\ A^\dagger(\mathbf{k}) & -\varepsilon_{\mathbf{k}}\sigma_0 \end{pmatrix} \begin{pmatrix} \hat{a} \\ \hat{b} \end{pmatrix} = E_{\mathbf{k}} \begin{pmatrix} \hat{a} \\ \hat{b} \end{pmatrix}. \quad (\text{B.5})$$

Then, from

$$\varepsilon_{\mathbf{k}}\sigma_0\hat{a} + A(\mathbf{k})\hat{b} = E_{\mathbf{k}}\hat{a}, \quad (\text{B.6})$$

and multiplying both sides of the equation with $A(\mathbf{k})^\dagger$, as well as using that $A(\mathbf{k})A(\mathbf{k})^\dagger = |A_{\mathbf{k}}|^2\sigma_0$, we obtain

$$\hat{b} = \frac{A(\mathbf{k})^\dagger}{|A_{\mathbf{k}}|^2} (E_{\mathbf{k}} - \varepsilon_{\mathbf{k}})\hat{a}. \quad (\text{B.7})$$

Therefore, the first two eigenvectors, which have the same eigenvalues, can be expressed as

$$\Psi_1 = \begin{pmatrix} \hat{a}_1 \\ \frac{A(\mathbf{k})^\dagger}{|A_{\mathbf{k}}|^2} (E_{\mathbf{k}} - \varepsilon_{\mathbf{k}})\hat{a}_1 \end{pmatrix}, \quad \Psi_2 = \begin{pmatrix} \hat{a}_2 \\ \frac{A(\mathbf{k})^\dagger}{|A_{\mathbf{k}}|^2} (E_{\mathbf{k}} - \varepsilon_{\mathbf{k}})\hat{a}_2 \end{pmatrix}. \quad (\text{B.8})$$

The next two eigenvectors can be obtained from a similar eigenvalue problem with the eigenenergy $E_{\mathbf{k}} = -\sqrt{\varepsilon_{\mathbf{k}}^2 + |A_{\mathbf{k}}|^2}$. From the following equation

$$\varepsilon_{\mathbf{k}}\sigma_0\hat{a} + A(\mathbf{k})\hat{b} = -E_{\mathbf{k}}\hat{a}, \quad (\text{B.9})$$

we obtain

$$\hat{a} = -\frac{A(\mathbf{k})}{E_{\mathbf{k}} + \varepsilon_{\mathbf{k}}}\hat{b}. \quad (\text{B.10})$$

The last two eigenvectors can then be expressed as

$$\Psi_3 = \begin{pmatrix} -\frac{A(\mathbf{k})}{E_{\mathbf{k}} + \varepsilon_{\mathbf{k}}}\hat{b}_3 \\ \hat{b}_3 \end{pmatrix}, \quad \Psi_4 = \begin{pmatrix} -\frac{A(\mathbf{k})}{E_{\mathbf{k}} + \varepsilon_{\mathbf{k}}}\hat{b}_4 \\ \hat{b}_4 \end{pmatrix}. \quad (\text{B.11})$$

For our purposes, the set of eigenvectors should be orthonormal, meaning that $\langle \Psi_i | \Psi_i \rangle = 1$ and $\langle \Psi_i | \Psi_j \rangle = 0$ for $i \neq j$. For the two first eigenvectors we have

$$\begin{aligned} |\hat{a}_1|^2 = |\hat{a}_2|^2 &= \frac{|A_{\mathbf{k}}|^2}{|A_{\mathbf{k}}|^2 + (E_{\mathbf{k}} - \varepsilon_{\mathbf{k}})^2}, \\ |\hat{b}_3|^2 = |\hat{b}_4|^2 &= \frac{(E_{\mathbf{k}} + \varepsilon_{\mathbf{k}})^2}{(E_{\mathbf{k}} + \varepsilon_{\mathbf{k}})^2 + |A_{\mathbf{k}}|^2}. \end{aligned} \quad (\text{B.12})$$

The transformation matrix takes the form

$$\hat{P} = \begin{pmatrix} \hat{a}_1 & \hat{a}_2 & -\frac{A(\mathbf{k})}{E_{\mathbf{k}} + \varepsilon_{\mathbf{k}}} \hat{b}_3 & -\frac{A(\mathbf{k})}{E_{\mathbf{k}} + \varepsilon_{\mathbf{k}}} \hat{b}_4 \\ \frac{A(\mathbf{k})^\dagger (E_{\mathbf{k}} - \varepsilon_{\mathbf{k}})}{|A_{\mathbf{k}}|^2} \hat{a}_1 & \frac{A(\mathbf{k})^\dagger (E_{\mathbf{k}} - \varepsilon_{\mathbf{k}})}{|A_{\mathbf{k}}|^2} \hat{a}_2 & \hat{b}_3 & \hat{b}_4 \end{pmatrix}. \quad (\text{B.13})$$

This transformation matrix should be unitary. We therefore consider

$$\begin{aligned} \hat{a}_1 &= \frac{|A_{\mathbf{k}}|}{\sqrt{|A_{\mathbf{k}}|^2 + (E_{\mathbf{k}} - \varepsilon_{\mathbf{k}})^2}} \begin{pmatrix} 1 \\ 0 \end{pmatrix}, \\ \hat{a}_2 &= \frac{|A_{\mathbf{k}}|}{\sqrt{|A_{\mathbf{k}}|^2 + (E_{\mathbf{k}} - \varepsilon_{\mathbf{k}})^2}} \begin{pmatrix} 0 \\ 1 \end{pmatrix}, \\ \hat{b}_3 &= \frac{(E_{\mathbf{k}} + \varepsilon_{\mathbf{k}})}{\sqrt{(E_{\mathbf{k}} + \varepsilon_{\mathbf{k}})^2 + |A_{\mathbf{k}}|^2}} \begin{pmatrix} 1 \\ 0 \end{pmatrix}, \\ \hat{b}_4 &= \frac{(E_{\mathbf{k}} + \varepsilon_{\mathbf{k}})}{\sqrt{(E_{\mathbf{k}} + \varepsilon_{\mathbf{k}})^2 + |A_{\mathbf{k}}|^2}} \begin{pmatrix} 0 \\ 1 \end{pmatrix}. \end{aligned} \quad (\text{B.14})$$

Based on these, \hat{P} can be rewritten as

$$\hat{P} = \begin{pmatrix} \hat{v}_{\mathbf{k}} & \hat{v}_{\mathbf{k}} \\ -\hat{v}_{\mathbf{k}}^\dagger & \hat{v}_{\mathbf{k}} \end{pmatrix}, \quad (\text{B.15})$$

with

$$\hat{v}_{\mathbf{k}} = \frac{E_{\mathbf{k}} + \varepsilon_{\mathbf{k}}}{\sqrt{(E_{\mathbf{k}} + \varepsilon_{\mathbf{k}})^2 + |A_{\mathbf{k}}|^2}} \sigma_0, \quad \hat{v}_{\mathbf{k}} = \frac{-1}{\sqrt{(E_{\mathbf{k}} + \varepsilon_{\mathbf{k}})^2 + |A_{\mathbf{k}}|^2}} A(\mathbf{k}). \quad (\text{B.16})$$

Free energy of a fermionic system

In all the research projects discussed in this thesis, the free energy is an important quantity because it determines the preferred state of the system. In this Appendix, we derive the free energy for a fermionic system. Our starting point is a diagonal Hamiltonian on the form

$$H = H_0 + \sum_{\mathbf{k}, \alpha} E_{\mathbf{k}, \alpha} \gamma_{\mathbf{k}, \alpha}^\dagger \gamma_{\mathbf{k}, \alpha}. \quad (\text{C.1})$$

Here, H_0 is the constant part of the Hamiltonian, and $\gamma_{\mathbf{k}, \alpha}^\dagger$ ($\gamma_{\mathbf{k}, \alpha}$) is a creation (annihilation) operator for a fermion with momentum \mathbf{k} and e.g. a spin quantum number α . Moreover, $E_{\mathbf{k}, \alpha}$ are the energies of the associated single-particle states where the chemical potential, as well as e.g. the effect of a spin-splitting field, is absorbed. The grand canonical partition function for the system is expressed as

$$Z = \text{tr}(e^{-\beta H}) = \sum_{\{n_{\mathbf{k}, \alpha}\}} \langle \{n_{\mathbf{k}, \alpha}\} | e^{-\beta H} | \{n_{\mathbf{k}, \alpha}\} \rangle. \quad (\text{C.2})$$

Here, $\{n_{\mathbf{k}, \alpha}\}$ is a many-particle state defined by the occupation numbers of the single-particle states $|n_{\mathbf{k}, \alpha}\rangle$, where $\hat{n}_{\mathbf{k}, \alpha} |n_{\mathbf{k}, \alpha}\rangle = \gamma_{\mathbf{k}, \alpha}^\dagger \gamma_{\mathbf{k}, \alpha} |n_{\mathbf{k}, \alpha}\rangle = n_{\mathbf{k}, \alpha} |n_{\mathbf{k}, \alpha}\rangle$. Inserting the expression for our Hamiltonian in Eq. (C.1), we obtain

$$Z = \sum_{\{n_{\mathbf{k}, \alpha}\}} e^{-\beta H_0} \langle \{n_{\mathbf{k}, \alpha}\} | e^{-\beta \sum_{\mathbf{k}, \alpha} E_{\mathbf{k}, \alpha} \hat{n}_{\mathbf{k}, \alpha}} | \{n_{\mathbf{k}, \alpha}\} \rangle. \quad (\text{C.3})$$

As the many-particles states $\{n_{\mathbf{k},\alpha}\}$ are eigenstates of the Hamiltonian, we simply obtain

$$Z = \sum_{\{n_{\mathbf{k},\alpha}\}} e^{-\beta H_0} \prod_{\mathbf{k},\alpha} e^{-\beta E_{\mathbf{k},\alpha} n_{\mathbf{k},\alpha}}. \quad (\text{C.4})$$

As the occupation numbers for the different single-particle states are independent in the grand canonical ensemble, we can rewrite the above expression as a product of sums over the occupation of single-particle states. As there can only be either 0 or 1 fermion in each single-particle state, the partition function can then be expressed as

$$Z = e^{-\beta H_0} \prod_{\mathbf{k},\alpha} \sum_{n_{\mathbf{k},\alpha}=0,1} e^{-\beta E_{\mathbf{k},\alpha} n_{\mathbf{k},\alpha}} = e^{-\beta H_0} \prod_{\mathbf{k},\alpha} (1 + e^{-\beta E_{\mathbf{k},\alpha}}). \quad (\text{C.5})$$

Using the relation between the free energy F and partition function $Z = e^{-\beta F}$, the free energy of our system can be expressed as

$$F = H_0 - \frac{1}{\beta} \sum_{\mathbf{k},\alpha} \ln(1 + e^{-\beta E_{\mathbf{k},\alpha}}). \quad (\text{C.6})$$

Chandrasekhar-Clogston limit

Consider a single-band, spin-singlet superconductor with a gap around the Fermi level in the band structure. The gap is assumed to originate with a constant attractive interaction potential that is active in a thin shell $2\hbar\omega_c$ around the Fermi level. Further, the superconductor is subjected to a spin-splitting field h that breaks the degeneracy of the spin-up and spin-down energy bands. The free energy of the superconductor can then be expressed as

$$F^{\text{SC}} = N \frac{\Delta^2}{V} + \sum_{\mathbf{k}} (\varepsilon_{\mathbf{k}} - E_{\mathbf{k}}) - \frac{1}{\beta} \sum_{\mathbf{k}, \alpha} \ln(1 + e^{-\beta E_{\mathbf{k}, \alpha}}). \quad (\text{D.1})$$

For the discussion in this Appendix, the temperature will be set to zero. We first consider the case without a spin-splitting field. In this case, the free energy of the superconducting state is

$$F^{\text{SC}}(h = 0) \approx N \frac{\Delta_0^2}{V} + \sum_{\mathbf{k}} (\varepsilon_{\mathbf{k}} - E_{\mathbf{k}}). \quad (\text{D.2})$$

There are here no contributions from the \ln term as the temperature is set to zero and we are only summing over positive energies. Next, we take $h > 0$. As the superconducting gap is not affected by h at $T = 0$, the free energy is then

$$F^{\text{SC}}(h \neq 0) = N \frac{\Delta_0^2}{V} + \sum_{\mathbf{k}} (\varepsilon_{\mathbf{k}} - E_{\mathbf{k}}) - \frac{1}{\beta} \sum_{\mathbf{k}} \left[\ln(1 + e^{-\beta(\sqrt{\varepsilon_{\mathbf{k}}^2 + \Delta_0^2} - h)}) + \ln(1 + e^{-\beta(\sqrt{\varepsilon_{\mathbf{k}}^2 + \Delta_0^2} + h)}) \right]. \quad (\text{D.3})$$

While the second ln-term can be neglected, the first one can contribute for $h > \sqrt{\varepsilon_{\mathbf{k}}^2 + \Delta_0^2}$. We can express this as

$$F^{\text{SC}}(h \neq 0) \approx N \frac{\Delta_0^2}{V} + \sum_{\mathbf{k}} (\varepsilon_{\mathbf{k}} - E_{\mathbf{k}}) - \sum'_{\mathbf{k}} (h - \sqrt{\varepsilon_{\mathbf{k}}^2 + \Delta_0^2}), \quad (\text{D.4})$$

where the prime on the last momentum sum puts the restriction that $h > \sqrt{\varepsilon_{\mathbf{k}}^2 + \Delta_0^2}$. We then see that the free energy of the superconductor is unaffected by a spin-splitting field smaller than the superconducting gap. As we have considered the superconducting state both in the presence and the absence of a spin-splitting field, we move on to the case of the normal state of the system ($\Delta_0 = 0$). The free energy of the normal state in the presence of a spin-splitting field can be expressed as

$$F^{\text{N}}(h \neq 0) = \sum_{\mathbf{k}} (\varepsilon_{\mathbf{k}} - |\varepsilon_{\mathbf{k}}|) - \frac{1}{\beta} \sum_{\mathbf{k}, \alpha} \ln(1 + e^{-\beta(|\varepsilon_{\mathbf{k}}| - \alpha h)}). \quad (\text{D.5})$$

Summing over spin, the ln term becomes

$$-\frac{1}{\beta} \sum_{\mathbf{k}} \left[\ln(1 + e^{-\beta(|\varepsilon_{\mathbf{k}}| - h)}) + \ln(1 + e^{-\beta(|\varepsilon_{\mathbf{k}}| + h)}) \right], \quad (\text{D.6})$$

which vanishes at $h \rightarrow 0$. For $h > 0$, on the other hand, the first part can contribute for $h > \varepsilon_{\mathbf{k}}$. As the normal state has no gap in the band structure, the free energy is then altered as soon as $h > 0$. The change in the normal state free energy due to the introduction of a spin-splitting field is expressed as

$$F^{\text{N}}(h = 0) - F^{\text{N}}(h \neq 0) = \sum_{|\varepsilon_{\mathbf{k}}| < h} (h - |\varepsilon_{\mathbf{k}}|). \quad (\text{D.7})$$

We then see that the normal state free energy is lowered in the presence of a spin-splitting field, in contrast to the case of the superconducting state unless the spin-splitting field is larger than the gap.

Starting from zero field, the free energy of the superconducting state is lower than the free energy of the normal state by an amount

$$F^{\text{N}}(h=0) - F^{\text{Sc}}(h=0) = \sum_{\mathbf{k}} (E_{\mathbf{k}} - |\varepsilon_{\mathbf{k}}|) - N \frac{\Delta_0^2}{V}, \quad (\text{D.8})$$

which is referred to as the condensation energy. However, as the normal state free energy is lowered in the presence of a spin-splitting field, the free energies of the two states will eventually become equal as the field is increased. At this point, the system transitions from a superconducting to a normal state. Comparing Eqs. (D.7) and (D.8), we can therefore obtain an expression for the maximum spin-splitting field that superconductivity can coexist with. We thus write

$$\sum_{\mathbf{k}} (E_{\mathbf{k}} - |\varepsilon_{\mathbf{k}}|) - N \frac{\Delta_0^2}{V} = \sum_{\mathbf{k}}^{|\varepsilon_{\mathbf{k}}| < h} (h - |\varepsilon_{\mathbf{k}}|). \quad (\text{D.9})$$

First, consider the right-hand-side of the equation. In the thermodynamic limit, we go over to an integral over energy $\sum_{\mathbf{k}} \rightarrow \int D(\varepsilon) d\varepsilon$. We then have

$$\sum_{\mathbf{k}}^{|\varepsilon_{\mathbf{k}}| < h} (h - |\varepsilon_{\mathbf{k}}|) = 2 \int_0^h d\varepsilon N_0 (h - |\varepsilon|), \quad (\text{D.10})$$

where we have approximated the density of states with the density of states at the Fermi-level. Calculating the integral

$$\sum_{\mathbf{k}}^{|\varepsilon_{\mathbf{k}}| < h} (h - |\varepsilon_{\mathbf{k}}|) = N_0 h^2, \quad (\text{D.11})$$

gives us the right hand side of Eq. (D.9). In order to calculate the left hand side of Eq. (D.9), we again substitute the summation with integration and approximate the density of states with the density of states at the Fermi level. We then obtain for the first term on the left-hand-side

$$Q_1 \equiv \sum_{\mathbf{k}} (E_{\mathbf{k}} - |\varepsilon_{\mathbf{k}}|) = \int_{-\hbar\omega_c}^{\hbar\omega_c} d\varepsilon N_0 (\sqrt{\varepsilon^2 + \Delta_0^2} - |\varepsilon|), \quad (\text{D.12})$$

where we have used that the superconducting gap is assumed to only be present in a thin shell around the Fermi-level. Performing the integration, we find that

$$\begin{aligned}
Q_1 = & 2N_0 \left[\int_0^{\hbar\omega_c} \sqrt{|\varepsilon|^2 + \Delta_0^2} d|\varepsilon| - \int_0^{\hbar\omega_c} |\varepsilon| d|\varepsilon| \right] = \\
& N_0 \left[\hbar\omega_c \sqrt{\hbar^2\omega_c^2 + \Delta_0^2} + \Delta_0^2 \ln(\sqrt{\hbar^2\omega_c^2 + \Delta_0^2} + \hbar\omega_c) - \Delta_0^2 \ln(|\Delta_0|) - \hbar^2\omega_c^2 \right].
\end{aligned} \tag{D.13}$$

Cleaning up the expression

$$Q_1 = N_0 \left[\hbar^2\omega_c^2 \left(\sqrt{1 + \frac{\Delta_0^2}{\hbar^2\omega_c^2}} - 1 \right) + \Delta_0^2 \ln \left(\frac{\hbar\omega_c}{|\Delta_0|} \left(\sqrt{1 + \frac{\Delta_0^2}{\hbar^2\omega_c^2}} + 1 \right) \right) \right], \tag{D.14}$$

we next make the usual approximation $\Delta_0 \ll \hbar\omega_c$. Using that $\sqrt{1+x^2} - 1 \approx \frac{x^2}{2}$ and $\sqrt{1+x^2} - 1 \approx 2$ for $x \ll 1$, we then obtain

$$Q_1 = N_0 \frac{\Delta_0^2}{2} \left(1 + 2 \ln \left(2 \frac{\hbar\omega_c}{|\Delta_0|} \right) \right). \tag{D.15}$$

The only remaining piece in the puzzle is then the second term on the left-hand-side of Eq. (D.9). Using the gap equation

$$\Delta_0 = \frac{1}{N} \sum_{\mathbf{k}} V \frac{\Delta_0}{\sqrt{\varepsilon^2 + \Delta_0^2}} \frac{1}{2} \tanh \left(\frac{\beta}{2} (\sqrt{\varepsilon^2 + \Delta_0^2}) \right), \tag{D.16}$$

this second term Q_2 is expressed as

$$\begin{aligned}
Q_2 \equiv & -N \frac{\Delta_0^2}{V} = -\frac{1}{2} \sum_{\mathbf{k}} \frac{\Delta_0^2}{\sqrt{\varepsilon^2 + \Delta_0^2}} \tanh \left(\frac{\beta}{2} (\sqrt{\varepsilon^2 + \Delta_0^2}) \right) = \\
& -\frac{1}{2} \Delta_0^2 \int_{-\hbar\omega_c}^{\hbar\omega_c} D(\varepsilon) d\varepsilon \frac{1}{\sqrt{\varepsilon^2 + \Delta_0^2}} \tanh \left(\frac{\beta}{2} (\sqrt{\varepsilon^2 + \Delta_0^2}) \right).
\end{aligned} \tag{D.17}$$

As we integrate over a thin shell around the Fermi-level, we can once again approximate the density of states with the density of states at the Fermi-level. Further, as we are working at zero temperature $\tanh \left(\frac{\beta}{2} (\sqrt{\varepsilon^2 + \Delta_0^2}) \right) \approx 1$. Then,

$$\begin{aligned}
Q_2 = & -\Delta_0^2 N_0 \int_0^{\hbar\omega_c} d|\varepsilon| \frac{1}{\sqrt{|\varepsilon|^2 + \Delta_0^2}} = \\
& -\Delta_0^2 \frac{N_0}{2} \left[\ln\left(\frac{\hbar\omega_c}{\sqrt{\hbar^2\omega_c^2 + \Delta_0^2}} + 1\right) - \ln\left(\frac{\hbar\omega_c}{\sqrt{\hbar^2\omega_c^2 + \Delta_0^2}} - 1\right) \right].
\end{aligned} \tag{D.18}$$

Once again, we use that $\Delta_0 \ll \hbar\omega_c$

$$Q_2 = -\Delta_0^2 N_0 \ln\left(2\frac{\hbar\omega_c}{\Delta_0}\right). \tag{D.19}$$

Combining together all the parts, we then obtain

$$N_0 \frac{\Delta_0^2}{2} \left(1 + 2\ln\left(2\frac{\hbar\omega_c}{|\Delta_0|}\right)\right) - \Delta_0^2 N_0 \ln\left(2\frac{\hbar\omega_c}{\Delta_0}\right) = N_0 h^2. \tag{D.20}$$

We then see that a transition to the normal state takes place when

$$h_c = \frac{\Delta_0}{\sqrt{2}}. \tag{D.21}$$

This limit on the spin-splitting field that a spin-singlet superconductor can coexist with is referred to as the Chandrasekhar-Clogston limit.

Schrieffer-Wolff transformation

In this Appendix, we will discuss a canonical transformation referred to as the Schrieffer–Wolff transformation (SWt). Historically, this transformation was first used by Luttinger and Kohn [147]. The name of the transformation does, however, stem from a later article by Schrieffer and Wolff where they connected the Anderson and Kondo models used to describe itinerant electrons interacting with magnetic impurities [148]. In the third paper [3] included in this thesis, we have used this transformation to transform the interaction between itinerant electrons and magnetic impurities into an effective interaction between magnetic impurities mediated by itinerant electrons.

Suppose we have a non-perturbed Hamiltonian H_0 and introduce a small perturbation $\Delta H = \lambda\alpha$ where λ is a smallness parameter. In the third paper [3] included in this thesis, the perturbation is the interaction between the conductance electrons and the localized magnetic moments. We start by performing a unitary transformation UHU^\dagger , where $U = e^{iS}$. Then, using the Taylor expansion for $e^x = 1 + x + \frac{x^2}{2!} + \frac{x^3}{3!} + \dots$, we obtain that

$$\begin{aligned} \tilde{H} = e^{iS} H e^{-iS} &= \left(1 + (iS) + \frac{(iS)^2}{2!} + \dots \right) H \left(1 + (-iS) + \frac{(-iS)^2}{2!} + \dots \right) = \\ &= H + i[S, H_0] + i[S, \Delta H] - \frac{1}{2}[S, [S, H_0]] - \frac{1}{2}[S, [S, \Delta H]] + \dots = \\ &= H_0 + \Delta H + i[S, H_0] + i[S, \Delta H] - \frac{1}{2}[S, [S, H_0]] + O(\lambda^3). \end{aligned} \tag{E.1}$$

As we have considered λ to be small, we ignore the higher order terms in the above equation. Next, we define S such that the first order terms are

eliminated, $\Delta H + i[S, H_0] = 0$. Therefore, the effective Hamiltonian will be $\tilde{H} = H_0 + \frac{i}{2}[S, \Delta H]$.

As explained above, the Schrieffer-Wolff transformation consists of a unitary transformation that is chosen in order to eliminate linear terms in the perturbation. The unitary transformation is determined by the choice of S , which will vary from one system to the other. For the system that we have considered in the third paper [3] included in this thesis, a suitable Ansatz for S is

$$S = \sum_{\substack{\mathbf{k}, \mathbf{k}' \\ \alpha, \beta}} (A_{\mathbf{k}, \mathbf{k}'} \gamma_{\alpha, \beta}^\dagger \gamma_{\mathbf{k}, \alpha} \gamma_{\mathbf{k}', \beta} + B_{\mathbf{k}, \mathbf{k}'} \gamma_{\mathbf{k}, \alpha}^\dagger \gamma_{-\mathbf{k}', -\beta}^\dagger + C_{\mathbf{k}, \mathbf{k}'} \gamma_{-\mathbf{k}, -\alpha} \gamma_{\mathbf{k}', \beta} + D_{\mathbf{k}, \mathbf{k}'} \gamma_{-\mathbf{k}, -\alpha} \gamma_{-\mathbf{k}', -\beta}^\dagger). \quad (\text{E.2})$$

By inserting this Ansatz into $[S, H_0]$, computing the commutator, and requiring that $\Delta H + i[S, H_0] = 0$, the coefficients A, B, \dots can be determined. As the linear terms in the perturbation have then been eliminated, the effective Hamiltonian can be obtained by calculating $[S, \Delta H]$ and inserting the result into the expression for \tilde{H} .

Bibliography

- [1] A. Ghanbari, V. K. Risinggård, and J. Linder, *Scientific Reports* **11**, 5028 (2021).
- [2] A. Ghanbari, E. Erlandsen, and J. Linder, *Phys. Rev. B* **104**, 054502 (2021).
- [3] A. Ghanbari and J. Linder, *Phys. Rev. B* **104**, 094527 (2021).
- [4] A. Ghanbari, E. Erlandsen, A. Sudbø, and J. Linder, (2021), arXiv:2109.13245 [cond-mat.supr-con] .
- [5] S. Wolf and D. Treger, *IEEE Transactions on Magnetics* **36**, 2748 (2000).
- [6] S. A. Wolf, D. D. Awschalom, R. A. Buhrman, J. M. Daughton, S. von Molnár, M. L. Roukes, A. Y. Chtchelkanova, and D. M. Treger, *Science* **294**, 1488 (2001).
- [7] N. F. Mott, *Proceedings of the Royal Society of London. Series A - Mathematical and Physical Sciences* **156**, 368 (1936).
- [8] I. A. Campbell, A. Fert, and R. Pomeroy, *Philosophical Magazine* **15**, 977 (1967).
- [9] A. Fert and I. A. Campbell, *Phys. Rev. Lett.* **21**, 1190 (1968).
- [10] M. N. Baibich, J. M. Broto, A. Fert, F. N. Van Dau, F. Petroff, P. Etienne, G. Creuzet, A. Friederich, and J. Chazelas, *Phys. Rev. Lett.* **61**, 2472 (1988).
- [11] G. Binasch, P. Grünberg, F. Saurenbach, and W. Zinn, *Phys. Rev. B* **39**, 4828 (1989).
- [12] J. Daughton, *Thin Solid Films* **216**, 162 (1992), papers presented at the International Workshop on Science and Technology of Thin Films for the 21st Century, Evanston,IL, USA, July 28-August 2, 1991.
- [13] S. Tehrani, E. Chen, M. Durlam, T. Zhu, and H. Goronkin, in *International Electron Devices Meeting. Technical Digest* (1996) pp. 193–196.

-
- [14] S. Tehrani, E. Chen, M. Durlam, M. DeHerrera, J. Slaughter, J. Shi, and G. Kerszykowski, *Journal of Applied Physics* **85**, 5822 (1999).
- [15] T. Miyazaki and N. Tezuka, *Journal of Magnetism and Magnetic Materials* **139**, L231 (1995).
- [16] J. S. Moodera, L. R. Kinder, T. M. Wong, and R. Meservey, *Phys. Rev. Lett.* **74**, 3273 (1995).
- [17] M. Julliere, *Physics Letters A* **54**, 225 (1975).
- [18] J. E. Hirsch, *Phys. Rev. Lett.* **83**, 1834 (1999).
- [19] K. Uchida, S. Takahashi, K. Harii, J. Ieda, W. Koshibae, K. Ando, S. Maekawa, and E. Saitoh, *Nature* **455**, 778 (2008).
- [20] E. Saitoh, M. Ueda, H. Miyajima, and G. Tatara, *Appl. Phys. Lett.* **88**, 182509 (2006).
- [21] A. V. Chumak, V. I. Vasyuchka, A. A. Serga, and B. Hillebrands, *Nature Physics* **11**, 453 (2015).
- [22] A. A. Serga, A. V. Chumak, and B. Hillebrands, *Journal of Physics D: Applied Physics* **43**, 264002 (2012).
- [23] P. De Gennes, *Physics Letters* **23**, 10 (1966).
- [24] G. Deutscher and F. Meunier, *Phys. Rev. Lett.* **22**, 395 (1969).
- [25] J. J. Hauser, *Phys. Rev. Lett.* **23**, 374 (1969).
- [26] J. Linder and J. W. A. Robinson, *Nature Physics* **11**, 307 (2015).
- [27] F. S. Bergeret, A. F. Volkov, and K. B. Efetov, *Phys. Rev. Lett.* **86**, 4096 (2001).
- [28] J. W. A. Robinson, J. D. S. Witt, and M. G. Blamire, *Science* **329**, 59 (2010).
- [29] T. S. Khaire, M. A. Khasawneh, W. P. Pratt, and N. O. Birge, *Phys. Rev. Lett.* **104**, 137002 (2010).
- [30] D. Sprungmann, K. Westerholt, H. Zabel, M. Weides, and H. Kohlstedt, *Phys. Rev. B* **82**, 060505 (2010).

-
- [31] X. L. Wang, A. Di Bernardo, N. Banerjee, A. Wells, F. S. Bergeret, M. G. Blamire, and J. W. A. Robinson, *Phys. Rev. B* **89**, 140508 (2014).
- [32] J. W. Bray, *Journal of Electronic Materials* **24**, 1767 (1995).
- [33] R. Schwall, *IEEE Transactions on Magnetics* **23**, 1287 (1987).
- [34] T. Otto, *Safety for Particle Accelerators* (Springer Nature, 2021).
- [35] B. Josephson, *Physics Letters* **1**, 251 (1962).
- [36] T. Ryhänen, H. Seppä, R. Ilmoniemi, and J. Knuutila, *Journal of Low Temperature Physics* **76**, 287 (1989).
- [37] D. Koelle, R. Kleiner, F. Ludwig, E. Dantsker, and J. Clarke, *Rev. Mod. Phys.* **71**, 631 (1999).
- [38] M. Faley, U. Poppe, K. Urban, V. Y. Slobodchikov, Y. V. Maslennikov, A. Gapelyuk, B. Sawitzki, and A. Schirdewan, *Appl. Phys. Lett.* **81**, 2406 (2002).
- [39] J. Mannhart, *Superconductor Science and Technology* **9**, 49 (1996).
- [40] H. Hilgenkamp and J. Mannhart, *Rev. Mod. Phys.* **74**, 485 (2002).
- [41] R. D. Parks, ed., *Superconductivity 1st edition*. (CRC Press, 1969).
- [42] P. Morel and P. W. Anderson, *Phys. Rev.* **125**, 1263 (1962).
- [43] J. Bardeen, L. N. Cooper, and J. R. Schrieffer, *Phys. Rev.* **108**, 1175 (1957).
- [44] M. Peiniger and H. Piel, *IEEE Transactions on Nuclear Science* **32**, 3610 (1985).
- [45] M. Casas, J. M. Getino, M. de Llano, A. Puente, R. M. Quick, H. Rubio, and D. M. van der Walt, *Phys. Rev. B* **50**, 15945 (1994).
- [46] C. Kittel and P. McEuen, *Introduction to solid state physics (8th ed.)* (John Wiley & Sons, 1996).
- [47] J. F. Cochran and D. E. Mapother, *Phys. Rev.* **111**, 132 (1958).

-
- [48] B. T. Matthias, T. H. Geballe, and V. B. Compton, *Rev. Mod. Phys.* **35**, 1 (1963).
- [49] J. Eisenstein, *Rev. Mod. Phys.* **26**, 277 (1954).
- [50] D. D. Osheroff, R. C. Richardson, and D. M. Lee, *Phys. Rev. Lett.* **28**, 885 (1972).
- [51] F. Steglich, J. Aarts, C. D. Bredl, W. Lieke, D. Meschede, W. Franz, and H. Schäfer, *Phys. Rev. Lett.* **43**, 1892 (1979).
- [52] C. Geibel, S. Thies, D. Kaczorowski, A. Mehner, A. Grauel, B. Seidel, U. Ahlheim, R. Helfrich, K. Petersen, C. D. Bredl, and F. Steglich, *Zeitschrift für Physik B Condensed Matter* **83**, 305 (1991).
- [53] C. Geibel, C. Schank, S. Thies, H. Kitazawa, C. D. Bredl, A. Böhm, M. Rau, A. Grauel, R. Caspary, R. Helfrich, U. Ahlheim, G. Weber, and F. Steglich, *Zeitschrift für Physik B Condensed Matter* **84**, 1 (1991).
- [54] C. Petrovic, P. G. Pagliuso, M. F. Hundley, R. Movshovich, J. L. Sarrao, J. D. Thompson, Z. Fisk, and P. Monthoux, *Journal of Physics: Condensed Matter* **13**, L337 (2001).
- [55] D. Jérôme, A. Mazaud, M. Ribault, and K. Bechgaard, *J. Physique Lett.* **41**, 95 (1980).
- [56] J. G. Bednorz and K. A. Müller, *Zeitschrift für Physik B Condensed Matter* **64**, 189 (1986).
- [57] M. K. Wu, J. R. Ashburn, C. J. Torng, P. H. Hor, R. L. Meng, L. Gao, Z. J. Huang, Y. Q. Wang, and C. W. Chu, *Phys. Rev. Lett.* **58**, 908 (1987).
- [58] P. Dai, B. Chakoumakos, G. Sun, K. Wong, Y. Xin, and D. Lu, *Physica C: Superconductivity* **243**, 201 (1995).
- [59] H. Hosono and K. Kuroki, *Physica C: Superconductivity and its Applications* **514**, 399 (2015).
- [60] C. C. Tsuei and J. R. Kirtley, *Rev. Mod. Phys.* **72**, 969 (2000).
- [61] F. Wang and D. H. Lee, *Science* **332**, 200 (2011).

-
- [62] H. Hosono and K. Kuroki, *Physica C: Superconductivity and its Applications* **514**, 399 (2015).
- [63] K. Ishida, H. Mukuda, Y. Kitaoka, K. Asayama, Z. Q. Mao, Y. Mori, and Y. Maeno, *Nature* **396**, 658 (1998).
- [64] E. Hassinger, P. Bourgeois-Hope, H. Taniguchi, S. René de Cotret, G. Grissonnanche, M. S. Anwar, Y. Maeno, N. Doiron-Leyraud, and L. Taillefer, *Phys. Rev. X* **7**, 011032 (2017).
- [65] A. Chronister, A. Pustogow, N. Kikugawa, D. A. Sokolov, F. Jerzembeck, C. W. Hicks, A. P. Mackenzie, E. D. Bauer, and S. E. Brown, *PNAS* **118** (2021).
- [66] Y. Wang, Z. Chen, T. Shi, B. Moritz, Z.-X. Shen, and T. P. Devereaux, *Phys. Rev. Lett.* **127**, 197003 (2021).
- [67] K. Kuboki, *Journal of the Physical Society of Japan* **70**, 2698 (2001).
- [68] A. J. Leggett, *Rev. Mod. Phys.* **47**, 331 (1975).
- [69] W. Meissner and R. Ochsenfeld, *Naturwissenschaften* **21**, 787 (1933).
- [70] D. Cribier, B. Jacrot, L. Madhav Rao, and B. Farnoux, *Physics Letters* **9**, 106 (1964).
- [71] W. Fite and A. G. Redfield, *Phys. Rev. Lett.* **17**, 381 (1966).
- [72] A. A. Abrikosov, *JETP* **5**, 1174 (1957).
- [73] U. Essmann and H. Träuble, *Physics Letters A* **24**, 526 (1967).
- [74] F. London and H. London, *Proc. R. Soc. Lond. A* **149**, 71 (1935).
- [75] A. B. Pippard, *Proc. R. Soc. Lond. A* **203**, 210–223 (1950).
- [76] P. De Gennes, *Superconductivity of Metals and Alloys (P.A. Pincus, Trans.; 1st ed.)* (CRC Press, 1999).
- [77] A. Aharoni, *Introduction to the Theory of Ferromagnetism*, Vol. 109 (Clarendon Press, 2000).
- [78] W. Heisenberg, *Zeitschrift für Physik* **49**, 619 (1928).
- [79] A. I. Buzdin, *Rev. Mod. Phys.* **77**, 935 (2005).

-
- [80] E. A. Demler, G. B. Arnold, and M. R. Beasley, *Phys. Rev. B* **55**, 15174 (1997).
- [81] P. Fulde and R. A. Ferrell, *Phys. Rev.* **135**, A550 (1964).
- [82] A. Larkin and Y. N. Ovchinnikov, *Soviet Physics-JETP* **20**, 762 (1965).
- [83] F. S. Bergeret, M. Silaev, P. Virtanen, and T. T. Heikkilä, *Rev. Mod. Phys.* **90**, 041001 (2018).
- [84] B. S. Chandrasekhar, *Appl. Phys. Lett.* **1**, 7 (1962).
- [85] A. M. Clogston, *Phys. Rev. Lett.* **9**, 266 (1962).
- [86] B. Sutherland, *Phys. Rev. B* **34**, 5208 (1986).
- [87] E. H. Lieb, *Phys. Rev. Lett.* **62**, 1201 (1989).
- [88] A. Mielke, *J. Phys. A: Math. Gen.* **24**, 3311 (1991).
- [89] H. Tasaki, *Phys. Rev. Lett.* **69**, 1608 (1992).
- [90] A. Mielke and H. Tasaki, *Communications in Mathematical Physics* **158**, 341 (1993).
- [91] H. Tasaki, *Phys. Rev. Lett.* **73**, 1158 (1994).
- [92] S. Miyahara, S. Kusuta, and N. Furukawa, *Physica C: Superconductivity* **460-462**, 1145 (2007).
- [93] N. B. Kopnin, T. T. Heikkilä, and G. E. Volovik, *Phys. Rev. B* **83**, 220503 (2011).
- [94] R. Bistritzer and A. H. MacDonald, *Proceedings of the National Academy of Sciences* **108**, 12233 (2011).
- [95] Y. Cao, V. Fatemi, S. Fang, K. Watanabe, T. Taniguchi, E. Kaxiras, and P. Jarillo-Herrero, *Nature* **556**, 43 (2018).
- [96] H. Suhl, B. T. Matthias, and L. R. Walker, *Phys. Rev. Lett.* **3**, 552 (1959).
- [97] H. A. Kramers, *Physica* **1**, 182 (1934).

-
- [98] P. W. Anderson, *Phys. Rev.* **79**, 350 (1950).
- [99] C. Zener, *Phys. Rev.* **82**, 403 (1951).
- [100] M. A. Ruderman and C. Kittel, *Phys. Rev.* **96**, 99 (1954).
- [101] T. Kasuya, *Progress of Theoretical Physics* **16**, 45 (1956).
- [102] K. Yosida, *Phys. Rev.* **106**, 893 (1957).
- [103] A. M. Black-Schaffer, *Phys. Rev. B* **81**, 205416 (2010).
- [104] M. Sherafati and S. Satpathy, *Phys. Rev. B* **83**, 165425 (2011).
- [105] Q. Liu, C.-X. Liu, C. Xu, X.-L. Qi, and S.-C. Zhang, *Phys. Rev. Lett.* **102**, 156603 (2009).
- [106] N. E. Alekseevskii, I. A. Garifullin, B. I. Kochelaev, and E. G. Kharakhash'yan, *Zh. Eksp. Teor. Fiz.* **72**, 1523 (1977).
- [107] B. Kochelaev, L. Tagirov, and M. Khusainov, *Zh. Eksp. Teor. Fiz.* **76**, 578 (1979).
- [108] M. G. Khusainov, *Zh. Eksp. Teor. Fiz.* **109**, 524 (1996).
- [109] D. N. Aristov, S. V. Maleyev, and A. G. Yashenkin, *Z. Phys. B* **102**, 467 (1997).
- [110] M. M. Valizadeh, *International Journal of Modern Physics B* **30**, 1650234 (2016).
- [111] F. Parhizgar, R. Asgari, S. H. Abedinpour, and M. Zareyan, *Phys. Rev. B* **87**, 125402 (2013).
- [112] H. Imamura, P. Bruno, and Y. Utsumi, *Phys. Rev. B* **69**, 121303 (2004).
- [113] J.-J. Zhu, D.-X. Yao, S.-C. Zhang, and K. Chang, *Phys. Rev. Lett.* **106**, 097201 (2011).
- [114] I. Dzialoshinskii, *Soviet Physics Jetp* **5**, 1259 (1957).
- [115] T. Moriya, *Phys. Rev.* **120**, 91 (1960).

-
- [116] F. Delgado, J. J. Palacios, and J. Fernández-Rossier, *Phys. Rev. Lett.* **104**, 026601 (2010).
- [117] S. Loth, K. von Bergmann, M. Ternes, A. F. Otte, C. P. Lutz, and A. J. Heinrich, *Nature Physics* **6**, 340 (2010).
- [118] B. Dieny, V. S. Speriosu, S. S. P. Parkin, B. A. Gurney, D. R. Wilhoit, and D. Mauri, *Phys. Rev. B* **43**, 1297 (1991).
- [119] R. Jungblut, R. Coehoorn, M. Johnson, J. Aan de Stegge, and A. Reinders, *Journal of Applied Physics* **75**, 6659 (1994).
- [120] T. Moran, J. Gallego, and I. K. Schuller, *Journal of Applied Physics* **78**, 1887 (1995).
- [121] W. H. Meiklejohn and C. P. Bean, *Phys. Rev.* **102**, 1413 (1956).
- [122] J. Nogués and I. K. Schuller, *Journal of Magnetism and Magnetic Materials* **192**, 203 (1999).
- [123] Y. Zhu, A. Pal, M. G. Blamire, and Z. H. Barber, *Nature Materials* **16**, 195 (2017).
- [124] L. R. Tagirov, *Phys. Rev. Lett.* **83**, 2058 (1999).
- [125] A. I. Buzdin, A. V. Vedyayev, and N. V. Ryzhanova, *Europhysics Letters (EPL)* **48**, 686 (1999).
- [126] A. F. Andreev, *JETP* **46**, 1823 (1964).
- [127] C. Bruder, *Phys. Rev. B* **41**, 4017 (1990).
- [128] J. M. Byers and M. E. Flatté, *Phys. Rev. Lett.* **74**, 306 (1995).
- [129] G. Deutscher and D. Feinberg, *Applied Physics Letters* **76**, 487 (2000).
- [130] D. Beckmann, H. B. Weber, and H. v. Löhneysen, *Phys. Rev. Lett.* **93**, 197003 (2004).
- [131] S. Russo, M. Kroug, T. M. Klapwijk, and A. F. Morpurgo, *Phys. Rev. Lett.* **95**, 027002 (2005).
- [132] C. R. Hu, *Phys. Rev. Lett.* **72**, 1526 (1994).

-
- [133] T. Löfwander, V. S. Shumeiko, and G. Wendin, *Supercond. Sci. Technol.* **14**, R53 (2001).
- [134] P. de Gennes and D. Saint-James, *Physics Letters* **4**, 151 (1963).
- [135] Y. Tanaka and S. Kashiwaya, *Phys. Rev. Lett.* **74**, 3451 (1995).
- [136] M. Matsumoto and H. Shiba, *J. Phys. Soc. Jpn* **64**, 1703 (1995).
- [137] Y. S. Barash, H. Burkhardt, and D. Rainer, *Phys. Rev. Lett.* **77**, 4070 (1996).
- [138] J. Geerk, X. X. Xi, and G. Linker, *Zeitschrift für Physik B Condensed Matter* **73**, 329 (1988).
- [139] J. Lesueur, L. Greene, W. Feldmann, and A. Inam, *Physica C: Superconductivity* **191**, 325 (1992).
- [140] M. Covington, R. Scheuerer, K. Bloom, and L. H. Greene, *Appl. Phys. Lett.* **68**, 1717 (1996).
- [141] C. R. Hu and X. Z. Yan, *Phys. Rev. B* **60**, R12573 (1999).
- [142] J.-X. Zhu and C. S. Ting, *Phys. Rev. B* **61**, 1456 (2000).
- [143] J. M. Park, Y. Cao, K. Watanabe, T. Taniguchi, and P. Jarillo-Herrero, *Nature* **590**, 249 (2021).
- [144] Y. Cao, J. M. Park, K. Watanabe, T. Taniguchi, and P. Jarillo-Herrero, *Nature* **595**, 526 (2021).
- [145] W. Qin and A. H. MacDonald, *Phys. Rev. Lett.* **127**, 097001 (2021).
- [146] A. Ozaeta, P. Virtanen, F. S. Bergeret, and T. T. Heikkilä, *Phys. Rev. Lett.* **112**, 057001 (2014).
- [147] J. M. Luttinger and W. Kohn, *Phys. Rev.* **97**, 869 (1955).
- [148] J. R. Schrieffer and P. A. Wolff, *Phys. Rev.* **149**, 491 (1966).

Self-consistent solution for the magnetic exchange interaction mediated by a superconductor

Sci. Rep. **11**, 5028 (2021)

Authors

Atousa Ghanbari
Vetle K. Risinggård
Jacob Linder



OPEN

Self-consistent solution for the magnetic exchange interaction mediated by a superconductor

Atousa Ghanbari, Vetle K. Risinggård & Jacob Linder[✉]

We theoretically determine the magnetic exchange interaction between two ferromagnets coupled by a superconductor using a tight-binding lattice model. The main purpose of this study is to determine how the self-consistently determined superconducting state influences the exchange interaction and the preferred ground-state of the system, including the role of impurity scattering. We find that the superconducting state eliminates RKKY-like oscillations for a sufficiently large superconducting gap, making the anti-parallel orientation the ground state of the system. Interestingly, the superconducting gap is larger in the parallel configuration than in the anti-parallel configuration, giving a larger superconducting condensation energy, even when the preferred ground state is anti-parallel. We also show that increasing the impurity concentration in the superconductor causes the exchange interaction to decrease, likely due to an increasing localization of the mediating quasiparticles in the superconductor.

The Ruderman–Kittel–Kasuya–Yosida (RKKY) is an indirect exchange interaction between localized spins mediated by itinerant electrons in metals¹. This interaction played an important role in the discovery of giant magnetoresistance (GMR)^{2,3} and has been studied in numerous materials^{4–9}.

The combination of magnetic and superconducting materials has been widely studied due to interesting features which cannot be observed in separate materials^{10–19}. Recently, the influence of superconductivity on the magnetic state was experimentally studied in a superconducting spin valve (SSV), GdN–Nb–GdN²⁰. On the basis of the de Gennes model²¹, it was shown that the superconductor promoted an anti-parallel configuration as the ground-state configuration. In the de Gennes model, a superconductor in an anti-parallel SSV has a higher critical temperature T_c than in the parallel orientation, leading to a larger superconducting gap in the anti-parallel configuration.

The interaction between localized magnetic moments through dirty *s*-wave superconductors^{22–24} has previously been found to contain two contributions. One contribution is from the usual RKKY interaction and a second contribution from a longer ranged interaction, decaying exponentially over the superconducting coherence length ξ and with a weaker power-law suppression, which favors an antiferromagnetic alignment. Later, the interaction through a *d*-wave superconductor with an anisotropic order parameter was studied²⁵. It was shown on the basis of analytical approximations that this interaction, similarly to the *s*-wave case, contains one oscillatory term and one term favoring an anti-parallel configuration. The oscillations occur when the length of the superconductor (L_S) is smaller than the coherence length (ξ) while the term favoring an anti-ferromagnetic configuration of the system occurs when $L_S > \xi$. The latter term was found to be proportional to the superconducting gap. Very recently, it was experimentally shown that in a *d*-wave SSV, the anti-parallel ground-state was favored for some specific lengths of the superconducting system and that nodal quasiparticles likely played a central role in mediating the magnetic coupling²⁶.

In this work, we address numerically and, importantly, self-consistently the effect of conventional *s*-wave singlet superconductors on the indirect exchange coupling (J) between two ferromagnetic contacts in a F–S–F structure. The free energy of the system, which is the main quantity of interest in this work, is manifested in a clear experimental observable: namely, the ground-state magnetic configuration of the system. Previous works considering superconducting spin-valves have also considered the superconducting transition temperature as a quantity of interest with respect to possible cryogenic applications. However, a shift in the preferred magnetic

Department of Physics, Center for Quantum Spintronics, Norwegian University of Science and Technology, 7491 Trondheim, Norway. ✉email: jacob.linder@ntnu.no

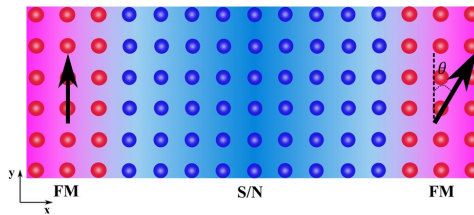


Figure 1. Schematic illustration of a superconducting spin valve (SSV) with magnetic moment of the two ferromagnets aligned at relative angle θ . Two cases will be consider here, one with $\theta = 0^\circ$ which is called P orientation and the other one is AP orientation with $\theta = 180^\circ$.

orientation (parallel (P: $\theta = 0^\circ$) or antiparallel (AP: $\theta = 180^\circ$)) of the spin-valve will also be a relevant quantity in this regard. Therefore, determining how the interaction between the ferromagnets depends on the superconducting layer is a task which is both of fundamental and possible practical interest. In contrast to Refs.^{22–25}, we compute the order parameter self-consistently and account for both the superconducting proximity effect in the ferromagnets and the magnetic proximity effect in the superconducting region. The self-consistent computation of the superconducting order parameter includes not only the effect of the magnetic configuration on the local spin density of the quasiparticles mediating the RKKY interaction, but also the effect of the magnetic configuration on the magnitude of the superconducting gap. This is an important result because as we show in the results section, the difference in gap-magnitude between the parallel and anti-parallel configuration does affect the RKKY-coupling between the ferromagnets. Due to the proximity effect between the superconductors and the ferromagnet, the superconducting gap can be strongly affected by the magnetic configuration, and thus requires a self-consistent calculation, unlike Refs.^{22–24} that considered isolated magnetic impurities. In a singlet superconductor, electrons with zero total spin and opposite momentum constitute the Cooper pairs: ($k \uparrow, -k \downarrow$). These Cooper pairs can penetrate into a weak ferromagnet (FM) which has been brought in contact with the superconductor²⁷ in an oscillatory fashion. Bringing another ferromagnetic layer in contact with this bilayer makes the SSV.

We first briefly reproduce the well-known RKKY-like oscillations of an F–N–F system to contrast these results with what happens in the superconducting state. We consider a finite size system in two dimensions, meaning that we do not assume periodic boundary conditions in any direction. Then, by substituting the central part with a singlet superconductor which leads to a F–S–F structure (Fig. 1), we demonstrate that two types of behaviour take place. For thin superconductors, J oscillates around zero whereas for thick ones the coupling takes values $J > 0$, favoring the AP configuration ($\theta = 180^\circ$), and reduces monotonically as the length is further increased. When the central part is a superconductor with small gap connected to two weakly polarized ferromagnets, we only find RKKY-like oscillations mediated by quasiparticles in the superconductor. In contrast, when the superconducting gap is large or if the exchange field in the ferromagnet is strong, $J > 0$ and the interaction displays either a pure monotonic decay or with superimposed oscillations.

Afterwards, we consider the effect of impurities on J in the F–S–F spin valve. When considering the impurity average $\langle J \rangle_{\text{imp}}$ for a large number of realizations with random impurity configurations, we find that increasing the impurity concentration in the superconductor causes the exchange interaction to decrease. This is likely due to an increasing localization of the mediating quasiparticles in the superconductor^{28,29}.

Theory

The indirect exchange interaction between the ferromagnets in F–N–F or F–S–F structures is defined by $J = F^{\uparrow\uparrow} - F^{\uparrow\downarrow}$. Here, $F^{\uparrow\uparrow}$ is the free energy when the ferromagnetic contacts have a parallel (P) orientation ($\theta = 0^\circ$) and $F^{\uparrow\downarrow}$ is the free energy when they have an anti-parallel (AP) orientation ($\theta = 180^\circ$). In this work, we only consider P and AP configurations as the possible ground states. This assumption is possible as we will consider strong anisotropy easy-axis, macrospin ferromagnets where the exchange stiffness is large enough to preclude any inhomogeneous textures, such as domain walls or spin spirals. Moreover, we do not consider the Dzyaloshinskii–Moryia-type³⁰ interactions at the interfaces, which may lead to noncollinear magnetization configurations. Therefore, the free energy of such a system is defined by

$$F = H_0 - \frac{1}{\beta} \sum_n \ln(1 + e^{-\beta E_n/2}). \quad (1)$$

Here, $\beta = \frac{1}{k_B T}$ and k_B is the Boltzmann constant and T is the temperature. H_0 is a constant term to be specified later, which consists of a superconducting constant term (H_0^S) and chemical potential constant term (H_0^{μ}). H_0^S arises as a result of performing a mean-field approximation while H_0^{μ} is due to a symmetrization of the Hamiltonian. Moreover, E_n is the n th eigenvalue and will be calculated by means of diagonalizing a tight-binding Hamiltonian for the structure of interest. The Hamiltonian is as follows,

$$H = - \sum_{(i,j),\alpha} t_{ij} c_{i\alpha}^\dagger c_{j\alpha} - \sum_{i,\alpha} \mu_i n_{i\alpha} - \sum_i U_i n_{i\uparrow} n_{i\downarrow} - \sum_{i\alpha\beta} (\mathbf{h}_i^\delta \cdot \boldsymbol{\sigma})_{\alpha\beta} c_{i\alpha}^\dagger c_{i\beta} \tag{2}$$

Here, $c_{i\alpha}^\dagger$ ($c_{i\alpha}$) creates (annihilates) an electron with spin α at site $i = (i_x, i_y)$ with $i_x = 1, \dots, N_x$ and $i_y = 1, \dots, N_y$. Also, t_{ij} is the hopping integral between nearest-neighbor sites and we assume that it has a constant value t . μ_i is the chemical potential at site i while $n_{i\alpha} = c_{i\alpha}^\dagger c_{i\alpha}$ is the number operator. The fourth term in the Hamiltonian represents the local exchange interaction with h_i^δ being the strength of this field in the left ($\delta = L$) or right ($\delta = R$) ferromagnets. Also, $h_i^L = h_i(0, 1, 0)$, $h_i^R = h_i(\sin(\theta), \cos(\theta), 0)$ and $\boldsymbol{\sigma} = (\sigma_x, \sigma_y, \sigma_z)$ the Pauli matrices. Although considering h as a fixed input parameter is a standard approach in much of the literature, we have also checked if our results hold when the magnetization is solved self-consistently as well. A brief study of f with self-consistent magnetization is included in the Supplementary information. We find that solving the magnetization self-consistently has very little effect on the results for the case when we have open boundary conditions along the y -direction. It does not change the physics for the 2D system compared to using a fixed input-value for h . We consider a singlet superconductor for the central part, modelling the interaction as an on-site attractive U as the third term of Hamiltonian. $U_i = U > 0$ is the local attractive interaction which creates Cooper pairs in the superconductor while it is zero elsewhere. We treat the interaction term by a mean-field approximation to simplify the problem,

$$- \sum_i U_i n_{i\uparrow} n_{i\downarrow} = - \sum_i U_i \left(c_{i\uparrow}^\dagger c_{i\downarrow}^\dagger \langle c_{i\downarrow} c_{i\uparrow} \rangle + c_{i\downarrow} c_{i\uparrow} \langle c_{i\uparrow}^\dagger c_{i\downarrow}^\dagger \rangle - \langle c_{i\downarrow} c_{i\uparrow} \rangle \langle c_{i\uparrow}^\dagger c_{i\downarrow}^\dagger \rangle \right) \tag{3}$$

If we define superconducting gap as $\Delta_i = -U_i \langle c_{i\downarrow} c_{i\uparrow} \rangle$, then

$$- \sum_i U_i n_{i\uparrow} n_{i\downarrow} = \sum_i \left(c_{i\uparrow}^\dagger c_{i\downarrow}^\dagger \Delta_i + c_{i\downarrow} c_{i\uparrow} \Delta_i^* \right) + H_0^S \tag{4}$$

where we have defined

$$H_0^S = \sum_i \frac{|\Delta_i|^2}{U_i} \tag{5}$$

The Hamiltonian does not contain any constant mean-field term containing the magnetic order parameter since we do not solve for the magnetization self-consistently.

We proceed to explain how the eigenvalues E_n are obtained. Our Hamiltonian Eq. (2) is bilinear in the fermion operators and can be diagonalized. Choosing the following basis,

$$W^\dagger = \left[D_1^\dagger \ D_2^\dagger \ D_3^\dagger \ \dots \ D_{N_y}^\dagger \right], \tag{6}$$

where we have defined

$$D_{i_y}^\dagger = \left[B_{(1,i_y)}^\dagger \ B_{(2,i_y)}^\dagger \ B_{(3,i_y)}^\dagger \ \dots \ B_{(N_x,i_y)}^\dagger \right] \tag{7}$$

with $i_y = 1, \dots, N_y$ and

$$B_i^\dagger = \left[c_{i\uparrow}^\dagger \ c_{i\downarrow}^\dagger \ c_{i\uparrow} \ c_{i\downarrow} \right], \tag{8}$$

the Hamiltonian may now be written as

$$H = H_0 + \frac{1}{2} W^\dagger S W = H_0 + \frac{1}{2} \sum_{ij} B_i^\dagger h_{ij} B_j \tag{9}$$

Here, H_0 is the constant term that we discussed previously, and

$$S = \begin{bmatrix} S_{11} & \dots & S_{1,N_y} \\ \vdots & \ddots & \vdots \\ S_{N_y,1} & \dots & S_{N_y,N_y} \end{bmatrix} \tag{10}$$

with

$$S_{i_y j_y} = \begin{bmatrix} h_{(1,i_y)(1,j_y)} & \dots & h_{(1,i_y)(N_x,j_y)} \\ \vdots & \ddots & \vdots \\ h_{(N_x,i_y)(1,j_y)} & \dots & h_{(N_x,i_y)(N_x,j_y)} \end{bmatrix} \tag{11}$$

Finally, the 4×4 matrix for interaction between sites i and j is

$$h_{ij} = - \left[\frac{t}{2} (\delta_{i_x, j_x-1} + \delta_{i_x, j_x+1}) + \mu_i \delta_{i_x, j_x} \right] \delta_{i_y, j_y} \tau_3 \sigma_0 - \left[\frac{t}{2} (\delta_{i_y, j_y-1} + \delta_{i_y, j_y+1}) + \mu_i \delta_{i_y, j_y} \right] \delta_{i_x, j_x} \tau_3 \sigma_0 + \left[-h_i^z \tau_3 \sigma_z - h_i^x \tau_3 \sigma_x - h_i^y \tau_3 \sigma_y + \Delta_{i_x, i_y} i \tau^+ \sigma_y - \Delta_{i_x, i_y}^* i \tau^- \sigma_y \right] \delta_{i_x, j_x} \delta_{i_y, j_y}. \tag{12}$$

Here, $\tau_m \sigma_l = \tau_m \otimes \sigma_l$ and $\tau^\pm = \frac{1}{2}(\tau_1 \pm i\tau_2)$. S is Hermitian and can be diagonalized numerically. Note that we are considering a finite size 2D system without any periodic boundary conditions. The 2D model is an approximation that is necessary because doing the calculations in 3D becomes numerically too demanding in terms of computational time. Although it could be interesting to consider how a 3D computation alters the result, we do not expect any qualitatively new effects. Diagonalizing the Hamiltonian by introducing a new basis gives

$$H = H_0 + \frac{1}{2} \sum_n E_n \gamma_n^\dagger \gamma_n. \tag{13}$$

The eigenfunctions for S are

$$\Phi_n^\dagger = [\phi_{1n}^\dagger \ \phi_{2n}^\dagger \ \dots \ \phi_{N_y n}^\dagger], \tag{14}$$

where we have defined

$$\begin{aligned} \phi_{i_y, n}^\dagger &= [\varphi_{(1, i_y), n}^\dagger \ \varphi_{(2, i_y), n}^\dagger \ \dots \ \varphi_{(N_x, i_y), n}^\dagger], \\ \varphi_{(i_x, i_y), n}^\dagger &= [v_{(i_x, i_y), n}^* \ v_{(i_x, i_y), n}^* \ \omega_{(i_x, i_y), n}^* \ \chi_{(i_x, i_y), n}^*]. \end{aligned} \tag{15}$$

The original creation and annihilation operators $\{c^\dagger, c\}$ now can be expressed with new quasiparticle operators,

$$\begin{aligned} c_{i\uparrow} &= \sum_n v_{i,n} \gamma_n, \quad c_{i\downarrow} = \sum_n v_{i,n} \gamma_n, \\ c_{i\uparrow}^\dagger &= \sum_n \omega_{i,n} \gamma_n, \quad c_{i\downarrow}^\dagger = \sum_n \chi_{i,n} \gamma_n. \end{aligned} \tag{16}$$

Using these, we obtain a self-consistency equation for Δ_i ,

$$\Delta_i = -U_i \sum_n v_{i,n} \omega_{i,n}^* (1 - f(E_n/2)). \tag{17}$$

The local density of states (LDOS) is the density of states at one site and in our model it can be calculated for $T = 0$. The number of charges at site i is given by

$$\rho_i = \sum_\alpha \langle c_{i\alpha}^\dagger c_{i\alpha} \rangle. \tag{18}$$

At an arbitrary temperature, the number of charges at site i is

$$\rho_i = \int_{-\infty}^{+\infty} N_i(E) f(E) dE. \tag{19}$$

Here, $N_i(E)$ is the local density of states at site i and $f(E)$ is the Fermi-Dirac distribution with energy E measured relative the chemical potential. When $T = 0$, we know that $f(E) = 1$ for $E < 0$ and $f(E) = 0$ when $E > 0$. Therefore, the LDOS takes the form:

$$N_i(E) = \sum_n (|v_{in}|^2 + |v_{in}^\dagger|^2) \delta(E_n/2 - E). \tag{20}$$

In our model, the proximity effect of the superconductor into the ferromagnets (induced Cooper pair correlations) is quantified by the anomalous Green function $F_i = -\langle c_{i\downarrow} c_{i\uparrow} \rangle$. Also, the inverse proximity effect causing an induction of magnetic polarization in the superconductor is accounted for by $M_i^y = \langle S_i^y \rangle$ where the $\langle \dots \rangle$ notation denotes expectation value. The spin operator is $S_i^y = \sum_{\alpha\beta} c_{i\alpha}^\dagger (\sigma_{\alpha\beta})_y c_{i\beta}$. Therefore, the magnetization along the y -direction in the system is given by

$$M_i^y = \sum_n i(-v_{in}^* v_{in} + v_{in}^* v_{in}) f\left(\frac{E_n}{2}\right) \tag{21}$$

Equation (17) is solved self-consistently. By considering an initial value for the gap, we diagonalize the Hamiltonian to obtain the eigenvalues (E_n), and eigenfunctions [Eq. (14)] to compute $v_{i,n}$ and $\omega_{i,n}$. By means of Eq. (17), we can then compute a new value for the gap and once again diagonalize the Hamiltonian with the new value for the gap. This process is repeated until the relative change in the gap value between iterations is smaller than the convergence criterion. The criterion for numerical convergence of the superconducting gap is set to be a relative change of 5×10^{-4} . To ensure that the self-consistent solution converges to the ground-state, we have checked several possible initial values for the superconducting order parameter.

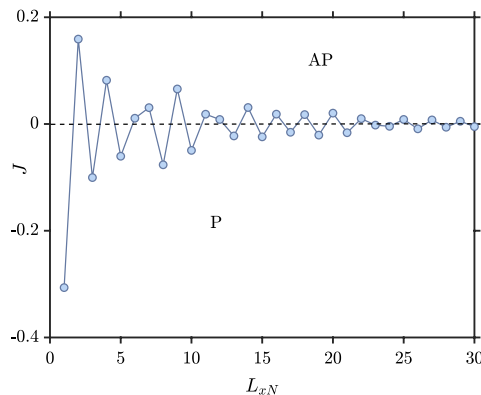


Figure 2. The indirect exchange interaction J between the two ferromagnetic contacts mediated by a normal material (F–N–F structure) when $L_y = 10$, $L_{xF} = 2$, $\mu_N = 0.8t$, $\mu_F = 0.9t$, $|h_i^L| = |h_i^R| = h_i = 1t$ and $k_B T = 0.01t$.

Results

F–N–F junction, briefly revisited. The main purpose of this paper is to investigate the indirect exchange coupling between two ferromagnets separated by a superconductor when solving self-consistently for the order parameter and taking into account both the proximity effect and the inverse proximity effect. We will consider a large range of h -values corresponding to either weakly polarized ferromagnets, such as PdNi, or strongly polarized elemental ferromagnets like Co or Fe. Before considering the superconducting case, it is worth considering briefly a three layer F–N–F structure as shown in Fig. 1. We include this treatment so that the reader can more easily contrast the normal and superconducting case. We choose a representative set of parameters as $L_y = 10$, $L_{xF} = 2$, $\mu_N = 0.8t$, $\mu_F = 0.9t$, and $k_B T = 0.01t$. In our notation, L_y is the number of lattice sites along the y -axis and L_{xF} is the number of lattice sites along the x -axis in the ferromagnets. The length of the ferromagnetic part has little influence on the final results in the F–N–F case and also does not change the results qualitatively in the F–S–F case. Therefore, we have chosen a small value for L_{xF} to reduce the required time of the numerical simulations. Both ferromagnetic contacts have the same exchange field strength and the magnetization is directed along \hat{y} ($|h_i^L| = |h_i^R| = h_i$). As the length of the normal part increases, the amplitude of the well-known RKKY-like oscillations in the F–N–F structure decreases as shown in Fig. 2. These oscillations indicate a switching between P and AP configurations as the ground-state of the junction: $J > 0$ corresponds to an AP configuration, while $J < 0$ corresponds to a P configuration.

Figure 3 shows J as a function of the exchange field strength in the ferromagnets (h_i) for several different normal region lengths. It demonstrates that J not only oscillates as a function of L_{xN} , but also as a function of h_i . The oscillations stem from the fact that the eigenstates for the quasiparticle excitations in the system interfere constructively or destructively at the ferromagnetic contacts, depending on the length L_{xN} and the exchange field h_i since both these quantities determine the phase-change of an eigenstate as one moves across the normal metal.

Despite the oscillations for small exchange field strengths, J monotonically decreases when h_i becomes sufficiently large. This decay is likely related to the depletion in the number of available states around the Fermi level in the ferromagnetic part as shown in Fig. 4.

F–S–F junction. We now turn to the main topic of this manuscript, namely a study of how the exchange interaction between two ferromagnets is mediated by an s -wave superconductor. Our results for the RKKY interaction in the superconducting state will be relevant for materials which have a (nearly) isotropic superconducting gap and where the ratio Δ/μ between the gap Δ and the Fermi energy μ is relatively large. The reason for the latter criterion is that large values of the gap is required in the lattice BdG formalism in order to work with systems that have a computationally manageable size. Although our model is simplified and approximative, there exists materials which matches the parameter-choice in our manuscript for the energy scales involved. One such superconducting material is FeSe³¹ which is known to have a large ratio Δ/μ of order ~ 0.1 , as in our parameter choice. The exact crystal structure of FeSe differs from our model and its full tight-binding model is more complex than the simple model used in our manuscript, but the projection of the FeSe crystal structure onto the plane is in fact a square lattice. Another material with a high ratio Δ/μ is FeTe_{0.6}Se_{0.4}³² which would also resemble our parameter-choice in terms of the relative size of the gap and Fermi energy.

In Fig. 5, we plot J against the length of the superconducting region for three different on-site pairing interactions $U/t = 1$, $U/t = 1.5$ and $U/t = 2$. The superconducting gap Δ tends to zero for a short superconductor with a weak superconducting interaction U . For the case of $U/t = 1$, J is the same as the F–N–F case. This is simply

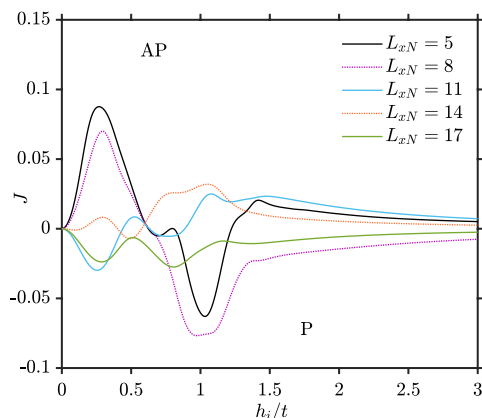


Figure 3. Indirect exchange interaction as a function of the exchange field strength of the ferromagnets for the F–N–F structure). Here, $L_y = 10$, $L_{xF} = 2$, $\mu_N = 0.8t$, $\mu_F = 0.9t$ and $k_B T = 0.01t$.

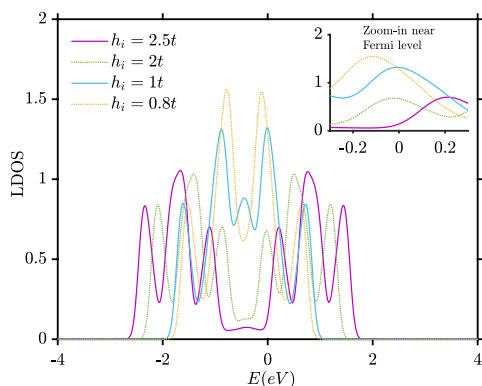


Figure 4. Local density of states (LDOS) for the (2,2) site inside the left ferromagnet as a function of energy for 4 different h_i . Here, $L_y = 10$, $L_{xF} = 2$, $L_{xS} = 8$, $\mu_N = 0.8t$, $\mu_F = 0.9t$, $k_B T = 0.01t$. The dashed box indicates an area around the Fermi energy.

because Δ is zero for short superconductors and when L_{xS} has increased sufficiently to render Δ non-zero, $J \rightarrow 0$ since the distance between the ferromagnets is then too large.

For the case of $U/t = 1.5$, there are two mechanisms competing against each other. One is the conventional RKKY-like oscillations mediated by quasiparticles. The other mechanism is the blocking of states that can mediate the interaction due to the superconducting gap. This can be seen from blue curve of Fig. 5. For short superconductors, the RKKY-like oscillations are approximately the same as in the F–N–F case because the gap is too small to block any significant fraction of the quasiparticles. For longer superconductors the gap increases and dominates the indirect exchange interaction J .

Figure 6a,b show that for $L_{xS} = 4$ and $L_{xS} = 5$, the gap is finite in both the P and AP configuration, but still RKKY-like oscillations dominate as seen in Fig. 5 for $U/t = 1.5$. However, as L_{xS} increases in Fig. 6c,d, Δ becomes sufficiently large to block the oscillations caused by quasiparticles. Now, we see that $\Delta_P > \Delta_{AP}$ which leads to $J > 0$, favoring an AP magnetic configuration as the ground state. At first glance, this might seem strange since a larger Δ in the P configuration should give a larger superconducting condensation energy gain compared to the AP configuration. However, the configuration with the largest gap will also block the largest amount of quasiparticles that can mediate the interaction between the ferromagnets and lower the free energy. In our numerical simulations, we find that when the gap is large enough in magnitude, it is the latter blocking effect that determines the ground-state of the system. Hence, $\Delta_P > \Delta_{AP}$ causes $J > 0$.

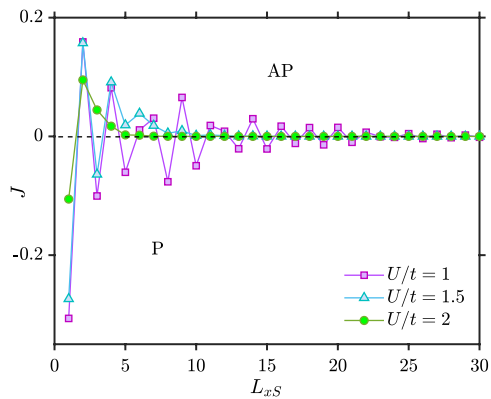


Figure 5. J vs the length of superconducting part (L_{xS}) for the F-S-F structure. When $L_y = 10$, $L_{xF} = 2$, $\mu_S = 0.8t$, $\mu_F = 0.9t$, $k_B T = 0.01t$, $|h_y^L| = |h_y^R| = h_i = 1t$.

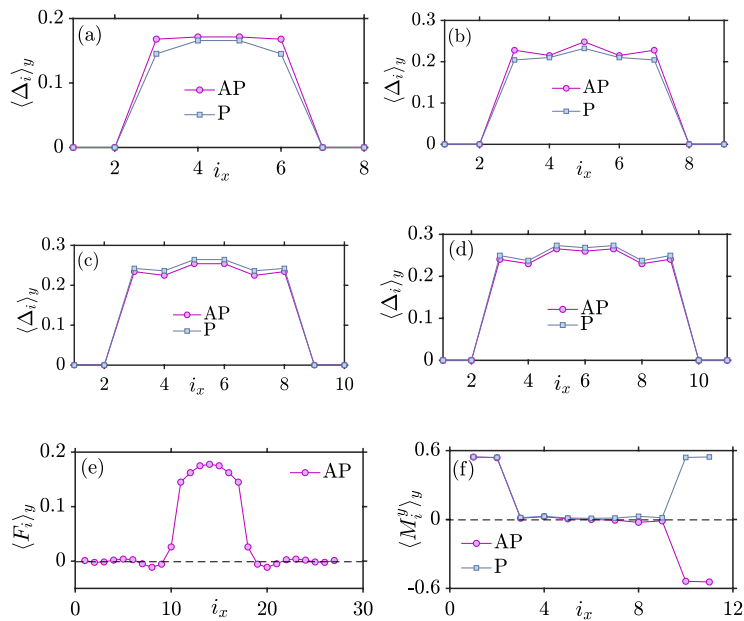


Figure 6. AP and P superconducting gaps (Δ_{AP} and Δ_P) when $U/t = 1.5$, $h_i = 1t$, $k_B T = 0.01t$, $\mu_S = 0.8t$ and $\mu_F = 0.9t$ (a) $L_{xS} = 4$ (b) $L_{xS} = 5$ (c) $L_{xS} = 6$ (d) $L_{xS} = 7$. (e) Superconducting proximity effect inside the ferromagnets when $U/t = 1.5$, $h_i = 0.5t$, $k_B T = 0.01t$, $\mu_S = 0.8t$, $\mu_F = 0.9t$, $L_{xS} = 7$ and $L_{xF} = 10$. (f) Layer-dependent magnetization for P and AP when $U/t = 1.5$, $h_i = 1t$, $k_B T = 0.01t$, $\mu_S = 0.8t$, $\mu_F = 0.9t$, $L_{xS} = 7$ and $L_{xF} = 2$. The $\langle \dots \rangle_y$ notation denotes averaging over the y -direction and i is a lattice site along the x -direction.

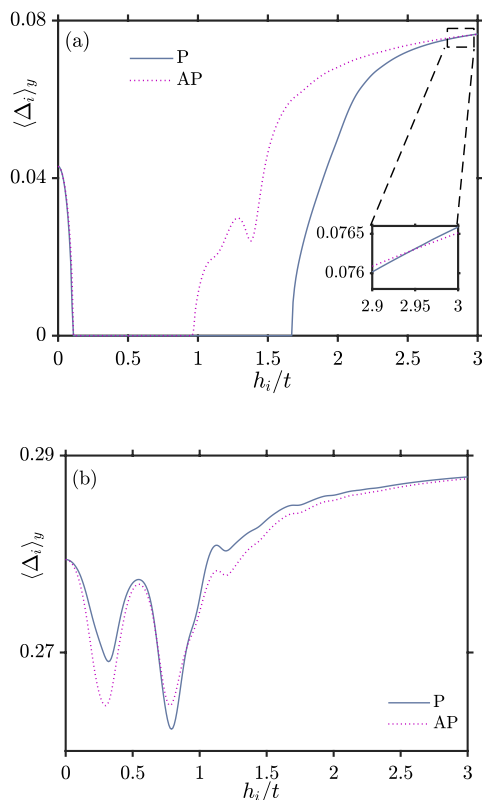


Figure 7. Superconducting gap vs h_i when $L_{XS} = 8$, $k_B T = 0.01t$, $\mu_S = 0.8t$ and $\mu_F = 0.9t$. (a) $U/t = 1$ (b) $U/t = 1.5$.

In Fig. 6, we demonstrate the presence of a superconducting proximity effect inside the ferromagnets. Whereas the gap Δ_i vanishes inside the ferromagnets due to the absence of an attractive interaction U_i in those regions in our model, the anomalous Green function ($-c_{i\downarrow}c_{i\uparrow}$) is finite in the ferromagnets, as shown in Fig. 6e. In that plot, we have considered larger ferromagnets ($L_{xF} = 10$) so that the oscillatory nature of the Cooper pairs penetrating inside the ferromagnets is better shown. On the other hand, an inverse proximity effect is also present: the induction of a magnetization induced inside the superconductor due to the exchange field of the ferromagnets. The layer-dependent magnetization is shown in Fig. 6(f).

It is often assumed in the literature that the AP configuration in a superconducting spin valve should give the largest superconducting gap. The rationale behind this assumption is that the induced magnetization in the superconducting region of the F–S–F structure is weakest in the AP configuration, leading to the least amount of pair-breaking. However, as we will discuss below, this is a simplified picture which neglects a key process in the spin valve: crossed Andreev reflection. The effect on Δ of various pair-breaking processes in equilibrium F–S–F structures has been studied previously, but primarily in layers with monoatomic thickness^{33–38}. In Ref.³⁷, it was stated that $\Delta_P < \Delta_{AP}$ at any temperature for sufficiently large thicknesses. In our work, we instead find that the opposite inequality holds for sufficiently large thicknesses of the superconductor.

For $U/t = 2$ in Fig. 5 one observes a monotonic decrease of J as a function of L_{XS} . This behavior occurs both for a strong pairing interaction U or when the exchange field h_i is large. We have already explained why it occurs for strong U , leading to a large gap. To explain why it occurs for a large exchange field, we consider the behaviour of Δ as a function of exchange field strength: this is shown in Fig. 7a for $U/t = 1$ and Fig. 7b for $U/t = 1.5$.

In both cases, for large enough h_i , there exists a specific h_i value which marks the transition from $\Delta_P < \Delta_{AP}$ to $\Delta_P > \Delta_{AP}$. The reason for this transition can be explained in terms of a competition between the pair-breaking influence of the induced exchange field in the superconductor and inverse crossed Andreev reflection (CAR)³⁹, which we proceed to explain.

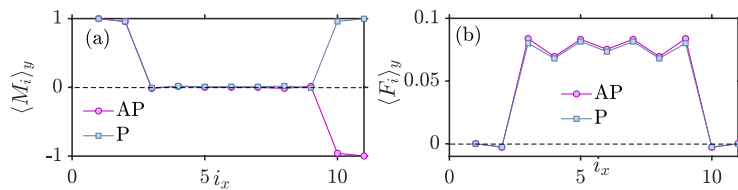


Figure 8. (a) Layer-dependent magnetization for P and AP (b) Proximity effect of superconductor inside the ferromagnets when $U/t = 1$, $h_i = 2.5t$, $k_B T = 0.01t$, $\mu_S = 0.8t$, $\mu_F = 0.9t$ and $L_{XS} = 7$.

In a superconducting spin valve, a magnetization is induced inside the superconductor. The corresponding induced exchange field is stronger in the case of P orientation than the AP one. As a result of this induced exchange field, the opposite spin electrons in the Cooper pair accumulate different phases in the superconductor, ultimately leading to a loss of phase coherence and Cooper-pair breaking. As the induced exchange field is stronger in the P case, the destructive effect of the ferromagnets is more severe in the P orientation than the AP. If this was the only mechanism, the superconducting gap should always be smaller in the P orientation ($\Delta_P < \Delta_{AP}$).

On the other hand, inverse crossed Andreev reflection is another pair breaking mechanism in competition with the pair breaking effect of the induced exchange field. What happens here is that spin up and down electrons in a Cooper pair move into separate ferromagnets. This is in contrast to the usual proximity effect mediated by local Andreev reflection, where both electrons (and thus the entire pair) leak into a single material. Crossed Andreev reflection is thus a non-local process. In the AP orientation, the electrons tunnel into the spin majority band of the two ferromagnets while in the P orientation one spin goes to a majority band while the other one goes to the minority band of the other ferromagnet.

As the exchange field becomes stronger, CAR becomes less probable to occur in the P configuration since the minority band involved in the process gradually vanishes. In the half-metallic limit, there is no longer any conducting minority band to enable CAR in the P configuration. Therefore, the destructive effect of CAR is stronger in the AP case, thus making the gap smaller ($\Delta_{AP} < \Delta_P$).

The configuration giving the largest Δ then depends on which of the two described effects that dominates. From Fig. 7, the fact that Δ_P overtakes Δ_{AP} in magnitude at a critical value for the exchange field h_i indicates that crossed Andreev reflection dominates in this regime. This reduces the leakage of superconductivity into the ferromagnets, and enhances the gap. It can be done by means of rotating the magnetization direction of one of the ferromagnets, for example with the help of an external magnetic field.

Figure 7a also demonstrates an example of reentrant superconductivity which can occur in superconducting spin valves, enabling a switching of superconductivity on and off possible. This is usually done by varying thickness of one of the ferromagnets in a superconducting spin valve^{14,40}. The suppression of superconductivity by the ferromagnet becomes particularly effective at certain ferromagnet thicknesses L_F . At these values of L_F , the different quasiparticle trajectories inside the ferromagnet interfere in such a manner that they minimize the superconducting condensate wave function at the interface with the superconductor. The interference occurs since the quasiparticles amplitudes are quantum mechanically determined from sum over all classical trajectories. Since phases picked up along these trajectories not only depend on the length of the trajectory, but also the magnitude of the exchange field, varying h also leads to reentrant behavior of superconductivity in our case.

Another interesting aspect of this plot (Fig. 7a) is that superconductivity is eventually enhanced when h_i/t increases compared to the case $h_i = 0$ without magnetization. In other words, strong magnetization enhances superconductivity. The reason for this effect can be understood by considering the mechanisms causing a suppression of superconductivity: local Andreev reflection occurring at a single interface in the system, crossed Andreev-reflection (CAR) occurring at both interfaces in the system, and the pair-breaking magnetic moment induced in the superconducting region when the exchange-field is finite. In the case of no exchange field ($h_i = 0$), the two first mechanisms listed above are then at play and reduce the superconducting gap. When exchange field is strong, the gap is seen to be enhanced compared to the $h_i = 0$ case in Fig. 7. Moreover, as seen from Fig. 7, the gap becomes almost identical in both the P and AP configuration. This indicates that the reason for the enhancement compared to $h_i = 0$ cannot be CAR or the induced magnetic moment (Fig. 8a), because these two mechanisms act very differently in the P and AP configuration. Instead, the reason is the first mechanism listed above: the behavior of local Andreev reflection. Namely, as the exchange field grows in magnitude, the ferromagnets become closer to being half-metallic (only conducting in one spin-band). For a half-metal/superconductor interface, there is in fact no proximity effect at all (in Fig. 8b, the proximity effect goes to zero quickly in the ferromagnets). As only one spin-type is available in the half-metal, no Andreev reflection can take place and the Cooper pairs are confined to the superconductor. Therefore, unlike the case for $h_i = 0$, there is now no leakage of Cooper pairs into the ferromagnetic regions. This results in a stronger superconducting condensate, since the leakage of pairs into the magnetic regions is absent.

In Fig. 9, we show how J in a superconducting spin valve behaves with respect to exchange field. The interaction between the ferromagnets weakens the longer the superconductor is. Despite of a small region where the P orientation is the ground state, it is clearly seen that AP is mostly the dominating ground state, especially as h_i becomes large. As we mentioned previously, this is as a result of Δ_P exceeding the magnitude of Δ_{AP} . Similarly to the F–N–F case, for high enough exchange field h_i the number of available conduction electron states near

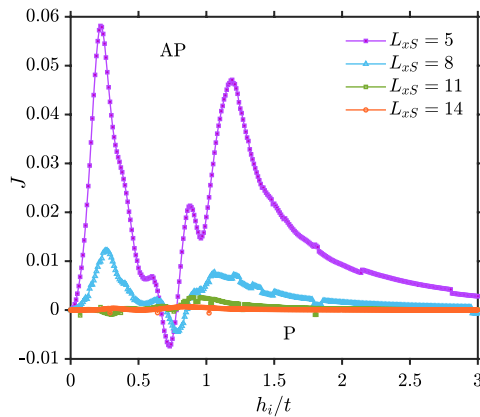


Figure 9. F–S–F, $L_y = 10, L_{xF} = 2, \mu_S = 0.8t, \mu_F = 0.9t, k_B T = 0.01t, U = 1.5$.

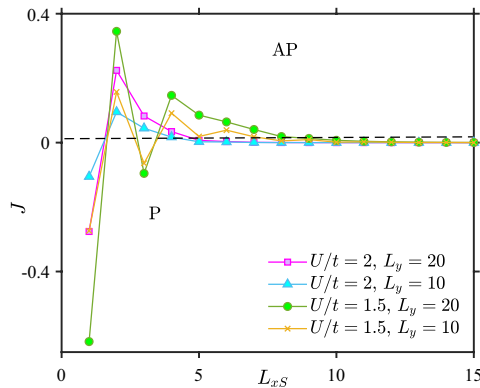


Figure 10. F–S–F, $L_{xF} = 2, \mu_S = 0.8t, \mu_F = 0.9t, k_B T = 0.01t$.

the Fermi level that can become spin-polarized and mediate the interaction monotonically decreases, leading to a corresponding reduction of the indirect exchange interaction.

In Ref.⁴¹, the authors showed that the critical temperature difference $\Delta T_c \equiv T_c(P) - T_c(AP)$ in a superconducting spin-valve could have both positive and negative sign if the thicknesses of the ferromagnets were unequal. The authors considered very thin superconductors $L_S \ll \xi_S$. In our manuscript, we do not consider such thin superconductors and instead focus on the regime $L_S > \xi_S$. Moreover, Ref.⁴¹ obtained the sign change in ΔT_c when assuming a strong Fermi-vector mismatch between the F and S regions, whereas we do not consider layers with a strong Fermi-vector mismatch. In our regime, we do not observe any sign-change in the indirect exchange interaction J as we vary the thickness of one of the ferromagnets while keeping the other fixed. This indicates that the interference effects causing the sign change in $T_c(P) - T_c(AP)$ in Ref.⁴¹ are suppressed for superconductors larger than the coherence length and when there is no strong Fermi-vector mismatch between the layers.

The relevant length-scales under consideration in our system are the superconducting coherence length $\xi = \hbar v_F / \pi \Delta$, the ferromagnetic coherence length $\xi_F = \hbar v_F / \pi h$, and the Fermi wavelength $\lambda_F = k_F^{-1}$. We have considered several different parameter choices for the length of the superconductor and the coherence length (by varying U). Therefore, the relative size of these length-scales is not a fixed number in our paper. However, considering a representative parameter set $L_S/a = 10, U/t = 1.5, h/t = 1.0$, we find that $\xi_S / \lambda_F \approx 3.5, \xi_F / \lambda_F \approx 1.2$. In this work, we have not considered the possible influence of the electromagnetic proximity effect^{42,43} on the RKKY interaction between the ferromagnets, which could be an interesting extension to consider.

To close this section, we investigate the effect of the width of the structure on the indirect interaction between the ferromagnets in Fig. 10. Increasing the width of the structure leads to more available states which makes the

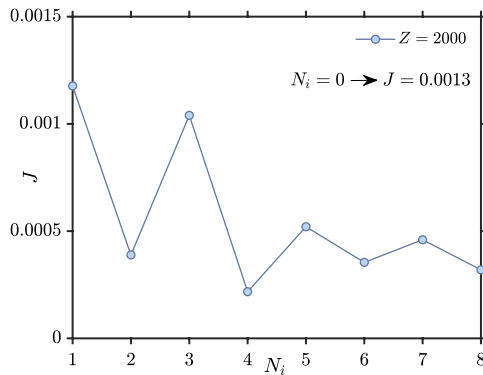


Figure 11. Indirect exchange interaction J between the ferromagnets versus number of impurities (N_i). We have considered J averaged over 2000 different impurity configurations, using $L_y = 10, L_{xF} = 2, L_{xS} = 10, \mu_S = 0.8t, \mu_F = 0.9t, k_B T = 0.01t, U/t = 1.5$ and $h_i = 1t$.

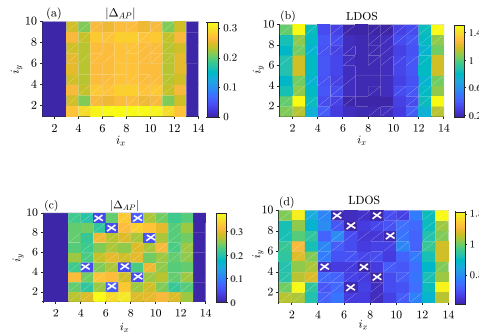


Figure 12. Left column: anti-parallel superconducting gap ($|\Delta_{AP}|$). Right column: local density of states (LDOS) plots. We have used $L_{xS} = 10, L_y = 10, L_{xF} = 2, \mu_S = 0.8t, \mu_F = 0.9t, U/t = 1.5, h_i = 1t$ and $\Phi = 0.036$. (a, b) clean F-S-F ($N_i = 0$). (c, d) dirty F-S-F with 8% impurity concentration ($N_i = 8$).

interaction J between the ferromagnets larger. However, it does not change the fact that the system prefers the AP orientation as the ground state for sufficiently strong superconductors.

We finally consider the effect of impurities on J . To this end, we consider randomly located impurities in the superconducting part. Impurity atoms are not chosen from edge atoms and atoms at the interfaces with ferromagnets. Here, we consider the impurity-averaged exchange interaction J over a large set of different impurity configurations. We define Z as the number of impurity configurations that we have averaged over. The Hamiltonian of the system including impurity scattering is as follows

$$H = - \sum_{(ij),\alpha} t_{ij} c_{i\alpha}^\dagger c_{j\alpha} + \sum_{i,\alpha} (V_i^{\text{imp}} - \mu_i) n_{i\alpha} + \sum_{i\alpha\beta} (\mathbf{h}_i \cdot \boldsymbol{\sigma})_{\alpha\beta} c_{i\alpha}^\dagger c_{i\beta} - \sum_i U_i n_{i\uparrow} n_{i\downarrow}. \quad (22)$$

Here V_i^{imp} is the potential describing the impurity strength at site i . In Fig. 11, we consider J as a function of the number of impurities in the system for $U/t = 1.5, h_i = 1t$ and $V_i^{\text{imp}} = 2t$, averaging over $Z = 2000$ configurations. We see that J decays in an oscillatory fashion as the number of impurities randomly placed in the superconductor increases.

To understand the behavior of J , we consider both how the magnitude and the LDOS changes for the F-S-F structure when comparing the clean case and the case with impurities. Consider first the case with zero impurities and zero magnetic field, shown in Fig. 12a,b. The LDOS has its minimum value in the middle of structure while $|\Delta_{AP}|$ is maximal at the middle of structure, as expected. When adding impurities, in Fig. 12c,d, $|\Delta_{AP}|$ will tend to zero around the impurity atoms. Their location is marked with white crosses. Interestingly, the average LDOS in the dirty F-S-F case (Fig. 12d) has increased in comparison to the clean F-S-F (Fig. 12b) case. At first

glance, this might indicate that more available quasiparticle states are available to mediate the exchange interaction between the ferromagnets. This should lead to an increase in J compared to the clean case $N_i = 0$. However, Fig. 11 shows the opposite: J is reduced compared to the clean case. We attribute this decrease in J with increasing impurity concentration to an increasing localization of quasiparticles^{28,29}. When the localization increases, the interaction J should be reduced, as seen in Fig. 11.

Concluding remarks

In conclusion, we have considered the magnetic exchange interaction J and the preferred equilibrium magnetic configuration in a 2D superconducting spin valve with an s -wave superconductor, solving self-consistently for the superconducting order parameter. We find that the qualitative dependence of J on the separation distance between the ferromagnets can behave differently on the basis of the strength of the superconducting gap and the strength of the exchange field in the ferromagnets. RKKY-like oscillations are observed when the superconducting gap Δ is small, whereas a monotonic decay is observed when Δ is larger. In the latter case, the AP configuration is always preferred even though the gap is larger in the P configuration. We explain this in terms of a competition between a proximity-induced pair-breaking magnetization in the superconductor and crossed Andreev reflection. Adding randomly localized impurities to the superconductor led to an oscillatory decrease of J with increasing impurity concentration.

Received: 5 December 2020; Accepted: 5 February 2021

Published online: 03 March 2021

References

- Ruderman, M. A. & Kittel, C. Indirect exchange coupling of nuclear magnetic moments by conduction electrons. *Phys. Rev.* **96**, 99–102. <https://doi.org/10.1103/PhysRev.96.99> (1954).
- Baibich, M. N. *et al.* Giant magnetoresistance of (001)Fe/(001)Cr magnetic superlattices. *Phys. Rev. Lett.* **61**, 2472–2475. <https://doi.org/10.1103/PhysRevLett.61.2472> (1988).
- Binasch, G., Grünberg, P., Saurenbach, F. & Zinn, W. Enhanced magnetoresistance in layered magnetic structures with antiferromagnetic interlayer exchange. *Phys. Rev. B* **39**, 4828–4830. <https://doi.org/10.1103/PhysRevB.39.4828> (1989).
- Zhu, J.-J., Yao, D.-X., Zhang, S.-C. & Chang, K. Electrically controllable surface magnetism on the surface of topological insulators. *Phys. Rev. Lett.* **106**, 097201. <https://doi.org/10.1103/PhysRevLett.106.097201> (2011).
- Abanin, D. A. & Pesin, D. A. Ordering of magnetic impurities and tunable electronic properties of topological insulators. *Phys. Rev. Lett.* **106**, 136802. <https://doi.org/10.1103/PhysRevLett.106.136802> (2011).
- Sherafati, M. & Satpathy, S. Rkky interaction in graphene from the lattice green's function. *Phys. Rev. B* **83**, 165425. <https://doi.org/10.1103/PhysRevB.83.165425> (2011).
- Hosseini, M. V. & Askari, M. Ruderman–Kittel–Kasuya–Yosida interaction in Weyl semimetals. *Phys. Rev. B* **92**, 224435. <https://doi.org/10.1103/PhysRevB.92.224435> (2015).
- Liu, Q., Liu, C.-X., Xu, C., Qi, X.-L. & Zhang, S.-C. Magnetic impurities on the surface of a topological insulator. *Phys. Rev. Lett.* **102**, 156603. <https://doi.org/10.1103/PhysRevLett.102.156603> (2009).
- Chesi, S. & Loss, D. Rkky interaction in a disordered two-dimensional electron gas with Rashba and Dresselhaus spin-orbit couplings. *Phys. Rev. B* **82**, 165303. <https://doi.org/10.1103/PhysRevB.82.165303> (2010).
- Ryazanov, V. V. *et al.* Coupling of two superconductors through a ferromagnet: Evidence for a π junction. *Phys. Rev. Lett.* **86**, 2427–2430. <https://doi.org/10.1103/PhysRevLett.86.2427> (2001).
- Robinson, J. W. A., Witt, J. D. S. & Blamire, M. G. Controlled injection of spin-triplet supercurrents into a strong ferromagnet. *Science* **329**, 59–61. <https://doi.org/10.1126/science.1189246> (2010).
- Eschrig, M., Kopu, J., Cuevas, J. C. & Schön, G. Theory of half-metal/superconductor heterostructures. *Phys. Rev. Lett.* **90**, 137003. <https://doi.org/10.1103/PhysRevLett.90.137003> (2003).
- Lutchyn, R. M., Sau, J. D. & Das Sarma, S. Majorana fermions and a topological phase transition in semiconductor–superconductor heterostructures. *Phys. Rev. Lett.* **105**, 077001. <https://doi.org/10.1103/PhysRevLett.105.077001> (2010).
- Tagirov, L. R. Low-field superconducting spin switch based on a superconductor/ferromagnet multilayer. *Phys. Rev. Lett.* **83**, 2058–2061. <https://doi.org/10.1103/PhysRevLett.83.2058> (1999).
- Baek, B., Rippard, W. H., Benz, S. P., Russek, S. E. & Dresselhaus, P. D. Hybrid superconducting–magnetic memory device using competing order parameters. *Nat. Commun.* **5**, 3888. <https://doi.org/10.1038/ncomms4888> (2014).
- Linder, J. & Robinson, J. W. A. Superconducting spintronics. *Nat. Phys.* **11**, 307. <https://doi.org/10.1038/nphys3242> (2015).
- Eschrig, M. Spin-polarized supercurrents for spintronics: a review of current progress. *Rep. Prog. Phys.* **78**, 104501. <https://doi.org/10.1088/0034-4885/78/10/104501> (2015).
- Buzdin, A. I. Proximity effects in superconductor–ferromagnet heterostructures. *Rev. Mod. Phys.* **77**, 935–976. <https://doi.org/10.1103/RevModPhys.77.935> (2005).
- Bergeret, F. S., Volkov, A. F. & Efetov, K. B. Odd triplet superconductivity and related phenomena in superconductor–ferromagnet structures. *Rev. Mod. Phys.* **77**, 1321–1373. <https://doi.org/10.1103/RevModPhys.77.1321> (2005).
- Zhu, Y., Pal, A., Blamire, M. G. & Barber, Z. H. Superconducting exchange coupling between ferromagnets. *Nat. Mater.* **16**, 195. <https://doi.org/10.1038/nmat4753> (2017).
- De Gennes, P. Coupling between ferromagnets through a superconducting layer. *Phys. Lett.* **23**, 10–11. [https://doi.org/10.1016/0031-9163\(66\)90229-0](https://doi.org/10.1016/0031-9163(66)90229-0) (1966).
- Alekssevskij, N., Garifullin, I., Kharakhash'yan, E. & Kochelaev, B. Electron paramagnetic resonance for localized magnetic states in the superconducting layer system. *Zh. Eksp. Teor. Fiz.* **72**, 1523–1533 (1977).
- Kochelaev, B., Tagirov, L. & Khusainov, M. Spatial dispersion of the spin susceptibility of conductivity electrons in superconductors. *Zh. Eksp. Teor. Fiz.* **76**, 578–587 (1979).
- Khusainov, M. G. Z. Indirect RKKY exchange and magnetic states of ferromagnet–superconductor superlattices. *Eksp. Teor. Fiz.* **109**, 524 (1996).
- Aristov, D. N., Maleyev, S. V. & Yashenkin, A. G. Rkky interaction in layered superconductors with anisotropic pairing. *Z. Phys. B* **102**, 467–471. <https://doi.org/10.1103/PhysRev.96.996> (1997).
- Di Bernardo, A. *et al.* Nodal superconducting exchange coupling. *Nat. Mater.* **18**, 1–7. <https://doi.org/10.1038/s41563-019-0476-3> (2019).
- Eschrig, M. Spin-polarized supercurrents for spintronics. *Phys. Today* **64**, 43. <https://doi.org/10.1063/1.3541944> (2011).

28. Maekawa, S. & Fukuyama, H. Localization effects in two-dimensional superconductors. *J. Phys. Soc. Jpn.* **51**, 1380. <https://doi.org/10.1143/JPSJ.51.1380> (1981).
29. Ma, M. & Lee, P. A. Localized superconductors. *Phys. Rev. B* **32**, 5658–5667. <https://doi.org/10.1103/PhysRev.96.997> (1985).
30. Dmitrienko, V. E., Ovchinnikova, E. N., Kokubun, J. & Ishida, K. Dzyaloshinskii–Moriya interaction: How to measure its sign in weak ferromagnets?. *JETP Lett.* **92**, 383–387. <https://doi.org/10.1134/S0021364010180050> (2010).
31. Liu, D. *et al.* Electronic origin of high-temperature superconductivity in single-layer FeSe superconductor. *Nat. Commun.* **3**, 1–6. <https://doi.org/10.1038/ncomms1946> (2012).
32. Okazaki, K. *et al.* Superconductivity in an electron band just above the fermi level: Possible route to BCS–BEC superconductivity. *Sci. Rep.* **4**, 1–6. <https://doi.org/10.1038/srep04109> (2014).
33. Melin, R. Superconducting cross-correlations in ferromagnets: implications for thermodynamics and quantum transport. *J. Phys. Condens. Matter* **13**, 6445. <https://doi.org/10.1088/0953-8984/13/30/301> (2001).
34. Apinyan, V. & Melin, R. Microscopic theory of non local pair correlations in metallic F/S/F trilayers. *Eur. Phys. J. B* **25**, 373. <https://doi.org/10.1140/epjb/e20020042> (2002).
35. H. Jirari, R. M. & Stefanakis, N. Proximity effect in multiterminal hybrid structures. *Eur. Phys. J. B* **31**, 125. <https://doi.org/10.1140/epjb/e2003-00016-8> (2003).
36. Buzdin, A. & Daumens, M. Inversion of the proximity effect in hybrid ferromagnet-superconductor-ferromagnet structures. *Europhys. Lett.* **64**, 510. <https://doi.org/10.1209/epl/i2003-00252-0> (2003).
37. Melin, R. & Feinberg, D. What is the value of the superconducting gap of a F/S/F trilayer? *Europhys. Lett.* **65**, 96. <https://doi.org/10.1209/epl/i2003-10051-1> (2004).
38. Melin, R. Microscopic theory of equilibrium properties of F/S/F trilayers with weak ferromagnets. *Eur. Phys. J. B* **39**, 249. <https://doi.org/10.1140/epjb/e2004-00188-7> (2004).
39. Beckmann, D., Weber, H. B. & Löhneysen, H. Evidence for crossed Andreev reflection in superconductor–ferromagnet hybrid structures. *Phys. Rev. Lett.* **93**, 197003. <https://doi.org/10.1103/PhysRevLett.93.197003> (2004).
40. Fominov, Y. V., Chchelkatchev, N. M. & Golubov, A. A. Nonmonotonic critical temperature in superconductor/ferromagnet bilayers. *Phys. Rev. B* **66**, 014507. <https://doi.org/10.1103/PhysRev.96.998> (2002).
41. Mironov, S. V. & Buzdin, A. Standard, inverse, and triplet spin-valve effects in $F_1/s/f_2$ systems. *Phys. Rev. B* **89**, 144505. <https://doi.org/10.1103/PhysRev.96.999> (2014).
42. Mironov, S., Mel'nikov, A. & Buzdin, A. Electromagnetic proximity effect in planar superconductor-ferromagnet structures. *Appl. Phys. Lett.* **113**, 022601. <https://doi.org/10.1063/1.5037074> (2018).
43. Devizorova, Z., Mironov, S. V., Mel'nikov, A. S. & Buzdin, A. Electromagnetic proximity effect controlled by spin-triplet correlations in superconducting spin-valve structures. *Phys. Rev. B* **99**, 104519. <https://doi.org/10.1103/PhysRevLett.61.24720> (2019).

Acknowledgements

This work was supported by the Research Council of Norway through its Centres of Excellence funding scheme grant 262633 QuSpin. We thank L. G. Johnsen for useful discussions. We also thank A. Di Bernardo and O. Millo for very helpful comments.

Author contributions

J.L. came up with the idea for the project. A.B.G. performed the analytical and numerical calculations with support from V.K.R. All authors contributed to the discussion of the results and the writing of the manuscript.

Competing interests

The authors declare no competing interests.

Additional information

Supplementary information The online version contains supplementary material available at <https://doi.org/10.1038/s41598-021-83620-3>.

Correspondence and requests for materials should be addressed to J.L.

Reprints and permissions information is available at www.nature.com/reprints.

Publisher's note Springer Nature remains neutral with regard to jurisdictional claims in published maps and institutional affiliations.



Open Access This article is licensed under a Creative Commons Attribution 4.0 International License, which permits use, sharing, adaptation, distribution and reproduction in any medium or format, as long as you give appropriate credit to the original author(s) and the source, provide a link to the Creative Commons licence, and indicate if changes were made. The images or other third party material in this article are included in the article's Creative Commons licence, unless indicated otherwise in a credit line to the material. If material is not included in the article's Creative Commons licence and your intended use is not permitted by statutory regulation or exceeds the permitted use, you will need to obtain permission directly from the copyright holder. To view a copy of this licence, visit <http://creativecommons.org/licenses/by/4.0/>.

© The Author(s) 2021

Effect of midgap states on the magnetic
exchange interaction mediated by a *d*-wave
superconductor

Phys. Rev. B **104**, 054502 (2021)

Authors

Atousa Ghanbari
Eirik Erlandsen
Jacob Linder

Effect of midgap states on the magnetic exchange interaction mediated by a d -wave superconductorAtousa Ghanbari, Eirik Erlandsen , and Jacob Linder*Center for Quantum Spintronics, Department of Physics, Norwegian University of Science and Technology, NO-7491 Trondheim, Norway*

(Received 14 January 2021; revised 26 July 2021; accepted 27 July 2021; published 4 August 2021)

We theoretically study the indirect interaction between two ferromagnetic contacts located on the surface of a d -wave superconductor. When the magnets are connected to a $\{010\}$ edge of the superconductor we find an oscillating RKKY interaction that varies in sign as the distance between the magnetic contacts is varied. However, when coupling the magnets to an $\{110\}$ edge of the superconductor, we find that the presence of midgap states qualitatively changes the results. The ground state of the system is then found to always favor alignment of the magnets as this configuration most strongly suppresses the midgap states, leading to a larger condensation energy, which dominates over the intrinsic RKKY interaction.

DOI: [10.1103/PhysRevB.104.054502](https://doi.org/10.1103/PhysRevB.104.054502)**I. INTRODUCTION**

Superconductors with d -wave symmetry have an anisotropic order parameter, which drops to zero along some nodal directions [1–3]. A $\{110\}$ edge of a $d_{x^2-y^2}$ superconductor has been shown to feature dispersionless surface states with zero energy, called midgap states [4]. The appearance of midgap states for such an edge is related to the fact that the order parameter in a 45° rotated coordinate system takes the form d_{xy} , introducing opposite signs for the pair potential experienced by particles undergoing specular and Andreev reflections at the surface. The $\{110\}$ edge also gives rise to a zero bias conductance peak [5], which is a result of the presence of the midgap states [6]. Such a zero-bias conductance peak has been experimentally observed in the high- T_c cuprate superconductors [7–10] and has been important in determining the pairing symmetry of these superconductors.

The indirect exchange interaction between two localized spins, mediated by the itinerant electrons of a host material, was first introduced by Ruderman, Kittel, Kasuya, and Yosida, and is known as the RKKY interaction [11–13]. In this indirect exchange interaction, itinerant electrons of the host material scatter off a localized spin, and the wave functions of the scattered electrons interfere with each other giving rise to alternating regions with high density of spin up/down. This leads to the well-known RKKY oscillations in the spin-spin interaction strength, which decrease with the distance R between the two localized spins as R^{-D} , where D is the dimensionality of the system. RKKY interaction has been investigated in various materials ranging from normal metals [11,13], to one- and two-dimensional electron gases [14,15], two-dimensional structures like graphene [16–20], and topological insulators [21–23].

For a system consisting of magnetic impurities embedded in a superconductor, the influence of superconductivity on the indirect impurity-impurity interaction has also been studied [24,25]. For a conventional s -wave superconductor, when the

distance between the impurities is larger than the superconducting coherence length, the interaction between them is found to be antiferromagnetic in character and suppressed compared to the normal metal case. The suppression is caused by the superconducting gap reducing the number of states close to the Fermi level that can mediate the interaction. Below the coherence length, the behavior is similar to the normal metal case with an oscillatory RKKY interaction that changes sign with distance. However, nonperturbative treatments have shown that Yu-Shiba-Rusinov (YSR) bound states can give rise to mainly antiferromagnetic behavior even at distances shorter than the coherence length [26]. Further, for impurities on the surface of a three-dimensional topological insulator with proximity-induced s -wave superconductivity, the RKKY interaction favors the impurity spins to be in-plane and antiparallel [27]. For a spin-valve structure consisting of two ferromagnetic insulators connected by an s -wave superconductor, experiments have shown that anti-alignment of the magnets is still favored [28].

Conventional s -wave superconductors do however typically have coherence lengths far exceeding the decay length of the RKKY interaction. On the other hand, d -wave superconductors can feature very short coherence lengths of the order of nanometers [29], offering an intriguing platform for studying the interplay between superconductivity and RKKY interaction, as the characteristic length scales of both phenomena are comparable. RKKY interaction between magnetic impurities mediated by a d -wave superconductor with an anisotropic order parameter of the type $d_{x^2-y^2}$ has lead to similar behavior as in the s -wave case [30]. Further, for a spin-valve structure involving a $d_{x^2-y^2}$ superconductor, nodal quasiparticles close to the Fermi surface have been observed to mediate interaction that favors anti-alignment of the magnetic insulators for a sufficiently large superconductor thickness [31].

As the gapped band structure of a superconductor suppresses the RKKY interaction, it is of interest to investigate the effect the presence of midgap states have on the

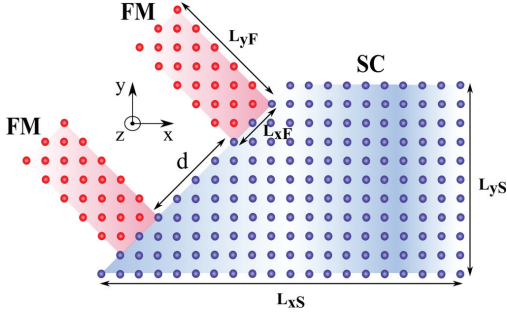


FIG. 1. Schematic illustration of a d -wave superconductor with midgap surface states mediating the indirect exchange interaction between two ferromagnetic contacts. We will consider configurations where the magnetization of the two magnets is either parallel (P) or antiparallel (AP). For comparison, the ferromagnetic contacts will also be attached to the lower, nondiagonal edge of the superconductor. The lengths indicated on the figure will in the main text be specified by the number of atomic distances.

interaction. We therefore consider a $d_{x^2-y^2}$ superconductor and calculate the exchange interaction between two ferromagnetic contacts located on a diagonal $\{110\}$ edge, as illustrated in Fig. 1. The superconductor is modelled by an extended BCS tight-binding Hamiltonian on a square lattice and connected to the metallic magnets through a hopping term across the interface. The results are obtained through a self-consistent solution of the Bogoliubov-de Gennes (BdG) equations [32]. To put the results into context, we consider the cases of a normal metal and an isotropic s -wave superconductor, in addition to the d -wave superconductor. In all three cases, we investigate the interaction between ferromagnetic contacts located on both diagonal and nondiagonal edges.

For magnetic contacts located on a diagonal edge of a d -wave superconductor, we find that the system always favors alignment of the two magnets. The variation in the strength of the magnetic exchange interaction as we vary the distance between the magnets is small compared to the magnitude of the interaction itself. We attribute these results to the aligned magnets more efficiently suppressing the midgap states than the anti-aligned configuration. Although the aligned magnets induce a stronger spin splitting in the superconductor, suppressing the gap, the reduction of the midgap states leads to an overall larger gap and increased condensation energy. The parallel magnet configuration is therefore the ground state of the system.

The paper is organized as follows. In Sec. II we introduce the model and methodology. Then, in Sec. III we present and discuss the results. Finally, in Sec. IV we provide a summary of the findings. The phase diagram of our d -wave superconductor model for a square system with continuous boundary conditions is included in the Appendix.

II. MODEL AND METHODS

By means of a tight-binding Hamiltonian on a square lattice, we model the attractive electron-electron interaction in a

superconductor:

$$H^{\text{SC}} = - \sum_{(i,j),\alpha} t_{ij} c_{i\alpha}^\dagger c_{j\alpha} - \sum_i \mu_i n_{i\alpha} - \sum_i U_i n_{i\uparrow} n_{i\downarrow} + \sum_{(ij),\alpha \neq \alpha'} V_{ij} n_{i\alpha} n_{j\alpha'} + \sum_{(ij),\alpha} V'_{ij} n_{i\alpha} n_{j\alpha}. \quad (1)$$

Here, $c_{i\alpha}^\dagger$ is a creation operator creating an electron with spin α on lattice site $i = (i_x, i_y)$. The hopping amplitude is denoted by t_{ij} , and μ_i is the chemical potential. The third term represents on-site attractive interactions between opposite spins, where the number operator is $n_{i\alpha} = c_{i\alpha}^\dagger c_{i\alpha}$. This term gives rise to conventional spin singlet isotropic s -wave superconductivity. The fourth and fifth terms represent nearest-neighbor interaction between opposite or equal spins, respectively. These terms can give rise to d -wave, p -wave, or extended s -wave pairing for an attractive interaction potential. For the purposes of this paper, we will set V'_{ij} to zero as we will not be interested in the possibility of equal spin pairing. As shown in the Appendix, the above model without V'_{ij} can give rise to a d -wave superconductor for a suitable choice of chemical potential.

A. Analytical methods

Through a mean-field treatment, we simplify the interaction terms. The on-site part of the interaction becomes

$$- \sum_i U_i n_{i\uparrow} n_{i\downarrow} = - \sum_i U_i (c_{i\uparrow}^\dagger c_{i\downarrow}^\dagger \langle c_{i\downarrow} c_{i\uparrow} \rangle + c_{i\downarrow} c_{i\uparrow} \langle c_{i\uparrow}^\dagger c_{i\downarrow}^\dagger \rangle - \langle c_{i\downarrow} c_{i\uparrow} \rangle \langle c_{i\uparrow}^\dagger c_{i\downarrow}^\dagger \rangle). \quad (2)$$

Defining the superconducting gap for the on-site interaction as $\Delta_i = -U_i \langle c_{i\downarrow} c_{i\uparrow} \rangle$, we obtain

$$- \sum_i U_i n_{i\uparrow} n_{i\downarrow} = \sum_i (c_{i\uparrow}^\dagger c_{i\downarrow}^\dagger \Delta_i + c_{i\downarrow} c_{i\uparrow} \Delta_i^*) + H_0^S, \quad (3)$$

where we have defined

$$H_0^S = \sum_i \frac{|\Delta_i|^2}{U_i}. \quad (4)$$

The on-site interaction U_i will be taken to a constant $U \geq 0$ in the superconductor, and zero elsewhere. Once again, performing a mean-field treatment, the attractive nearest-neighbor interaction term becomes

$$\sum_{(ij),\alpha \neq \alpha'} V_{ij} n_{i\alpha} n_{j\alpha'} = \sum_{(ij),\alpha \neq \alpha'} V_{ij} (c_{j\alpha'}^\dagger c_{i\alpha}^\dagger \langle c_{i\alpha} c_{j\alpha'} \rangle + c_{i\alpha} c_{j\alpha'} \langle c_{j\alpha'}^\dagger c_{i\alpha}^\dagger \rangle - \langle c_{j\alpha'}^\dagger c_{i\alpha}^\dagger \rangle \langle c_{i\alpha} c_{j\alpha'} \rangle). \quad (5)$$

We then define the nearest-neighbor pairing amplitude

$$F_{ij}^{\alpha\alpha'} = \langle c_{i\alpha} c_{j\alpha'} \rangle, \quad (6)$$

transforming Eq. (5) into

$$\sum_{(ij),\alpha \neq \alpha'} V_{ij} (c_{j\alpha'}^\dagger c_{i\alpha}^\dagger F_{ij}^{\alpha\alpha'} + c_{i\alpha} c_{j\alpha'} (F_{ij}^{\alpha\alpha'})^\dagger) + H_0^d, \quad (7)$$

where

$$H_0^d = - \sum_{(i,j), \alpha \neq \alpha'} V_{ij} |F_{ij}^{\alpha\alpha'}|^2. \quad (8)$$

As $\sum_{(i,j)} V_{ij} |F_{ij}^{\uparrow\downarrow}|^2 = \sum_{(i,j)} V_{ji} |F_{ij}^{\downarrow\uparrow}|^2$, we can rewrite $H_0^d = - \sum_{(i,j)} |F_{ij}^{\uparrow\downarrow}|^2 (V_{ij} + V_{ji})$, and similarly

$$\begin{aligned} & \sum_{(i,j), \alpha \neq \alpha'} V_{ij} (c_{j\alpha'}^\dagger c_{i\alpha}^\dagger F_{ij}^{\alpha\alpha'} + c_{i\alpha} c_{j\alpha'} (F_{ij}^{\alpha\alpha'})^\dagger) \\ &= \sum_{(ij)} (c_{i\downarrow}^\dagger c_{i\uparrow}^\dagger F_{ij}^{\uparrow\downarrow} + c_{i\uparrow} c_{j\downarrow} (F_{ij}^{\uparrow\downarrow})^\dagger) (V_{ij} + V_{ji}). \end{aligned} \quad (9)$$

In the following, we will take the nearest-neighbor interaction to be $V_{ji} = V_{ij} = V \leq 0$ (corresponding to an attractive interaction) in the superconductor and zero elsewhere. The mean-field extended tight-binding Hamiltonian now takes the form

$$\begin{aligned} H_{mf}^{SC} &= H_0 - \sum_{(i,j), \alpha} t_{ij} c_{i\alpha}^\dagger c_{j\alpha} - \sum_{i, \alpha} \mu_i n_{i\alpha} \\ &+ \sum_i (c_{i\uparrow}^\dagger c_{i\downarrow}^\dagger \Delta_i + c_{i\downarrow} c_{i\uparrow} \Delta_i^*) \\ &+ 2 \sum_{(ij)} V (c_{i\downarrow}^\dagger c_{i\uparrow}^\dagger F_{ij}^{\uparrow\downarrow} + c_{i\uparrow} c_{j\downarrow} (F_{ij}^{\uparrow\downarrow})^\dagger), \end{aligned} \quad (10)$$

where $H_0 = H_0^S + H_0^d$.

The metallic ferromagnets that are attached to the superconductor are described by the following tight-binding Hamiltonian:

$$\begin{aligned} H^{FM} &= - \sum_{(i,j), \alpha} t_{ij} c_{i\alpha}^\dagger c_{j\alpha} - \sum_{i, \alpha} \mu_i n_{i\alpha} \\ &- \sum_{i\alpha\beta} h_i^\delta (\sigma_z)_{\alpha\beta} c_{i\alpha}^\dagger c_{i\beta}. \end{aligned} \quad (11)$$

The last term represents the coupling between the spin of an electron at site i and the local magnetic exchange field, giving rise to ferromagnetism. The local exchange field h_i^δ is taken to produce a spin splitting in the z direction in spin space, giving rise to a magnetization that could in general be either in-plane or out-of-plane in real space. Our model does not separate these cases as the magnetism is simply introduced through a spin splitting. Orbital effects on the superconductor arising from the magnets, not considered in this model, can be limited by keeping the magnetization in-plane [33]. The Pauli matrices are denoted by σ , and the index δ separates the local

exchange field of each of the two magnets with $\delta = L, R$ for the leftmost and rightmost magnet, respectively. The sign of the local exchange field can be either the same or opposite for the two magnets, giving rise to parallel (P) or antiparallel (AP) ferromagnets. Outside of the magnets, the local magnetic exchange field is set to zero. The coupling between the magnets and the superconductor is introduced by having a nonzero hopping amplitude t_{ij} across the ferromagnet-superconductor interfaces. The region outside of the superconductor and magnets is considered to be vacuum and decoupled from the rest of the system with a vanishing hopping amplitude.

After diagonalization, the free energy of the system will be expressed as

$$F = H_0 - \frac{1}{2} \sum_{n=1}^{2N} E_n - \frac{1}{\beta} \sum_{n=1}^{2N} \ln(1 + e^{-\beta E_n}), \quad (12)$$

where E_n is the quasiparticle energy associated with quantum number n , and N is the number of lattice sites. The magnetic exchange interaction is computed as the difference in free energy between the configurations with parallel and antiparallel magnets

$$J = F^{\uparrow\uparrow} - F^{\uparrow\downarrow}, \quad (13)$$

which includes both the RKKY interaction mediated by the quasiparticles as well as the effect of the magnetic configurations on the condensation energy of the superconductor.

The Hamiltonian $H = H^{SC} + H^{FM}$ is diagonalized by means of the BdG method in order to compute the eigenvalues E_n and eigenstates γ_n . The diagonalized Hamiltonian will then take the form

$$H = H_0 - \frac{1}{2} \sum_{n=1}^{2N} E_n + \sum_{n=1}^{2N} E_n \gamma_n^\dagger \gamma_n. \quad (14)$$

In order to perform the diagonalization, we start by rewriting the Hamiltonian as $H = H_0 + \frac{1}{2} \sum_{ij} B_i^\dagger h_{ij} B_j$ where we have introduced the basis

$$B_i^\dagger = [c_{i\uparrow}^\dagger \quad c_{i\downarrow}^\dagger \quad c_{i\uparrow} \quad c_{i\downarrow}]. \quad (15)$$

Here, h_{ij} is a 4×4 matrix that takes the following form for $i \neq j$

$$h_{ij} = \begin{bmatrix} -t & 0 & 0 & -2V F_{ij} \\ 0 & -t & 2V F_{ji} & 0 \\ 0 & 2V (F_{ij})^* & +t & 0 \\ -2V (F_{ji})^* & 0 & 0 & +t \end{bmatrix}, \quad (16)$$

and for $i = j$

$$h_{ij} = \begin{bmatrix} -\mu_i + \sum_\delta h_i^\delta & 0 & 0 & \Delta_i \\ 0 & -\mu_i - \sum_\delta h_i^\delta & -\Delta_i & 0 \\ 0 & -(\Delta_i)^* & 0 & 0 \\ (\Delta_i)^* & 0 & 0 & +\mu_i + \sum_\delta h_i^\delta \end{bmatrix}. \quad (17)$$

Writing the Hamiltonian on matrix form $H = H_0 + \frac{1}{2} W^\dagger S W$, and introducing the matrix P , we diagonalize the Hamiltonian $H = H_0 + \frac{1}{2} W^\dagger P^\dagger P S P^\dagger P W = H_0 + \frac{1}{2} \tilde{W}^\dagger S_d \tilde{W}$. The eigenvectors of S

are

$$\begin{aligned} \Phi_n^\dagger &= [\varphi_{1n}^* \quad \cdots \quad \varphi_{in}^* \quad \cdots \quad \varphi_{Nn}^*], \\ \varphi_{in}^* &= [v_{in}^* \quad v_{in}^* \quad \omega_{in}^* \quad \chi_{in}^*], \end{aligned} \quad (18)$$

such that

$$P^\dagger = [\Phi_1 \quad \Phi_2 \quad \dots \quad \Phi_{4N}]. \quad (19)$$

We next use $P^\dagger \tilde{W} = W$ along with

$$\tilde{W}^\dagger = [\gamma_1^\dagger \dots \gamma_{4N}^\dagger], \quad (20)$$

and the relations between the quasiparticle operators that are not independent of each other. There are then $2N$ remaining independent quasiparticle operators with corresponding eigenvalues. The creation and annihilation operators $\{c^\dagger, c\}$ can then be expressed in terms of quasiparticle creation and annihilation operators $\{\gamma^\dagger, \gamma\}$:

$$\begin{aligned} c_{i\uparrow} &= \sum_{n=1}^{2N} v_{i,n} \gamma_n + \omega_{i,n}^* \gamma_n^\dagger, & c_{i\downarrow} &= \sum_{n=1}^{2N} v_{i,n} \gamma_n + \chi_{i,n} \gamma_n^\dagger, \\ c_{i\uparrow}^\dagger &= \sum_{n=1}^{2N} \omega_{i,n} \gamma_n + v_{i,n}^* \gamma_n^\dagger, & c_{i\downarrow}^\dagger &= \sum_{n=1}^{2N} \chi_{i,n} \gamma_n + v_{i,n}^* \gamma_n^\dagger. \end{aligned} \quad (21)$$

Inserting these relations into the definition of the gap for the on-site interaction, we obtain the self-consistent gap equation

$$\Delta_i = -U_i \sum_{n=1}^{2N} [(\chi_{i,n}^* v_{i,n} - v_{i,n} \omega_{i,n}^*) f(E_n) + v_{i,n} \omega_{i,n}^*]. \quad (22)$$

For the nearest-neighbor pairing amplitudes, we introduce a simplified notation $F_{ij}^{\uparrow\downarrow} = F_{ij}$. Further, $F_{i,i+\hat{x}}$ is expressed as $F_i^{\hat{x}+}$ and likewise $F_{i+\hat{x},i}^- \equiv F_i^{\hat{x}-}$ and so on. Inserting the expressions from Eq. (21) into the definitions of the pairing amplitudes, we obtain

$$\begin{aligned} F_i^{x\pm} &= \sum_{n=1}^{2N} [(\omega_{i,n}^* v_{i\pm\hat{x},n} - v_{i,n} \chi_{i\pm\hat{x},n}^*) f(E_n) + v_{i,n} \chi_{i\pm\hat{x},n}^*], \\ F_i^{\pm x} &= \sum_{n=1}^{2N} [(\omega_{i\pm\hat{x},n}^* v_{i,n} - v_{i\pm\hat{x},n} \chi_{i,n}^*) f(E_n) + v_{i\pm\hat{x},n} \chi_{i,n}^*], \\ F_i^{y\pm} &= \sum_{n=1}^{2N} [(\omega_{i,n}^* v_{i\pm\hat{y},n} - v_{i,n} \chi_{i\pm\hat{y},n}^*) f(E_n) + v_{i,n} \chi_{i\pm\hat{y},n}^*], \\ F_i^{\pm y} &= \sum_{n=1}^{2N} [(\omega_{i\pm\hat{y},n}^* v_{i,n} - v_{i\pm\hat{y},n} \chi_{i,n}^*) f(E_n) + v_{i\pm\hat{y},n} \chi_{i,n}^*]. \end{aligned} \quad (23)$$

As we are interested in the effect of the midgap states on the indirect interaction between two ferromagnetic leads connected to the superconductor, establishing the presence of midgap states is of importance. This can be achieved by calculating the single particle local density of states (LDOS), which should have a peak around zero energy in the presence of midgap states. The number of charges on lattice site i is given by $\rho_i = \sum_\alpha \langle c_{i\alpha}^\dagger c_{i\alpha} \rangle$, but this quantity can also be expressed as $\rho_i = \int_{-\infty}^{+\infty} N_i(E) f(E) dE$. Here $N_i(E)$ is the local density of states at site i , and $f(E)$ is the Fermi-Dirac distribution with energy E measured relative to the chemical potential. At $T = 0$, we have $f(E) = 1$ for $E < 0$ and $f(E) = 0$ when $E > 0$. Comparing the above two expressions for the number

of charges on lattice site i , the LDOS can then be expressed as

$$\begin{aligned} N_i(E) &= \sum_{n=1}^{2N} [(|\omega_{i,n}|^2 + |\chi_{i,n}|^2) \delta(E + E_n) \\ &\quad + (|v_{i,n}|^2 + |v_{i,n}|^2) \delta(E - E_n)]. \end{aligned} \quad (24)$$

Another quantity of interest is the magnetization on lattice site i , $\mathbf{M}_i = \langle \mathbf{S}_i \rangle$. Here, the spin operator is defined as $\mathbf{S}_i = \sum_{\alpha\beta} c_{i\alpha}^\dagger \boldsymbol{\sigma}_{\alpha\beta} c_{i\beta}$. The magnetization in the z direction can then be expressed as

$$\begin{aligned} M_i^z &= \sum_{n=1}^{2N} [(|v_{i,n}|^2 + |\chi_{i,n}|^2 - |\omega_{i,n}|^2 - |v_{i,n}|^2) f(E_n) \\ &\quad + |\omega_{i,n}|^2 - |\chi_{i,n}|^2]. \end{aligned} \quad (25)$$

B. Computational methods

The computational part of this study consists of numerically diagonalizing the Hamiltonian and self-consistently solving the equations for either the on-site superconducting gap [Eq. (22)] or the nearest-neighbor pairing amplitudes [Eq. (23)], depending on whether the superconductor is taken to be of the isotropic s -wave type or the d -wave type. Iterative solution of these equations require an initial value for the gap function/pairing amplitudes, and a convergence criterion in order to determine when a solution has been obtained. In this paper, the convergence criterion was that the relative change in the gap/pairing amplitudes from one iteration to the next should be less than 1×10^{-4} for the d -wave and 1×10^{-3} for the s -wave state. The initial values for the d -wave state are listed in the Appendix and the initial value for the s -wave gap Δ was set to $0.5t$.

III. RESULTS AND DISCUSSION

We first investigate the presence of midgap surface states, i.e., zero-energy states existing on an edge of a superconductor. As displayed in Fig. 2, we calculate the LDOS for different points on an s -wave and a d -wave superconductor without magnetic contacts. One of the points is located at the diagonal edge, one of the points is in the bulk, and the third point is on the lower horizontal edge. Only on the diagonal edge of the d -wave superconductor, Fig. 2(b1), there is a peak around zero-energy signaling the presence of midgap states. In this figure, the chemical potential has been set to $\mu_S = 0.7t$, which gives rise to an asymmetric density of states around $E = 0$ for our tight-binding model as the gap in the electron spectrum is opened away from the middle of the band.

As the presence of midgap states has been established, we move on to results for the indirect interaction between magnetic leads attached to a normal metal, an s -wave superconductor, and finally a d -wave superconductor.

A. Normal state

To put the results for the superconductors into context, we start with the case of magnetic leads connected by a normal metal ($V = U = 0$). The indirect exchange interaction J is presented in Fig. 3. For the horizontal edge, the result is the expected RKKY oscillations that are damped with increasing

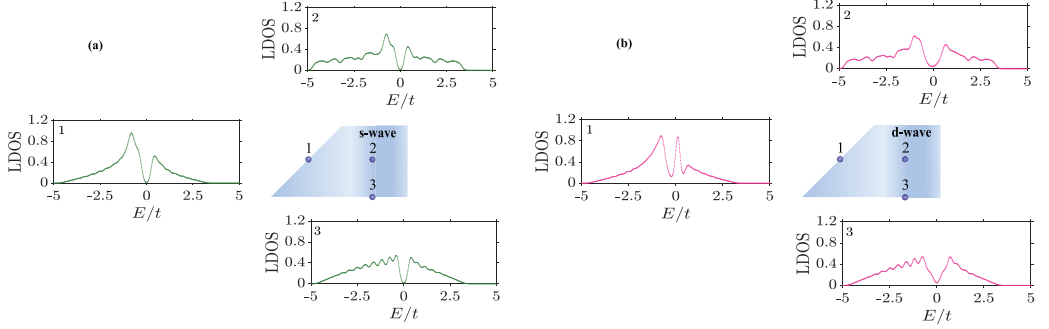


FIG. 2. Local density of states (LDOS) for different points of an s -wave superconductor (a) and a d -wave superconductor (b), showing the presence of midgap states on the diagonal edge of the d -wave superconductor. In both cases the size of the structure is $L_{xS} = 34$ and $L_{yS} = 30$. For the s -wave results we have taken $U/t = 2$ and $V = 0$, while for the d -wave results we have taken $U = 0$ and $V/t = -1$. In both cases we have set the chemical potential $\mu_S = 0.7t$.

distance between the magnets. For the diagonal edge, the results are more peculiar, showing an enhanced interaction when the electrodes are close to the endpoints of the diagonal edge. Investigating the LDOS for $E = 0$ in Fig. 4, the reason becomes clear. Close to the edges of the system, the LDOS increases in magnitude and exhibits Friedel-like oscillations due to the abruptly vanishing charge density at the edge. The oscillatory and increased LDOS close to the edges correspondingly affects the RKKY interaction when the electrodes are close to the edge.

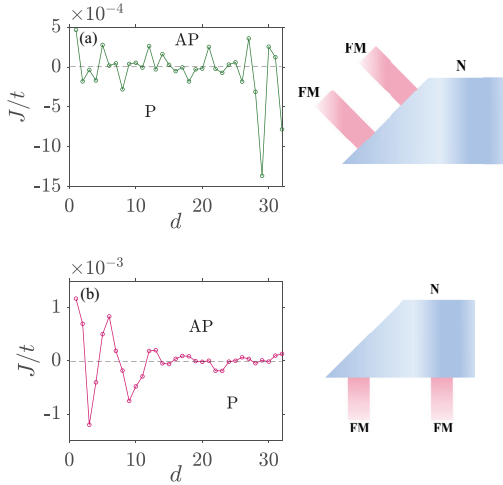


FIG. 3. Normal metal: Indirect exchange interaction between magnetic leads connected to a diagonal (a) and a horizontal (b) edge of a normal metal, presented as a function of the distance between the leads. Here, the chemical potential in the normal metal is set to $\mu_N = 0.9t$ and the chemical potential in the ferromagnets is set to $\mu_F = 1.2t$. Further, $h_i = 2t$, $L_{xN} = 40$, $L_{yN} = 40$, $L_{xF} = 2$, $L_{yF} = 10$, and $V = U = 0$. In both subfigures, the leftmost magnet was fixed two lattice points away from the endpoint of the edge.

B. s -Wave pairing

We then move on to the case of magnetic leads connected by an isotropic s -wave superconductor ($V = 0$). The results for the indirect exchange interaction are presented in Fig. 5. In this case, there are two competing effects: The conventional RKKY interaction and the blocking of the states that can mediate the interaction due to the gap around the Fermi level in the band structure. For a weak attractive interaction U in the superconductor, the RKKY interaction dominates, giving rise to an oscillating behavior. For larger U , the gap becomes larger and can block more of the states that can mediate the interaction between the magnets. The interaction then displays a damping behavior instead of oscillations, and an antiparallel configuration of the magnets is preferred [34]. For the diagonal edge, the electrodes have been kept further away from the endpoints of the edge. For a weak attractive interaction U , the enhanced RKKY oscillations occurring when the electrodes are close to the end-points can, however, still be observed, as explained previously. On the other hand, when the strength of

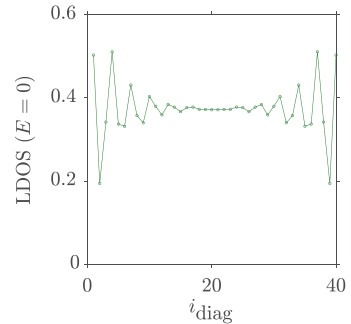


FIG. 4. Normal metal: Local density of states (LDOS) for $E = 0$ at the diagonal edge in the absence of magnetic contacts. The system size is $L_{xN} = 40$ and $L_{yN} = 40$, $V = U = 0$, and the chemical potential in the normal metal is $0.9t$.

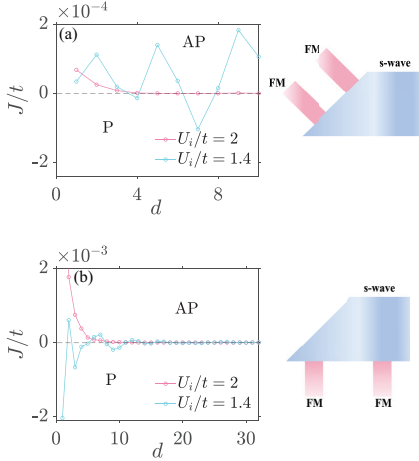


FIG. 5. *s*-Wave : Indirect exchange interaction between magnetic leads connected to a diagonal (a) and a horizontal (b) edge of a *s*-wave superconductor. Here $\mu_S = 0.9t$, $\mu_F = 1.2t$, $h_i = 2t$, $L_{xS} = 40$, $L_{yS} = 40$, $L_{xF} = 2$, $L_{yF} = 10$, and $V = 0$. For the diagonal edge, the leftmost magnet is fixed 13 lattice points away from the endpoint of the edge, while for the horizontal edge, the leftmost magnet is fixed 2 lattice points away from the endpoint.

the attractive interaction is increased, increasing the superconducting gap, we see that J is damped to zero for sufficiently large magnet separation also for the diagonal edge. Thus, in the *s*-wave case, the qualitative behavior of J is the same regardless of which edge we consider.

C. *d*-Wave pairing

Finally, we consider the main result of this paper, which is how the magnetic leads interact when separated by a *d*-wave superconductor ($U = 0$). The results for the indirect interaction between the magnetic leads is presented in Fig. 6. For the horizontal edge, the interaction displays an oscillating behavior and varies in sign as a function of the distance between the magnetic contacts. The results for the diagonal edge, on the other hand, show a qualitatively different behavior. The system now always prefers alignment of the ferromagnets and the interaction varies little with distance. Further, increasing h_i now leads to a larger difference in free energy between the parallel and antiparallel magnet configurations.

The result that a parallel magnet configuration is strongly favored for the diagonal edge is surprising as one would expect that the parallel configuration induces a larger magnetization in the superconductor, which suppresses the gap and lowers the condensation energy. A particularly large induced magnetization in the superconductor should be expected in the presence of midgap states, which can give rise to a giant magnetic moment when subjected to a spin splitting [4,35,36]. In accordance with this, we find a sizable induced magnetization on the diagonal edge. As previously discussed in the literature, the magnetization induced in a superconductor due to

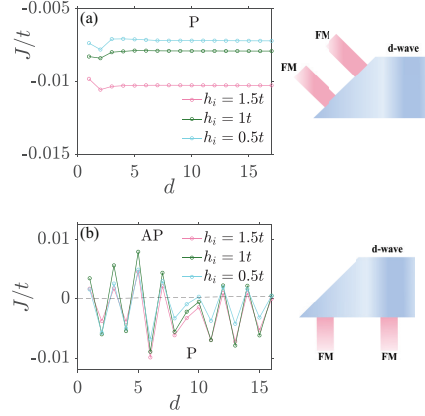


FIG. 6. *d*-Wave : Indirect exchange interaction between magnetic leads connected to a diagonal (a) and a horizontal (b) edge of a *d*-wave superconductor. Here $\mu_S = 0.7t$, $\mu_F = 1t$, $V/t = -1$, $L_{xF} = 2$, $L_{yF} = 10$, and $U = 0$. For the diagonal edge, the leftmost magnet is fixed only 2 lattice points away from the endpoint of the edge in order to maximize the number of data points. The *d*-wave diagonal edge results are not sensitive to how close the magnets are to the endpoints of the edge. Further $L_{xS} = 34$, $L_{yS} = 30$. For the horizontal edge, the leftmost magnet is fixed 10 lattice points away from the endpoint, and $L_{xS} = 40$, $L_{yS} = 20$.

proximity to a ferromagnet can be either aligned or anti-aligned with the magnetization of the ferromagnet [37–39]. A physical picture for the origin of an anti-aligned induced magnetization is that there are contributions from Cooper pairs where one of the two electrons is located in the ferromagnet, aligned with the local magnetization, leaving a Cooper pair partner with opposite spin in the superconductor. In the present system the induced magnetization tends to be anti-aligned with the magnetization of the magnetic contacts, as displayed in Figs. 7(a) and 7(b).

The effect of introducing the magnets is, however, not solely to reduce the gap due to an induced effective spin splitting in the superconductor. The induced spin splitting also splits the midgap states away from their resonance point at zero energy, suppressing the midgap states. As the gap close to the edge to begin with is strongly suppressed by the midgap states, the effect of reducing the midgap states, causing the superconducting order parameter to recover at the edge, is stronger than the effect of the spin splitting on the condensation energy. As the parallel configuration most effectively produces a spin splitting in the superconductor, this configuration features the largest condensation energy, giving rise to the behavior that is observed in Fig. 6(a).

Investigating the constant term in the Hamiltonian $H_0 = \sum_i H_{0,i}$, the difference between $H_{0,i}$ for the parallel and antiparallel configurations is presented in Fig. 7(c). The figure shows that H_0 , which is a positive quantity, is largest for the parallel configuration, corresponding to a larger gap. In turn, this produces a larger condensation energy that lowers the free energy of the system. From the figure, it is clear that the

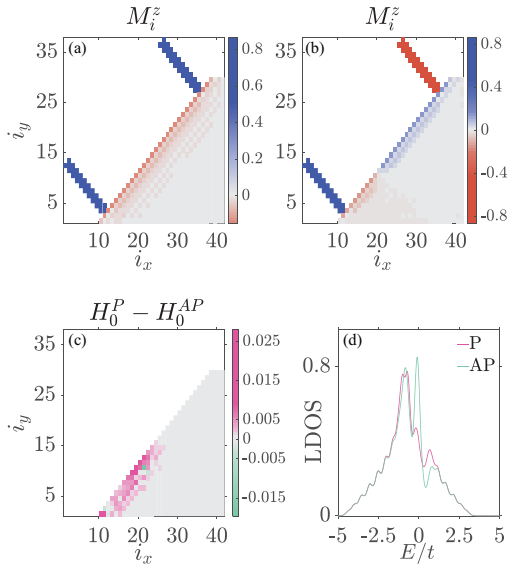


FIG. 7. *d*-Wave: Magnetization on each lattice site for the parallel (a) and antiparallel (b) configuration of magnets. The difference in $H_{0,i}$ between the parallel and antiparallel configurations is presented in (c). The local density of states (LDOS) for the 11th lattice site (from the left) of the diagonal edge is presented in (d), showing that the midgap states are more suppressed for the parallel magnet configuration. Here we have taken the same parameters as in Fig. 6(a), apart from a larger exchange field of $h_i = 2t$ in order to more clearly show the differences between the two configurations.

main contribution to the difference in condensation energy between the magnetic configurations comes from the transition region where the antiparallel configuration has a reduced edge magnetization. LDOS results from this region are presented in Fig. 7(d). While the AP configuration in this region has a clear midgap peak around zero energy, the midgap states for the P configuration have been split and suppressed by the induced spin splitting.

We close by discussing briefly experimental considerations and possible choices of materials for observation of the *d*-wave results presented in this paper. While the system sizes in the presented calculations are limited by computational considerations, the presented results are expected to be robust also for larger systems. As RKKY interaction typically decays below experimentally accessible values over short length scales of the order of nanometers, the separation between the magnetic contacts typically needs to be kept small. This might however only apply to the RKKY dominated indirect interaction that we observe for the horizontal edge of the *d*-wave superconductor. The preference of alignment of the ferromagnets when attached to a diagonal edge of a *d*-wave superconductor is expected to also be observable for larger magnet separation as the indirect interaction in this case is not dominated by itinerant carriers, but rather arises from the parallel configuration more efficiently inducing a spin

splitting, suppressing the localized midgap states. The distance the magnets can interact over is then limited by the length scale determining how far away from a magnet the midgap states still experience a spin splitting. If the magnet separation is much larger than this decay length of the induced spin splitting along the edge, the spin splitting arising from each magnet decays before interacting with the spin splitting arising from the other magnet. There is then no difference between the two magnet configurations when it comes to suppression of midgap states, and the parallel configuration is no longer favored. For an *s*-wave superconductor in proximity to a ferromagnet, the proximity-induced magnetization decays over a length scale of the superconducting coherence length [40]. A natural length scale for the decay of the induced spin splitting in the present case would then be the effective coherence length corresponding to the strongly suppressed order parameter at the edge. As the coherence length is inversely proportional to the order parameter, the magnets will then be able to interact over distances considerably larger than the bulk coherence length.

Experimental investigation of our main finding would consist of attaching magnetic leads to a {110} edge of a *d*-wave superconductor. The indirect interaction between the magnets can then be established by determining the energy barrier of switching between the two magnet configurations through an external magnetic field. Our prediction is that ferromagnetic alignment of the magnets will be preferred for a wide range of magnet separation distances. Possible material choices could be YBCO [2,7,29] for the *d*-wave superconductor featuring midgap states, and a nickel-alloy-like $\text{Ni}_{80}\text{Co}_{20}$ [41] for the magnetic contacts.

IV. SUMMARY

We have investigated the indirect exchange interaction between two ferromagnetic leads connected to a superconductor as a function of the separation between the magnets, showing that the presence of zero-energy surface states in a *d*-wave superconductor can qualitatively change the results. When the magnets are connected to an edge without zero-energy surface states we find a normal oscillating RKKY behavior. However, when the magnets are connected to an edge featuring zero-energy surface states, the strength of the magnetic exchange interaction is shifted away from zero, always favoring alignment of the magnetization in the two magnets, as the aligned configuration produces a larger superconducting condensation energy.

ACKNOWLEDGMENTS

This work was supported by the Research Council of Norway through its Centres of Excellence funding scheme, Grant No. 262633, QuSpin.

APPENDIX: PHASE DIAGRAM

In order to choose the parameters such that the superconductor used in the study is in a *d*-wave state, we obtain a starting point by considering a square system with continuous boundary conditions in both the *x* and *y* directions and no

attached magnetic leads. The relevant Hamiltonian is the one in Eq. (1) with $U_i = V_{ij} = 0$. We introduce Fourier transformations for the electron operators $c_{i\alpha} = \frac{1}{\sqrt{N}} \sum_{\mathbf{k}} e^{i\mathbf{k} \cdot \mathbf{i}} c_{\mathbf{k},\alpha}$ where $\mathbf{i} = (i_x, i_y)$ and N is the number of lattice sites. After the mean-field approximation, Eq. (1) then becomes

$$\begin{aligned} H^{\text{SC}} = & - \sum_{(i,j),\alpha} t c_{i\alpha}^\dagger c_{j\alpha} - \sum_{i,\alpha} \mu_i n_{i\alpha} \\ & + \sum_{i,\alpha \neq \alpha'} V [n_{i\alpha} n_{i+\hat{x},\alpha'} + n_{i\alpha} n_{i-\hat{x},\alpha'} + n_{i\alpha} n_{i+\hat{y},\alpha'} \\ & + n_{i\alpha} n_{i-\hat{y},\alpha'}] \\ = & \sum_{\mathbf{k},\sigma} \zeta_{\mathbf{k}} c_{\mathbf{k},\sigma}^\dagger c_{\mathbf{k},\sigma} + \sum_{\mathbf{k}} [(\Gamma_{\mathbf{k}})^\dagger c_{\mathbf{k}\downarrow}^\dagger c_{-\mathbf{k}\uparrow}^\dagger + \Upsilon_{\mathbf{k}} c_{\mathbf{k}\uparrow} c_{-\mathbf{k}\downarrow}] \\ & + H_0^{\text{SC}}. \end{aligned} \quad (\text{A1})$$

Here $H_0^{\text{SC}} = -2NV(|F^{\hat{x}+}|^2 + |F^{\hat{x}-}|^2 + |F^{\hat{y}+}|^2 + |F^{\hat{y}-}|^2)$,

$$\begin{aligned} F^{x\pm} &= \frac{1}{N} \sum_{\mathbf{k}} e^{\mp i\mathbf{k} \cdot \hat{x}} (c_{\mathbf{k},\uparrow} c_{-\mathbf{k},\downarrow}), \\ F^{y\pm} &= \frac{1}{N} \sum_{\mathbf{k}} e^{\mp i\mathbf{k} \cdot \hat{y}} (c_{\mathbf{k},\uparrow} c_{-\mathbf{k},\downarrow}), \end{aligned} \quad (\text{A2})$$

and we have defined,

$$\begin{aligned} \Upsilon_{\mathbf{k}} &= 2V(e^{-i\mathbf{k} \cdot \hat{x}} (F^{\hat{x}+})^\dagger + e^{i\mathbf{k} \cdot \hat{x}} (F^{\hat{x}-})^\dagger \\ &+ e^{-i\mathbf{k} \cdot \hat{y}} (F^{\hat{y}+})^\dagger + e^{i\mathbf{k} \cdot \hat{y}} (F^{\hat{y}-})^\dagger), \\ \Gamma_{\mathbf{k}} &= 2V(e^{i\mathbf{k} \cdot \hat{x}} (F^{\hat{x}+})^\dagger + e^{-i\mathbf{k} \cdot \hat{x}} (F^{\hat{x}-})^\dagger \\ &+ e^{i\mathbf{k} \cdot \hat{y}} (F^{\hat{y}+})^\dagger + e^{-i\mathbf{k} \cdot \hat{y}} (F^{\hat{y}-})^\dagger), \\ \varepsilon_{\mathbf{k}} &= -2t[\cos(\mathbf{k} \cdot \hat{x}) + \cos(\mathbf{k} \cdot \hat{y})] - \mu. \end{aligned} \quad (\text{A3})$$

Further, $t = t_{ij}$ and $V = V_{ij}$.

Following the BdG method [32], we consider the following basis in order to diagonalize the Hamiltonian

$$B_{\mathbf{k}}^\dagger = [c_{\mathbf{k}\uparrow}^\dagger \quad c_{\mathbf{k}\downarrow}^\dagger \quad c_{-\mathbf{k}\uparrow} \quad c_{-\mathbf{k}\downarrow}]. \quad (\text{A4})$$

Then full Hamiltonian can be written as $H = H_0 + \frac{1}{2} \sum_{\mathbf{k}} B_{\mathbf{k}}^\dagger H_{\mathbf{k}} B_{\mathbf{k}}$, where $H_0 = H_0^{\text{SC}} + \sum_{\mathbf{k}} \varepsilon_{\mathbf{k}}$ and $H_{\mathbf{k}}$ is

$$H_{\mathbf{k}} = \begin{bmatrix} \varepsilon_{\mathbf{k}} & 0 & 0 & -(\Upsilon_{\mathbf{k}})^\dagger \\ 0 & \varepsilon_{\mathbf{k}} & (\Gamma_{\mathbf{k}})^\dagger & 0 \\ 0 & \Gamma_{\mathbf{k}} & -\varepsilon_{\mathbf{k}} & 0 \\ -\Upsilon_{\mathbf{k}} & 0 & 0 & -\varepsilon_{\mathbf{k}} \end{bmatrix}. \quad (\text{A5})$$

Using the unitary matrix $P_{\mathbf{k}}$ the diagonalized form of the Hamiltonian will be $H^{\text{SC}} = H_0 + \frac{1}{2} \sum_{\mathbf{k}} B_{\mathbf{k}}^\dagger P_{\mathbf{k}}^\dagger P_{\mathbf{k}} H_{\mathbf{k}} P_{\mathbf{k}} P_{\mathbf{k}} B_{\mathbf{k}} = H_0 + \frac{1}{2} \sum_{\mathbf{k}} \tilde{B}_{\mathbf{k}}^\dagger \tilde{H}_{\mathbf{k}} \tilde{B}_{\mathbf{k}} = H_0 - \frac{1}{2} \sum_{\mathbf{k},\sigma} E_{\mathbf{k},\sigma} + \sum_{\mathbf{k},\sigma} E_{\mathbf{k},\sigma} \gamma_{\mathbf{k},\sigma}^\dagger \gamma_{\mathbf{k},\sigma}$. The relationship between the normal electron operators

TABLE I. Sets of initial values.

	F^{x+}	F^{x-}	F^{y+}	F^{y-}
d -wave	1	1	-1	-1
s -wave extended	1	1	1	1
$p_x + ip_y$	1	-1	i	$-i$
Normal state	0	0	0	0

and the quasiparticle operators is then

$$\begin{bmatrix} v_{\mathbf{k},\uparrow} & v_{\mathbf{k},\downarrow} & \omega_{-\mathbf{k},\uparrow}^* & \omega_{-\mathbf{k},\downarrow}^* \\ v_{\mathbf{k},\uparrow} & v_{\mathbf{k},\downarrow} & \chi_{-\mathbf{k},\uparrow}^* & \chi_{-\mathbf{k},\downarrow}^* \\ \omega_{\mathbf{k},\uparrow} & \omega_{\mathbf{k},\downarrow} & v_{-\mathbf{k},\uparrow}^* & v_{-\mathbf{k},\downarrow}^* \\ \chi_{\mathbf{k},\uparrow} & \chi_{\mathbf{k},\downarrow} & v_{-\mathbf{k},\uparrow}^* & v_{-\mathbf{k},\downarrow}^* \end{bmatrix} \begin{bmatrix} \gamma_{\mathbf{k}\uparrow} \\ \gamma_{\mathbf{k}\downarrow} \\ \gamma_{-\mathbf{k}\uparrow}^\dagger \\ \gamma_{-\mathbf{k}\downarrow}^\dagger \end{bmatrix} = \begin{bmatrix} c_{\mathbf{k}\uparrow} \\ c_{\mathbf{k}\downarrow} \\ c_{-\mathbf{k}\uparrow}^\dagger \\ c_{-\mathbf{k}\downarrow}^\dagger \end{bmatrix}, \quad (\text{A6})$$

where the columns are the eigenvectors of $H_{\mathbf{k}}$. The pairing amplitudes can then be expressed as

$$\begin{aligned} F^{x\pm} &= \frac{1}{N} \sum_{\mathbf{k},\sigma} [e^{\mp i\mathbf{k} \cdot \hat{x}} v_{\mathbf{k},\sigma} \chi_{\mathbf{k},\sigma}^* (1 - f(E_{\mathbf{k},\sigma})) \\ &+ e^{\pm i\mathbf{k} \cdot \hat{x}} \omega_{\mathbf{k},\sigma}^* v_{\mathbf{k},\sigma} f(E_{\mathbf{k},\sigma})], \\ F^{y\pm} &= \frac{1}{N} \sum_{\mathbf{k},\sigma} [e^{\mp i\mathbf{k} \cdot \hat{y}} v_{\mathbf{k},\sigma} \chi_{\mathbf{k},\sigma}^* (1 - f(E_{\mathbf{k},\sigma})) \\ &+ e^{\pm i\mathbf{k} \cdot \hat{y}} \omega_{\mathbf{k},\sigma}^* v_{\mathbf{k},\sigma} f(E_{\mathbf{k},\sigma})]. \end{aligned} \quad (\text{A7})$$

Finally, the free energy of the system is

$$F = H_0 - \frac{1}{2} \sum_{\mathbf{k},\sigma} E_{\mathbf{k},\sigma} - \frac{1}{\beta} \sum_{\mathbf{k},\sigma} \ln(1 + e^{-\beta E_{\mathbf{k},\sigma}}). \quad (\text{A8})$$

For different values of chemical potential and temperature, we then solve the self-consistent equations for the pairing amplitudes through iteration, using the different sets of initial values listed in Table I. We then compare the resulting free energies [Eq. (A8)] and determine the favored phase of the system. The phase diagram is presented in Fig. 8. The choices for the initial values are determined by the expressions for the

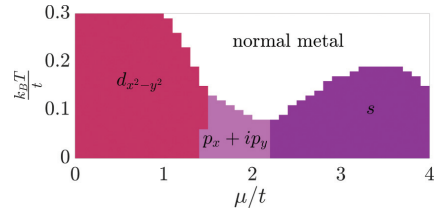


FIG. 8. Phase diagram for the tight-binding Hamiltonian with attractive nearest-neighbor interaction between opposite spins $V = -1t$. Here, T is the temperature, k_B is the Boltzmann constant, μ is the chemical potential, and t is the hopping amplitude.

gap functions [42]

$$\begin{aligned}\Delta_d &= (V/4)(F^{\hat{x}+} + F^{\hat{x}-} - F^{\hat{y}+} - F^{\hat{y}-}), \\ \Delta_s &= (V/4)(F^{\hat{x}+} + F^{\hat{x}-} + F^{\hat{y}+} + F^{\hat{y}-}),\end{aligned}$$

$$\Delta_{p_x} = (V/2)(F^{\hat{x}+} - F^{\hat{x}-}),$$

$$\Delta_{p_y} = (V/2)(F^{\hat{y}+} - F^{\hat{y}-}). \quad (\text{A9})$$

-
- [1] P. Monthoux, A. V. Balatsky, and D. Pines, *Phys. Rev. B* **46**, 14803 (1992).
- [2] D. A. Wollman, D. J. Van Harlingen, W. C. Lee, D. M. Ginsberg, and A. J. Leggett, *Phys. Rev. Lett.* **71**, 2134 (1993).
- [3] C. C. Tsuei, J. R. Kirtley, C. C. Chi, Lock See Yu-Jahnes, A. Gupta, T. Shaw, J. Z. Sun, and M. B. Ketchen, *Phys. Rev. Lett.* **73**, 593 (1994).
- [4] C.-R. Hu, *Phys. Rev. Lett.* **72**, 1526 (1994).
- [5] Y. Tanaka and S. Kashiwaya, *Phys. Rev. Lett.* **74**, 3451 (1995).
- [6] S. Kashiwaya, Y. Tanaka, M. Koyanagi, H. Takashima, and K. Kajimura, *Phys. Rev. B* **51**, 1350 (1995).
- [7] J. Geerk, X. Xi, and G. Linker, *Z. Phys. B* **73**, 329 (1988).
- [8] J. Lesueur, L. Greene, W. Feldmann, and A. Inam, *Physica C: Superconductivity* **191**, 325 (1992).
- [9] I. Iguchi, W. Wang, M. Yamazaki, Y. Tanaka, and S. Kashiwaya, *Phys. Rev. B* **62**, R6131(R) (2000).
- [10] J. Y. T. Wei, N.-C. Yeh, D. F. Garrigus, and M. Strasiak, *Phys. Rev. Lett.* **81**, 2542 (1998).
- [11] K. Yosida, *Phys. Rev.* **106**, 893 (1957).
- [12] M. A. Ruderman and C. Kittel, *Phys. Rev.* **96**, 99 (1954).
- [13] T. Kasuya, *Prog. Theor. Phys.* **16**, 45 (1956).
- [14] Y. Yafet, *Phys. Rev. B* **36**, 3948 (1987).
- [15] H. Imamura, P. Bruno, and Y. Utsumi, *Phys. Rev. B* **69**, 121303(R) (2004).
- [16] A. M. Black-Schaffer, *Phys. Rev. B* **81**, 205416 (2010).
- [17] E. Kogan, *Phys. Rev. B* **84**, 115119 (2011).
- [18] S. Saremi, *Phys. Rev. B* **76**, 184430 (2007).
- [19] M. Sherafati and S. Satpathy, *Phys. Rev. B* **83**, 165425 (2011).
- [20] E. H. Hwang and S. Das Sarma, *Phys. Rev. Lett.* **101**, 156802 (2008).
- [21] M. Shiranzadei, H. Cheraghchi, and F. Parhizgar, *Phys. Rev. B* **96**, 024413 (2017).
- [22] J.-J. Zhu, D.-X. Yao, S.-C. Zhang, and K. Chang, *Phys. Rev. Lett.* **106**, 097201 (2011).
- [23] Q. Liu, C.-X. Liu, C. Xu, X.-L. Qi, and S.-C. Zhang, *Phys. Rev. Lett.* **102**, 156603 (2009).
- [24] V. M. Galitski and A. I. Larkin, *Phys. Rev. B* **66**, 064526 (2002).
- [25] P. W. Anderson and H. Suhl, *Phys. Rev.* **116**, 898 (1959).
- [26] N. Y. Yao, L. I. Glazman, E. A. Demler, M. D. Lukin, and J. D. Sau, *Phys. Rev. Lett.* **113**, 087202 (2014).
- [27] A. A. Zyuzin and D. Loss, *Phys. Rev. B* **90**, 125443 (2014).
- [28] Y. Zhu, A. Pal, M. G. Blamire, and Z. H. Barber, *Nat. Mater.* **16**, 195 (2017).
- [29] U. Welp, W. K. Kwok, G. W. Crabtree, K. G. Vandervoort, and J. Z. Liu, *Phys. Rev. Lett.* **62**, 1908 (1989).
- [30] D. Aristov, S. Maleyev, and A. Yashenkin, *Z. Phys. B* **102**, 467 (1997).
- [31] A. Di Bernardo, S. Komori, G. Livanas, G. Divitini, P. Gentile, M. Cuoco, and J. W. Robinson, *Nat. Mater.* **18**, 1194 (2019).
- [32] P. G. De Gennes, *Superconductivity Of Metals And Alloys* (CRC Press, Boca Raton, FL, 1999).
- [33] F. S. Bergeret, M. Silaev, P. Virtanen, and T. T. Heikkilä, *Rev. Mod. Phys.* **90**, 041001 (2018).
- [34] A. Ghanbari, V. K. Risinggård, and J. Linder, *Sci. Rep.* **11**, 5028 (2021).
- [35] C.-R. Hu and X.-Z. Yan, *Phys. Rev. B* **60**, R12573(R) (1999).
- [36] J.-X. Zhu and C. S. Ting, *Phys. Rev. B* **61**, 1456 (2000).
- [37] F. S. Bergeret, A. F. Volkov, and K. B. Efetov, *Rev. Mod. Phys.* **77**, 1321 (2005).
- [38] F. S. Bergeret, A. Levy Yeyati, and A. Martín-Rodero, *Phys. Rev. B* **72**, 064524 (2005).
- [39] M. Y. Kharitonov, A. F. Volkov, and K. B. Efetov, *Phys. Rev. B* **73**, 054511 (2006).
- [40] F. S. Bergeret, A. F. Volkov, and K. B. Efetov, *Phys. Rev. B* **69**, 174504 (2004).
- [41] S. S. P. Parkin and D. Mauri, *Phys. Rev. B* **44**, 7131 (1991).
- [42] K. Kuboki, *J. Phys. Soc. Jpn.* **70**, 2698 (2001).


RKKY interaction in a spin-split superconductor

Phys. Rev. B **104**, 094527 (2021)

Authors | Atousa Ghanbari
Jacob Linder

RKKY interaction in a spin-split superconductor

Atousa Ghanbari and Jacob Linder

Center for Quantum Spintronics, Department of Physics, Norwegian University of Science and Technology, NO-7491 Trondheim, Norway (Received 9 May 2021; revised 7 August 2021; accepted 23 September 2021; published 30 September 2021)

We determine theoretically the interaction between two magnetic impurities embedded in a spin-split s -wave superconductor. The spin-splitting in the superconductor gives rise to two different interaction types between the impurity spins, depending on whether their spins lie in the plane perpendicular to the spin-splitting field (Heisenberg) or not (Ising). For impurity separation distances exceeding ξ_S , we find that the magnitude of the spin-splitting can determine whether an antiferromagnetic or ferromagnetic alignment of the impurity spins is preferred by the RKKY interaction. Moreover, the Ising and Heisenberg terms of the RKKY interaction alternate on being the dominant term and their magnitudes oscillate as a function of distance between the impurities.

DOI: [10.1103/PhysRevB.104.094527](https://doi.org/10.1103/PhysRevB.104.094527)**I. INTRODUCTION**

Superconductors have been experimentally demonstrated to exhibit strongly modified spin-dependent transport properties [1,2] with respect to normal metals, such as spin relaxation times [3–6] and magnetoresistance effects [7]. Consequently, superconductors have the potential to advance research on spintronic devices, in which the spin of the electron is utilized as the information carrier instead of the electronic charge [8–10]. Intrinsically coexisting ferromagnetism and superconductivity, proposed more than 60 years ago [11–13], is only possible under rather strict conditions. On the other hand, by creating hybrid structures of ferromagnetic and superconducting materials, it is possible to study the interplay between these orders by virtue of the proximity effect [14].

The Ruderman–Kittel–Kasuya–Yosida (RKKY) interaction [15–17] between magnetic impurities is an exchange interaction mediated by conduction electrons of the host material that the impurities are embedded in. This interaction has been vastly studied in different materials with spin-degeneracy, including systems with Dirac fermion excitations [18–20] and superconducting materials [21–26]. In a clean metal, the RKKY interaction decays as R^{-D} where R is the distance between the impurities and D is the dimension of the system. Likewise, the interaction decays faster in higher dimensions also in superconducting systems.

In the presence of spin-degeneracy, the RKKY interaction between magnetic impurities is isotropic in spin space and has no preferred direction for the impurity magnetic moments. On the other hand, it has been shown that in spin nondegenerate systems, the interaction can have different terms of the types Heisenberg, Ising, and Dzyaloshinskii–Moriya (DM) [27], depending on the spin structure of the host material. For instance, in a uniformly spin polarized system the Ising term arises [28] whereas in systems with spin-orbit interactions a DM interaction term can emerge [29–33]. In particular, the interaction between magnetic impurities located on top of an s -wave superconductor with Rashba spin-orbit coupling has

been found to feature an additional DM term due to the spin-orbit coupling in the superconductor [34]. Similar results have been obtained for the interaction between magnetic impurities on top of a topological insulator with proximity-induced superconductivity from an s -wave superconductor [35].

To the best of our knowledge, the RKKY interaction between magnetic impurities in a spin-split superconductor (see Fig. 1) has not been studied. Such superconductors have in recent years been demonstrated to give rise to interesting spin-dependent thermoelectric effects and spin diffusion properties [36]. Due to the spin-splitting, the density of states in the superconductor acquires a large spin-dependent particle-hole asymmetry. Therefore, one might expect that the RKKY interaction could be modified compared to both the purely superconducting case and the case of a superconductor with spin-orbit interaction.

In practice, a spin-split superconductor is achieved by either exposing a spin-film superconductor to a strong in-plane magnetic field or by growing a thin-film superconductor on top of a ferromagnetic insulator. In this case, the thickness of the superconductor has to be much smaller than the magnetic penetration depth λ . When the superconductor has a thickness smaller than the superconducting coherence length ξ_S , it can be well approximated by a superconductor coexisting with a homogeneous spin-splitting field.

In this paper, we will consider the RKKY interaction between two magnetic impurity atoms embedded in a spin-split conventional s -wave superconductor, contrasting it to the interaction between magnetic impurities in a normal metal subject to a spin-splitting field. While the RKKY interaction, in the normal metal case, is mediated by electrons, the RKKY in the superconducting case is mediated by quasiparticles that are a mix of electron and hole excitations. However, in both the superconducting and normal case a spin-splitting field induced via proximity to a ferromagnetic insulator lifts the spin degeneracy of the system. This causes the RKKY-interaction to have two parts: a Heisenberg- and Ising-term. In the present context, a Heisenberg term denotes the interaction energy

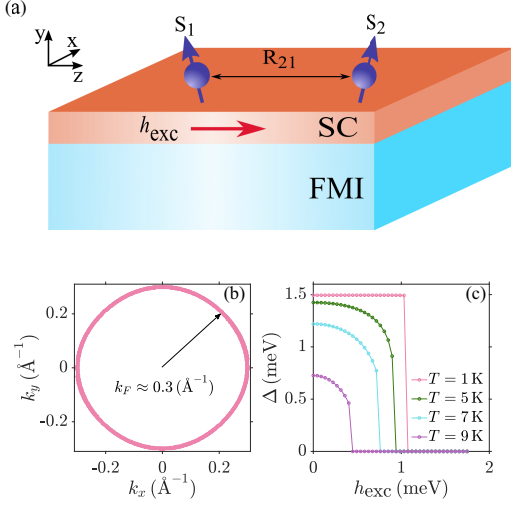


FIG. 1. (a) Schematic illustration of a possible experimental realization of the system. A thin-film superconductor is placed on top of a ferromagnetic insulator. Quasiparticle reflection at the interface to the ferromagnetic insulator induces an effective spin-splitting field inside the superconductor. (b) Circular Fermi-surface with Fermi vector magnitude of 0.3 \AA^{-1} used in our calculations. (c) Superconducting gap as a function of external exchange field for different temperature magnitudes.

obtained when the impurity spins lie in the plane perpendicular to the spin-splitting field. The Ising term describes the interaction for the case when the impurity spins are collinear with the spin-splitting field.

We find that it is possible to switch between an AFM and FM interaction between the magnetic impurities by adjusting the magnitude of the spin-splitting field. While this effect is in principle attainable even in the normal-state of the system, it is considerably more robust in the superconducting state where it occurs in a much larger regime of separation distances between the impurities compared to the normal state. We discuss a possible experimental way to adjust the spin-splitting field strength in order to see this effect. Moreover, we find that the magnitudes of the Ising and Heisenberg terms of the RKKY interaction oscillate as a function of distance between the impurities, causing them to take turns on which is the dominant term.

This paper is structured as follows. We introduce the methodology used to compute the RKKY interaction in Sec. II. In Sec. III, we present a numerical evaluation of the expression for the RKKY interaction and discuss the underlying physics of its behavior. Finally, we summarize our findings in Sec. IV.

II. MODEL AND METHODS

We consider a thin film s-wave superconductor in presence of a spin-splitting field, which causes a spin-splitting in the

electron bands, as shown in Fig. 1. The superconductor is modelled by a tight-binding Hamiltonian including an attractive interaction between the electrons

$$H_0 = - \sum_{(i,j),\sigma} t_{ij} c_{i,\sigma}^\dagger c_{j,\sigma} + \sum_i V c_{i,\uparrow}^\dagger c_{i,\downarrow}^\dagger c_{i,\downarrow} c_{i,\uparrow} - \sum_{i,\sigma} (\sigma h_{\text{exc}} + \mu) c_{i,\sigma}^\dagger c_{i,\sigma}. \quad (1)$$

The first term represents the nearest-neighbor hopping term with $t_{ij} = t$ being the hopping parameter. The second term is the BCS on-site attractive interaction with $V < 0$ being the pairing strength. In the third term, h_{exc} is the spin-splitting field. In our model, we consider this field to be oriented in the z direction, which is assumed to lie in the film plane of the superconductor. The Meissner response of the superconductor is well known to be suppressed in a thin-film geometry when the field is applied in plane and we may neglect orbital effects.

We consider the system having continuous boundary conditions along both in-plane directions (x and z axes here). Using a Fourier transformation $c_{i\alpha} = \frac{1}{\sqrt{N}} \sum_{\mathbf{k}} e^{-i\mathbf{k}\cdot\mathbf{r}_i} c_{\mathbf{k},\alpha}$ where N is the total number of the lattice points, leads to the following form of the Hamiltonian in the k space:

$$H_0 = \sum_{\mathbf{k},\sigma} (\zeta_{\mathbf{k}} - \sigma h_{\text{exc}}) c_{\mathbf{k},\sigma}^\dagger c_{\mathbf{k},\sigma} + \sum_{\mathbf{k}\mathbf{k}'} V c_{\mathbf{k},\uparrow}^\dagger c_{-\mathbf{k},\downarrow}^\dagger c_{-\mathbf{k}',\downarrow} c_{\mathbf{k}',\uparrow}, \quad (2)$$

where $\zeta_{\mathbf{k}} = -2t[\cos(k_x a_x) + \cos(k_z a_z)] - \mu$ and in it $a_x(a_z)$ is the lattice constant along $x(z)$ axis, also μ is the chemical potential. Here, we have redefined $V/N \rightarrow V$.

Performing a mean-field treatment, we introduce the superconducting gap

$$\Delta = -V \sum_{\mathbf{k}'} \langle c_{-\mathbf{k}',\downarrow} c_{\mathbf{k}',\uparrow} \rangle. \quad (3)$$

We then obtain

$$H_0 = \sum_{\mathbf{k},\sigma} (\zeta_{\mathbf{k}} - \sigma h_{\text{exc}}) c_{\mathbf{k},\sigma}^\dagger c_{\mathbf{k},\sigma} - \sum_{\mathbf{k},\sigma} \Delta c_{\mathbf{k},\uparrow}^\dagger c_{-\mathbf{k},\downarrow} - \sum_{\mathbf{k},\sigma} \Delta^* c_{-\mathbf{k},\downarrow} c_{\mathbf{k},\uparrow} - \frac{|\Delta|^2}{V}. \quad (4)$$

Using the following transformation (see Appendix A for details),

$$\begin{pmatrix} c_{\mathbf{k},\sigma} \\ c_{-\mathbf{k},-\sigma}^\dagger \end{pmatrix} = \begin{pmatrix} v_{\mathbf{k}} & \sigma v_{\mathbf{k}} \\ -\sigma v_{\mathbf{k}} & v_{\mathbf{k}} \end{pmatrix} \begin{pmatrix} \gamma_{\mathbf{k},\sigma} \\ \gamma_{-\mathbf{k},-\sigma}^\dagger \end{pmatrix}, \quad (5)$$

where

$$v_{\mathbf{k}} = \frac{1}{\sqrt{2}} \sqrt{1 + \frac{\zeta_{\mathbf{k}}}{\sqrt{\zeta_{\mathbf{k}}^2 + \Delta^2}}}, \quad v_{\mathbf{k}} = \frac{1}{\sqrt{2}} \sqrt{1 - \frac{\zeta_{\mathbf{k}}}{\sqrt{\zeta_{\mathbf{k}}^2 + \Delta^2}}}, \quad (6)$$

the diagonalized form of H_0 will be

$$H_0 = -\frac{|\Delta|^2}{V} + \sum_{\mathbf{k}} \zeta_{\mathbf{k}} - \sum_{\mathbf{k}} E_{\mathbf{k}} + \sum_{\mathbf{k},\sigma} E_{\mathbf{k},\sigma} \gamma_{\mathbf{k},\sigma}^\dagger \gamma_{\mathbf{k},\sigma}. \quad (7)$$

Here, $E_k = \sqrt{\zeta_k^2 + \Delta^2}$ and $E_{k,\sigma} = E_k - \sigma h_{\text{exc}}$. Expressing the electron operators in terms of the quasiparticle operators Eq. (5), the gap equation takes the form

$$1 = -\frac{V}{2} \sum_k \frac{1}{2} \frac{1}{\sqrt{\zeta_k^2 + \Delta^2}} \left[\tanh \left(\frac{\beta}{2} (\sqrt{\zeta_k^2 + \Delta^2} - h_{\text{exc}}) \right) + \tanh \left(\frac{\beta}{2} (\sqrt{\zeta_k^2 + \Delta^2} + h_{\text{exc}}) \right) \right]. \quad (8)$$

In this paper, the gap equation is solved self-consistently. Further, the free energy of the system is given by

$$F = -\frac{|\Delta|^2}{V} + \sum_k \zeta_k - \sum_k E_k - \frac{1}{\beta} \sum_{k,\sigma} \ln(1 + e^{-\beta E_{k,\sigma}}). \quad (9)$$

An important characteristic length scale in the system is the superconducting coherence length ξ_S , which is indicative of the size of the Cooper pairs. In the BCS formalism, this quantity for an isotropic s -wave superconductor is given by $\xi_S = \frac{\hbar v_F}{\pi \Delta_0}$, where \hbar is the reduced Plank constant, v_F is the Fermi velocity, and Δ_0 is the superconducting gap at zero temperature. The Fermi velocity is $v_F = \frac{1}{\hbar} \frac{d\zeta_k}{dk} |_{k=k_F}$.

The main purpose of this paper is to determine the indirect exchange interaction between two magnetic impurity atoms mediated by the quasiparticles inside a superconductor described by the Hamiltonian in Eq. (1). The coupling between the quasiparticle spins and the magnetic impurities will be treated perturbatively. The total Hamiltonian can then be written as

$$H = H_0 + \Delta H, \quad (10)$$

in which the first part is the nonperturbative Hamiltonian given by Eq. (1) and the second part is the perturbation defined by

$$\Delta H = J \sum_{j=1}^2 S_j \cdot s_j. \quad (11)$$

Here, J is the strength of the interaction between the spin of an impurity atom (S_j) and an itinerant spin (s_j) at lattice site j . The impurity spin is treated classically like a normal vector and itinerant spin is treated quantum mechanically and represented by the operator $s_j = \sum_{\alpha\beta} \sigma_{\alpha\beta} c_{j\alpha}^\dagger c_{j\beta}$. Here, $\sigma = (\sigma_x, \sigma_y, \sigma_z)$ is the Pauli matrix vector. Performing a Fourier transformation, the perturbation term in the Hamiltonian becomes

$$\Delta H = \sum_{k,k'} \sum_{\alpha,\beta} \frac{J}{N} e^{i(k-k')\cdot r_j} (S_j \cdot \sigma_{\alpha\beta}) c_{k,\alpha}^\dagger c_{k',\beta}. \quad (12)$$

By means of Eq. (5), we change the $c_{k,\alpha}$ operators into quasiparticle operators. Then, by means of a Schrieffer-Wolff transformation (SWT), the effective interaction between the magnetic impurity atoms is obtained to second order in the coupling J . To obtain the effective interaction, we consider a unitary matrix U of the form $U = e^{iS}$. The unitary transformation of the total Hamiltonian H is then

$$\tilde{H} = U H U^\dagger = e^{iS} H e^{-iS}. \quad (13)$$

The above equation may be expanded as

$$\tilde{H} = H_0 + \Delta H + i[S, H_0] + i[S, \Delta H] + O(J^3), \quad (14)$$

where we take $S = JS'$ and discard higher order terms in J . This leads to the following effective Hamiltonian for the system:

$$\tilde{H} = H_0 + \Delta H + i[S, H_0] + i[S, \Delta H]. \quad (15)$$

We now choose the unitary transformation S so that $\Delta H + i[S, H_0] = 0$ and the effective Hamiltonian becomes $\tilde{H} = H_0 + i[S, \Delta H]$. In order to accomplish this, we consider the following Ansatz for S :

$$S = \sum_{\substack{k,k' \\ \alpha,\beta}} (A_{k,k'} \gamma_{k,\alpha}^\dagger \gamma_{k',\beta} + B_{k,k'} \gamma_{k,\alpha}^\dagger \gamma_{-k',-\beta} + C_{k,k'} \gamma_{-k,-\alpha} \gamma_{k',\beta} + D_{k,k'} \gamma_{-k,-\alpha} \gamma_{-k',-\beta}). \quad (16)$$

Computing the commutator $[S, H_0]$, and requiring $\Delta H + i[S, H_0] = 0$, the coefficients in S are found to be

$$\begin{aligned} A_{k,k'} &= i \sum_j \frac{J}{N} e^{i(k-k')\cdot r_j} (S_j \cdot \sigma_{\alpha\beta}) \frac{v_k^* v_{k'}}{E_{k',\beta} - E_{k,\alpha}}, \\ B_{k,k'} &= -\beta i \sum_j \frac{J}{N} e^{i(k-k')\cdot r_j} (S_j \cdot \sigma_{\alpha\beta}) \frac{v_k^* v_{k'}}{E_{-k',-\beta} + E_{k,\alpha}}, \\ C_{k,k'} &= \alpha i \sum_j \frac{J}{N} e^{i(k-k')\cdot r_j} (S_j \cdot \sigma_{\alpha\beta}) \frac{v_k^* v_{k'}}{E_{k',\beta} + E_{-k,-\alpha}}, \\ D_{k,k'} &= \alpha \beta i \sum_j \frac{J}{N} e^{i(k-k')\cdot r_j} (S_j \cdot \sigma_{\alpha\beta}) \frac{v_k^* v_{k'}}{-E_{-k',-\beta} + E_{-k,-\alpha}}. \end{aligned} \quad (17)$$

The final form of the effective Hamiltonian \tilde{H} is obtained after calculating $[S, \Delta H]$. In this Hamiltonian, we neglect terms representing feedback from the impurity spin on the superconductor. Feedback from the impurities would ideally be included by self-consistently taking into account both the effect of the presence of the superconductor on the impurity spins and the effect of the impurity spins on the superconducting gap, giving rise to spatial variation of the superconducting order parameter. As the density of impurities in the system is very low, neglecting feedback from the impurities can be justified.

Computing the expectation value of the effective Hamiltonian \tilde{H} (given explicitly in Appendix B) leads to two different terms in the interaction energy between the two magnetic impurities: a 2D Heisenberg-like (E_H) and Ising-like (E_I) interaction

$$\langle \tilde{H} \rangle = E_0 + 2E_I (S_1^z S_2^z) + 2E_H (S_1^x S_2^x + S_1^y S_2^y), \quad (18)$$

where E_0 is a constant. In Sec. III, we will consider these E_I and E_H terms in more detail analytically and then evaluate them numerically to determine the nature of the RKKY interaction in a spin-split superconductor.

III. RESULTS AND DISCUSSION

A. Analytical

The physical significance of the RKKY interaction terms E_I and E_H is described as follows. The Ising term E_I determines the strength of the interaction between the magnetic impurities when they are oriented collinearly to the spin-splitting field. For $E_I > 0$, the interaction prefers an AFM alignment of the impurity spins. For $E_I < 0$, they prefer a FM

alignment. The Heisenberg term E_H determines the strength of the interaction between the magnetic impurities when they lie in the plane perpendicular to the spin-splitting field. The same considerations regarding the sign for E_H hold as for the Ising term.

The explicit expression for the RKKY Ising-like interaction between the spin of impurity atom 1 and the spin of impurity atom 2 is found to be

$$E_I = -\frac{1}{2} \sum_{k,k'} \left(\frac{J}{N}\right)^2 e^{i(k'-k)\cdot R_{21}} \left[(|v_k v_{k'}|^2 + |v_k v_{k'}|^2) \left(\frac{n(E_{k,\uparrow}) - n(E_{k',\uparrow})}{E_{k,\uparrow} - E_{k',\uparrow}} + \frac{n(E_{k,\downarrow}) - n(E_{k',\downarrow})}{E_{k,\downarrow} - E_{k',\downarrow}} \right) - 2v_k^* v_{k'} v_k^* v_{k'} \right. \\ \times \left(\frac{n(E_{k',\uparrow}) - n(E_{k,\uparrow})}{E_{k',\uparrow} - E_{k,\uparrow}} + \frac{n(E_{k',\downarrow}) - n(E_{k,\downarrow})}{E_{k',\downarrow} - E_{k,\downarrow}} \right) - 2v_k^* v_{k'} v_k^* v_{k'} \left(\frac{1 - n(E_{k,\uparrow}) - n(E_{k',\downarrow})}{E_{k,\downarrow} + E_{k',\uparrow}} + \frac{1 - n(E_{k,\downarrow}) - n(E_{k',\uparrow})}{E_{k',\uparrow} + E_{k,\downarrow}} \right) \\ \left. + \left(\frac{1 - n(E_{k,\uparrow}) - n(E_{k',\downarrow})}{E_{k,\uparrow} + E_{k',\downarrow}} + \frac{1 - n(E_{k,\downarrow}) - n(E_{k',\uparrow})}{E_{k,\downarrow} + E_{k',\uparrow}} \right) 2v_k^* v_{k'} v_k^* v_{k'} \right]. \quad (19)$$

Here, $R_{21} = r_2 - r_1$ is the relative distance between the two impurity atoms and $n(E_{k,\sigma}) = (1 + e^{\beta E_{k,\sigma}})^{-1}$ is the Fermi-Dirac distribution function. The Heisenberg-like term in the RKKY interaction energy is

$$E_H = -\frac{1}{2} \sum_{k,k'} \left(\frac{J}{N}\right)^2 e^{i(k'-k)\cdot R_{21}} \left[(|v_k v_{k'}|^2 + |v_k v_{k'}|^2) \left(\frac{n(E_{k,\uparrow}) - n(E_{k',\downarrow})}{E_{k,\downarrow} - E_{k',\uparrow}} + \frac{n(E_{k,\downarrow}) - n(E_{k',\uparrow})}{E_{k',\uparrow} - E_{k,\downarrow}} \right) - 2v_k^* v_{k'} v_k^* v_{k'} \right. \\ \times \left(\frac{n(E_{k',\downarrow}) - n(E_{k,\uparrow})}{E_{k',\downarrow} - E_{k,\uparrow}} + \frac{n(E_{k',\uparrow}) - n(E_{k,\downarrow})}{E_{k',\uparrow} - E_{k,\downarrow}} \right) - 2v_k^* v_{k'} v_k^* v_{k'} \left(\frac{1 - n(E_{k,\uparrow}) - n(E_{k',\uparrow})}{E_{k',\uparrow} + E_{k,\uparrow}} + \frac{1 - n(E_{k,\downarrow}) - n(E_{k',\downarrow})}{E_{k',\downarrow} + E_{k,\downarrow}} \right) \\ \left. + \left(\frac{1 - n(E_{k,\uparrow}) - n(E_{k',\uparrow})}{E_{k,\uparrow} + E_{k',\uparrow}} + \frac{1 - n(E_{k,\downarrow}) - n(E_{k',\downarrow})}{E_{k,\downarrow} + E_{k',\downarrow}} \right) 2v_k^* v_{k'} v_k^* v_{k'} \right]. \quad (20)$$

In the limiting case of $h_{\text{exc}} = 0$, the two above terms are equal. The system then displays a normal 3D Heisenberg-like interaction between the two impurity atoms hosted by an s -wave superconductor, which is spin isotropic as it should.

B. Numerical

Proceeding to a numerical evaluation of E_H and E_I , we consider a system of $N = 800 \times 800$ lattice points in the xz plane. We choose V so that the zero-temperature superconducting gap takes the value $\Delta \approx 1.5$ meV. The lattice constants are set to $a_x = a_z = 3.5$ Å. The hopping parameter and chemical potential magnitudes are taken to be $t = 0.2$ eV and $\mu = -0.6$ eV, respectively. The chemical potential is chosen to provide us with a circular Fermi surface as shown in Fig. 1(b). The superconducting gap at $T = 0$ K, the Fermi velocity, the Fermi wave vector, and coherence length take the values $\Delta_0 = 1.49$ meV, $v_F = 1.91 \times 10^5 \frac{\text{m}}{\text{s}}$, $k_F \approx 0.3$ Å⁻¹, and $\xi_S = 269$ Å, respectively.

Figure 1(c) illustrates the gap versus the spin-splitting field for different temperatures. A nontrivial solution to the gap equation does not guarantee that the superconducting phase is the ground state of the system. For each temperature and field strength, the ground state of the system (either $\Delta = 0$ or $\Delta \neq 0$) has therefore been determined by computing the free energy of the system given in Eq. (9). At $T \approx 0$ K the largest spin-splitting, which allows for a superconducting phase as the ground state is approximately $h_{\text{exc}} \approx 0.7\Delta_0$, which is

around 1.07 meV with our set of parameters. This is consistent with the Clogston-Chandrasekhar limit. It is also seen from the figure that increasing temperature reduces the gap until a phase transition occurs at the critical temperature, which is around $T_C = 9.829$ K for $h_{\text{exc}} = 0$. A superconductor with a similar set of parameters as chosen above is niobium (Nb) with a critical temperature $T_C \approx 9.2$ K [37].

1. Low temperatures $T \ll T_c$

We start by considering temperatures well within the superconducting phase $T \ll T_c$ and here set $T = 1$ K. The strength of the exchange interaction between the impurity spins and the quasiparticle spins is taken to be $J = 1$ meV. For $h_{\text{exc}} = 0$, the RKKY energies Eq. (19) and Eq. (20) are presented as a function of the distance between the two impurity atoms in Fig. 2(a). The RKKY energy goes to zero as R_{21} increases as seen in the inset of Fig. 2(a). The effect of the superconducting gap is primarily to shift the RKKY energy above zero for distances larger than coherence length ξ_S . Consequently, the interaction prefers an AFM orientation of the impurity spins at such distances. In the normal state of the system, the RKKY signal changes sign between FM and AFM alignment, also for large distances. These results are consistent with previous literature.

Considering instead the case where the spin-splitting field h_{exc} is present, an interesting possibility with regard to the tunability of the RKKY interaction opens up. Since the RKKY

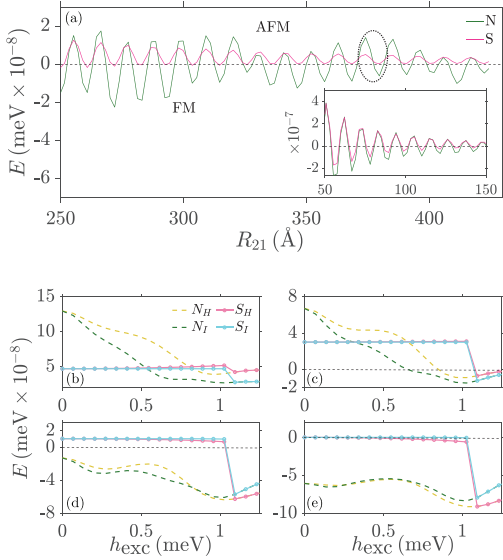


FIG. 2. (a) RKKY energy vs R_{21} when $h_{\text{exc}} = 0$. The inset represents the energies for distances smaller than coherence length. Furthermore, the energies as a function of exchange field for (b) $R_{21} = 374.7\text{\AA}$, (c) $R_{21} = 376.18\text{\AA}$, (d) $R_{21} = 377.59\text{\AA}$, and (e) $R_{21} = 379\text{\AA}$ are computed. Here, $N_H(N_I)$ is the Heisenberg (Ising) RKKY interaction energy for the normal state of the system while $S_H(S_I)$ is Heisenberg (Ising) RKKY interaction energy for the superconducting phase. The temperature is fixed at 1 k.

interaction E is positive in the superconducting state at $h_{\text{exc}} = 0$ for $R_{21} > \xi_S$ whereas it oscillates in the normal-state, driving the system through a phase transition by increasing h_{exc} above its critical value will change the sign of the RKKY interaction whenever the oscillations in the normal state causes $E < 0$. We illustrate this in Figs. 2(b)–2(e), which shows the RKKY energies at four different separation distances taken from the dashed oval region marked in Fig. 2(a).

It can be seen from Figs. 2(c)–2(e) that by increasing h_{exc} one can change the RKKY energy sign from AFM alignment into FM alignment and vice versa. In contrast to the normal state of the system where E varies significantly with h_{exc} , the RKKY interaction in the superconducting phase is practically independent of h_{exc} in comparison. This can be understood from the fact that the superconducting gap changes very slowly as a function of h_{exc} for low temperatures, as seen in Fig. 1(c). As a result, an abrupt change occurs once the phase transition to the normal state takes place, which can cause a sign change in the RKKY interaction. A sign change can in principle also occur in the normal state of the system, as shown in Fig. 2(c), but this effect is far less robust than the one observed in the superconducting state. In the normal state of the system, the sign change can only occur at carefully chosen separation distances R_{21} , whereas the sign change occurs in the superconducting state for a much larger set of separation distances. More precisely, when the separation distance

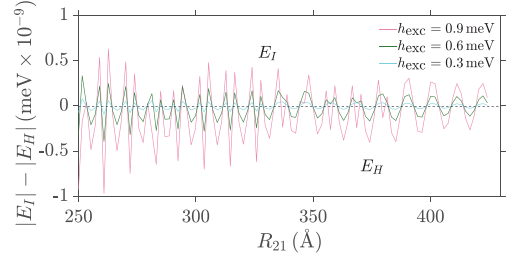


FIG. 3. Difference between the Ising and Heisenberg energies for three different values of the spin-splitting field at $T = 1$ K for the superconducting state.

between the impurities is larger than the coherence length, the sign change occurs in the superconducting state whenever the normal-state RKKY oscillations cause E to be negative. In principle, above the coherence length, this corresponds to half of all separation distances.

It is also of interest to determine whether the interaction between the magnetic impurities in the system favor their spins being collinear with the spin-splitting field or lying in the plane perpendicular to it. To this end, we compute the difference between the magnitude of the Ising and Heisenberg energies ($|E_I| - |E_H|$) as a function of distance between the impurities for several different values of the spin-splitting field in the superconducting phase (Fig. 3). The term, which is largest in magnitude will dictate whether the interaction prefers the impurity spins to orient in the plane normal to the exchange field or collinearly with it. The sign of the largest term thereafter determines whether the interaction prefers the impurity spins to orient parallel or antiparallel. The difference in magnitude between the Ising and Heisenberg interaction energies oscillates as a function of separation distance, making the two interaction terms take turns on being dominant.

2. High temperatures $T \lesssim T_c$

In order to show the effect of temperature on the results, we consider in this section $T = 4$ K, taken to represent the regime $T \lesssim T_c$. Similarly to the previous section, we first compute the change in the RKKY energy as a function of R_{21} when no spin-splitting field is present for both the normal state and superconducting phase of the system in Fig. 4(a). The results are qualitatively similar to the low-temperature case. For $R_{21} \ll \xi_S$, the signal oscillates both in the normal and superconducting state, while above ξ_S the interaction between the magnetic impurities is AFM in the superconducting state.

When the spin-splitting field is present, as shown in Figs. 4(b)–4(e), the RKKY interaction in the superconducting state is more strongly affected by a change in h_{exc} than in the low-temperature case considered in the previous section. This can be understood from the exchange field having a larger effect on the superconducting order parameter at higher temperatures, as displayed in Fig. 1(c). As a result, it becomes easier to change the sign of the RKKY interaction energies E_I and E_H by increasing h_{exc} while still remaining in the superconducting phase of the system. In fact, it can be seen

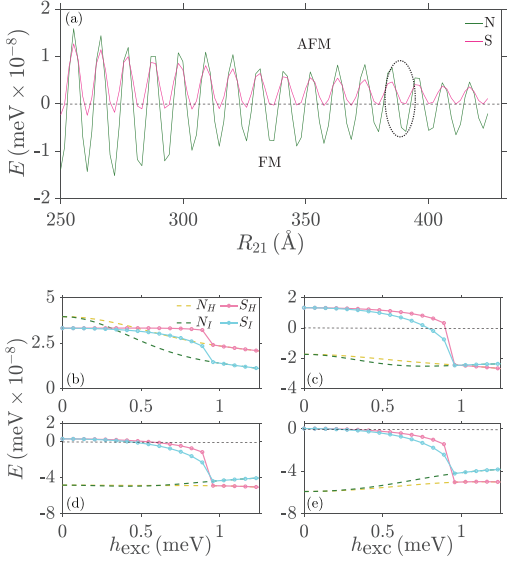


FIG. 4. (a) RKKY energy vs R_{21} when $h_{\text{exc}} = 0$. The RKKY energies as a function of exchange field for (b) $R_{21} = 386.561 \text{\AA}$, (c) $R_{21} = 387.975 \text{\AA}$, (d) $R_{21} = 388.908 \text{\AA}$, and (e) $R_{21} = 390.803 \text{\AA}$ are computed. Here, $N_H(N_I)$ is Heisenberg (Ising) RKKY interaction energy for normal metal state and $S_H(S_I)$ is Heisenberg (Ising) RKKY interaction energy for the superconducting phase. The temperature is fixed at 4 K.

from Figs. 4(c)–4(e) that the sign change can occur for much lower spin-splitting fields than in the low-temperature case. We also find that a sign change of the RKKY interaction becomes more difficult to achieve in the normal state of the system and no such sign change is observed in any of the plots in Fig. 4. In fact, the sign change now only occurs at highly selective separation distances R_{21} in the normal state where the RKKY oscillations cause the interaction to almost vanish.

Moreover, Fig. 5 shows that the interaction between the two impurity spins still oscillates between Heisenberg and

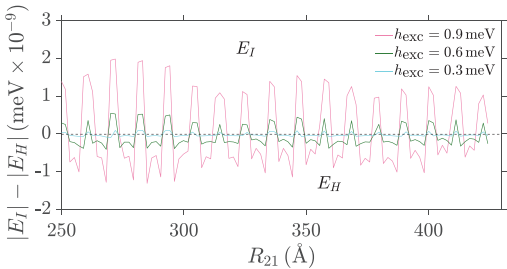


FIG. 5. Difference between the Ising and Heisenberg energies for three different external values of the spin-splitting field at $T = 4 \text{ K}$ for the superconducting state.

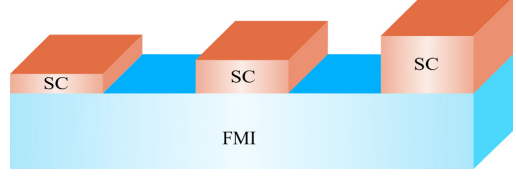


FIG. 6. Possible experimental setup that can be used to test the effect on the RKKY energies when changing the effective Zeeman-splitting in the superconductor. By growing several superconducting layers on top of a ferromagnetic insulator and making the thickness of each superconducting layer different, the effective spin-splitting experienced by magnetic impurities placed on top of the superconducting surfaces will be different. The thickness of the superconducting layers should in all cases be much smaller than the penetration depth λ and smaller than the superconducting coherence length ξ_S in order to justify the approximation of a homogeneous spin-splitting field.

Ising terms as a function of the distance between the two impurity spins even for the case of higher temperatures $T \lesssim T_c$. The magnitude of the oscillations in Fig. 5 increases with h_{exc} in both cases. This is reasonable since the spin-rotational invariance becomes more strongly broken with increasing h_{exc} , making the Ising and Heisenberg configurations more distinct in energy.

3. Discussion of experimental aspects

We close this section by discussing possible experimental realizations of the proposed system. The magnitude of the spin-splitting field h_{exc} can be readily tuned by an external magnetic field. Alternatively, the spin-splitting can be induced by proximity coupling the superconductor to a ferromagnetic insulator (FMI), as displayed in Fig. 6. An effective spin-splitting field in the superconductor then arises from quasiparticle reflections at the interface between the superconductor and the ferromagnet. The spin-splitting field can be assumed to be uniform if the thickness of the superconductor is much smaller than the coherence length. Also, the magnitude of the spin-splitting scales as one over the thickness of the superconducting layer [36]. The effective exchange field in the superconductor h_{exc} can therefore be tuned through the thickness of the superconducting layer. Figure 6 illustrates such a set up where several superconducting samples with varying thickness are grown on top of the same FMI layer. Magnetic impurity spins placed on the top surface of the superconductor will then couple via quasiparticles that experience different values of the effective h_{exc} , depending on the thickness of the superconducting layer.

For RKKY interaction in spin-polarized systems [28], an important point to note is that the preferred direction of the impurity spins will not be solely determined by the RKKY interaction. There are also local effective anisotropy terms of the type $E_z(S_j^z)^2$ and $E_{xy}[(S_j^x)^2 + (S_j^y)^2]$ for both impurities $j = 1, 2$ that are contained in E_0 in Eq. (18). Moreover, when inducing a magnetization in the superconductor, there will be a coupling between the induced magnetization and the impurities, which is first order in the perturbation parameter

J and therefore able to dominate over the RKKY interaction for sufficiently large spin-splitting. As the interaction between the impurity spins and the homogeneous magnetization of the superconductor will be equal for both impurities, this interaction will act to align the impurity spins. If the spin-splitting arises from an external magnetic field, there will in addition be a direct Zeeman coupling to the impurity spins. This direct Zeeman coupling, which would otherwise typically be the dominant interaction determining the impurity spin orientation, can be avoided by inducing the spin-splitting through proximity to a ferromagnet.

We want to underline that, although there will be other interactions influencing the magnetic impurity configuration, the RKKY interaction is detectable in experiments as it is the only interaction that depends on the relative orientation of the impurity spins and the distance between them. A possible experiment probing the RKKY interaction could be as follows. Consider the setup in Fig. 6. The impurity spins in the superconductor will prefer to align due to the coupling to the exchange field. Using, e.g., spin-polarized scanning tunneling microscopy, the energy needed to flip one of the two spins can be measured [38,39]. The energy necessary to flip this spin at a given impurity separation distance will be decided by the RKKY interaction as well as other present interactions. By subtracting the energy necessary to flip a spin in the absence of RKKY interaction (when there is no other impurity nearby), the RKKY interaction can then be determined.

IV. SUMMARY

In conclusion, we have determined the RKKY interaction between magnetic impurities in a spin-split superconductor, in which case the interaction becomes anisotropic in spin space. The magnitudes of the Ising and Heisenberg terms of the RKKY interaction alternate on being the dominant term and oscillate as a function of distance between the impurities, both at low temperatures $T \ll T_c$ and high temperatures $T \lesssim T_c$.

We also demonstrate that it is possible to change the preferred orientation of the RKKY interaction from an antiferromagnetic configuration of impurity spins to a parallel configuration by adjusting the magnitude of the spin-splitting field h_{exc} . Such an effect is in principle also attainable in the normal state of the system, but the effect is considerably more robust in the superconducting state where it occurs for a much larger set of separation distances between the impurities compared to the normal state.

ACKNOWLEDGMENTS

We thank E. Erlandsen for fruitful discussions. This work was supported by the Research Council of Norway through its Centres of Excellence funding scheme Grant No. 262633.

APPENDIX A: BOGOLIUBOV-DE GENNES TRANSFORMATION

In this section, we give a brief derivation of Bogoliubov-de Gennes transformation in Eq. (5). We first rewrite Eq. (4) as follows:

$$\begin{aligned} H_0 &= \frac{1}{2} \sum_{k,\sigma} \begin{pmatrix} c_{k,\sigma}^\dagger & c_{-k,-\sigma} \end{pmatrix} \begin{pmatrix} \zeta_k - \sigma h_{\text{exc}} & -\sigma \Delta \\ -\sigma \Delta & -\zeta_k - \sigma h_{\text{exc}} \end{pmatrix} \\ &\times \begin{pmatrix} c_{k,\sigma} \\ c_{-k,-\sigma}^\dagger \end{pmatrix} - \frac{|\Delta|^2}{V} + \sum_k \zeta_k \\ &= \frac{1}{2} \sum_{k,\sigma} \varphi_{k,\sigma}^\dagger M \varphi_{k,\sigma} - \frac{|\Delta|^2}{V} + \sum_k \zeta_k. \end{aligned} \quad (\text{A1})$$

In order to diagonalize the Hamiltonian, we consider the unitary matrix $P_{k,\sigma}$ of the form

$$\begin{aligned} P_{k,\sigma}^\dagger &= (\Phi_{k,\sigma}^+ \Phi_{k,\sigma}^-), \\ \Phi^+ &= \begin{pmatrix} v_k \\ -\sigma v_k \end{pmatrix}, \Phi^- = \begin{pmatrix} \sigma v_k \\ v_k \end{pmatrix}, \end{aligned} \quad (\text{A2})$$

where Φ^+ and Φ^- are eigenvectors of M . The Hamiltonian then takes the form

$$H_0 = \frac{1}{2} \sum_{k,\sigma} \tilde{\varphi}_{k,\sigma}^\dagger \tilde{M} \tilde{\varphi}_{k,\sigma} - \frac{|\Delta|^2}{V} + \sum_k \zeta_k. \quad (\text{A3})$$

We have used

$$\begin{aligned} \tilde{M} &= \begin{pmatrix} E_{k,\sigma}^+ & 0 \\ 0 & E_{k,\sigma}^- \end{pmatrix}, \\ \tilde{\varphi}_{k,\sigma} &= P_{k,\sigma} \varphi_{k,\sigma} = \begin{pmatrix} \gamma_{k,\sigma} \\ \gamma_{-k,-\sigma}^\dagger \end{pmatrix}. \end{aligned} \quad (\text{A4})$$

Here, the quasiparticle energies are $E_{k,\sigma}^\pm = \pm \sqrt{\zeta_k^2 + (-\sigma \Delta)^2} - \sigma h_{\text{exc}}$. Using $P_{k,\sigma}^\dagger \tilde{\varphi}_{k,\sigma} = \varphi_{k,\sigma}$ leads to the transformation between normal creation and annihilation operators and quasiparticle creation and annihilation operators [Eq. (5)].

APPENDIX B: EFFECTIVE HAMILTONIAN

In order to obtain the Ising and Heisenberg terms of the RKKY interaction, we calculate the expectation value of the effective Hamiltonian following the procedure outlined in Sec. II. We then obtain

$$\begin{aligned} \langle \tilde{H} \rangle &= \sum_{k,\sigma} E_{k,\sigma} n(E_{k,\sigma}) - \frac{1}{2} \sum_{k,k'} \sum_{i,j} \left(\frac{J}{N} \right)^2 e^{i(k'-k) \cdot (r_j - r_i)} \left[|v_k v_{k'}|^2 \frac{n(E_{k,\alpha}) - n(E_{k',\beta})}{E_{k',\beta} - E_{k,\alpha}} S_i^{\alpha\beta} S_j^{\beta\alpha} + \alpha \beta v_k^* v_{k'} v_{-k}^* v_{-k'} \right. \\ &\times \frac{n(E_{k',\beta}) - n(E_{k,\alpha})}{E_{k',\beta} - E_{k,\alpha}} S_i^{\alpha\beta} S_j^{\alpha,-\beta} + (-\alpha \beta) v_k^* v_{-k'} v_{k'} v_{-k}^* \left. \frac{n(E_{k,\alpha}) + n(E_{-k',-\beta}) - 1}{E_{-k',-\beta} + E_{k,\alpha}} S_i^{\alpha\beta} S_j^{\alpha,-\beta} \right] \end{aligned}$$

$$\begin{aligned}
 & + v_k^* v_k v_{k'}^* v_{k'} \frac{-n(E_{k,\alpha}) - n(E_{-k',-\beta}) + 1}{E_{k,\alpha} + E_{-k',-\beta}} S_i^{\alpha\beta} S_j^{\beta\alpha} - v_{k'} v_{k'}^* v_k v_k^* \frac{n(E_{-k,-\alpha}) + n(E_{k',\beta}) - 1}{E_{k',\beta} + E_{-k,-\alpha}} S_i^{\alpha\beta} S_j^{\beta\alpha} \\
 & - (-\beta\alpha) v_{k'} v_{k'}^* v_k v_k^* \frac{-n(E_{-k,-\alpha}) - n(E_{k',\beta}) + 1}{E_{k',\beta} + E_{-k,-\alpha}} S_i^{\alpha\beta} S_j^{\alpha,-\beta} + (\beta\alpha) v_{-k}^* v_{-k} v_k^* v_k \frac{n(E_{-k,-\alpha}) - n(E_{-k',-\beta})}{E_{-k,-\alpha} - E_{-k',-\beta}} S_i^{\alpha\beta} S_j^{\alpha,-\beta} \\
 & + |v_k v_k^*|^2 \frac{n(E_{-k',-\beta}) - n(E_{-k,-\alpha})}{E_{-k,-\alpha} - E_{-k',-\beta}} S_i^{\alpha\beta} S_j^{\beta\alpha} \Big]. \tag{B1}
 \end{aligned}$$

Here, we have defined $S_i^{\alpha\beta} = S_j \cdot \sigma_{\alpha\beta}$. The first term is a constant that is not relevant for the RKKY interaction. Performing the Pauli matrix products, the second term in Eq. (B1) leads to the RKKY interaction presented in Eqs. (19) and (20).

-
- [1] J. Linder and J. W. A. Robinson, *Nat. Phys.* **11**, 307 (2015).
 [2] M. Eschrig, *Rep. Prog. Phys.* **78**, 104501 (2015).
 [3] F. Hübner, M. J. Wolf, D. Beckmann, and H. v. Löhneysen, *Phys. Rev. Lett.* **109**, 207001 (2012).
 [4] I. V. Bobkova and A. M. Bobkov, *JETP Lett.* **101**, 118 (2015).
 [5] H. Yang, S.-H. Yang, S. Takahashi, S. Maekawa, and S. S. P. Parkin, *Nat. Mater.* **9**, 586 (2010).
 [6] Y. Yafet, *Phys. Lett. A* **98**, 287 (1983).
 [7] G.-X. Miao, A. V. Ramos, and J. S. Moodera, *Phys. Rev. Lett.* **101**, 137001 (2008).
 [8] I. Žutić, J. Fabian, and S. Das Sarma, *Rev. Mod. Phys.* **76**, 323 (2004).
 [9] M. Johnson and R. H. Silsbee, *Phys. Rev. Lett.* **55**, 1790 (1985).
 [10] M. N. Baibich, J. M. Broto, A. Fert, F. Nguyen Van Dau, F. Petroff, P. Etienne, G. Creuzet, A. Friederich, and J. Chazelas, *Phys. Rev. Lett.* **61**, 2472 (1988).
 [11] V. L. Ginzburg, *ZhETF* **31**, 202 (1957) [*Sov. Phys. JETP* **4**, 153 (1957)].
 [12] B. T. Matthias and H. Suhl, *Phys. Rev. Lett.* **4**, 51 (1960).
 [13] L. Gor'kov and A. Rusinov, *Zh. Eksp. Teor. Fiz.* **46**, 1363 (1964) [*Sov. Phys. JETP* **19**, 922 (1964)].
 [14] Y. A. Izyumov, Y. N. Proshin, and M. G. Khusainov, *Phys. Usp.* **45**, 109 (2002).
 [15] K. Yosida, *Phys. Rev.* **106**, 893 (1957).
 [16] T. Kasuya, *Prog. Theor. Phys.* **16**, 45 (1956).
 [17] M. A. Ruderman and C. Kittel, *Phys. Rev.* **96**, 99 (1954).
 [18] A. M. Black-Schaffer, *Phys. Rev. B* **81**, 205416 (2010).
 [19] M. Sherafati and S. Satpathy, *Phys. Rev. B* **83**, 165425 (2011).
 [20] Q. Liu, C.-X. Liu, C. Xu, X.-L. Qi, and S.-C. Zhang, *Phys. Rev. Lett.* **102**, 156603 (2009).
 [21] N. E. Alekseevskii, I. A. Garifullin, B. I. Kochelaev, and E. G. Kharakhash'yan, *Zh. Eksp. Teor. Fiz.* **72**, 1523 (1977) [*JETP* **45**, 799 (1977)].
 [22] B. Kochelaev, L. Tagirov, and M. Khusainov, *Zh. Eksp. Teor. Fiz.* **76**, 578 (1979) [*JETP* **49**, 578 (1979)].
 [23] M. G. Khusainov, *Zh. Eksp. Teor. Fiz.* **109**, 524 (1996) [*JETP* **82**, 278 (1996)].
 [24] D. N. Aristov, S. V. Maleyev, and A. G. Yashenkin, *Z. Phys. B* **102**, 467 (1997).
 [25] A. Di Bernardo, S. Komori, G. Livanas, G. Divitini, P. Gentile, M. Cuoco, and J. W. A. Robinson, *Nat. Mater.* **18**, 1194 (2019).
 [26] A. Ghanbari, V. K. Risinggård, and J. Linder, *Sci. Rep.* **11**, 5028 (2021).
 [27] V. E. Dmitrienko, E. N. Ovchinnikova, J. Kokubun, and K. Ishida, *JETP Lett.* **92**, 383 (2010).
 [28] F. Parhizgar, R. Asgari, S. H. Abedinpour, and M. Zareyan, *Phys. Rev. B* **87**, 125402 (2013).
 [29] H. Imamura, P. Bruno, and Y. Utsumi, *Phys. Rev. B* **69**, 121303(R) (2004).
 [30] J.-J. Zhu, D.-X. Yao, S.-C. Zhang, and K. Chang, *Phys. Rev. Lett.* **106**, 097201 (2011).
 [31] M. Shiranazaei, H. Cheraghchi, and F. Parhizgar, *Phys. Rev. B* **96**, 024413 (2017).
 [32] M. V. Hosseini and M. Askari, *Phys. Rev. B* **92**, 224435 (2015).
 [33] H.-R. Chang, J. Zhou, S.-X. Wang, W.-Y. Shan, and D. Xiao, *Phys. Rev. B* **92**, 241103(R) (2015).
 [34] A. Heimes, D. Mandler, and P. Kotetes, *New J. Phys.* **17**, 023051 (2015).
 [35] A. A. Zyuzin and D. Loss, *Phys. Rev. B* **90**, 125443 (2014).
 [36] F. S. Bergeret, M. Silaev, P. Virtanen, and T. T. Heikkilä, *Rev. Mod. Phys.* **90**, 041001 (2018).
 [37] M. Peiniger and H. Piel, *IEEE Trans. Nucl. Sci.* **32**, 3610 (1985).
 [38] S. Loth, K. von Bergmann, M. Ternes, A. F. Otte, C. P. Lutz, and A. J. Heinrich, *Nat. Phys.* **6**, 340 (2010).
 [39] F. Delgado, J. J. Palacios, and J. Fernández-Rossier, *Phys. Rev. Lett.* **104**, 026601 (2010).

Going beyond the Chandrasekhar-Clogston limit in a flat-band superconductor

arXiv:2109.13245 (2021)

Authors

Atousa Ghanbari*
Eirik Erlandsen*
Asle Sudbø
Jacob Linder

*These authors contributed equally to this work.

Going beyond the Chandrasekhar-Clogston limit in a flat-band superconductor

Atousa Ghanbari,* Eirik Erlandsen,* Asle Sudbø, and Jacob Linder†
 Center for Quantum Spintronics, Department of Physics, Norwegian University of Science and Technology,
 NO-7491 Trondheim, Norway

The Chandrasekhar-Clogston limit normally places stringent conditions on the magnitude of the magnetic field that can coexist with spin-singlet superconductivity, restricting the critical induced Zeeman shift to a fraction of the superconducting gap. Here, we consider a model system where the spin-singlet Cooper pairing in a dispersive band crossing the Fermi level is boosted by an additional flat-band located away from the Fermi level. The boosting of the pairing in the dispersive band allows for nontrivial solutions to the coupled gap equations for spin-splitting fields considerably larger than the superconducting gaps at zero field. Further, the additional Cooper pairing in the flat-band, away from the Fermi level, increases the superconducting condensation energy without affecting the paramagnetic susceptibility of the system, making the free energy favor the superconducting state. This opens up the possibility for spin-singlet superconductivity beyond the standard Chandrasekhar-Clogston limit.

Introduction. – Coexistence of superconductivity and magnetism is essential within the field of superconducting spintronics [1–8], which relies on stabilizing superconductors in proximity to magnetic materials and realizing phenomena such as spin-polarized supercurrents [9–11]. Moreover, spin-split superconductors can give rise to very large thermoelectric effects [12–17], which can be used to convert excess heat into useful energy.

Magnetism is, however, usually detrimental to superconductivity. Orbital effects induced in a superconductor due to a magnetic field can be suppressed by making the superconductor sufficiently thin and applying the magnetic field in-plane [16, 18, 19]. The critical magnetic field is then determined by the Zeeman-splitting that the superconducting state can survive [20, 21]. As the normal state of the system has a nonzero density of states at the Fermi level, the free energy can be lowered in the presence of a spin-splitting field by spin-polarizing the system. A spin-singlet superconductor with a gap around the Fermi level [22], on the other hand, has no zero-temperature paramagnetic susceptibility and is unable to lower its energy in the same way. When the Zeeman energy gain in the normal state becomes as large as the superconducting condensation energy, the system therefore transitions to the normal state. This places an upper bound on the spin-splitting field that a conventional superconductor can coexist with $h = \Delta_0/\sqrt{2} \approx 0.7 \Delta_0$ [20, 21], referred to as the Chandrasekhar-Clogston limit. Here Δ_0 is the superconducting gap at zero field. Bypassing the Chandrasekhar-Clogston limit requires e.g. spin-triplet or Fulde-Ferrell-Larkin-Ovchinnikov (FFLO) pairing [23, 24], introduction of spin-orbit coupling in the system [25], or an applied voltage bias driving the superconductor out of equilibrium [26].

Fermionic flat-band systems are systems containing one or more fermionic energy bands with vanishing or small dispersion [27, 28]. Such bands can be gener-

ated by realizing particular tight-binding models [29–35] in e.g. artificial electronic lattices [36–39] or optical lattices filled with ultracold fermionic atoms [40, 41]. Flat-bands can also be realized in twisted or lattice mismatched multilayers such as twisted bilayer graphene [28, 42–45], where the flat-bands are defined in a mini-Brillouin zone corresponding to a long-wavelength superlattice arising from the mismatch between the periodic structures in the separate layers. Flat-band systems are appealing for superconductivity as a larger density of states at the Fermi level normally leads to a larger superconducting transition temperature. Early studies identified that the presence of a flat-band could in fact give rise to a linear dependence of the transition temperature on the strength of the attractive interactions [46, 47], generating hope of achieving high critical temperatures. With the discovery of superconductivity in magic-angle twisted-bilayer graphene [43], interest in flat-band superconductivity rocketed [48–52]. Recently, it has also been discovered that superconductivity in twisted trilayer graphene can survive in-plane magnetic fields beyond the Chandrasekhar-Clogston limit [53], which has been interpreted as an indication of spin-triplet pairing [53, 54].

In this Letter, we consider a two-band model system for a spin-split superconductor, in which a dispersive band crosses the Fermi level and a flat-band is located in the vicinity of the Fermi level. We consider both attractive intra- and interband scattering, giving rise to two coupled self-consistency equations for the spin-singlet pairing amplitudes associated with the two bands. The additional Cooper pairing in the flat-band gives rise to an increase in the condensation energy, without affecting the zero-temperature paramagnetic susceptibility of the system as the flat-band does not cross the Fermi level. The free energy is therefore minimized by the superconducting state beyond the Chandrasekhar-Clogston limit. Moreover, as the flat-band is located away from the Fermi level, quasiparticle excitations associated with

the flat-band are energetically costly also for large spin-splitting, making the flat-band contributions to the gap equations more resilient to spin-splitting fields than the contributions from the dispersive band. We therefore find that the spin-singlet pairing in this system can survive spin-splitting fields significantly larger than the superconducting gaps at zero field. We close by discussing how the physics captured by our model can be realized in experiments.

Model. – Our system is described by an interacting two-band Hamiltonian on the form

$$H = \sum_{i,\mathbf{k},\sigma} \varepsilon_{i,\mathbf{k},\sigma} c_{i,\mathbf{k},\sigma}^\dagger c_{i,\mathbf{k},\sigma} + \frac{1}{N} \sum_{i,j,\mathbf{k},\mathbf{k}'} V_{ij}(\mathbf{k}, \mathbf{k}') c_{i,\mathbf{k},\uparrow}^\dagger c_{i,-\mathbf{k},\downarrow}^\dagger c_{j,-\mathbf{k}',\downarrow} c_{j,\mathbf{k}',\uparrow}. \quad (1)$$

Here, $c_{i,\mathbf{k},\sigma}$ is an annihilation operator for an electron in band i with momentum \mathbf{k} , and spin σ . The non-interacting part of the Hamiltonian describes the dispersive band with energies $\varepsilon_{1,\mathbf{k},\sigma} = -2t[\cos(k_x) + \cos(k_y)] - \mu - \sigma h$ and the flat-band with energies $\varepsilon_{2,\mathbf{k},\sigma} = -\mu_0 - \sigma h$. The strength of the spin-splitting field is still h , the number of lattice sites is denoted by N , and μ is the chemical potential. Further, μ_0 is the shift of the flat band away from the Fermi-level. With this parametrization, the Fermi level is moved relative to the dispersive band when μ is varied, while the separation of the flat-band and the Fermi level is fixed. The band structure in the absence of spin-splitting is illustrated in Fig. 1 (a-b). The Hamiltonian in Eq. (1) is similar to the one used in Ref. [46], which discussed boosting of the pairing in a dispersive band through the presence of a flat-band. However, no spin-splitting field was considered in Ref. [46].

The interaction term in the Hamiltonian allows for attractive BCS-type intraband and interband scattering [55]. The interaction is taken to be attractive in a thin shell of width $2h\omega_c$ around the Fermi level

$$V_{ij}(\mathbf{k}, \mathbf{k}') = \begin{cases} V_{ij} > 0, & |\varepsilon_{i,\mathbf{k}}|, |\varepsilon_{j,\mathbf{k}'}| \leq h\omega_c, \\ 0, & \text{otherwise.} \end{cases} \quad (2)$$

Here, $\varepsilon_{i,\mathbf{k}}$ is defined from $\varepsilon_{i,\mathbf{k},\sigma} = \varepsilon_{i,\mathbf{k}} - \sigma h$, and V_{ij} is the band-dependent attractive interaction strength. In the following, we neglect any hybridization between the bands or other changes to the normal state band structure arising from the interaction, and investigate up to what values of h the attractive interaction can give rise to superconductivity.

Performing a standard mean-field theory, defining spin-singlet gaps $\Delta_i(\mathbf{k}) = \frac{1}{N} \sum_{j,\mathbf{k}'} V_{ij}(\mathbf{k}, \mathbf{k}') \langle c_{j,-\mathbf{k}',\downarrow} c_{j,\mathbf{k}',\uparrow} \rangle$, and introducing the necessary Bogoliubov-de Gennes transformation,

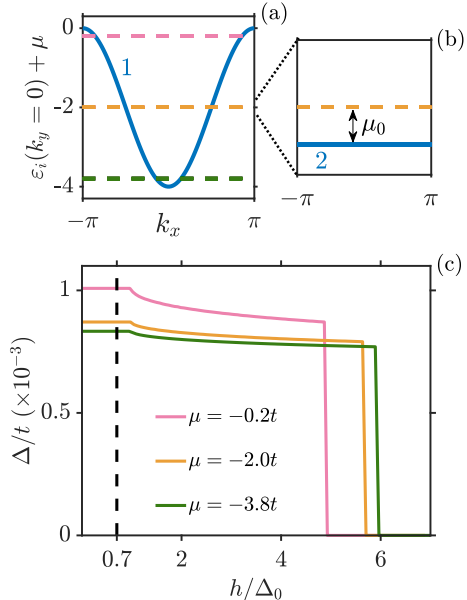


FIG. 1. (a-b) Illustration of the band structure of the two-band model in the absence of spin-splitting. Dashed lines represent three different values of the chemical potential $\mu = -0.2t, -2t, \text{ and } -3.8t$. The flat-band is fixed μ_0 below the Fermi level, which is illustrated by the blue line 2 in (b) for a specific choice of the chemical potential. (c) Superconducting gap versus the ratio between the strength of the spin-splitting field and the gap at zero field for the three different chemical potentials in (a). The Chandrasekhar-Clogston limit is indicated by the vertical dashed line. The parameters have been set to $t = 1, T = 0, V_{11} = V_{12} = V_{21} = V_{22} = 0.01t, \mu_0 = 0.00495t$, and $\hbar\omega_c = 0.05t$.

the coupled gap equations take the form

$$\Delta_i(\mathbf{k}) = \frac{1}{N} \sum_{j,\mathbf{k}'} V_{ij}(\mathbf{k}, \mathbf{k}') \frac{\Delta_j(\mathbf{k}')}{2E_{j,\mathbf{k}'}} \times \frac{1}{2} \left[\tanh\left(\frac{\beta}{2} E_{j,\mathbf{k}',\uparrow}\right) + \tanh\left(\frac{\beta}{2} E_{j,\mathbf{k}',\downarrow}\right) \right]. \quad (3)$$

Here, $E_{i,\mathbf{k}} = \sqrt{\varepsilon_{i,\mathbf{k}}^2 + |\Delta_i(\mathbf{k})|^2}$, the quasiparticle energies are $E_{i,\mathbf{k},\sigma} = E_{i,\mathbf{k}} - \sigma h$, and $\beta = 1/(k_B T)$ is inverse temperature. The free energy, which determines whether the superconducting state minimizes the free energy, is expressed as

$$F = \frac{1}{4} \sum_{i,\mathbf{k},\sigma} \frac{\Delta_i^2(\mathbf{k})}{E_{i,\mathbf{k}}} \tanh\left(\frac{\beta}{2} E_{i,\mathbf{k},\sigma}\right) + \sum_{i,\mathbf{k}} (\varepsilon_{i,\mathbf{k}} - E_{i,\mathbf{k}}) - \frac{1}{\beta} \sum_{i,\mathbf{k},\sigma} \ln(1 + e^{-\beta E_{i,\mathbf{k},\sigma}}). \quad (4)$$

The first term in this expression is simply a generalization of the term $N\Delta^2/V$, which it reduces to for the case of a single electron band.

Results. – For simplicity, we start with the case where all the interaction strengths are equal ($V_{11} = V_{12} = V_{21} = V_{22} = V$). In this case, the two coupled gap equations in Eq.(3) reduce to a single self-consistent equation for the gap $\Delta = \Delta_1 = \Delta_2$. By numerically solving this gap equation and ensuring that the free energy in Eq. (4) is minimized, we determine the value of the gap as a function of the strength of the spin-splitting field h . The results at zero-temperature are presented in Fig. 1 (c) for different values of the chemical potential μ . As displayed in this figure, a non-zero superconducting gap can exist for spin-splitting fields significantly larger than the gap at zero field Δ_0 .

In the more familiar case of a superconductor with a single dispersive band crossing the Fermi level, the superconducting gap vanishes when the field strength reaches the Chandrasekhar-Clogston limit and the normal state minimizes the free energy. In Fig. 1(c), this limit is indicated by a vertical dashed line. The mechanism for this transition is easily seen from the expression for the free energy in Eq. (4) if we limit ourselves to the contributions from $i = 1$, corresponding to the dispersive band. For the superconductor, as long as the spin-splitting is smaller than the gap, all the quasiparticle energies are positive and the last term in the free energy vanishes. For the normal state, on the other hand, there is no gap in the excitation spectrum and the energies $E_{1,\mathbf{k},\sigma} = |\varepsilon_{1,\mathbf{k}}| - \sigma h$ can turn negative, giving rise to negative contributions from the last term in the free energy. This corresponds to a lowering of the normal state free energy through the system becoming spin-polarized. Comparing the rest of the free energy for the two phases gives rise to the condensation energy, favoring the superconducting state. When the strength of the spin-splitting field is increased, the lowering of the free energy of the normal state eventually dominates over the condensation energy, and the normal state prevails.

In the present case, there are additional contributions to the free energy arising from the flat band. As long as the quasiparticle energies $E_{2,\mathbf{k},\sigma}$ are shifted away from the Fermi level by $|\mu_0| > h$, these energies will always be positive even without a gap. At zero temperature there are then no contributions from the last term in the free energy arising from the flat-band, regardless

of whether the system is in the superconducting or normal state. The effect of the flat-band on the free energy is then simply to significantly increase the condensation energy due to its large density of states. We therefore find that having a nonzero gap minimizes the free energy also beyond the Chandrasekhar-Clogston limit. Moreover, when the spin-splitting becomes larger than Δ_0 , the gaps in the separate spin-bands no longer overlap and the superconducting state is able to lower its free energy by spin-polarizing the quasiparticles as discussed in Ref. [56]. Such "gapless" superconductivity arises from time-reversal symmetry breaking [57, 58] and has been encountered in e.g. systems with magnetic impurities [59, 60] and in the presence of a magnetic field [61, 62].

Turning to the gap equation, for a spin-splitting field larger than the gap, the energies $E_{1,\mathbf{k}',\uparrow}$ and $E_{1,\mathbf{k}',\downarrow}$ on the right-hand-side of Eq. (3) can end up with opposite signs, leading to a cancellation of the contributions. The first contributions to go are those with the smallest energies $E_{1,\mathbf{k}'}$, i.e. the most important contributions from the dispersive band. For the flat-band, on the other hand, the quasiparticle energies are always positive for $|\mu_0| > h$. The flat-band contributions to the gap equation are therefore robust towards spin-splitting. By having the flat-band sufficiently close to the Fermi level ($|\mu_0| < V/2$), solutions to the gap equation can then be guaranteed as long as $h < |\mu_0|$. The spin-splitting field that can coexist with superconductivity is then, in other words, limited by $|\mu_0|$, where the value of $|\mu_0|$ that can produce a superconducting solution is limited by the interaction strength V .

The dependence of the gap equation on the strength of the spin-splitting field can be observed in Fig. 1 (c), and is most easily seen by considering the pink curve corresponding to $\mu = -0.2t$. For $h < \Delta_0$, the curve is flat as the spin-splitting has no effect on the contributions to the gap equation. Then, as $h > \Delta_0$, contributions from the dispersive band start cancelling out, leading to a decrease in the gap. This corresponds to the minimum energy of breaking a Cooper pair becoming zero, as discussed by Abrikosov in the context of gapless superconductivity in the presence of magnetic impurities [63]. In the present case, a non-zero superconducting gap exists until around $h > |\mu_0|$, beyond which the flat-band no longer contributes to the gap equation.

We next demonstrate how our results are influenced by band-dependence of the interaction strengths. We first consider the effect of reducing the interband scattering by taking $V_{12} = V_{21}$ smaller than $V_{11} = V_{22}$. Solving the coupled gap equations and checking the free energy, we obtain the results in Fig. 2. As the dominant contributions to the gap equations arise from the flat-band, we find that Δ_2 , which obtains contributions from $V_{21}\Delta_1$ and $V_{22}\Delta_2$, is not strongly affected by a reduction of

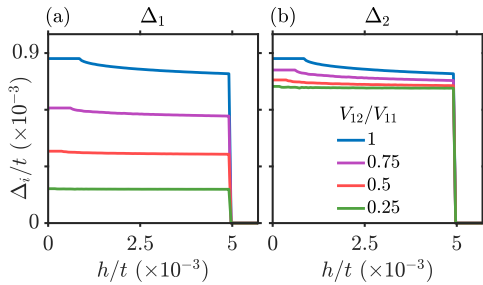


FIG. 2. (a) Δ_1 (b) Δ_2 as a function of the strength of the spin-splitting field h for four different ratios of V_{12}/V_{11} . The parameters are set to $t = 1$, $T = 0$, $\mu_0 = 0.00495t$, $V_{11} = V_{22} = 0.01t$, $V_{12} = V_{21}$, $\hbar\omega_c = 0.05t$, and $\mu = -2t$.

V_{21} . On the other hand, Δ_1 obtains contributions from $V_{11}\Delta_1$ and $V_{12}\Delta_2$, and a reduction of V_{12} therefore leads to a significant reduction of Δ_1 . Substantial pairing in the dispersive band crossing the Fermi level therefore requires a sufficiently large interband interaction strength. In all cases, the gaps survive until $h > |\mu_0|$, which is considerably larger than the gaps at zero field.

Finally, we consider the case where we also increase the intraband interaction in the dispersive band compared to the intraband interaction in the flat-band. The results for Δ_1 are displayed in Fig. 3, showing that significantly increasing V_{11} only leads to a moderate increase in Δ_1 as the dominant contributions to the gap equations still arise from the flat-band due to its large density of states. A moderate increase in Δ_1 has little impact on the results for Δ_2 which therefore varies little when we increase V_{11} . The gaps once again survive until $h > |\mu_0|$, where the magnitude of $|\mu_0|$ that can still provide a nontrivial solution to the gap equations is determined by how large we take V_{22} .

Outlook. – We have presented a mechanism for how a spin-singlet superconductor can survive beyond the Chandrasekhar-Clogston limit. The mechanism relies on having a dispersive band crossing the Fermi level, an additional flat band nearby, sufficient intra-band interaction in the flat band, and some interband scattering. Realization in experiments requires a thin-film superconductor with a, preferably tunable, induced spin-splitting. The spin-splitting can be achieved by exposing the superconductor to a strong in-plane magnetic field, or to a combination of a ferromagnet and an external field where the additional external field provides the tunability of the strength of the spin-splitting [26]. The necessary band structure could be realized in artificial electronic lattices, optical lattices, or in twisted multilayers. The especially relevant case of a dispersive band on top of a flat band

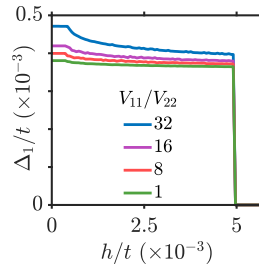


FIG. 3. The gap Δ_1 as a function of the strength of the spin-splitting field h for four different ratios of V_{11}/V_{22} . The parameters are set to $t = 1$, $T = 0$, $\mu_0 = 0.00495t$, $V_{22} = 0.01t$, $V_{12} = V_{21} = 0.005t$, $\hbar\omega_c = 0.05t$, and $\mu = -2t$.

corresponds to the limiting case where the chemical potential in Fig. 1 is taken almost down to the bottom of the band, e.g. $\mu = -4t + \mu_0$. Importantly, the flatness of the flat-band should be stable in the presence of spin-splitting. Finally, the interactions could originate with phonons in twisted multilayers or be engineered in artificial systems. The choice of interactions in Fig. 1 could e.g. in principle correspond to the electrons in both bands coupling similarly to Einstein phonons. As shown in Fig. 2 and 3, the results for the critical field are, however, quite robust to band-dependence of the interaction strengths, allowing for reduction of the interband scattering as well as for a much larger intraband scattering in the dispersive band than in the flat-band.

More exhaustive studies of realistic systems, taking into account the details of the band structure and the interactions, should be performed in order to more closely relate the results to experiments. Special attention should be paid to the theoretical approach when a flat-band is present and when the Fermi energy is not dominating the other energy scales in the system, which e.g. can be the case when the chemical potential is close to the bottom of the conduction band. Future work could also look into whether other superconducting phases, such as an FFLO state, could be favored in parts of the parameter regime.

Summary. – Our results demonstrate that spin-singlet superconductivity beyond the Chandrasekhar-Clogston limit could be possible in flat-band systems. Future studies should perform more detailed calculations for realistic systems in order to more closely connect the findings to experiments.

We thank Even Thingstad for valuable discussions. We acknowledge financial support from the Research Council of Norway Grant No. 262633 “Center of Excellence on Quantum Spintronics” and Grant No. 323766.

- * These authors contributed equally to this work
† Corresponding author: jacob.linder@ntnu.no
- [1] J. Linder and J. W. A. Robinson, *Nature Physics* **11**, 307 (2015).
 - [2] M. Eschrig, *Phys. Today* **64**, 43 (2011).
 - [3] A. Singh, S. Voltan, K. Lahabi, and J. Aarts, *Phys. Rev. X* **5**, 021019 (2015).
 - [4] Y. C. Tao and J. G. Hu, *Journal of Applied Physics* **107**, 041101 (2010).
 - [5] A. I. Buzdin, *Rev. Mod. Phys.* **77**, 935 (2005).
 - [6] S. Takahashi and S. Maekawa, *Phys. Rev. Lett.* **88**, 116601 (2002).
 - [7] T. Wakamura, H. Akaike, Y. Omori, Y. Niimi, S. Takahashi, A. Fujimaki, S. Maekawa, and Y. Otani, *Nature Materials* **14**, 675 (2015).
 - [8] S. Takahashi and S. Maekawa, *Japanese Journal of Applied Physics* **51**, 010110 (2011).
 - [9] R. S. Keizer, S. T. B. Goennenwein, T. M. Klapwijk, G. Miao, G. Xiao, and A. Gupta, *Nature* **439**, 825 (2006).
 - [10] T. S. Khaire, M. A. Khasawneh, W. P. Pratt, and N. O. Birge, *Phys. Rev. Lett.* **104**, 137002 (2010).
 - [11] J. W. A. Robinson, J. D. S. Witt, and M. G. Blamire, *Science* **329**, 59 (2010).
 - [12] A. Ozaeta, P. Virtanen, F. S. Bergeret, and T. T. Heikkilä, *Phys. Rev. Lett.* **112**, 057001 (2014).
 - [13] P. Machon, M. Eschrig, and W. Belzig, *Phys. Rev. Lett.* **110**, 047002 (2013).
 - [14] F. Giazotto, J. W. A. Robinson, J. S. Moodera, and F. S. Bergeret, *Appl. Phys. Lett.* **105**, 062602 (2014).
 - [15] P. Machon, M. Eschrig, and W. Belzig, *New Journal of Physics* **16**, 073002 (2014).
 - [16] F. S. Bergeret, M. Silaev, P. Virtanen, and T. T. Heikkilä, *Rev. Mod. Phys.* **90**, 041001 (2018).
 - [17] S. Kolenda, M. J. Wolf, and D. Beckmann, *Phys. Rev. Lett.* **116**, 097001 (2016).
 - [18] R. Meservey, P. M. Tedrow, and P. Fulde, *Phys. Rev. Lett.* **25**, 1270 (1970).
 - [19] R. Meservey, P. M. Tedrow, and R. C. Bruno, *Phys. Rev. B* **11**, 4224 (1975).
 - [20] B. S. Chandrasekhar, *Applied Physics Letters* **1**, 7 (1962).
 - [21] A. M. Clogston, *Phys. Rev. Lett.* **9**, 266 (1962).
 - [22] J. Bardeen, L. N. Cooper, and J. R. Schrieffer, *Phys. Rev.* **108**, 1175 (1957).
 - [23] P. Fulde and R. A. Ferrell, *Phys. Rev.* **135**, A550 (1964).
 - [24] A. I. Larkin and Y. N. Ovchinnikov, *Zh. Eksp. Teor. Fiz.* **47**, 1136 (1964).
 - [25] R. C. Bruno and B. B. Schwartz, *Phys. Rev. B* **8**, 3161 (1973).
 - [26] J. A. Ouassou, T. D. Vethaak, and J. Linder, *Phys. Rev. B* **98**, 144509 (2018).
 - [27] D. Leykam, A. Andreanov, and S. Flach, *Advances in Physics: X* **3**, 1473052 (2018).
 - [28] L. Balents, C. R. Dean, D. K. Efetov, and A. F. Young, *Nature Physics* **16**, 725 (2020).
 - [29] B. Sutherland, *Phys. Rev. B* **34**, 5208 (1986).
 - [30] E. H. Lieb, *Phys. Rev. Lett.* **62**, 1201 (1989).
 - [31] A. Mielke, *Journal of Physics A: Mathematical and General* **24**, 3311 (1991).
 - [32] H. Tasaki, *Phys. Rev. Lett.* **69**, 1608 (1992).
 - [33] S. Miyahara, K. Kubo, H. Ono, Y. Shimomura, and N. Furukawa, *Journal of the Physical Society of Japan* **74**, 1918 (2005).
 - [34] A. Ramachandran, A. Andreanov, and S. Flach, *Phys. Rev. B* **96**, 161104 (2017).
 - [35] A. Sil and A. K. Ghosh, *Journal of Physics: Condensed Matter* **31**, 245601 (2019).
 - [36] A. Tadjine, G. Allan, and C. Delerue, *Phys. Rev. B* **94**, 075441 (2016).
 - [37] W.-X. Qiu, S. Li, J.-H. Gao, Y. Zhou, and F.-C. Zhang, *Phys. Rev. B* **94**, 241409 (2016).
 - [38] M. R. Slot, T. S. Gardenier, P. H. Jacobse, G. C. P. van Miert, S. N. Kempkes, S. J. M. Zevenhuizen, C. M. Smith, D. Vanmaekelbergh, and I. Swart, *Nature Physics* **13**, 672 (2017).
 - [39] R. Drost, T. Ojanen, A. Harju, and P. Liljeroth, *Nature Physics* **13**, 668 (2017).
 - [40] S. Taie, T. Ichinose, H. Ozawa, and Y. Takahashi, *Nature Communications* **11**, 257 (2020).
 - [41] G.-B. Jo, J. Guzman, C. K. Thomas, P. Hosur, A. Vishwanath, and D. M. Stamper-Kurn, *Phys. Rev. Lett.* **108**, 045305 (2012).
 - [42] R. Bistritzer and A. H. MacDonald, *Proceedings of the National Academy of Sciences* **108**, 12233 (2011).
 - [43] Y. Cao, V. Fatemi, S. Fang, K. Watanabe, T. Taniguchi, E. Kaxiras, and P. Jarillo-Herrero, *Nature* **556**, 43 (2018).
 - [44] Z. Zhang, Y. Wang, K. Watanabe, T. Taniguchi, K. Ueno, E. Tutuc, and B. J. LeRoy, *Nature Physics* **16**, 1093 (2020).
 - [45] J. M. Park, Y. Cao, K. Watanabe, T. Taniguchi, and P. Jarillo-Herrero, *Nature* **590**, 249 (2021).
 - [46] S. Miyahara, S. Kusuta, and N. Furukawa, *Physica C: Superconductivity* **460-462**, 1145 (2007).
 - [47] N. B. Kopnin, T. T. Heikkilä, and G. E. Volovik, *Phys. Rev. B* **83**, 220503 (2011).
 - [48] R. Ojajarvi, T. Hyart, M. A. Silaev, and T. T. Heikkilä, *Phys. Rev. B* **98**, 054515 (2018).
 - [49] A. Bussmann-Holder, H. Keller, A. Simon, and A. Bianconi, *Condensed Matter* **4** (2019), 10.3390/condmat4040091.
 - [50] Y. W. Choi and H. J. Choi, *Phys. Rev. B* **98**, 241412 (2018).
 - [51] B. Lian, Z. Wang, and B. A. Bernevig, *Phys. Rev. Lett.* **122**, 257002 (2019).
 - [52] F. Schrodi, A. Aperis, and P. M. Oppeneer, *Phys. Rev. Research* **2**, 012066 (2020).
 - [53] Y. Cao, J. M. Park, K. Watanabe, T. Taniguchi, and P. Jarillo-Herrero, *Nature* **595**, 526 (2021).
 - [54] W. Qin and A. H. MacDonald, *Phys. Rev. Lett.* **127**, 097001 (2021).
 - [55] H. Suhl, B. T. Matthias, and L. R. Walker, *Phys. Rev. Lett.* **3**, 552 (1959).
 - [56] G. Sarma, *Journal of Physics and Chemistry of Solids* **24**, 1029 (1963).
 - [57] K. H. Bennemann and J. B. Ketterson, *Superconductivity - Conventional and Unconventional Superconductors* (Springer-Verlag, Berlin Heidelberg, 2008).
 - [58] G. Sun, D. Y. Xing, J. Dong, and M. Liu, *Phys. Rev. B* **65**, 174508 (2002).
 - [59] A. A. Abrikosov and L. P. Gor'kov, *Zh. Eksp. i Teor. Fiz.* **39** (1960).

- [60] F. Reif and M. A. Wolf, *Rev. Mod. Phys.* **36**, 238 (1964).
[61] K. Maki, *Physics Physique Fizika* **1**, 127 (1964).
[62] P. G. de Gennes and M. Tinkham, *Physics Physique Fizika* **1**, 107 (1964).
[63] A. A. Abrikosov, *Fundamentals of the Theory of Metals* (Elsevier Science Publishers, Amsterdam, 1988).

ISBN 978-82-326-6602-7 (printed ver.)
ISBN 978-82-326-6330-9 (electronic ver.)
ISSN 1503-8181 (printed ver.)
ISSN 2703-8084 (online ver.)



NTNU

Norwegian University of
Science and Technology